

Collision Processes in Low-Temperature Hydrogen Plasmas

R.K. Janev^{1,2}, D. Reiter¹, U. Samm¹

Abstract

Collision processes among the constituents of low-temperature hydrogen plasmas (e , H , H^+ , H^- , H_2 , H_2^+ , H_3^+) play a key role in technical plasma applications as well as in the boundary regions of magnetically confined fusion plasmas. In this work a review of the current knowledge on their cross sections is presented.

Collision processes of electronically and vibrationally excited species are also included in the present review. The energy range in which these processes are considered extends from thermal energies to several hundreds electronvolts (and to the keV region for some heavy-particle collision processes). The available experimental and theoretical cross section information is critically assessed and presented in form of analytic fit functions, convenient for use in plasma applications.

¹Institut für Plasmaphysik, Forschungszentrum Jülich GmbH, EURATOM Association, Trilateral Euregio Cluster, D-52425 Jülich, Germany

²Macedonian Academy of Sciences and Arts, 1000 Skopje, Macedonia

Contents

1	Introduction	7
2	Collision Processes of Hydrogen Atoms	8
2.1	Electron impact processes	8
2.1.1	Excitation	8
	A Transitions from the ground state: $nl = 1s$. . .	8
	B Transitions between excited states: $n \rightarrow m$. . .	10
2.1.2	Ionization	11
	A Ionization of the ground- and $n = 2, 3$ excited states	11
	B Ionization of $n \geq 4$ states	12
2.1.3	Radiative electron attachment	12
2.1.4	$H(n \geq 1)$ formation in electron-proton collisions	13
	A Radiative recombination	13
	B Three-body recombination	14
2.2	Proton impact processes	14
2.2.1	Excitation	15
	A Transitions from the ground state: $nl = 1s$. . .	15
	B Transitions between excited states: $n \rightarrow m$. . .	16
2.2.2	Ionization	18
2.2.3	Charge transfer	19
2.2.4	Three-body diatomic association	20
2.3	Atom-atom collision processes	20
2.3.1	Excitation transfer, Penning ionization and spin exchange	21
2.3.2	Excitation (de-excitation) and ionization of Rydberg atoms	21
2.3.3	Associative and non-associative ionization	22
2.3.4	Three-body diatomic association	22
3	Collision Processes of H^- Ions	23
3.1	Electron impact processes	23
3.1.1	Electron detachment	23
3.1.2	Other processes	23
3.2	Proton impact processes	24
3.2.1	Mutual neutralization of H^+ and H^-	24
3.2.2	Associative (AD) and non-associative (Det) detachment .	25
3.3	Collisions of H^- with H	25
3.3.1	Resonant charge exchange	26
3.3.2	Associative (AD) and non-associative (Det) detachment .	26

4	Collision Processes of Electrons with Hydrogen Molecules	27
4.1	Vibrational excitation of $H_2(X^1\Sigma_g^+)$	27
4.1.1	Vibrational excitation via $H_2^-(X^2\Sigma_u^+, B^2\Sigma_g^+)$ resonant states	28
4.1.2	Vibrational excitation via $H_2^*(N^1\Lambda_u)$ excited states	29
4.2	Electronic excitation processes	30
4.2.1	Excitation of singlet states from $X^1\Sigma_g^+$	33
A	Excitation from $X^1\Sigma_g^+(v = 0)$	33
B	Excitation from $X^1\Sigma_g^+(v \geq 1)$	35
C	Dissociative excitation cross sections	37
D	$v - v'$ resolved excitation cross sections	37
4.2.2	Excitation of triplet states from $X^1\Sigma_g^+$	39
A	Excitation from $X^1\Sigma_g^+(v = 0)$	39
B	Excitation from $X^1\Sigma_g^+(v \geq 1)$	40
4.2.3	Excitation transitions between excited states	41
4.3	Ionization processes	42
4.3.1	Ionization from the ground electronic state, $X^1\Sigma_g^+(v)$	43
4.3.2	Ionization from excited electronic states of H_2	45
4.4	Dissociative electron attachment	46
4.4.1	Dissociative attachment on $H_2(X^1\Sigma_g^+; v)$	47
4.4.2	Dissociative attachment on electr. excited $H_2^*(N^{1,3}\Lambda_\sigma)$	48
4.5	Dissociation and ionization of $H_2(N^{1,3}\Lambda_\sigma)$ via resonant, doubly excited and auto-ionizing states.	49
4.5.1	Dissociation of $H_2(^1\Sigma_g^+; v)$ via H_2^- resonant states	49
4.5.2	Dissociation and ionization of H_2 via doubly excited states	50
4.5.3	Auto-ionization and pre-dissociation of excited electronic states	50
A	Auto-ionization	51
B	Pre-dissociation	51
4.6	The metastable ($c^3\Pi_u; v = 0$) state	53
4.6.1	Electron-impact excitation from ($c^3\Pi_u; v = 0$)	53
4.6.2	Ionization of ($c^3\Pi_u; v = 0$) state	54
4.6.3	Electron attachment on ($c^3\Pi_u; v = 0$) state	54
5	Collision Processes of Protons with Hydrogen Molecules	55
5.1	Vibrational excitation	56
5.2	Charge transfer processes	58
5.2.1	Proton charge exchange with $H_2(X^1\Sigma_g^+; v)$	58
A	Initial v -state resolved cross sections	59
B	$v - v'$ resolved charge exchange cross sections	60
5.2.2	Proton charge exchange with $H_2(N^{1,3}\Lambda_\sigma; v), N \geq 2$	60
5.3	Proton impact dissociation of H_2	61
5.4	Proton impact electronic excitation and ionization of H_2	62
5.4.1	Electronic excitation	62
5.4.2	Ionization processes	63

6	Collision Processes of H^-, H and H_2 with Hydrogen Molecules	63
6.1	Collisions of H^- with H_2	64
6.1.1	Electron detachment	64
6.1.2	Other processes	64
6.2	Collisions of H with H_2	65
6.2.1	Vibrational excitation and de-excitation ($V - T$ transfer) .	65
6.2.2	Dissociation	66
6.3	$H_2 - H_2$ collisions	66
6.3.1	Vibrational ($V - V$) transfer	66
6.3.2	Dissociation	67
6.4	Collisions of H^- , H^* and H_2 with electronically excited H_2 . . .	67
7	Collision Processes of H_2^+	68
7.1	Collision processes with electrons	69
7.1.1	Vibrational excitation	69
7.1.2	Dissociative excitation	70
A	Total DE cross section	70
B	DE cross sections for individual vibrational levels	71
7.1.3	Dissociative recombination	72
A	Total DR cross section	73
B	DR cross sections for individual initial vibrational states of $H_2^+(v)$	74
C	n -distribution of excited dissociation products .	75
D	Relation of $\sigma_{DR}(v \rightarrow n)$ with state selective as- sociative ionization of $H + H(n)$	76
7.1.4	Dissociative ionization	77
7.2	Collisions of $H_2^+(v)$ with H Atoms	78
7.2.1	Vibrational excitation and de-excitation of $H_2^+(v)$	78
7.2.2	Charge exchange	79
A	Charge exchange with $H(1s)$	79
B	Charge exchange with $H(n \geq 2)$	80
7.2.3	Dissociation	80
7.3	Collisions of H_2^+ with H_2	82
7.3.1	Vibrational excitation (de-excitation) and charge transfer .	82
A	Vibrational excitation cross sections	83
B	State-selective charge transfer and associated ex- citation (de-excitation)	83
C	Total charge transfer cross section	85
7.3.2	Collision induced dissociation of $H_2^+(v_i)$	86
A	Total CID cross section	87
B	CID cross sections for individual initial v_i states	87
C	Other collision induced dissociative processes .	88
7.3.3	H_3^+ ion formation	88
A	State-selective cross sections	89

Contents

	B	Total cross sections	90	
	C	Proton and atom transfer cross sections	91	
7.4		Collisions of $H_2^+(v_i)$ with H^-	92	
	7.4.1	$H_2^+ - H^-$ mutual neutralization	92	
	7.4.2	Associative and non-associative detachment	94	
8		Collision Processes of H_3^+	95	
	8.1	Collision processes of H_3^+ with electrons	95	
		8.1.1 Vibrational excitation	95	
		8.1.2 Dissociative excitation	96	
		8.1.3 Dissociative recombination (DR)	97	
		A	Total cross section and channel branching ratios for $H_3^+(v_3 = 0)$ DR	98
		B	Quantum state distribution of DR reaction products	99
		C	Total DR cross section for $H_3^+(v_3 \geq 0)$	100
		8.1.4	Ion-pair formation	100
	8.2	Collision processes of H_3^+ with H	101	
		8.2.1	H_3^+ dissociation	101
		8.2.2	Dissociative charge transfer	102
	8.3	$H_3^+ - H_2$ collisions	102	
		8.3.1	Proton transfer reaction	103
		8.3.2	Collision induced dissociation of H_3^+	103
		8.3.3	Dissociative electron capture and fast H_2 production	105
		8.3.4	Slow H^+ production processes	106
	8.4	Collision processes of H_3^+ with H^-	107	
		8.4.1	Dissociative mutual neutralization	107
		8.4.2	Dissociative electron detachment	107
9		Concluding Remarks	108	
		References	111	
10		Tables	130	
11		Figures	163	

1 Introduction

Low-temperature hydrogen plasmas exist in various astrophysical and laboratory environments, and their study is relevant for many technological plasma applications. Despite of their relatively simple chemical composition ($e, H, H^+, H^-, H_2, H_2^+, H_3^+$), their kinetics is extremely complex. This is, basically, due to the facts that the number of quantum states of atomic and molecular species involved in collision kinetics is very large (electronic and ro-vibrational excited states), and that the atomic and molecular collision kinetics are coupled by many inter-conversion processes. On the other hand, the relatively simple internal (electronic and ro-vibrational) structure of hydrogen plasma constituents provides a facilitating circumstance for theoretical and experimental studies of their collision processes. The quantitative information on the differential and integral characteristics of these processes (e.g., reaction cross sections or rate coefficients, energy, angular and quantum-state distribution of reaction products, etc) provides the key for understanding and interpretation of observed properties of hydrogen plasmas.

In the present work we shall review and present the cross section information on the collision processes taking place in hydrogen plasmas in the temperature range from 0.01 eV to several hundreds eV. This temperature range covers the typical temperature conditions of many astrophysical and laboratory plasmas, including the edge plasmas of thermonuclear fusion devices.

The collision processes that will be considered in the present work include: electron- and proton-impact excitation (electronic and vibrational) and ionization of neutral plasma particles, electron-ion (atomic and molecular) recombination, excitation and ionization, processes of formation and destruction of H^- and H_3^+ ions, and electron and heavy-particle exchange in ion-neutral particle collisions. Particular attention will be given to processes involving electronically and/or vibrationally excited states. Elastic processes between hydrogen plasma constituents are excluded from the scope of present review.

The purpose of the present work is to provide an exhaustive and critically assessed information on the cross sections of above mentioned inelastic collision processes, and to identify those processes for which such information is still not available in the literature. The physics of the considered processes will not be discussed in detail; the interested reader is directed to the various existing textbooks and specialized monographs [1–10]. The cross section information on the majority of processes considered in the present review has been subject to critical assessment in several previous publications [11–15]. The present review will make an appropriate use of these assessments, but will be more exhaustive in its scope, and will reflect the recent progress in cross section generation (see, e.g., the collections [16, 17]). Much of the previously assessed cross section information for considered processes can be accessed via Internet [18–20]. As a rule, the cross sections for considered collision processes and reactions will be presented in form of analytic fit functions, representing the original or critically assessed data with a high ($\sim 1 - 2\%$) accuracy. The analytic fit expressions have physically correct

2 Collision Processes of Hydrogen Atoms

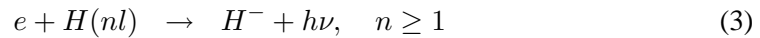
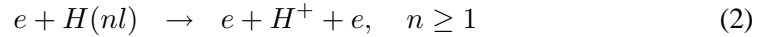
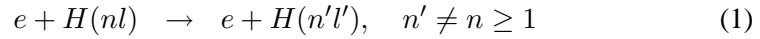
asymptotic behaviour at both low (or threshold) and high energies. Only in a limited number of cases the fits have a polynomial form, in which case the energy range of fit validity is always specified.

The organization of the present review is as follows. In Sections 2 and 3, we discuss the collision processes of H atoms and H^- ions, respectively. Sections 4 and 5 are devoted to collision processes of hydrogen molecules with electrons and protons, respectively, and in Section 6 the collision processes of H , H_2 and H^- with H_2 are considered. Sections 7 and 8 are devoted to collision processes of H_2^+ and H_3^+ , respectively, with other plasma constituents. Finally, in Section 9 some concluding remarks are given.

2 Collision Processes of Hydrogen Atoms

2.1 Electron impact processes

The inelastic electron impact processes of a hydrogen atom H , in a quantum state characterized by principal and angular momentum quantum numbers n and l , include



For most plasma applications, inclusion of the magnetic quantum number (m) in the characterization of the quantum state of a hydrogen atom is not required. Moreover, because of the energy degeneracy of angular momentum states of hydrogen atoms, l -resolved cross sections for the above reactions are required only for the lowest n -levels (e.g., $n \leq 3$), while for the higher levels ($n \geq 4$) a statistical distribution of l -populations is usually assumed. The l -mixing processes $nl \rightarrow nl'$ are usually very strong and quickly establish a statistical distribution of l -sub-states.

The processes (1) - (3) have been extensively studied in the past, but mostly for the ground ($nl = 1s$) initial state. For the $n \geq 2$ states, mainly theoretical studies of processes (1) and (2) exist. (Reaction (3) for $n \geq 2$ has not been studied so far.)

The most recent critical assessment of the cross sections for the processes (1) and (2) has been performed in Ref. [13], and it supersedes the previous assessments [11], [21]. The cross section information in the present Section is based upon that of Ref. [13].

2.1.1 Excitation

A Transitions from the ground state: $nl = 1s$

The cross sections for transitions $1s \rightarrow nl$ with $n = 2,3$ will be given for each sub-state l , while for $n \geq 4$ only the total (l -unresolved) cross section will be presented. The cross section will be given in analytic form based upon fits of best

2.1 Electron impact processes

experimental (for $1s \rightarrow 2l; 3l$ only) and theoretical data (see [13]). The analytic expression for $1s \rightarrow 2l$ cross section has the form [13], [22]

$$\sigma(1s \rightarrow 2l) = [a + b(E - \Delta E)](\times 10^{-16} \text{ cm}^2), 10.2 < E \leq 11.56 \quad (4a)$$

$$= c(\times 10^{-16} \text{ cm}^2), 11.56 \leq E \leq 12.23 \quad (4b)$$

$$= \frac{\sigma_0}{\Delta E x} \left[A_0 \ln(x) + \sum_{j=1}^5 \frac{A_j}{x^{j-1}} \right] (\times 10^{-16}), E \geq 12.23 \quad (4c)$$

where $\sigma_0 = 5.984$, $\Delta E = 10.2$ eV (the threshold energy), $x = \frac{E}{\Delta E}$, and the collision energy E is expressed in eV units. See Figure 3 on page 163. The fitting parameters a, b, c , and A_i are given in Table 1.

For transitions $1s \rightarrow 3l$ and $1s \rightarrow n (= 4, 5)$, the analytic expression for the cross section fitted to experimental (for $1s \rightarrow 3l$) and best theoretical data has the form

$$\sigma(1s \rightarrow 3l; n = 4, 5) = \frac{\sigma_0}{\Delta E x} \left(1 - \frac{1}{x} \right)^\alpha \left(A_0 \ln(x) + \sum_{j=1}^4 \frac{A_j}{x^{j-1}} \right) (\times 10^{-16} \text{ cm}^2) \quad (5)$$

where $\sigma_0 = 5.984$, ΔE is threshold energy, $x = \frac{E}{\Delta E}$, and E and ΔE are expressed in eV units. See, again, Figure 3 on page 163. The values of fitting parameters α and A_i , as well as of ΔE , for considered transitions are given in Table 2.

For the $1s \rightarrow n (\geq 6)$ transitions, a good description of the cross section is provided by the semi-empirical formula of Johnson [21], which agrees to within 5–10% with the results of Born and Born-Rudge approximations [23]. The Johnson formula (a semi-empirical modification of the Born-Bethe formula) has the form

$$\begin{aligned} \sigma(1s \rightarrow n \geq 6) &= \frac{1.76}{y_n x_n} [1 - \exp(-r_1 y_n x_n)] \times \\ &\left[A_n \left(\ln(x_n) + \frac{1}{2x_n} \right) + [B_n - A_n \ln\left(\frac{2}{y_n}\right)] \left(1 - \frac{1}{x_n} \right) \right] \\ &(\times 10^{-16} \text{ cm}^2) \end{aligned} \quad (6)$$

$$x_n = \frac{E}{\Delta E_n}, \quad y_n = 1 - \frac{1}{n^2}, \quad A_n = 2f_{1n}/y_n, \quad r_1 = 0.45 \quad (7a)$$

$$B_n = \frac{4}{n^3 y_n^2} \left(1 + \frac{4}{3y_n} - \frac{0.603}{y_n^2} \right) \quad (7b)$$

where $\Delta E_n = 13.6(1 - 1/n^2)$ (eV) is the threshold energy, f_{1n} is the oscillator strength for $1s \rightarrow n$ transition, and collision energy E is expressed in eV units. The analytic expression for f_{1n} can be found elsewhere [4, 13, 21], and is given by Eqs. (11-13) below.

The accuracy of the presented cross sections is:

for $1s \rightarrow n (\leq 4)$: 10 – 20% for $E \leq 80$ eV and 10% for $E > 80$ eV;

for $1s \rightarrow n (\geq 5)$: 15 – 30% for $E \leq 80$ eV and 15 – 20% for $E > 80$ eV.

2 Collision Processes of Hydrogen Atoms

B Transitions between excited states: $n \rightarrow m$

The electron-impact induced transitions between excited states of H have been less studied than those from the ground state. The transition between $2s$ and $2p$ states has been treated by the perturbation theory [24] and the cross section is obtained in analytic form (see also [11])

$$\sigma(2s \rightarrow 2p) = \frac{8.617}{E} \ln(1.14 \times 10^4 E) (\times 10^{-15} \text{cm}^2), \quad (8)$$

where the electron impact energy E is expressed in eV.

Extensive close-coupling cross section calculations, however, do exist for the $2l \rightarrow 3l'$ transitions [25–27], complemented with unitarized Born calculations [28]. The total cross section for $n = 2 \rightarrow n = 3$ transitions resulting from these calculations can be represented by an analytic expression identical to Eq. (5) with the fitting parameters [13]

$$\alpha = 1.3196, A_0 = 38.906, A_1 = 5.2373, A_2 = 119.25, \\ A_3 = -595.39, A_4 = 816.71.$$

For other $n \rightarrow m$ transitions ($n \geq 2, m \geq 4$), the semi-empirical formula of Johnson [21] can be used to estimate the cross section. The results of this formula are consistent with the results of normalized Born approximation.

The Johnson formula for $n \rightarrow m$ transitions has the form [21]

$$\sigma(n \rightarrow m) = \frac{1.76n^2}{y_{nm}x_{nm}} [1 - \exp(-r_n y_{nm} x_{nm})] \times \quad (9) \\ \times \left[A_{nm} \left(\ln(x_{nm}) + \frac{1}{2x_{nm}} \right) + \left(B_{nm} - A_{nm} \ln \left(\frac{2n^2}{y_{nm}} \right) \right) \left(1 - \frac{1}{x_{nm}} \right) \right] \\ (\times 10^{-16} \text{cm}^2)$$

$$x_{nm} = \frac{E}{\Delta E_{nm}}, \Delta E_{nm} = 13.6 \left(\frac{1}{n^2} - \frac{1}{m^2} \right), y_{nm} = 1 - \left(\frac{n}{m} \right)^2, r_n = \frac{1.94}{n^{1.57}} \quad (10a)$$

$$A_{nm} = \frac{2n^2 f_{nm}}{y_{nm}}, \quad B_{nm} = \frac{4n^4}{m^3 y_{nm}^2} \left(1 + \frac{4}{3y_{nm}} + \frac{b_n}{y_{nm}^2} \right), \quad (10b)$$

$$b_n = \frac{1}{n} \left(4.0 - \frac{18.63}{n} + \frac{36.24}{n^2} - \frac{28.09}{n^3} \right) \quad (10c)$$

where f_{nm} is the oscillator strength for $n \rightarrow m$ transition, and E is expressed in eV units.

The oscillator strength f_{nm} has the form [21]

$$f_{nm} = \frac{32}{3\sqrt{3}\pi} \frac{n}{m^3} \frac{1}{y_{nm}^3} g(n, y_{nm}) \quad (11)$$

2.1 Electron impact processes

$$g(n, y_{nm}) = g_0(n) + g_1(n) \frac{1}{y_{nm}} + g_2(n) \frac{1}{y_{nm}^2} \quad (12)$$

where the coefficients $g_j(n)$ have the values

$$g_0(1) = 1.1330, g_1(1) = -0.4059, g_2(1) = 0.0714 \quad (13a)$$

$$g_0(2) = 1.0785, g_1(2) = -0.2319, g_3(2) = 0.0295 \quad (13b)$$

and for $n \geq 3$ they are given by

$$g_0(n) = 0.9935 + \frac{0.2328}{n} - \frac{0.1296}{n^2} \quad (13c)$$

$$g_1(n) = -\frac{1}{n} \left(0.6282 - \frac{0.5598}{n} + \frac{0.5299}{n^2} \right) \quad (13d)$$

$$g_2(n) = \frac{1}{n^2} \left(0.3887 - \frac{1.181}{n} + \frac{1.470}{n^2} \right) \quad (13e)$$

We note that semi-empirical expressions for the $n \rightarrow m$ ($n \geq 1, m \geq n$) excitation cross section are available also in Ref. [29], but their accuracy is somewhat lower than that of Johnson's formula [8]. The accuracy of the above cross sections is:

for $n = 2 \rightarrow n = 3$: 10 – 30% for $E \leq 80$ eV and 10% for $E > 80$ eV;

for $n \rightarrow m$ ($n \geq 3$): 20 – 50% for $E \leq 80\Delta E_{nm}$ and 10 – 20% for $E > 80\Delta E_{nm}$.

See Figure 4 on page 163 for some selected transition cross sections.

2.1.2 Ionization

A Ionization of the ground- and $n = 2, 3$ excited states

Accurate ionization cross section measurement exist only for the ground ($1s$) [30] and metastable ($2s$) [31, 32] excited state. Theoretical cross section calculations for ionization from $1s, 2l$ and $3l$ states have been performed in the first Born approximation [33–35]. The recommended cross sections in Ref. [13] for ionization of $1s, 2l$ and $3l$ states have been based upon the above sets of data and fitted to the analytic expression (see Figure 5 on page 164)

$$\sigma_{ion} = \frac{10^{-13}}{I_n E} \left[A_0 \ln(E/I_n) + \sum_{j=1}^5 A_j \left(1 - \frac{I_n}{E} \right)^j \right] (cm^2) \quad (14)$$

where I_n is the ionization potential (in eV units) of level n , $I_n = 13.6/n^2$, and E is the collision energy (in eV). The fitting parameters A_i are given in Table 3. The fits represent the recommended data with an r.m.s of 1 – 2%, or better. The estimated accuracy of the data represented by the fits is: 10% for $1s$ state in the entire energy region, for $n = 2$ states it is 10 – 30% for $E \leq 40$ eV and 10% for $E > 40$ eV, and for $n = 3$ it is 15 – 30% for $E \leq 30$ eV and 10% for $E > 30$ eV. For $n = 2, 3$, the uncertainty may be somewhat higher ($\sim 40\%$) in the near-threshold region.

2 Collision Processes of Hydrogen Atoms

B Ionization of $n \geq 4$ states

Ionization cross sections for $n \geq 4$ states are available from the first Born [34] and orthogonalized Born-Oppenheimer approximation [36]. The Born-Bethe-based semi-empirical formula of Johnson [21] gives results which agree within 5 – 10% with the results of first Born approximation [34] for energies $E \gtrsim 15I_n$ ($I_n = 13.6/n^2$ eV), while for $5I_n \lesssim E \lesssim 15I_n$ they are consistent with the results of Born-Oppenheimer approximation [36] within 10 – 30%. Only for $E < 5I_n$ ($\lesssim 5$ eV for $n \geq 4$) the uncertainty of Johnson's formula becomes larger. The Johnson formula for ionization of a level with principal quantum number n has the form [21]

$$\sigma_{ion}(n) = \frac{1.76n^2}{x_n} [1 - \exp(-r_n x_n)] \quad (15)$$

$$\times \left[A_n^{ion} \ln(x_n) + (B_n^{ion} - A_n^{ion} \ln(2n^2)) \left(1 - \frac{1}{x_n}\right)^2 \right] (\times 10^{-16} \text{ cm}^2)$$

$$A_n^{ion} = \frac{32n}{3\sqrt{3}\pi} \sum_{j=0}^2 \frac{g_j(n)}{j+3}, \quad r_n = 1.94/n^{1.57}, \quad x_n = E/I_n, \quad I_n = 13.6/n^2 \quad (16a)$$

$$B_n^{ion} = \frac{2}{3}n^2(5 + b_n), \quad b_n = \frac{1}{n} \left(4.0 - \frac{18.63}{n} + \frac{36.24}{n^2} - \frac{28.09}{n^3} \right). \quad (16b)$$

and the coefficients $g_j(n)$ are given by Eqs. (13).

We note that for the high- n states, the classical impulse (“binary encounter”) approximation should also give good ionization cross section estimates. The ionization cross section in this approximation has very simple form [29]

$$\sigma_{ion}^{BEA}(n) = \frac{5.886n^4}{x_n + 3.25} \left(1 - \frac{3}{5x_n} - \frac{2}{5x_n^2} \right) (\times 10^{-16} \text{ cm}^2) \quad (17)$$

where $x_n = E(\text{eV})/I_n(\text{eV})$.

2.1.3 Radiative electron attachment

The radiative attachment of electrons on $H(n)$, Eq. (3), has been studied only when the hydrogen atom is in its ground state ($n = 1$). The H^- ion formation by this process takes place at very low collision energies (electron affinity of H is 0.754 eV) and its cross section is rather small [37, 38]. Formation of H^- by other processes (e.g., by dissociative electron attachment on $H_2(v \geq 4)$; see subsection 4.1.4) is much more effective than by the radiative attachment process. The cross section for radiative electron attachment on $H(1s)$ can be represented by the following analytic expression [38]

$$\sigma_{att}^{rad}(H^-) = 1.971 \frac{E^{1/2}}{E_b + E} (\times 10^{-18} \text{ cm}^2) \quad (18)$$

2.1 Electron impact processes

where $E_b = 0.754$ eV and the collision energy E is expressed in eV (see Figure 6 on page 164). The radiative attachment rate coefficient (Maxwellian electron energy distribution) $\alpha_{att}^{rad} = \langle \sigma_{att}^{rad} v \rangle$ can be calculated in closed analytic form [38],

$$\alpha_{att}^{rad}(H^-) = 1.17 \left[2\pi^{1/2} \beta^{3/2} e^\beta + 1 - 2\beta {}_1F_1 \left(1, \frac{1}{2}; \beta \right) \right] (\times 10^{-10} cm^3/s) \quad (19)$$

where $\beta = E_b/T$ and ${}_1F_1(a, b; z)$ is the confluent hypergeometric function. For $\beta \gg 1$ and $\beta \ll 1$, the expression in square brackets in Eq. (19) tends to $3/(2\beta)$ and $(1 - 2\beta)$, respectively, i.e., when $T \rightarrow \infty$ then $\alpha_{att}^{rad}(H^-)$ tends to a finite value of $1.17 \times 10^{-10} cm^3/s$.

2.1.4 $H(n \geq 1)$ formation in electron-proton collisions

In order to complete the collisional scheme of electron impact processes involving $H(n)$ atoms, the formation of these atoms by radiative and three-body electron-proton recombination needs to be considered.

A Radiative recombination

The radiative recombination process



is inverse to the exhaustively studied photo-ionization process (see, e.g., [39]). The Maxwellian rate coefficient for radiative electron capture to $nl = 1s, 2s$ and $2p$ states is given by [11, 39]

$$\alpha_{rec}^{rad}(nl) = A_{nl} \left(\frac{I_n}{Ry} \right)^{1/2} \frac{\beta_n^{3/2}}{\beta_n + \chi_{nl}} (\times 10^{-14} cm^3/s) \quad (21)$$

where $I_n = 13.6/n^2$ eV is the ionization potential, $Ry = 13.60$ eV is the Rydberg constant, $\beta_n = I_n/T$, T is the temperature (expressed in eV) and the values of constants A_{nl} and χ_{nl} are

$$\begin{aligned} A_{1s} &= 3.92, & A_{2s} &= 2.47, & A_{2p} &= 6.22 \\ \chi_{1s} &= 0.35, & \chi_{2s} &= 0.12, & \chi_{2p} &= 0.61 \end{aligned}$$

For capture to $n \geq 3$ levels, $\alpha_{rec}^{rad}(n)$ can well be represented by the Kramers approximation

$$\alpha_{rec}^{rad}(n \geq 3) = 5.201 \beta_n^{3/2} E_1(\beta_n) \exp(\beta_n) (\times 10^{-14} cm^3/s) \quad (22)$$

where $E_1(\beta)$ is the exponential integral. For some selected nl states these rate coefficients are shown in Figure 7 on page 165. Accurate expansions for $\exp(\beta)$,

2 Collision Processes of Hydrogen Atoms

$E_1(\beta)$ can be found in [40]. When the states $2s$ and $2p$ are not treated separately, an alternative expression for $\alpha_{rec}^{rad}(n)$ is given by Johnson [21]

$$\alpha_{rec}^{rad,J}(n \geq 1) = 5.197 \exp(\beta_n) \sum_{j=0}^2 g_j(n) E_{j+1}(\beta_n) (\times 10^{-14} \text{cm}^3/\text{s}) \quad (23)$$

where, as before, $\beta_n = I_n/T$, $E_j(z)$ is the Schlömilch exponential integral, and $g_j(n)$ are the Gaunt factor coefficients, given by Eqs. (13).

As seen from Eqs. (21) and (22), $\alpha_{rec}^{rad}(n)$ decreases with increasing n and T . Only for $T \leq 2$ eV, $\alpha_{rec}^{rad}(1s)$ becomes larger than $10^{-13} \text{cm}^3/\text{s}$.

B Three-body recombination

The three-body recombination process



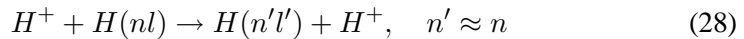
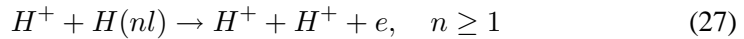
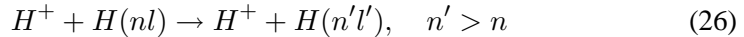
is inverse to electron-impact ionization of $H(n)$ and its rate coefficients for Maxwellian electron and proton energy distributions can be derived from the corresponding ionization rate coefficient $\alpha_{ion}(nl)$ by applying the detailed balance principle [4].

$$\alpha_{rec}^{3b}(n) = n^2 a_0^3 \left(\frac{\pi R y}{T} \right)^{3/2} \exp(\beta_n) \alpha_{ion}(n) \quad (25)$$

where $a_0 (= 0.529 \cdot 10^{-8} \text{cm})$ is the Bohr radius, T is expressed in eV and, as before, $\beta_n = I_n/T$. We note that $\alpha_{rec}^{3b} = \langle \langle \sigma_{rec}^{3b} v_1 v_2 \rangle \rangle$ is a double Maxwellian average of σ_{rec}^{3b} , (v_1, v_2 are the velocities of two continuum electrons). We further note that the units of σ_{rec}^{3b} are $\text{cm}^4 \cdot \text{s}$, and consequently those of α_{rec}^{3b} are cm^6/s . It follows from Eq. (25) that in three-body recombination the electron is predominantly captured into high- n states, where it becomes subject to a diffusion process in the n -space described by the Fokker-Planck equation [41]. The approximate solution leads to a $T^{-9/2}$ dependence of the total α_{rec}^{3b} . The three-body recombination process is effective only at high plasma densities. It should be mentioned that protons (or any other neutral or charged heavy particle M) may also ‘‘catalyze’’ the three-body recombination ($e + H^+ + M \rightarrow H(n) + M$), but the corresponding rate coefficients are two or more orders of magnitude smaller than that given by Eq. (25).

2.2 Proton impact processes

The most important collision processes of H^+ with $H(n)$ are



In the context of low temperature plasmas, the excitation and ionization processes (26) and (27) are important only when n is relatively high. The charge exchange

process (28), however, is an important process for all n . The l -mixing processes $nl \rightarrow nl'$ in (26) are usually very strong, and we shall assume that they quickly establish a statistical distribution of the l -sub-states. In the context of an energetic neutral hydrogen beam interaction with plasmas (for heating or diagnostic purposes), the proton-impact excitation and ionization processes become important also for all n -states.

2.2.1 Excitation

A Transitions from the ground state: $nl = 1s$

The cross section for the proton-impact $1s \rightarrow 2s$ transition has been measured in the energy range 5–26 keV/amu (amu = atomic mass unit) [42,43], and it has been theoretically calculated by a variety of highly accurate methods at low [44–50], intermediate [48–50] and high [14, 15, 51] energies. In the overlapping energy regions the experimental and theoretical results agree (10 – 20%) with each other. For the cross section of the $1s \rightarrow 2p$ transition, experimental data are available from 0.6 keV/amu to 700 keV/amu [42, 54–56] that are, again, in fair (10 – 20%) agreement with each other and with theoretical calculations [45–53]. The total $1s \rightarrow (n = 2)$ relative excitation cross section has also been measured [57] in the energy range 16 – 200 keV/amu, and, when normalized to highly accurate theoretical data of Ref. [58] at $E = 200$ keV/amu, it agrees with other theoretical data [48–50, 59] to within 10 – 15%. It also extends smoothly to the first Born approximation results [53].

A critical assessment of available cross section data for $1s \rightarrow 2s$ and $1s \rightarrow 2p$ transitions has been performed in Ref. [13] and the recommended cross section has been presented by the analytic expressions

$$\sigma(1s \rightarrow 2s) = a_1 \left[\frac{a_2 e^{-a_3 E}}{E^{a_4}} + \frac{a_5 e^{-a_6/E}}{1 + a_7 E^{a_8}} + \frac{e^{-a_9/E}}{E} \right] (\times 10^{-16} \text{ cm}^2) \quad (29a)$$

$$\sigma(1s \rightarrow 2p) = a_1 \left[\frac{a_2 e^{-a_3 E}}{E^{a_4}} + \frac{a_5 e^{-a_6/E}}{1 + a_7 E^{a_8}} + \frac{e^{-a_9/E} \ln(1 + a_{10} E)}{E} \right] (\times 10^{-16} \text{ cm}^2) \quad (29b)$$

where E is the laboratory energy of the proton and it is expressed in keV/amu. The fitting parameters a_i are given in Table 4. See Figure 8 on page 165. The total $1s \rightarrow (n = 2)$ excitation cross section can also be represented by Eq. (29b); the values of corresponding parameters a_i are also given in Table 4. While the uncertainty of cross sections represented by Eqs. (29) for energies below ~ 0.5 keV/amu can be of the order of a factor two, for energies above ~ 1 keV it is in the range 10 – 20%, with the 10% figure typical for the energies above 100 keV/amu.

Total relative cross section measurements for $1s \rightarrow n = 3, 4$ transitions are available in the energy range 16 – 200 keV/amu [57], while absolute cross section measurements have been reported for $1s \rightarrow np$, ($n = 3, 4, 5, 6$) transitions in

2 Collision Processes of Hydrogen Atoms

the range $\sim 20 - 700$ keV/amu [56]. For the total $1s \rightarrow n = 3, 4$ excitation cross sections accurate calculations have been performed by the advanced adiabatic method [46], the two-center atomic-orbital close-coupling method [59] and by the first Born approximation [53]. For the $1s \rightarrow n = 3$ transition accurate theoretical cross section data are also available from [48, 58, 60]. For the $1s \rightarrow n = 4 - 6$ transitions, apart from the experimental $1s \rightarrow 5p, 6p$ cross sections [18] also theoretical cross sections are available from the first Born approximation [53]. The critical assessment of the published $1s \rightarrow n = 3-6$ excitation cross section data in Ref. [13] has resulted in a set of recommended cross sections for these transitions that can be represented by the analytic expression

$$\sigma_{exc}(1s \rightarrow n = 3-6) = b_1 \left[\frac{b_2 e^{-b_3 E}}{E^{b_4} + b_5 E^{b_6}} + \frac{e^{-b_7/E} \ln(1 + b_8 E)}{E} \right] (\times 10^{-16} \text{cm}^2) \quad (30)$$

where E is expressed in keV/amu and the values of the fitting parameters b_i are given in Table 5. See, again, Figure 8 on page 165. The accuracy of the cross sections $\sigma_{exc}(1s \rightarrow n = 3-6)$ represented by Eq. (30) is similar to that of $\sigma_{exc}(1s \rightarrow n = 2)$.

For the transitions $\sigma_{exc}(1s \rightarrow n \geq 7)$, the excitation cross sections can be obtained from $\sigma_{exc}(1s \rightarrow n = 6)$ by using the scaling relation

$$\sigma_{exc}(1s \rightarrow n \geq 7) = \left(\frac{6}{n}\right)^3 \sigma_{exc}(1s \rightarrow n = 6) \quad (31)$$

B Transitions between excited states: $n \rightarrow m$

There are no experimental cross section measurements for $n \rightarrow m$, ($n \geq 2, m > n$) proton-impact excitation transitions. Cross section calculations for $n = 2 \rightarrow m = 3, 4, 5$ transitions have been performed by the advanced adiabatic method (AAM) [46] ($E \leq 30$ keV/amu), by the atomic-orbital close-coupling (AO-CC) method using a large expansion basis [59] (20 – 200 keV/amu), and by the symmetrized eikonal (SE) method [59] (2 keV/amu – 10 MeV/amu). For the $n = 3 \rightarrow m = 4$ transition cross section calculations have been performed by the AAM [46] and AO-CC method [59], while for $n = 3 \rightarrow m = 3, 4, 5$ transitions such calculations have also been carried out by the SE method [46]. The critical analysis of these cross sections performed in Ref. [13], together with the general Lodge formula for $n \rightarrow m$ transitions [61] (see below), has led to the following analytic fit expressions for $n = 2 \rightarrow m$ cross sections:

$$\sigma_{exc}(2 \rightarrow 3, 4, 5) = c_1 \left[\frac{c_2 e^{-c_3 E}}{E^{c_4}} + \frac{e^{-c_5/E} \ln(1 + c_6 E)}{E} \right] (\times 10^{-16} \text{cm}^2), \quad (32)$$

$$\sigma_{exc}(2 \rightarrow n) = A_n^{(2)} \sigma_{exc}(2 \rightarrow 5), \quad n = 6, 7, 8, 9, 10, \quad (33)$$

$$\sigma_{exc}(2 \rightarrow n \geq 11) = \left(\frac{10}{n}\right)^3 \sigma_{exc}(2 \rightarrow 10), \quad (34)$$

2.2 Proton impact processes

where the fitting parameters c_i in Eq. (32) are given in Table 6, the coefficients $A_n^{(2)}$ in Eq. (33) have the values

$$A_6^{(2)} = 0.4610, A_7^{(2)} = 0.2475, A_8^{(2)} = 0.1465, A_9^{(2)} = 0.0920, A_{10}^{(2)} = 0.0605$$

and the proton energy E in Eq. (32) is expressed in keV/amu (i.e.: amu=1 here). Cross sections for the $2 \rightarrow 3, 4$ transitions are shown in Figure 9 on page 166.

A similar analysis of the cross sections for $n = 3 \rightarrow m$ transitions has resulted in the following analytic expressions:

$$\sigma_{exc}(3 \rightarrow 4, 5, 6) = F(c_i, E), \quad i = 1 - 6 \quad (35)$$

$$\sigma_{exc}(3 \rightarrow n) = B_n^{(3)} \sigma_{exc}(3 \rightarrow 6), \quad n = 7, 8, 9, 10, \quad (36)$$

$$\sigma_{exc}(3 \rightarrow n \geq 11) = \left(\frac{10}{n}\right)^3 \sigma_{exc}(3 \rightarrow 10), \quad (37)$$

where $F(c_i, E)$ in Eq. (35) has the same form as the function on the right-hand-side of Eq. (32), with the fitting parameters given in Table 7, and the proton energy E expressed in keV/amu, and the coefficients $B_n^{(3)}$ in Eq. (36) have the values

$$B_7^{(3)} = 0.4670, B_8^{(3)} = 0.2545, B_9^{(3)} = 0.1540, B_{10}^{(3)} = 0.1000$$

The cross section for the $3 \rightarrow 4$ transition is included in Figure 9 on page 166. For the transitions $n \rightarrow m$, with $n \geq 4$, the Lodge-Percival-Richards (LPR) cross section formula [61] can be used. This formula has been obtained by combining the result of various low-and high-energy theoretical approximations. The LPR- (or, for brevity, the Lodge-) formula has the form ($m > n$):

$$\sigma_{exc}(n \rightarrow m) = \frac{0.88n^4}{\epsilon} [ADL + FGH] (\times 10^{-16} \text{ cm}^2) \quad (38)$$

$$\epsilon = \frac{E(\text{keV/amu})}{25}, \quad s = m - n, \quad D = \exp[-1/(nm\epsilon^2)] \quad (39a)$$

$$A = \frac{8}{3s} \left(\frac{m}{sn}\right)^3 \left(0.184 - \frac{0.04}{s^{2/3}}\right) \left(1 - \frac{0.2s}{nm}\right)^{1+2s}, \quad G = \frac{1}{2} \left(\frac{n^2\epsilon}{m - 1/m}\right)^3 \quad (39b)$$

$$L = \ln \left[\frac{1 + 0.53\epsilon^2 n(m - 2/m)}{1 + 0.4\epsilon} \right], \quad F = [1 - 0.3sD/(nm)]^{1+2s} \quad (39c)$$

$$H = [C_2(z_-, y) - C_2(z_+, y)], \quad C_2(z, y) = \frac{z^2 \ln(1 + 2z/3)}{2y + (3z/2)} \quad (39d)$$

$$z_{\pm} = 2 \left\{ \epsilon n^2 \left[(2 - n^2/m^2)^{1/2} \pm 1 \right] \right\}^{-1}, \quad y = [1 - D \ln(18s)/(4s)]^{-1} \quad (39e)$$

Note that the proton energy E in Eq. (39a) is expressed in units of keV/amu (here: amu=1). The accuracy of the cross section (38) for $s = m - n \leq 6$ is 20 – 25%

2 Collision Processes of Hydrogen Atoms

for energies above the cross section maximum, and 20 – 40% below the energy at which the cross section maximum occurs. For $s \geq 7$, the uncertainty progressively increases. Generally, the validity of the cross section (38) is restricted to $\epsilon \gtrsim (2/n)^2$. As is well known, the heavy-particle inelastic cross sections in the low-energy region ($\epsilon \ll 1$) decrease exponentially with decreasing collision energy, which is reflected in Eq. (38) by the factor D .

2.2.2 Ionization

Experimental cross section measurements for $H^+ + H(n)$ are available only for $n = 1$ in the collision energy range $\sim 10\text{keV} - 1.5\text{MeV}$ [62]. Accurate theoretical cross section calculations for proton-impact ionization of $H(1s)$ are available at low [46, 63], intermediate to high [45, 48, 58] and high [64] energies. In the energy region of validity of the applied theoretical methods the results of the calculations agree well with experimental data. Theoretical cross section calculations also exist for $H(n = 2)$ and $H(n = 3)$ [46, 64, 65], covering the energy range from 0.2 keV/amu to ~ 1 MeV/amu. The classical trajectory Monte Carlo (CTMC) calculations, performed in Ref. [65] also for higher n , demonstrate the n -scaling of the ionization cross section for $n \geq 3$.

The recommended ionization cross sections in $H^+ + H(n)$ collisions derived in Ref. [13] on the basis of a critical assessment of available data can all be represented by the analytic expression

$$\sigma_{ion}(n) = b_1 n^4 \left[\frac{\tilde{E}^{b_2} \exp(-b_3 \tilde{E})}{1 + b_4 \tilde{E}^{b_5}} + \frac{b_6 \exp(-b_7/\tilde{E}) \ln(1 + b_8 \tilde{E})}{\tilde{E}} \right] (\times 10^{-16} \text{cm}^2) \quad (40)$$

where \tilde{E} is the reduced energy

$$\tilde{E} = n^2 E \text{ (keV/amu)} \quad (41)$$

The values of fit parameters b_i are given in Table 8. See Figure 10 on page 166. As observed from Eq. (40), the ionization cross sections for $n \geq 3$ allow a scaling: $\tilde{\sigma}_{ion} = \sigma_{ion}(n)/n^4 = f(\tilde{E})$. While for $n \leq 3$ the proton-impact ionization cross sections are small in the energy region below ~ 100 eV, already for $n \geq 5$ they attain values $\gtrsim 10^{-15} \text{cm}^2$ at $E \simeq 100$ eV. The accuracy of cross sections given by Eq. (40) in the region $\tilde{E} < 0.1$ is difficult to estimate. For $\tilde{E} \gtrsim 1$ it is on the level of 20 – 30%, and better for $n = 1, 2$.

For the states with high n , cross section estimates can also be obtained from the analytic expression for $\sigma_{ion}(n)$ provided by the classical impulse approximation (BEA) [11, 29].

$$\sigma_{ion}^{BEA}(n) = 0, \quad \epsilon < 0.207 \quad (42a)$$

$$= 0.5867n^4 \left[\epsilon - \frac{0.164}{\epsilon^2} + \frac{0.1875}{\epsilon^2(1+\epsilon)} \right] (\times 10^{-16} \text{cm}^2), \quad 0.207 < \epsilon \leq 1.207 \quad (42b)$$

$$= \frac{1.467n^4}{\epsilon^2} \left(1 - \frac{0.15}{\epsilon^2 - 1} \right) (\times 10^{-16} \text{cm}^2), \quad \epsilon > 1.207, \quad (42c)$$

where

$$\epsilon^2 = n^2 E(\text{keV}/\text{amu})/25 \quad (43)$$

2.2.3 Charge transfer

The charge transfer reaction in $H^+ + H(n)$ collisions is characterized by large cross sections ($\sigma_{cx} \sim n^4 10^{-16} \text{cm}^2$) in the low-keV and eV regions, and is one of the most important heavy-particle collision processes in low-temperature plasmas. This reaction has been extensively studied both experimentally (for $n = 1$) [66–71] and theoretically (for various $n \geq 1$) (see [13] for references). For $n \lesssim 3$, dominant contribution to total charge transfer cross section at low energies gives the electron capture to final n' levels with $n' = n$ (resonant electron capture). For $n \gtrsim 3$, however, electron capture at low collision energies is also efficient to a group of n' levels around $n' = n$. The critical analysis of available theoretical and experimental (for $n = 1$) cross section information for $H^+ + H(n)$ charge collisions, performed in Ref. [13], has led to the following analytic fit expression to the best cross section data

$$\sigma_{cx}(n) = \frac{A_1 n^4 \ln(A_2/\tilde{E} + A_3)}{1 + A_4 \tilde{E} + A_5 \tilde{E}^{3.5} + A_6 \tilde{E}^{5.4}} (\times 10^{-16} \text{cm}^2) \quad (44)$$

where $\tilde{E} = n^2 E$ (keV/amu), see Figure 11 on page 167. The validity of this analytic fit of the cross sections extends over the energy range from sub-eV to several MeV. The values of fitting parameters A_i in Eq. (44) for $n = 1, 2, 3$ are given in Table 9. We note that the cross sections for $n \geq 4$ can be scaled: $\tilde{\sigma}_{cx} = \sigma_{cx}(n \geq 4)/n^4 = f(\tilde{E})$. We also note that the coefficients A_5 and A_6 for $n = 2, 3$ and $n \geq 4$ have the same values. The cross section (44) for $n = 2$ and $n \geq 3$ was based upon the quantal calculations [72, 73] at low energies, CTMC calculations [65] in the intermediate energy range, and the symmetrized eikonal method [74] at high energies. The high-energy behaviour of $\sigma_{cx}(1s)$ was determined from the second-order quantal calculations [75, 76]. The estimated accuracy of $\sigma_{cx}(n)$ cross sections for $n \geq 2$ is about 20 – 50% for $\tilde{E} \lesssim 1$, and 10 – 20% for $\tilde{E} > 1$. The fit for $\sigma_{cx}(n = 1)$ was based upon accurate experimental and theoretical data and its accuracy is 10 – 20% in the entire energy region (from ~ 0.1 eV up to 2 MeV) considered.

For $\tilde{E} < 10$ keV/amu, $\sigma_{cx}(n \geq 2)$ can also be estimated from the cross section expression resulting from the over-barrier transition model (OBM) for the process [5, 11, 77]

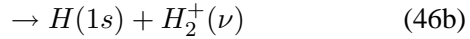
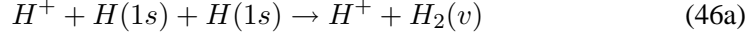
$$\sigma_{cx}^{OBM}(n \geq 2) = \frac{1.584 n^4}{1 + 0.42 \tilde{E}^{0.2} + 0.52 \tilde{E}^{0.5}} (\times 10^{-15} \text{cm}^2) \quad (45)$$

with $\tilde{E} = n^2 E$ (keV/amu).

2 Collision Processes of Hydrogen Atoms

2.2.4 Three-body diatomic association

In low-temperature, high-neutral-density hydrogen plasmas, the diatomic association in three body collisions



may also be important processes. The higher vibrational states (v) of $H_2(v)$ and $H_2^+(v)$ are preferentially populated in these reactions. Reactions (46a) and (46b) have recently been theoretically studied within the close-coupling approach of the "infinite order sudden approximation" (IOSA) with inclusion of all discrete vibrational states and a large number of discretized continuum states [78]. The total rate coefficients (summed over final v -states) of reactions (46a) and (46b) in the temperature region up to $\sim 3 \times 10^4$ K can be represented by analytic fits

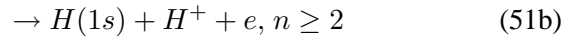
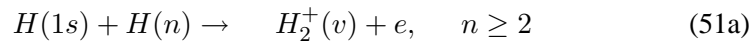
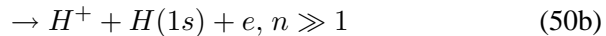
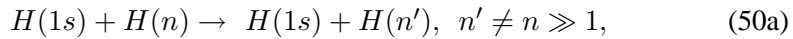
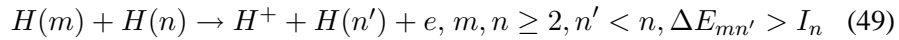
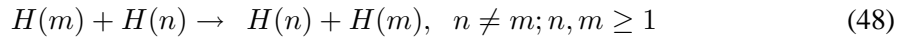
$$K_{3b}(H_2) = \frac{1.145}{T^{1.12}} (\times 10^{-29} \text{ cm}^6 / \text{s}) \quad (47a)$$

$$K_{3b}(H_2^+) = \frac{1.238}{T^{1.046}} (\times 10^{-29} \text{ cm}^6 / \text{s}) \quad (47b)$$

where T is expressed in Kelvin. The three-body association reactions of the type (46), with one of the neutral atoms in an excited state, have not been studied so far, but their rate coefficients can be expected to be much higher than those given by Eqs. (47).

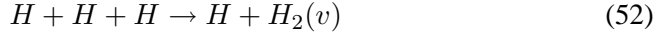
2.3 Atom-atom collision processes

The collision processes between hydrogen atoms in the low-energy region have cross sections comparable to those involving electrons and protons only when (at least) one of the neutral atoms is in an excited state. Among these processes the most important are:



2.3 Atom-atom collision processes

where $\Delta E_{n'n}$ is the $(n - n')$ energy level difference, and I_n is the ionization potential of level n . The ionization processes (49), (50b) and (51b) are governed by different dynamic mechanisms and have different cross section characteristics. When the neutral particle density in a low-temperature hydrogen plasma is high, the three-body diatomic association



may also be an important process.

2.3.1 Excitation transfer, Penning ionization and spin exchange

Resonant excitation transfer reaction (48) can proceed via two mechanisms: by a dipole allowed $m \rightarrow n$ (and, simultaneous $n \rightarrow m$) transition (or virtual emission and absorption of an optical photon), and by two-electron exchange interaction (simultaneous exchange of m - and n -state electrons from one to the other atom). These processes have been theoretically extensively studied in past [5, 6]. Generally, the cross section of dipole assisted resonant excitation transfer process is significantly larger than that due to a two-electron transfer. Its cross section for $m = 1s$ and $n = np$ states has the form [79, 80]

$$\sigma_{ex,tr} = \frac{3.145}{E^{1/2}} |d_{sp}|^2 (\times 10^{-14} cm^2) \quad (53a)$$

$$|d_{sp}|^2 = \frac{1}{3} \frac{2^8 n^7 (n-1)^{2n-5}}{(n+1)^{2n+5}} \quad (53b)$$

where d_{sp} is the $1s \rightarrow np$ dipole matrix element, and the relative collision energy E is expressed in eV units (see Figure 12 on page 167). The cross section for two-electron resonant excitation-process can be calculated by the methods described in [5].

The Penning ionization process (49) takes place when m is a metastable state (e.g., $m = 2s$) and the transition energy ΔE_{mn} is larger than the ionization potential I_n . This is, generally, an important process in low-temperature plasmas, and the specific reaction (49) has been subject to several studies (see e.g., [5], [81]). In the case of hydrogen atom, however, the strong l -mixing within a given n level, makes this process rather ineffective.

With the excitation transfer process, the process of spin exchange may be associated. The two processes are related to each other, and the cross section for spin exchange is [5, 80]

$$\sigma_{sp,ex} = \frac{1}{2} \sigma_{ex,tr} . \quad (54)$$

2.3.2 Excitation (de-excitation) and ionization of Rydberg atoms

An internal energy conversion model for excitation (de-excitation) and ionization processes (50) in atom-Rydberg atom slow collisions has been developed in [82].

2 Collision Processes of Hydrogen Atoms

The model relates the transitions of Rydberg electron with the electron capture dynamics of inner electron in the $H(1s) + H^+$ system, the motion of two electrons being coupled by a (long-distant) dipole interaction. The model also allows to describe the associative ionization process (51a), when $n \gg 1$.

A semi-quantal model for excitation and ionization in atom-Rydberg atom collisions has also been developed in [83]. The application of these models to $H + H(n \gg 1)$ collisions has been, however, rather limited.

2.3.3 Associative and non-associative ionization

The associative ionization process (51a) has been experimentally and theoretically studied for $n = 2s, 3s, 4s$ [84–86]. The cross section for $n = 2s$ is peaked at $E_m \simeq 3.25$ eV, with a peak value of $\simeq 2.5 \times 10^{-17} \text{ cm}^2$, and rapidly decreases with varying E on both sides of E_m . However, the cross sections for $n = 3s$ and $4s$ are large ($\gtrsim 10^{-16} \text{ cm}^2$) for $E \lesssim 1$ eV, and decrease rapidly for $E \gtrsim 2 - 3$ eV (due to the competing non-associative, Penning ionization). The mechanism of associative ionization in $H(1s) + H(ns)$ slow collisions is the formation of doubly excited $(2p\sigma_u)^2$ intermediary state during the course of collision and its auto-ionization at small internuclear distances. Due to multiplicity of reaction paths for formation of this intermediary state, the associative ionization cross sections in the region $\sim 0.1 - 1.5$ eV show pronounced oscillations. A manifestation of the $(2p\sigma_u)^2$ formation and decay mechanism for the associative ionization process is the E^{-1} dependence of its cross section (for $n \geq 3$) for $E \lesssim 0.1$ eV. By averaging the oscillations in the region $\sim 0.1 - 1.0$ eV, the associative ionization cross sections for $n = 3s, 4s$ of Refs. [85, 86] can be represented in scaled form

$$\sigma_{AI}(ns) = \frac{2.96n^4}{E} (\times 10^{-19} \text{ cm}^2), \quad E \leq 0.1 \text{ eV} \quad (55a)$$

$$= 2.96n^4 (\times 10^{-18} \text{ cm}^2), \quad 0.1 \leq E(\text{eV}) \leq 1.0 \quad (55b)$$

$$= \frac{2.96n^4}{E^{0.4n}} (\times 10^{-18} \text{ cm}^2), \quad E > 1.0 \text{ eV} \quad (55c)$$

where the baricentric (center of mass) energy E is expressed in eV units. The accuracy of the above fit is 20 – 40%, where 40% reflects the deviations of σ_{AI} values in the region 0.1 – 1.0 eV from their average value. It is unclear whether above expressions can be extrapolated to the $n \geq 5$ states, (see, however, sub-section 4.1.3D).

For the non-associative ionization channel (51b), cross section data are not available at present.

2.3.4 Three-body diatomic association

The three-body diatomic association reaction (52) with ground state atoms have been studied both experimentally [87] and theoretically [88] at very low temperatures ($T \lesssim 5,000\text{K}$). The theoretical and experimental data are given in temperature regions which do not overlap, and the two data sets cannot be smoothly

connected with each other. The rate coefficients for the three-body diatomic association in $H^+ + H + H$ system discussed in sub-section 2.2.4. are consistent with the theoretical data of Ref. [88], given the fact that the polarization interaction in $H^+ + H + H$ system and the additional charge-transfer assisted channel, ensure larger association rate coefficient in this system than in $H + H + H$. Normalizing the experimental data to the theoretical ones (after their extension to higher temperature by keeping the gradient unchanged), one arrives at the following analytic expression for rate coefficient of reaction (52)

$$K(H_2) = \frac{3.65}{T} (\times 10^{-30} \text{ cm}^6/\text{s}) \quad (56)$$

where T is expressed in Kelvin.

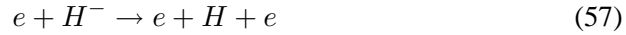
The validity of this expression extends up to $T \sim (2 - 3) \times 10^4 \text{ K}$, and its uncertainty is within 50%. From the similarity of three-body association mechanisms in $H^+ + H + H$ and $H + H + H$ systems, one can conclude that H_2 molecules formed in the latter system are also predominantly in highly excited vibrational states (the population weight increasing with the increase of vibrational level).

3 Collision Processes of H^- Ions

3.1 Electron impact processes

3.1.1 Electron detachment

The binding energy of loosely bound electron in H^- ion is only 0.754 eV and its detachment in collisions with other particles is fairly efficient. The process of electron detachment of H^- by electron impact



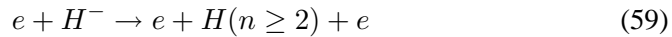
has been subject of numerous experimental and theoretical studies in the past (see, e.g., [12], [37] for references). The cross section of this reaction can be represented by the analytic fit

$$\begin{aligned} \sigma_{det}(H^-) = & \frac{2.06}{E} \ln(e + 2.335 \times 10^{-4} E) \exp\left(-\frac{13.75}{E^{0.868}}\right) \times \\ & \times \left[1 - \left(\frac{0.754}{E}\right)^2\right] (\times 10^{-13} \text{ cm}^2) \end{aligned} \quad (58)$$

where $e = 2.7182818\dots$ and E is expressed in eV units, see Figure 14 on page 168. A polynomial fit to this cross section is also given in [11].

3.1.2 Other processes

Other less important electron impact processes of H^- are



3 Collision Processes of H^- Ions

and



The cross sections for these processes, involving two electron transitions, are one to two orders of magnitude smaller than $\sigma_{det}(H^-)$ [89, 90]. These processes can, therefore, be excluded in low-temperature plasma kinetics studies. The experimental cross section for the double electron detachment reaction (60) from Ref. [90], measured in the energy range from threshold ($\simeq 16.8$ eV) to 800 eV, can be represented by the analytic expression

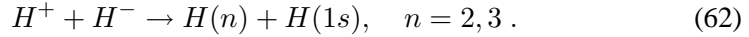
$$\sigma_{2-det}(H^-) = \frac{22.98}{E^{1.19}} \left[1 - \left(\frac{16.8}{E} \right)^{1.372} \right]^{0.822} \exp \left[-\frac{53.233}{E^{0.943}} \right] (\times 10^{-15} cm^2) \quad (61)$$

where E is expressed in eV (see Figure 15 on page 169). $\sigma_{2-det}(H^-)$ attains its maximum (of $\simeq 5.0 \times 10^{-17} cm^2$) at $E \simeq 65$ eV, to be compared with $\sigma_{det}(H^-) \simeq 2.3 \times 10^{-15} cm^2$ at the same energy.

3.2 Proton impact processes

3.2.1 Mutual neutralization of H^+ and H^-

By far the most important process in slow $H^+ + H^-$ collisions is their mutual neutralization by the electron capture reaction



The potential energy curve of initial ionic (quasi-molecular) state exhibits avoided crossings with the final $n = 2$ and $n = 3$ covalent states at favorable internuclear distances ($R_x(n = 2) \simeq 10.3a_0$ and $R_x(n \simeq 3) \simeq 35.8a_0$, a_0 being the Bohr radius of ground state electron in H -atom) at which strong non-adiabatic transitions populate the $n = 2$ and $n = 3$ electron capture channels. The $n = 1$ and $n \geq 4$ final states in reaction (62) are not populated, since the corresponding non-adiabatic couplings are either too weak, e.g., for $n = 1$ and $n = 4$, or do not exist at all (for $n \geq 5$).

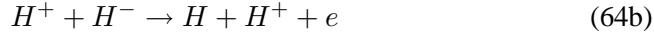
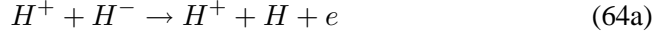
There have been many experimental [91, 92] and theoretical [93, 94] studies of reaction (62). The total experimental cross section for reaction (62) [91, 92], partitioned between the $n = 2$ and $n = 3$ channels on the basis of theoretical calculations, gives the cross sections $\sigma_{cx}(n = 2, 3)$ which can be represented by the following polynomial fits [11]

$$\ln \sigma_{cx}(n) = \sum_{j=0}^8 a_j (\ln E)^j, \quad n = 2, 3 \quad (63)$$

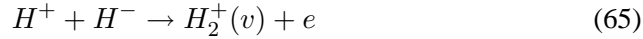
where σ_{cx} is expressed in cm^2 and the relative collision energy E is in eV units (see Figure 16 on page 169). The energy range in which the validity of above polynomial representation of $\sigma_{cx}(n)$ is valid is 0.1 eV - 20 keV. The values of coefficients a_j of polynomial fits (63) are given in Table 10.

3.2.2 Associative (AD) and non-associative (Det) detachment

Other less significant collision processes of H^+ with H^- include the non-associative reactions



and the associative detachment reaction



The direct proton impact electron detachment process (64a) has been studied both theoretically [95] and experimentally [96] and its cross-section becomes large ($\sim 10^{-15} \text{ cm}^2$) only in the keV energy region. Its cross section is given in an analytic fit form in Ref. [11].

The electron detachment reaction (64b) is a two-electron process: simultaneous capture of loosely bound electron from H^- and ionization of its tightly bound electron ("transfer ionization"). This process has also been studied experimentally in a wide energy range [97], but its cross section is small even at low (eV) collision energies. At low collision energies, reaction (64b) proceeds via formation of an intermediary auto-ionizing dissociative state H_2^{**} that decays in the vibrational continuum of H_2^+ ion [97].

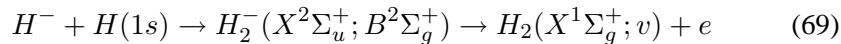
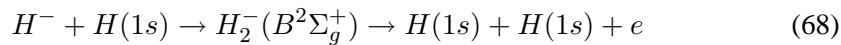
The associative detachment reaction (65, AD) proceeds via the same auto-ionizing dissociative state H_2^{**} , but it results from the decay of this state in the discrete vibrational spectrum of H_2^+ . This reaction has also been studied both experimentally [98] and theoretically [99]. Theoretical studies indicate that the lower vibrational states of H_2^+ ion are predominantly populated in reaction (65). The total cross section of associative detachment reaction can be represented (at least down to 10^{-3} eV) by the analytic fit

$$\sigma_{AD} = \frac{1.38}{E^{0.85}(1 + 0.065E^{2.70})} (\times 10^{-16} \text{ cm}^2) \quad (66)$$

where the relative collision energy E is expressed in eV (see Figure 17 on page 170). The cross section drops rapidly for $E \gtrsim 2$ eV due to the competing detachment channels (64a) and (64b). The nearly E^{-1} energy dependence of σ_{AD} is indicative for the processes proceeding via formation and decay of auto-ionizing dissociative states.

3.3 Collisions of H^- with H

The most important collision processes of H^- with ground state H atoms are



3 Collision Processes of H^- Ions

3.3.1 Resonant charge exchange

Charge exchange reaction (67) has resonant character and proceeds with high probability at low collision energies. It has been subject to numerous experimental [100, 101] and theoretical [102, 103] studies, and its cross section is well established. The critically assessed experimental cross section [12], extended at low and high collision by accurate theoretical calculations, can be represented by the analytic fit

$$\sigma_{cx}(H^-, H) = \frac{A_1 \ln(A_2/E + A_3)}{1 + A_4 E + A_5 E^{3.5} + A_6 E^{5.4}} (\times 10^{-15} \text{ cm}^2) \quad (70)$$

where the H^- -laboratory energy E is expressed in keV/amu, and the fitting parameters A_i have the values

$$A_1 = 1.326, A_2 = 23.588, A_3 = 2.3713 \\ A_4 = 0.4678, A_5 = 1.986 \times 10^{-2}, A_6 = 3.9747 \times 10^{-5}.$$

The accuracy of the fit is well within the experimental (and theoretical) uncertainty of the cross section (being $\sim 10 - 15\%$ for $E \lesssim 25$ keV/amu, and $15 - 30\%$ for $E > 25$ keV/amu). The fitted cross section is shown in Figure 18 on page 170.

3.3.2 Associative (AD) and non-associative (Det) detachment

The electron detachment processes (68) and (69) have also been studied both experimentally [100, 101, 104, 105] and theoretically [103, 106]. At low collision energies, the processes (68) and (69) result from the decay of quasi-stationary (auto-detachment) states $B^2\Sigma_g^+$ and $X^2\Sigma_u^+$ of H_2^- in the continuum and discrete vibrational spectrum of H_2 , respectively. The ground state $H_2^-(X^2\Sigma_u)(1s\sigma_g^2, 2p\sigma_u)$ is a shape resonance for $R \lesssim 3.0a_0$, while the excited state $H_2^-(B^2\Sigma_g)(1s\sigma_g, 2p\sigma_u^2)$ is a Feshbach resonance for $R \lesssim 4.9a_0$, where R is the internuclear distance and a_0 is the Bohr radius. The main contribution to the associative detachment reactions (69, AD) comes from the decay of $X^2\Sigma_u^+$ resonance.

The cross sections of these two reactions in the energy range ~ 0.1 eV – 20 keV can be represented by the analytic fit [11]

$$\ln \sigma = \sum_{j=0}^8 a_j (\ln E)^j \quad (71)$$

where σ and E ($= E_{CM}$) are expressed in units of cm^2 and eV, respectively, and the fitting coefficients a_j are given in Table 11. The fitted cross sections are depicted in Figure 19 on page 171. Cross sections for population of specific vibrational states in reaction (69) are given in [107].

At higher collision energies ($E \gtrsim 25$ keV/amu), a contribution to the cross section

of electron detachment reaction (68, Det) gives also the direct detachment mechanism.

Collision processes of H^- with excited hydrogen atoms $H(n \geq 2)$ have not been studied so far. It is expected, however, that electron detachment channels of type (68) and (69) should dominate in $H^- + H(n \geq 2)$ slow collisions and, thus, suppress the charge exchange channel.

4 Collision Processes of Electrons with Hydrogen Molecules

Collision processes of molecular hydrogen with other plasma constituents may involve changes in both the electronic and the nuclear (vibrational, rotational) motion of the molecule. In the present review, we shall consider only processes which involve changes of electronic and vibrational states of the molecule and exclude the processes involving rotational transitions. Such a position can be partly justified by the small amount of energy exchange (~ 0.01 eV) in such transitions and their long collision times (“frozen rotation”).

The state of vibrational excitation of a H_2 molecule in a given electronic state $N^{2S+1}\Lambda_\sigma^\pi$ significantly affects the cross section of the collision processes (here N denotes the united atom principal quantum number, S is the total electronic spin, Λ is the total angular momentum quantum number, σ is the label of its g/u -symmetry and π is the parity of the state). For inelastic electron-impact processes, the vibrational excitation of H_2 determines the reaction threshold, the transition energy and the overlap of initial and final state nuclear wave-functions (and, thereby, the magnitude of the cross section). In this context, the collision processes leading to formation or destruction of vibrational states of H_2 , in its ground or excited electronic states, are of particular importance for the overall collision kinetics of the plasma.

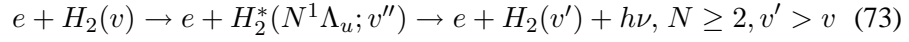
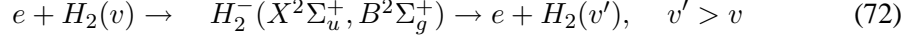
In the most part of the present section we shall discuss the collision processes of H_2 in its ground electronic state. The cross section information for the processes involving electronically excited initial states of H_2 is extremely limited, but the available information will be included in the discussions. The electronically excited states of H_2 are, generally, strongly radiatively coupled to the lower states (including the ground state). They may also have additional modes of decay: predissociation and auto-ionization. The information on these non-radiative decay processes of excited electronic states of H_2 is also quite limited.

4.1 Vibrational excitation of $H_2(X^1\Sigma_g^+)$

The homonuclear H_2 molecule does not possess a permanent dipole moment and, consequently, the excited vibrational states v do not exhibit spontaneous radiative decay. There are two basic electron-impact processes for excitation of vibrational

4 Collision Processes of Electrons with Hydrogen Molecules

states of H_2 molecules in their ground electronic state $X^1\Sigma_g^+$:



where v and $v' (> v)$ are the quantum numbers of initial and final vibrational states, and $N^1\Lambda_u$ is an excited electronic singlet state radiatively coupled to the ground state. The direct $v \rightarrow v'$ energy transfer excitation mechanism by electron impact is much less efficient than processes (72) and (73). (see, e.g., [108]).

4.1.1 Vibrational excitation via $H_2^-(X^2\Sigma_u^+, B^2\Sigma_g^+)$ resonant states

Experimental cross section measurements for the $v \rightarrow v'$ excitation in low-energy $e - H_2(v = 0)$ collisions have been performed in early sixties [109] and their large values ($\sim 10^{-17} \text{ cm}^2$ for 0-1 excitation) could be interpreted only in terms of the two-step reaction (72). Later cross section measurements [110] and theoretical calculations [111, 112] for $0 \rightarrow v'$ excitation have confirmed this interpretation. It should be noted, however, that the description of $0 \rightarrow v'$ excitations, when v' is not large, can be alternatively achieved also by other methods [113, 114], not explicitly involving the resonance concept [114]. The best results of these methods, however, agree with those of resonance theory.

The cross sections for $v \rightarrow v' (v \geq 1)$ excitation have been also calculated within the resonance theory [111, 112]. They show that the cross section for the $v \rightarrow v + \Delta v (\Delta v = 1, 2, 3\dots)$ excitation increases with increasing v , but rapidly decrease with increasing Δv . The experimental cross sections for $0 \rightarrow 1$ and $0 \rightarrow 2$ excitations [109, 110] can be appropriately fitted by the analytic expression

$$\sigma_{v,exc}^{(-)} = \frac{5.78\xi_v}{(\Delta E)^4} \frac{1}{x^2} \left(1 - \frac{1}{x}\right)^{6.11/(\Delta E)^{1/2}} (\times 10^{-16} \text{ cm}^2) \quad (74)$$

where $x = E/\Delta E$, ΔE is the energy difference of $v = 0$ and v' levels, and both E and ΔE are expressed in eV units. The ξ_v factor in Eq. (74) has values 1 and 0.628 for $0 \rightarrow 1$ and $0 \rightarrow 2$ transitions, respectively and the corresponding ΔE values are 0.516 and 1.003. These fits are shown in Figure 20 on page 171. We note that the theoretical cross sections for $0 \rightarrow 1$ and $0 \rightarrow 2$ transitions in Ref. [111] are by a factor $\sim 1.5 - 1.8$ smaller than the experimental ones.

For the $0 \rightarrow v'$ excitations, cross sections have also been derived from a Boltzmann analysis of electron swarm data [115] that are in fair agreement (within a factor of two, or so) with the calculated data [111]. We note that for initial $v \geq 1$, the process (72) can lead to both excitation ($v' > v$) and de-excitation ($v' < v$). The transitions with $\Delta v = |v' - v| = 1$ are always the dominant ones (and almost equal in magnitude).

The rate coefficients $K_{v,exc}^{(-)}(0 \rightarrow v')$ for the $0 \rightarrow v'$ excitations of H_2 via the process (72), obtained by Maxwellian averaging of theoretical cross sections [111],

4.1 Vibrational excitation of $H_2(X^1\Sigma_g^+)$

can be represented by the analytic fits [112]

$$\ln \left[K_{v,exc}^{(-)}(0 \rightarrow v') \right] = \frac{a_1}{T'^{a_2}} + \frac{a_3}{T'^{a_4}} + \frac{a_5}{T'^{a_6}} \quad (75)$$

where $T' = T/10^3$, T is the temperature (same for all reactants) expressed in K, and $K_{v,exc}^{(-)}$ is expressed in cm^3/s units. See Figure 21 on page 172 for transitions to $v' = 0, \dots, 10$ states. The fitting coefficients a_i are given in Table 12 for $v' = 0 - 10$. In view of the above mentioned underestimation of $\sigma_{v,exc}^{(-)}$ by the resonance theory, the values of $K_{v,exc}^{(-)}$ obtained from Eq. (75) have to be increased by a factor 1.5 - 1.8. The ‘‘elastic’’ $0 \rightarrow 0'$ transition is also covered by Eq. (75) and Table 12 and its rate coefficient (as well as the corresponding cross section) is about two or more (at $T' \lesssim 10K$) orders of magnitude larger than that for the $0 \rightarrow 1$ transition. The validity of the fit (75) extends from thermal to $T \sim 100$ eV temperatures.

We note that the $B^2\Sigma_g^+$ resonance H_2^- state has repulsive character and lies energetically close to the dissociative $b^3\Sigma_u^+$ state of H_2 (and for certain internuclear distances smaller than some $R_x \sim 1a_0$, above it). The $B^2\Sigma_g^+$ state can non-radiatively decay (by electron detachment) also to $b^3\Sigma_u^+$ state, which leads to dissociation of H_2 . The $B^2\Sigma_g^+$ state, lying energetically well above the $H_2(X^1\Sigma_g^+)$ state, can non-radiatively decay into the vibrational continuum of $H_2(X^1\Sigma_g^+, \epsilon)$, as well. The cross section of these dissociative processes will be discussed later on in sub-section 4.5.

4.1.2 Vibrational excitation via $H_2^*(N^1\Lambda_u)$ excited states

In contrast to the two-step process (72), in which the intermediate H_2^- resonant state decays non-radiatively to some vibrational state of $X^1\Sigma_g^+$ ground electronic state of H_2 , the decay of intermediate excited state $H_2(N^1\Lambda_u)$ ($N \geq 2$) in the process (73) takes place radiatively. The $v - v'$ excitation of H_2 mediated by the process (72) has, therefore, a larger cross section as compared to the channel mediated by the process (73). The cross section for a $v \rightarrow v'$ excitation via the process (73) is, obviously,

$$\sigma_{v,exc}^{(*)}(v \rightarrow v') = \sum_{v''} \sigma_{exc}^{el}(X^1\Sigma_g^+; v \rightarrow N^1\Lambda_u; v'') A(N^1\Lambda_u v'' \rightarrow X^1\Sigma_g^+; v') \quad (76)$$

where σ_{exc}^{el} is the electron-impact cross section for the $X^1\Sigma_g^+; v \rightarrow N^1\Lambda_u; v''$ excitation transition, and $A(N^1\Lambda_u v'' \rightarrow X^1\Sigma_g^+; v')$ is the probability for spontaneous radiative decay. Among all singlet excited electronic states of H_2 with u -symmetry, the two lowest excited states $B^1\Sigma_u^+$ and $C^1\Pi_u$ have the largest electron-impact excitation cross sections [11], and their radiative transition probabilities to the ground $X^1\Sigma_g^+$ state are also the largest. Therefore these two states are the most important ones for the $v \rightarrow v'$ excitation process (73). The involvement of transition probabilities $A_{if}(v'', v')$ in Eq. (76) causes that only for the $v \lesssim 4$ initial states the transitions with $|v' - v| = 1$ have the largest cross sections (in contrast to the process (72)).

4 Collision Processes of Electrons with Hydrogen Molecules

The first quantum mechanical cross section calculations for the process (73) have been performed for $v = 0$ and $N^1\Lambda_u = B^1\Sigma_u^+, C^1\Pi_u$ in Ref. [116]. Later on, they have been extended also to $v \geq 1$ [117]. The total $\sigma_{v,exc}^{(*)}(v \rightarrow v')$ cross sections, summed over the contributions from both $B^1\Sigma_u^+$ and $C^1\Pi_u$ states, can be found in Ref. [15] (only for selected v -values, but for all $v' = 0 - 14$). The cross sections $\sigma_{v,exc}^{(*)}(v \rightarrow v')$ for all v, v' combinations can be also accessed via Internet [20].

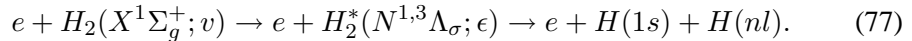
The rate coefficients $K_{v,exc}^{(*)}$ for $0 \rightarrow v'$ excitations of H_2 via the $B^1\Sigma_u^+$ and $C^1\Pi_u$ excited electronic states have been calculated by Maxwellian averaging of the cross sections of Ref. [117] and represented as analytic function of the form (75) [112]. The corresponding fitting parameters a_i are given in Table 13, including those for the $0 \rightarrow 0'$ transition. The validity of the fit (75) for $K_{v,exc}^{(*)}$ extends from thermal to temperatures of $\sim 200 - 300$ eV.

Vibrational excitation of H_2 via higher excited singlet states is negligible since the electronic excitation cross sections of these states are about one or more orders of magnitude smaller than those for $B^1\Sigma_u$ and $C^1\Pi_u$ states. We note that the radiative decay of $B^1\Sigma_u$ and $C^1\Pi_u$ states may take place not only to the discrete vibrational spectrum of $H_2(X^1\Sigma_g^+; v)$, but also to the vibrational continuum ($X^1\Sigma_g^+, \epsilon$), producing dissociation of H_2 . The corresponding cross sections for these dissociation processes will be discussed in sub-section 4.5.

4.2 Electronic excitation processes

The lowest singlet and triplet excited electronic states $N^{1,3}\Lambda_\sigma$ of H_2 are given in Table 14, together with their configuration ($1s\sigma_g; Nl\lambda_\sigma$), symmetry (subscript σ), and the quantum state of the excited electron in the dissociation limit, $H(1s) + H(nl)$. The potential energy diagrams of these states are given in Figs. 1 (singlet) on page 31 and 2 (triplet) on page 32.

Optically allowed electron transitions in molecules are subject to the selection rules: $g \leftrightarrow u$, $\Delta S = 0$ and $\Delta \Lambda = 0, \pm 1$. However, due to electron exchange effects in electron-impact excitation collisions at low energies, these selection rules are not strictly preserved. The cross sections for singlet-triplet (or *vice versa*) transitions ($\Delta S = 1$) may have magnitudes comparable to the cross sections for “spin-allowed” ($\Delta S = 0$) transitions in the region of their maximum. Only at collision energies above the energy of the cross section maximum, the cross section energy dependence of spin-allowed and spin-forbidden electron transitions is different (and, consequently, their magnitude as well): the former have an $E^{-1} \ln E$ behaviour, whereas the latter decrease much faster with energy, as E^{-3} . The magnitude of the maximum of excitation cross section is, generally, determined by the value of transition energy, ΔE ($\sigma_{exc}^{max} \sim \frac{1}{\Delta E^2}$). When the excited electronic state of H_2 has a repulsive, anti-bonding character (such as $b^3\Sigma_u^+$, for instance), the electron-impact excitation of that state leads to dissociation,



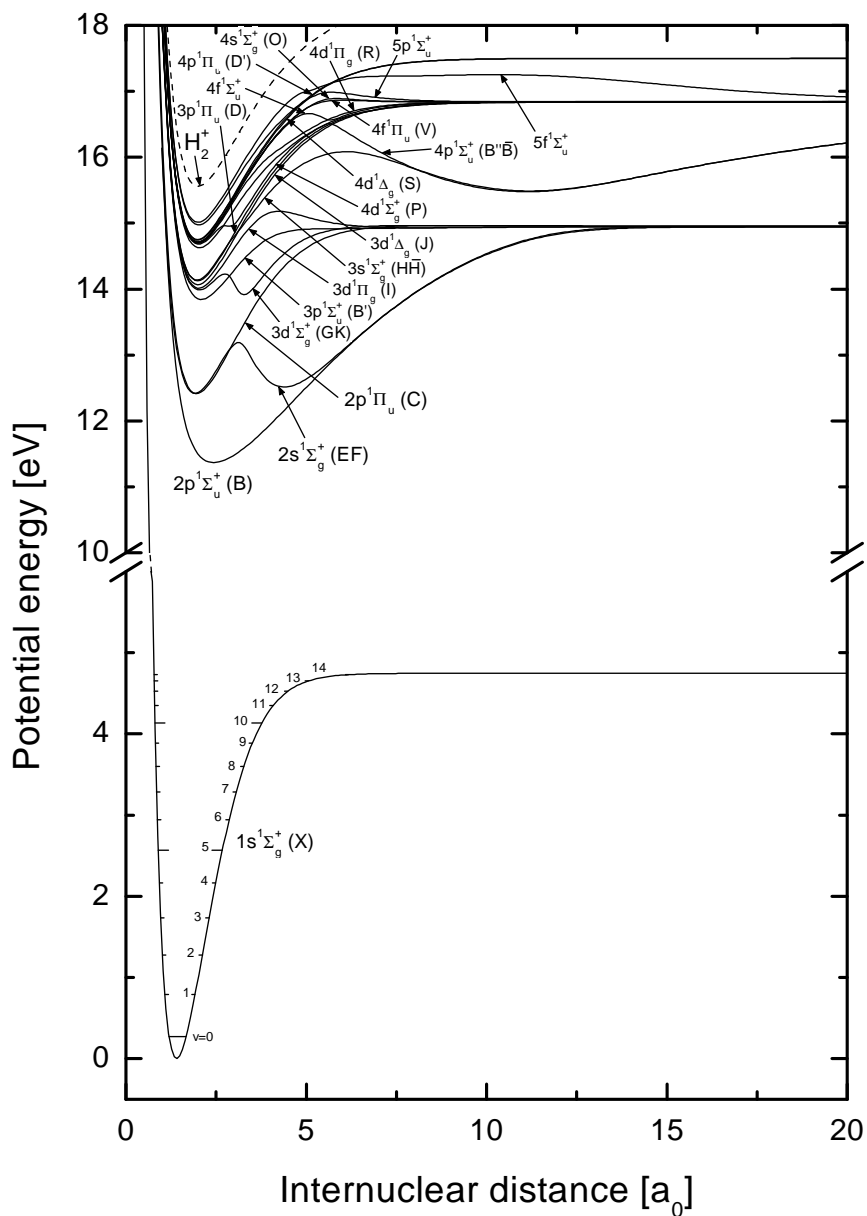


Figure 1: Potential energy diagrams for the singlet system of molecular hydrogen (figure kindly provided by D. Wunderlich, University Augsburg, Germany, 2003)

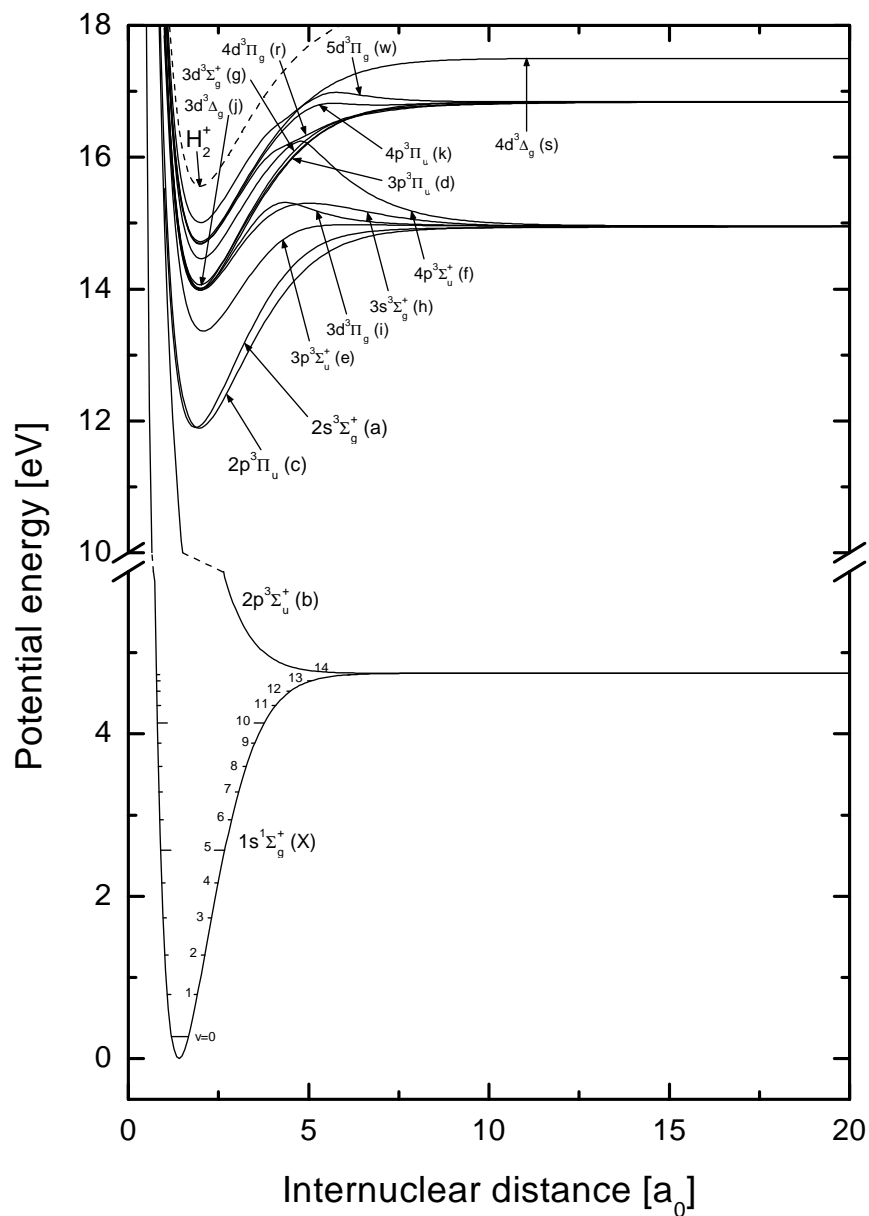


Figure 2: Potential energy diagrams for the triplet system of molecular hydrogen (figure kindly provided by D. Wunderlich, University Augsburg, Germany, 2003)

where ϵ is the continuum energy.

When the excited electronic state is bound, its vibrational spectrum has both a discrete part (bound vibrational states) and a continuous part (vibrational, or dissociative continuum). Therefore, the excitation of such a state can lead to two processes:

$$e + H_2(X^1\Sigma_g^+; v) \rightarrow e + H_2^*(N^{1,3}\Lambda_\sigma; v'), \quad (78)$$

$$e + H_2(X^1\Sigma_g; v) \rightarrow e + H_2^*(N^{1,3}\Lambda_\sigma; \epsilon') \rightarrow e + H(1s) + H(nl). \quad (79)$$

The dissociative excitation process (79) can take place when the “vertical” Franck-Condon transition from the initial v -state reaches that part of the potential energy curve of the excited state that lies above the dissociation limit of $N^{1,3}\Lambda_\sigma$ state. Obviously, this possibility appears most often for the higher initial vibrational states of $H_2(X^1\Sigma_g^+)$.

Some of the bound excited electronic state of H_2 have a potential barrier the top of which is above the dissociation limit (e.g., the $I^1\Pi_g, i^3\Pi_g$ and $h^3\Sigma_g^+$ states). The vibrational states of such excited electronic states, that energetically lie above the dissociation limit have quasi-stationary character and are unstable against dissociation (by quantum-mechanical tunnelling). Finally, if N is sufficiently high ($N \gtrsim 4$), most of its higher vibrational states lie energetically above the ground state ($X^2\Sigma_g^+; v = 0$) of H_2^+ ion. The excitation of such states will lead to $H_2^+(X^2\Sigma_g^+; v)$ production via auto-ionization (see next sub-section). We should also note that for high collision energies, doubly excited dissociative states of H_2 [such as, e.g., $(2p\sigma_u, nl\lambda|Q_2^1)\Pi_u$] can be also excited, which leads to production of two excited hydrogen atoms.

In the sub-sections below we will discuss the excitation cross sections for the processes $(X^1\Sigma_g^+; v) \rightarrow (N^1\Lambda_\sigma)$, $(X^1\Lambda_g^+; v) \rightarrow (N^3\Lambda_\sigma)$ and $(N^{1,3}\Lambda_\sigma) \rightarrow (N'^{1,3}\Lambda'_\sigma)$ separately.

4.2.1 Excitation of singlet states from $X^1\Sigma_g^+$

A Excitation from $X^1\Sigma_g^+(v = 0)$

Most of experimental and theoretical studies for electron-impact $(X^1\Sigma_g^+; v) \rightarrow (N^1\Lambda_\sigma; v'/\epsilon)$ excitation processes in H_2 have been performed for the $v = 0$ initial vibrational state. Experimental cross section measurements have been performed for $X^1\Sigma_g^+ \rightarrow B^1\Sigma_u^+$ [118, 119], for $X^1\Sigma_g^+ \rightarrow C^1\Pi_u$ [118–120], and for $X^1\Sigma_g^+ \rightarrow B', B''^1\Sigma_g^+, D, D'\Pi_u$ [119] transitions, generally in the energy range below ~ 350 eV. In the region around the cross section maximum ($\sim 40 - 50$ eV) the cross sections of Ref. [119] are about 25 – 30% larger than those of Ref. [118] for both $X \rightarrow B$ and $X \rightarrow C$ transitions. On the other hand, the cross section of Ref. [118] for $X \rightarrow C$ transition (available for $E \lesssim 80$ eV) agrees well with that of Ref. [120] that extends up to $E = 1000$ eV, which, on its turn, agrees well with the Born-Ochkur (B-O) calculations [121]. Systematic B-O cross section calculations for $X^1\Sigma_g^+(v = 0) \rightarrow B, B', B''^1\Sigma_u^+, C, D, D'\Pi_u, EF, H\bar{H}^1\Sigma_g^+$ and

4 Collision Processes of Electrons with Hydrogen Molecules

$I^1\Pi_g$, summed over the final v' -states, have been performed in [121]. Extensive excitation cross section calculations for dipole-allowed $X^1\Sigma_g^+(v = 0 - 14) \rightarrow B, B', B''^1\Sigma_u^+, C, D, D'^1\Pi_u$ transitions were performed by the impact parameter version of first Born approximation (IPM) [122] and summarized in [15]. Distorted wave calculations have also been performed for $X^1\Sigma_g^+(v = 0) \rightarrow C^1\Pi_u, EF\Sigma_g^+$ transitions [123].

For the excitations from ground vibrational state ($v = 0$), the Franck-Condon overlap with the vibrational continuum of excited electronic states is negligible small (except for B' state, see, e.g., Ref. [15]), and the dissociative channel (79) can be generally neglected. The cross sections for dipole allowed $X^1\Sigma_g^+(v = 0) \rightarrow N^1\Lambda_u$ excitations with $N = 2-4$ can all be represented by the analytic fit expression

$$\sigma_{exc}(X^1\Sigma_g^+(v = 0) \rightarrow N^1\Lambda_u) = \frac{5.984}{\Delta E x} \left(1 - \frac{1}{x}\right)^\alpha \times \left(A_1 + \frac{A_2}{x} + \frac{A_3}{x^2} + A_4 \ln(x)\right) (\times 10^{-16} \text{cm}^2) \quad (80)$$

where ΔE is the threshold energy, $x = E/\Delta E$ (both E and ΔE are expressed in eV), and α and A_i are fitting parameters. The values of these parameters, obtained from available experimental and theoretical data, are given in Table 15, together with the values of threshold energies. The expression (80) obviously has the correct physical behaviour at both low and high energies, see Figure 22 on page 172.

The cross sections of symmetry-forbidden transitions

$$X^1\Sigma_g^+(v = 0) \rightarrow EF^1\Sigma_g^+, H\bar{H}^1\Sigma_g^+, I^1\Pi_g$$

have an E^{-1} high-energy behaviour, and the available (and appropriately assessed) data can be represented by the analytic fit function (Figure 23 on page 173)

$$\sigma_{exc}(X^1\Sigma_g^+(v = 0) \rightarrow N^1\Lambda_g) = \frac{5.984A_1}{\Delta E x} \left(1 - \frac{1}{x}\right)^\alpha (\times 10^{-16} \text{cm}^2) \quad (81)$$

where ΔE and x have the same meaning as in Eq. (80). The values of parameters α and A_1 are given in Table 16.

The cross section for a dipole-allowed transition ($0 \rightarrow N$), as function of reduced energy $x = E/\Delta E$, is proportional to $f_{0N}/\Delta E_{0N}$, where f_{0N} is the dipole oscillator strength evaluated at the equilibrium distance $r_e = 1.4a_0$ of $H_2(X^1\Sigma_g^+; v = 0)$. Since starting from a certain sufficiently high state N_0 one has $f_{0N} \sim N^{-3}$, and since the $A_4 \ln(x)/x$ term in Eq. (80) dominates the cross section (except in the threshold region [$x \sim 1$]) (see Table 15), the following scaling relation follows for the $X^1\Sigma_g(v = 0) \rightarrow N^1\Lambda_u$ excitation cross sections within a given $^1\Lambda_u$ series

$$\sigma_{exc}(X^1\Sigma_g^+(v = 0) \rightarrow N^1\Lambda_u) = \left(\frac{N_0}{N}\right)^3 \left(\frac{\Delta E_{0N_0}}{\Delta E_{0N}}\right) \times \sigma_{exc}(X^1\Sigma_g^+(v = 0) \rightarrow N_0^1\Lambda_u), N > N_0. \quad (82)$$

4.2 Electronic excitation processes

For the $N^1\Sigma_u^+$ and $N^1\Pi_u$ series, the relation (82) becomes valid already for $N_0 = 3$.

For the symmetry-forbidden transitions $X^1\Sigma_g^+(v=0) \rightarrow N^1\Lambda_g$, the cross section is proportional to $f_{0N}(q)/\Delta E_{0N}$, where $f_{0N}(q)$ is the generalized oscillator strength and q is the transferred electron momentum. The variation of $f_{0N}(q)$ with q , evaluated at $r_e = 1.4a_0$, is rather strong [121], (with $f_{0N}(0) = 0$), and its N -dependence is unknown. The theoretical cross section data of Ref. [121] suggest the following (approximate) scaling relation (within a given $^1\Lambda_g$ series)

$$\begin{aligned} \sigma_{exc}(X^1\Sigma_g^+(v=0) \rightarrow N^1\Lambda_g) &= \left(\frac{N_0}{N}\right)^6 \left(\frac{\Delta E_{0N_0}}{\Delta E_{0N}}\right) \times \\ &\times \sigma_{exc}(X^1\Sigma_g^+(v=0) \rightarrow N_0^1\Lambda_g), N > N_0, \end{aligned} \quad (83)$$

starting already with $N_0 = 3$. In contrast to the scaling relation (82) for dipole-allowed transitions, the scaling (83) appears to be not very sensitive to the particular type of the $^1\Lambda_g$ series ($^1\Sigma_g$), or ($^1\Pi_g$).

B Excitation from $X^1\Sigma_g^+(v \geq 1)$: total cross sections

As mentioned earlier in this section, the overlap of nuclear wave-functions of vibrationally excited states of $X^1\Sigma_g^+$ electronic state with the wave-functions of vibrational continuum of an excited electronic state $N^1\Lambda_\sigma$ can be large (generally increasing with the increase of v), resulting in significant increase of the role of dissociation channel (79). In the present sub-section we shall discuss the total cross sections for $N^1\Lambda_\sigma$ excitation [i.e., the sum of the cross sections for the channels (78) and (79)], and in the next sub-section we shall discuss the cross sections for the dissociative excitation channel (79) alone. The cross section for excitation of all discrete vibrational states v' (summation over all v') is then the difference of the total cross section discussed in the present sub-section and that for dissociative excitation (see next sub-section).

Cross section calculations for excitation from $X^1\Sigma_g^+(v \geq 1)$ have been performed only for the dipole-allowed transitions to $N^1\Sigma_u^+$ and $N^1\Pi_u$ states with $N = 2 - 4$ by using the impact parameter method Ref. [122], and covering all initial vibrational states ($v = 0 - 14$). It has been found that total excitation cross sections for $X^1\Sigma_g^+(v) \rightarrow N^1\Lambda_u$ transitions allow an approximate scaling with respect to v [124, 125]. All $\sigma_{exc}(v)$ cross sections for the $X^1\Sigma_g^+(v) \rightarrow B^1\Sigma_u, C^1\Pi_u$ transitions can be represented in a unified form:

$$\sigma_{exc}^{tot}(X^1\Sigma_g^+; v) \rightarrow B, C = \sigma_0(x) \left[\frac{Ry}{\Delta E_{X\Lambda}(R_v^t)} \right]^3, \quad (84)$$

where $x = E/\Delta E_{X\Lambda}(R_v^t)$, $\Delta E_{X\Lambda}(R_v^t)$ is the vertical transition energy from the $X^1\Sigma_g^+(v)$ energy level to the $\Lambda (= B, C)$ potential energy curve taken at the outermost turning point R_v^t of $X^1\Sigma_g^+(v)$ level, $Ry = 13.6$ eV, and E and $\Delta E_{X\Lambda}$ are expressed in eV units. The common "shape function" $\sigma_0(x)$ has the form

4 Collision Processes of Electrons with Hydrogen Molecules

$$\sigma_0(x) = \frac{a_1}{x} \left(1 - \frac{1}{x}\right)^{a_2} \left[a_3 + \frac{a_4}{x} + \ln(x) \right] (\times 10^{-16} \text{cm}^2) \quad (85)$$

see Figure 24 on page 173. The values of transition energies $\Delta E_{X\Lambda}(R_v^t)$ and fitting parameters a_i entering Eqs. (84) and (85) are given in Table 17. The analytical expressions (84 -85) represent the calculated data for $\sigma_{exc}(v)$ with an accuracy better than $\sim 25\%$.

The $\sigma_{exc}(v)$ cross sections for $X^1\Sigma_g^+(v) \rightarrow B', B''^1\Sigma_u, D, D'^1\Pi_u$ transitions also allow scaling with v , but starting with $v = 1$, Ref. [125]. The excitation cross sections for these transitions from $v = 0$ and $v = 1$ initial states can be represented in the form [same as Eq. (85)]:

$$\begin{aligned} \sigma_{exc}^{tot} (X^1\Sigma_g(v=0,1) \rightarrow N^1\Lambda_u) &= \\ &= \frac{b_1}{x} \left(1 - \frac{1}{x}\right)^{b_2} \left[b_3 + \frac{b_4}{x} + \ln(x) \right] (\times 10^{-16} \text{cm}^2) \end{aligned} \quad (86)$$

where $x = E/\Delta E_{X\Lambda}(R_v^t)$ and $\Delta E_{X\Lambda}(R_v^t)$ has the same meaning as in Eqs. (84), (85). The values of $\Delta E_{X\Lambda}(R_v^t)$ and of the fitting parameters b_i are given in Table 18.

For the transitions from $v \geq 2$ vibrational states of $X^1\Sigma_g^+$ to $B', B''^1\Sigma_u$, and $D, D'^1\Pi_u^+$ excited states, the cross section can be represented in the form (Ref. [125]):

$$\sigma_{exc}^{tot} (X^1\Sigma_g^+(v \geq 2) \rightarrow N^1\Lambda_u) = F(v, x) \sigma_{exc} (X^1\Sigma_g^+(v=1) \rightarrow N^1\Lambda_u) \quad (87)$$

$$F(v, x) = \left[\frac{\Delta E_{X\Lambda}(R_1^t)}{\Delta E_{X\Lambda}(R_v^t)} \right]^{\alpha(v,x)} \beta(v, x), \quad (88)$$

where $\alpha(v, x)$ and $\beta(v, x)$ are given by

$$\alpha(v, x) = (1 + C_1 v^{C_2}) \left[C_3 + \left(\frac{2}{x} \right)^{C_4} \right] \quad (89a)$$

$$\begin{aligned} \beta(v, x) &= C_5 + C_6 v + \left(\frac{C_7}{x^{C_8}} + C_9 \right) v^2 \\ &+ C_{10} v^3 + \left(\frac{C_{11}}{x^{C_8}} + C_{12} \right) v^4. \end{aligned} \quad (89b)$$

The values of fitting parameters C_i are given in Table 19. The $\sigma_{exc}(v)$ cross sections provided by Eqs. (87-89) reproduce the calculated data of Refs. [122, 124] with an accuracy better than $\sim 15\%$. It is to be noted that for transitions to $D, D'^1\Pi_u$ states the coefficient C_i for $i \geq 6$ are all zero.

4.2 Electronic excitation processes

We note that the values of fitting parameters a_i, b_i and C_i in Eqs. (85), (86) and (89a), (89b) have been determined in conjunction with the use of most recent accurate variational calculations of potential energy curves for considered singlet states of H_2 . The information on the potential energy curves of these state is necessary to determine the vertical transition energy, $\Delta E_{X\Lambda}(R_v^t)$, on which the cross section for $X(v) \rightarrow N^1\Lambda_u$ transition sensitively depends.

C Dissociative excitation cross sections

Cross section calculations for dissociative excitation process (79) for dipole-allowed $X^1\Sigma_g^+(v) \rightarrow B, B', B''^1\Sigma_u^+, C, D, D'^1\Pi_u$ transitions have been performed in Ref. [122] for all initial v-states ($v = 0 - 14$). For the initial $v = 0$ state, dissociative excitation cross sections have been also calculated in the Born-Rudge approximation for $X^1\Sigma_g^+(v = 0) \rightarrow B'^1\Sigma_u^+$ and $X\Sigma_g^+(v = 0) \rightarrow EF^1\Sigma_g^+$ transitions in Ref. [126]. The energy behaviour of dissociative excitation cross sections $\sigma_{exc}^{diss}(v)$ is similar to that for the corresponding non-dissociative excitation reaction (78) and shows a maximum at $\sim 40 - 50 eV$. In Table 20, the values of cross sections $\sigma_{exc}^{diss}(v)$ from transitions to $B, B', B''^1\Sigma_u^+$ and $C, D, D'^1\Pi_u$ excited states are shown for $v = 0 - 14$ at the collision energy $E = 40 eV$.

The contribution of $\sigma_{exc}^{diss}(v)$ to the total excitation cross sections $\sigma_{exc}^{tot}(v)$, discussed in the preceding sub-section, can be appreciated from Table 21 in which the ratios $R(v) = \sigma_{exc}^{diss}(v)/\sigma_{exc}^{tot}(v)$ for the above mentioned excitation transitions are shown for all v-levels at the collision energy $E = 40 eV$. These values can be taken as typical for other collision energies as well. As discussed earlier, the contribution of $\sigma_{exc}^{diss}(v = 0)$ to $\sigma_{exc}^{tot}(v = 0)$ is small, except for the $X \rightarrow B'$ transition. The high ($\sim 40\%$) contribution of $\sigma_{exc}^{diss}(v = 0)$ to $\sigma_{exc}^{tot}(v = 0)$ for this transition is confirmed also by other calculations (e.g., $\sigma_{exc}^{diss}(v = 0)$ from Ref. [126] and $\sigma_{exc}^{tot}(v = 0)$ from Ref. [121]). With increasing v , the ratios $R(v)$ rapidly increase; they maximize in the range $v \sim 6 - 11$, and then begin to decrease. It is to be noticed that for $X \rightarrow B', B''$ transitions, the contribution of dissociative excitation process to total excitation cross section is substantial; most of the excitation from the levels $v = 6 - 12$ in the $X \rightarrow B'$ case leads to dissociation. The excited H -atoms formed by dissociative excitation of considered singlet states of H_2 are indicated in Table 14.

We mention that dissociative excitation cross section for $X^1\Sigma_g^+(v = 0) \rightarrow EF^1\Sigma_g^+$ transition has been calculated in Ref. [126]. At $E = 40 eV$, it constitutes 4.1% of $\sigma_{exc}^{tot}(EF)$.

D $v - v'$ resolved excitation cross sections .

In many plasma applications (e.g., plasma diagnostics based upon molecular band radiation), excitation cross sections from a specific initial vibrational state v to a specific vibrational state v' of excited electronic state are required. Such $v - v'$

4 Collision Processes of Electrons with Hydrogen Molecules

resolved excitation cross sections have not been so far published in the literature. However, in all theoretical calculations of excitation processes, the $v - v'$ resolved cross section calculations are actually performed, but are then summed over v' in order to obtain the excitation cross section for a given value of v . (Summation is also done over the vibrational continuum ϵ' .) Experimental excitation cross section also implicitly contain such summation over v' (or ϵ' for σ_{exc}^{diss}). Under the assumption that electronic transition matrix element is a slow varying function of internuclear distance, it can be factored in nuclear and electronic coordinates and the resulting total excitation cross section (including the vibrational continuum ϵ') is

$$\sigma_v^{tot} = \sum_{v'} F_{vv'} \sigma_v^{(0)} + \int F_{v\epsilon'} \sigma_v^{(0)} d\epsilon' \quad (90)$$

where $F_{vv'}$ and $F_{v\epsilon'}$ are the Franck-Condon factor and Franck-Condon density, respectively, and $\sigma_v^{(0)}$ does not (approximately) depends on v' . The first and second term in Eq. (90) represent the excitation cross section to bound vibrational states and to the vibrational continuum of excited electronic state, respectively, i.e. $\sigma_v^{tot} = \sigma_v^b + \sigma_v^{diss}$. Since Franck-Condon factors and Franck-Condon density satisfy the sum rule (closure relation):

$$\sum_{v'} F_{vv'} + \int_{\epsilon'} F_{v\epsilon'} d\epsilon' = 1, \quad (91)$$

it follows from Eq. (90) that the cross section $\sigma_{v,v'}^b$ for a $v - v'$ resolved excitation transition is

$$\sigma_{v,v'}^b = F_{vv'} \sigma_v^{tot}. \quad (92)$$

Analogously, the cross section $\sigma_{v,\epsilon'}^{diss}$ for a $v \rightarrow \epsilon'$ dissociative excitation transition to a continuum energy level ϵ' , is

$$\sigma_{v,\epsilon'}^{diss} = F_{v\epsilon'} \sigma_v^{tot}. \quad (93)$$

There exist well established procedures for calculations of the Franck-Condon factors $F_{vv'}$ and $F_{v\epsilon'}$. $F_{vv'}$ can be calculated analytically if the potential energy curves of the lower ($V_i(R)$) and the upper ($V_f(R)$) electronic states are approximated by Morse potentials [127]. Calculations of $F_{vv'}$ can also easily be carried out in the quasi-classical approximation [128]. The most accurate values for $F_{vv'}$ can, however, be obtained by solving numerically the Schrödinger equation for the nuclear motion in the potentials of the lower (i) and upper (f) electronic state, and then, from the obtained vibrational functions $\chi_v^{(i)}(R)$ and $\chi_{v'}^{(f)}(R)$ (R is the internuclear distance), calculate the square of their overlap integral

$$F_{vv'} = |\langle \chi_v^{(i)} | \chi_{v'}^{(f)} \rangle|^2 \quad (94)$$

4.2 Electronic excitation processes

This approach can also be used for calculation of $F_{ve'}$. The overlap of initial ($\chi_v^{(i)}(R)$) and final ($\chi_{e'}^{(f)}(R)$, continuum) vibrational functions in this case is dominantly determined by the region of R close to the classical turning point $R_{t,e'}^{(f)}$ on the upper potential ($U_f(R_{t,e'}^{(f)}) = \epsilon'$) and for $\chi_{e'}^{(f)}(R)$ one can use either an Airy function, or even a delta function approximation at the classical turning point. The application of any of these methods for determining $F_{vv'}$ and $F_{ve'}$ requires knowledge of accurately calculated potential energy curves of the electronic states involved. For a number of transitions between low-lying singlet states, complete sets of $F_{vv'}$ values are available in the literature [129, 130]. Different approximations for calculating $F_{ve'}$ are presented in [131].

4.2.2 Excitation of triplet states from $X^1\Sigma_g^+$

A Excitation from $X^1\Sigma_g^+(v=0)$

Except for the fully repulsive $b^3\Sigma_u^+$ state, all other low-lying excited triplet states of H_2 have bound character in the Franck-Condon region of the ground vibrational state of H_2 ($^1\Sigma_g^+$). Cross section measurements for excitation of triplet states have been done only for $b^3\Sigma_u^+$ [132, 133], and $a^3\Sigma_g^+$ and $c^3\Pi_u$ [118] states. Theoretical cross section calculations, using methods of varying accuracy (particularly in the low energy region), have been performed for excitation of $b^3\Sigma_u^+$ [126, 134–137], $a^3\Sigma_g^+$ [126, 135, 137, 138], $c^3\Pi_u$ [123, 126, 135, 137], and $e^3\Sigma_u^+$, $d^3\Pi_u$ [126] states. The excitation cross section of triplet states attain their maximum value in the range 14–16 eV, they rise sharply in the threshold region, and have an E^{-3} high-energy behaviour (following from the Born approximation). The results of the most involved theoretical calculations (such as the R-matrix [136], or second-order methods [135]) for excitation of $b^3\Sigma_u^+$ state agree well with experimental data of Ref. [133]. The theoretical and experimental cross section data also agree for the excitation of $a^3\Sigma_g^+$ state, but for the $c^3\Pi_u$ state the experimental data appear to be by a factor of two to three smaller than theoretical results. (In the analytical fit for this cross section given below, a compromise position was adopted between theoretical and experimental data.).

The critically assessed available cross sections for excitation of above discussed triplet states can be represented by the following analytic expression

$$\sigma_{exc}^{tot}(X^1\Sigma_g^+(v=0) \rightarrow N^3\Lambda_\sigma) = \frac{A}{x^3} \left(1 - \frac{1}{x^\beta}\right)^\gamma (\times 10^{-16} cm^2) \quad (95)$$

where $x = E/\Delta E$ and ΔE is the threshold energy, see Figure 25 on 174. The values of parameters A , β and γ in Eq. (95) for the considered transitions are given in Table 22, together with the values of threshold energies ΔE .

The cross section $\sigma_{exc}^{tot}(X \rightarrow b)$ is a fully dissociative excitation cross section. For other considered transitions, the contribution of dissociative excitation process

4 Collision Processes of Electrons with Hydrogen Molecules

(88) to σ_{exc}^{tot} is negligible (a few percents), except in the case of $X^1\Sigma_g^+ \rightarrow e^3\Sigma_u^+$ transition when it constitutes about 20% of $\sigma_{exc}^{tot}(X \rightarrow e)$ [126].

The excitation cross sections for triplet states of H_2 do show rapid decrease with increasing the principal quantum number N of the state (within a given $^3\Lambda_\sigma$ series), but the specific N dependence is not known. The ratios $\sigma(X \rightarrow d)/\sigma(X \rightarrow c)$ and $\sigma(X \rightarrow a)/\sigma(X \rightarrow e)$ show an approximate $(N_0/N)^2(\Delta E_{N_0}/\Delta E_N)^3$ scaling (with $N_0 = 2$, and $N = 3$, in these cases), but whether it is valid for, or can be extended to higher N is unclear.

B Excitation from $X^1\Sigma_g^+(v \geq 1)$

Cross section calculations for transitions from vibrationally excited $H_2(X^1\Sigma_g^+; v)$ to excited triplet states have been published only for the excitation of $b^3\Sigma_u^+$ dissociation state [134, 136, 139]. The quantum-mechanical calculations in Refs. [134] and [136] were done for $v \leq 9$ and $v \leq 4$, respectively.

In Ref. [139] the cross section calculations were performed for $v = 0 - 13$, but using the classical model for inelastic atomic processes [140] extended to collisions with molecules [141] (see next sub-section). These two sets of calculations disagree considerably for $v \geq 1$ (by factor greater than three) for energies below ~ 10 eV. The R-matrix cross sections from the region below ~ 10 eV can, however, be smoothly connected with the results of quantal calculations of Ref. [134]. By combining the results of Refs. [134] and [136], one can derive a set of cross sections for dissociative excitation via the $b^3\Sigma_u^+$ state for $v \leq 7$.

These cross sections can be represented in a scaled form

$$\sigma_{exc}^{diss}(b^3\Sigma_u^+)_v = \left(\frac{\Delta E_{v=0}}{\Delta E_v} \right)^{0.30} \sigma_{exc}^{diss}(b^3\Sigma_u^+)_0 \quad (96)$$

where ΔE_v is the threshold energy of initial vibration level v (the transition energy at the outermost classical turning point), and $\sigma_{exc}^{diss}(b^3\Sigma_u^+)_0$ is the dissociative excitation cross section from the level $v = 0$ level given by Eq. (66) with $x = E/\Delta E_{v=0}$. The small value of the exponent in the scaling factor indicates that the magnitude of $\sigma_{exc}^{diss}(b^3\Sigma_u^+)_v$ increases very slowly with the increase of v , despite the significant shift in threshold energies.

The values of vertical $X^1\Sigma_g^+(v) \rightarrow b^3\Sigma_u^+$ transition energies, ΔE_v , taken at the outermost classical turning point of the v -level in the $X^1\Sigma_g^+$ potential, are given in Table 23. The excitation energies, $E_{exc}(v)$, of vibrational levels of $H_2(X^1\Sigma_g^+; v)$ are also given in this table for reference. (The energy of the $v = 0$ level, $E_{v=0} = 0.269621$ eV, has been taken as zero.)

It is worthwhile to note that the excited states $a^3\Sigma_g^+$ and $c^3\Pi_u$ are mutually strongly (radiatively) coupled, and also strongly coupled to $b^3\Sigma_u^+$; their excitation results in quick decay to the $b^3\Sigma_u^+$ state and to production of two $H(1s)$ atoms. The rate coefficients for $H_2(X^1\Sigma_g^+; v)$ dissociation to $H(1s) + H(1s)$ via excitation of $b^3\Sigma_u^+$, $a^3\Sigma_g^+$ and $c^3\Pi_u$ states for $v = 0 - 10$ have been calculated in [112] and

4.2 Electronic excitation processes

can be represented by the analytic fit expression

$$\ln \left[K_{exc}^{diss} (b^3 \Sigma_u, a^3 \Sigma_g, c^3 \Pi_u) \right] = \frac{b_1}{T'^{b_2}} + \frac{b_3}{T'^{b_4}} + \frac{b_5}{T'^{2b_6}} \quad (97)$$

where $T' = T/10^3$ and temperature T is expressed in K . The fitting parameters b_i are given in Table 24. The small contribution to K_{exc}^{diss} from the excitation of some upper singlet states is also included in Eq. (97). The fit (97) is valid in the range $T' = 1K - 200K$.

It should be noted, however, that the higher triplet states, radiatively coupled to $a^3 \Sigma_g^+$ or $c^3 \Pi_u$ or directly to $b^3 \Sigma_u^+$, may also contribute to the $H(1s) + H(1s)$ dissociation of H_2 .

4.2.3 Excitation transitions between excited states

There are only a few cross section calculations for the excitation transition between the excited states of H_2 . They include the dipole- allowed transitions $B^1 \Sigma_u^+(v) \rightarrow I' \Pi_u$ [125] and $a^3 \Sigma_g^+(v) \rightarrow d^3 \Pi_u$, $c^3 \Pi_u(v) \rightarrow h^3 \Sigma_g^+$ and $c^3 \Pi_u(v) \rightarrow g^3 \Sigma_g^+$ [142] from all initial vibrational states v . The calculations have been performed within the impact parameter method. In view of small transition energy in these excitation processes, their cross sections are fairly large and exhibit a maximum at low collision energies (a few times of threshold energy).

In absence of more elaborate quantum-mechanical calculations for excitation transitions between excited states, one can use the method of Refs. [140,141] (GBB method) for rough estimates of the cross sections for these transitions. Being based upon classical mechanics, this method involves (besides the Franck-Condon factor) only the transition energy between the corresponding states. It can, therefore, be used to generate cross sections also for $v - v'$ resolved transitions.

If we introduce the notation: U_n , for the energy difference between initial $(\Lambda_\sigma; v)$ and final $(\Lambda'_\sigma; v')$ state; U_{n+1} , for the energy difference between $(\Lambda_\sigma; v)$ and $(\Lambda'_\sigma; v' + 1)$ states; and I_n , for the ionization potential of initial state, then the GBB excitation cross section for $(\Lambda_\sigma; v) \rightarrow (\Lambda'_\sigma; v')$ transition is given by [140,141]

$$\sigma_{exc} (\Lambda_\sigma; v \rightarrow \Lambda'_\sigma; v') = F_{\Lambda\Lambda'}(v, v') G_{\Lambda\Lambda'}(U_n, E) \quad (98)$$

where $F_{\Lambda\Lambda'}(v, v')$ is the Franck-Condon factor, and the function $G_{\Lambda\Lambda'}(U_n, E)$ has the form:

1. Dipole-allowed transitions; case $U_{n+1} - U_n \ll U_n$:

$$G_{\Lambda\Lambda'}(U_n, E) = \frac{\sigma_0}{U_n^2} \left[\frac{E}{(I_n + E)^3} \right]^{1/2} \Gamma(U_n, E) \Delta_n \times \left[1 - \left(\frac{I_n}{E} \right) + \left(\frac{4I_n}{3U_n} \right) \ln(e + \xi_n) \right] \quad (99a)$$

$$\Gamma(U_n, E) = \left(1 - \frac{U_n}{E}\right)^{I_n/(I_n+U_n)}, \xi_n = \left(\frac{E - U_n}{I_n}\right)^{1/2},$$

$$\Delta_n = \begin{cases} E - U_n; & U_n \leq E \leq U_{n+1} \\ U_{n+1} - U_n; & E \leq U_{n+1} \end{cases} \quad (99b)$$

2. Dipole-allowed transitions; case $U_{n+1} - U_n \gtrsim U_n$:

$$G_{\Lambda\Lambda'}(U_n, E) = Q(U_n, E) - Q(U_{n+1}, E) \quad (100a)$$

$$Q(U, E) = \frac{\sigma_0}{U^2} \left[\frac{I_n^2 E}{(I_n + E)^3} \right]^{1/2} \left(1 - \frac{U}{E}\right) \Gamma(U, E) \times$$

$$\times \left[\frac{U}{I_n} + \frac{2}{3} \left(1 - \frac{U}{2E}\right) \ln(e + \xi) \right] \quad (100b)$$

3. Dipole-forbidden transitions:

$$G_{\Lambda\Lambda'}(U_n, E) = \frac{\sigma_0(E - U_n)}{I_n(E + I_n)(E + I_n - U_n)}, \quad U_n \leq E \leq U_{n+1}, \quad (101a)$$

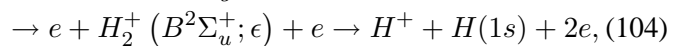
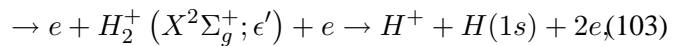
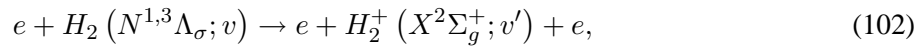
$$= \frac{\sigma_0(U_{n+1} - U_n)}{(E + I_n)(E + I_n - U_n)(E + I_n - U_{n+1})}, \quad E \geq U_{n+1}, \quad (101b)$$

where $\sigma_0 = 6.52 \times 10^{-16} \text{ cm}^2$, $e = 2.71828 \dots$ is the base of natural logarithm, and energies E, U_n, I_n are all expressed in eV units.

The cross sections calculated with the GBB model for excitation processes of atomic and molecular targets [139–141] show that their uncertainty is within a factor of two (or three) for dipole-allowed transitions and higher (up to a factor of five) for dipole-forbidden transitions.

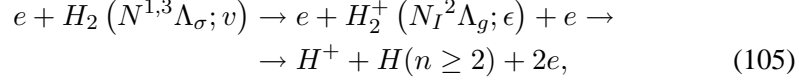
4.3 Ionization processes

The electron-impact ionization of a given $N^{1,3}\Lambda_\sigma(v)$ state of H_2 has three basic channels that involve the ground ($X^2\Sigma_g^+$) and first excited ($B^2\Sigma_u^+$) state of the H_2^+ ion :



where $\epsilon'(\epsilon)$ is the energy of vibrational continuum state.

Dissociative ionization of $H_2(N^{1,3}\Lambda_\sigma; v)$ is also possible by excitation of higher excited states $N_I^2\Lambda_\sigma$ of H_2^+ ion (all of which have repulsive character in the Frank-Condon region of the initial $H_2(N^{1,3}\Lambda_\sigma; v)$ state),



where $H(n)$ is an excited H atom. Below we shall discuss the cross sections for non-dissociative [reaction (102)] and dissociative [reaction (103) - (105)] ionization processes from the ground and excited electronic states of H_2 separately. As mentioned earlier, non-dissociative ionization of $H_2(N^{1,3}\Lambda_\sigma; v)$ can also occur by excitation of an excited state $(N'^{1,3}\Lambda'_\sigma; v')$ the energy of which is smaller than the dissociation energy of $H_2^+(X^2\Sigma_g^+; v=0)$, but above its ground state energy. This excitation-auto-ionization channel for non-dissociation ionization will be discussed in sub-section 4.5

4.3.1 Ionization from the ground electronic state, $X^1\Sigma_g^+(v)$

Accurate cross section measurement for ionization of $H_2(X^1\Sigma_g^+; v=0)$ from its ground electronic and vibrational state have been done both for the non-dissociative and dissociative channels [143–146]. Theoretical calculations have also been performed for all three ionization channels (102) -(104) for $v = 0 - 13$ [147] by using the GBB method (see next sub-section). The experimental dissociative ionization cross section contains contributions from both (103) and (104) channels, which can be separated out by using the theoretical cross sections (properly normalized) of Ref. [147] for $v = 0$. The resulting experimental cross sections for all three ionization channels from $X^1\Sigma_g^+(v=0)$ state of H_2 then can be fitted to the expressions

$$\sigma_{ion}^{ndiss}(^2\Sigma_g^+)_0 = \frac{1.828}{x} \left(1 - \frac{1}{x^{0.92}}\right)^{2.19} \ln(C_0 x) (\times 10^{-16} \text{cm}^2), \quad (106)$$

$$\sigma_{ion}^{diss}(^2\Sigma_g^+)_0 = \frac{0.02905}{x^{1.25}} \left(1 - \frac{1}{x^{2.78}}\right)^{1.886} \times (10^{-16} \text{cm}^2), \quad (107a)$$

$$\sigma_{ion}^{diss}(^2\Sigma_u^+)_0 = \frac{0.5927}{x^{1.20}} \left(1 - \frac{1}{x^{1.22}}\right)^{3.375} \times (10^{-16} \text{cm}^2), \quad (107b)$$

where $C_0 = 2.05\Delta E$, $X = E/\Delta E$, and ΔE is the threshold energy, equal to 15.42 eV, 18.15 eV and 30.6eV for the ionization via the channels (102), (103) and (104), respectively (or for Eqs. (106), (107a), and (107b), respectively, Figure 26 on page 174).

4 Collision Processes of Electrons with Hydrogen Molecules

In the non-dissociative ionization from $X(v = 0)$, the produced H_2^+ ($^2\Sigma_g^+$) ion is vibrationally excited. The population of H_2^+ ($^2\Sigma_g^+; v'$) vibrationally excited states from reaction (102) has been determined experimentally [148] and was found to be very close to that predicted on the basis of Franck-Condon vertical ionization transitions, see Table 25. The cross sections for state-selective ionization transitions $X^1\Sigma_g^+(v = 0) \rightarrow ^2\Sigma_g^+(v')$ are, thus, [see Eq. (92)]

$$\sigma_{ion}^{ndiss} (^1\Sigma_g^+(v = 0) \rightarrow ^2\Sigma_g^+(v')) = F_{0v'} \left[\sigma_{ion}^{ndiss} (^2\Sigma_g^+)_0 + \sigma_{ion}^{diss} (^2\Sigma_g^+)_0 \right] \quad (108)$$

where $F_{0v'}$ is the Franck-Condon factor. The second term in Eq. (108) is by two or more orders of magnitude smaller than the first one and can be neglected. The distribution of $F_{0v'}$ over v' is rather broad with a maximum at $v' = 1 - 3$. The dissociation energies $E_{H_2^+}^{diss}(v')$ of $H_2^+(v')$ levels are also given in Table 25.

The cross sections for non-dissociative ionization from vibrationally excited $X^1\Sigma_g^+(v \geq 1)$ states of H_2 have also been calculated up to $v = 13$ [147]. By normalizing the theoretical $v = 0$ cross section to experimental cross section represented by Eq. (106) in scaled energy units $x = E/\Delta E$, the calculated cross sections of Ref. [147] can be represented in the form

$$\sigma_{ion}^{ndiss} (^2\Sigma_g^+)_v = \left(\frac{\Delta E_{v=0}}{\Delta E_v} \right)^{1.15} \sigma_{ion}^{ndiss} (^2\Sigma_g^+)_0 \quad (109)$$

where ΔE_v is the threshold energy for the initial v -level in $X^1\Sigma_g^+$, and $\sigma_{ion}^{ndiss} (^2\Sigma_g^+)_0$ is given by the expression (106) with $x = E/\Delta E_v$ and $C_0 \rightarrow C_v = 2.05\Delta E_v$. In analogy with Eq. (108), the state-selective $v - v'$ non-dissociative ionization cross section via the $X^1\Sigma_g^+(v) \rightarrow X^2\Sigma_g^+(v')$ transition is given by

$$\sigma_{ion}^{ndiss} (^2\Sigma_g^+)_{v \rightarrow v'} \simeq F_{vv'} \sigma_{ion}^{ndiss} (^2\Sigma_g^+)_v, \quad (110)$$

where $F_{vv'}$ is the Franck-Condon factor and $\sigma_{ion}^{ndiss} (^2\Sigma_g^+)_v$ is given by Eq. (109). The contribution of $\sigma_{ion}^{diss} (^2\Sigma_g^+)_v$ in Eq. (110) has been neglected.

The GBB cross sections for dissociation ionization via the repulsive state $^2\Sigma_u^+$ of H_2^+ from various $v \geq 1$ initial vibrational levels of H_2 ($X^1\Sigma_g^+; v$) [147] can also be represented in a scaled form [149]. By normalizing the $\sigma_{ion}^{diss} (^2\Sigma_u^+)_{v=0}$ cross section of Ref. [147] to the experimental cross section represented by Eq. (107b), and taking the analytic expression (107b) as a basis for the scaling, the cross sections for dissociative ionization due to ionizing transitions $X^1\Sigma_g^+(v) \rightarrow B^2\Sigma_u^+(\epsilon)$ can be given in the form

$$\sigma_{ion}^{diss} (^2\Sigma_u^+)_v = \left(\frac{\Delta E_{v=0}}{\Delta E_v} \right)^{1.96} \sigma_{ion}^{diss} (^2\Sigma_u^+)_0, \quad (111)$$

where ΔE_v is the reaction threshold for the initial v -energy level, and $\sigma_{ion}^{diss} (^2\Sigma_u^+)_0$ is given by Eq. (107b) with $x = E/\Delta E_v$. The transition energies ΔE_v span a

large energy interval: from $\Delta E_{v=0} = 30.6\text{eV}$ to $\Delta E_{v=13} = 14.2\text{eV}$ (see Table 26). The GBB cross sections $\sigma_{ion}^{diss}(^2\Sigma_g^+, ^2\Sigma_u^+)$ of Ref. [147], normalized for $v = 0$ on the experiment [145], have been averaged over the Maxwellian electron velocity distribution, and the resulting rate coefficients fitted to the form [112]

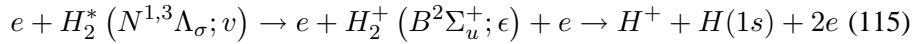
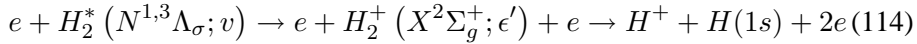
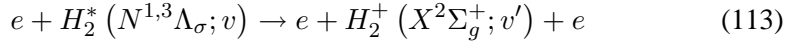
$$\ln \left[K_{ion}^{diss} (^2\Sigma_g^+, ^2\Sigma_u^+)_v \right] = \frac{C_1}{T^{C_2}} + C_3 + C_4 \exp(-C_5 T'), \quad T' = T/10^3, \quad (112)$$

where T is expressed in K , and the coefficients C_i are given in Table 26. The fit (112) is valid in the range $T' = 3K - 200K$.

Ionization of the $H_2(X^1\Sigma_g^+; v)$ molecule may take place via transitions to higher excited states of H_2^+ which all have a repulsive character and dissociate into $H^+ + H(n \geq 2)$ products [reaction (105)]. These states energetically lies significantly above the first ($B^2\Sigma_u^+$) excited states of H_2^+ and the dissociative ionization via these states is expected to have much smaller cross sections than when it proceeds via the ($B^2\Sigma_u^+$) state. The ionization of $H_2(X^1\Sigma_g^+)$ via excitation of doubly excited electronic states of H_2 will be discussed in sub-section 4.5.2.

4.3.2 Ionization from excited electronic states of H_2

There have been no published cross sections results for the ionization processes from excited electronic states of H_2 ,



A rough estimate of the cross sections for these processes can be made by using the GBB model [140, 141]. The cross section for the non-dissociative ionization channel (113) within GBB model is given by:

$$\sigma_{ion}^{ndiss} (^1\Sigma_g^+; v \rightarrow ^2\Sigma_g^+; v') = \frac{\sigma_0}{(\Delta E_{vv'})^2} F_{vv'} G_{ion}(x), \quad (116)$$

$$\sigma_0 = 6.52 \times 10^{-14} \text{cm}^2,$$

$$G_{ion}(x) = \frac{1}{x} \left(\frac{x-1}{x+1} \right)^{3/2} \left\{ 1 + \frac{2}{3} \left(1 - \frac{1}{2x} \right) \ln[e + (x-1)^{1/2}] \right\}, \quad (117)$$

where $\Delta E_{vv'}$ is the transition energy, $x = E/\Delta E_{vv'}$, $F_{vv'}$ is the Franck-Condon factor, and $e = 2.71828\dots$ is the base of natural logarithm. For the dissociation

4 Collision Processes of Electrons with Hydrogen Molecules

ionization processes (114) and (115), the general form of the GBB cross section is [140, 141]

$$\sigma_{ion}^{diss} ({}^1\Sigma_g^+; v \rightarrow {}^2\Sigma^+; \epsilon) = \sigma_0 \int_0^E F_v(\epsilon) g_{ion}(\Delta E_{v\epsilon}, I_v, E) d\epsilon \quad (118)$$

$$g_{ion} = \frac{1}{(\Delta E_{v\epsilon})^2} \left[\frac{E}{(I_v + E)^3} \right]^{1/2} \times \quad (119)$$

$$\times \Gamma(\Delta E_{v\epsilon}, E) \left[1 - \left(\frac{I_v}{E} \right) + \left(\frac{4I_v}{3\Delta E_{v\epsilon}} \right) \ln \xi \right]$$

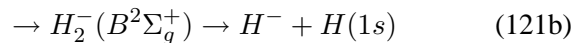
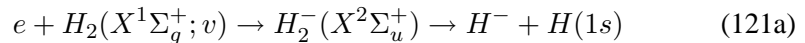
$$\Gamma(\Delta E_{v\epsilon}, E) = \left[1 - \frac{\Delta E_{v\epsilon}}{E} \right]^{I_v/(I_v + \Delta E_{v\epsilon})}, \quad \xi = e + \left(\frac{E - \Delta E_{v\epsilon}}{I_v} \right)^{1/2} \quad (120)$$

where $\Delta E_{v\epsilon} = I_v + \epsilon$, I_v is the ionization potential of $H_2^* (N^{1,3}\Lambda_g; v)$, $\epsilon = \epsilon(R)$ is the energy of $H_2^+ ({}^2\Sigma_{g,u})$ state above the dissociation limit (vibrational continuum), e is the base of natural logarithm and $F_v(\epsilon)$ is the Franck-Condon density for the $(N^{1,3}\Lambda_\sigma; v) \rightarrow ({}^2\Sigma_{g,u}^+; \epsilon(R))$ transition. $F_v(\epsilon)$ can be calculated in various approximations, the simplest of which is the δ -function approximation for the continuum wave-function at the classic turning point $R_{c,v}$ for the $v \rightarrow \epsilon$ vertical transition, $\epsilon(R_{c,v}) = E$. In this case the integral (118) can be evaluated in a straightforward manner.

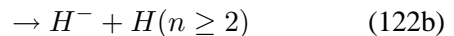
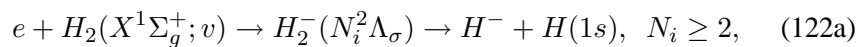
It has to be mention that the reliability of GBB model is not high (it usually overestimates the cross section), and a correction of the cross sections (117), (118) by a constant factor is desirable, provided there is an additional data source (or suitable theoretical arguments) for its determination. Perhaps a significantly better way for an approximate estimate of ionization cross sections from $(N^{1,3}\Lambda_\sigma; v)$ excited state of H_2 would be to approximately scale the corresponding ionization cross sections from $H_2(X^1\Sigma_g^+; v)$ considered in the preceding sub-section (i.e. by a mere change of the value of transition energies $\Delta E_{vv'}$ and $\Delta E_{v\epsilon}$). This scaling approach should be adequate particularly for the higher excited electronic states.

4.4 Dissociative electron attachment

Dissociative electron attachment (DA) on H_2 in the ground electronic state $X^1\Sigma_g^+$ with production of a negative H^- ion can proceed via several channels

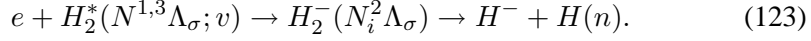


or via



4.4 Dissociative electron attachment

where $H_2^-(\dots)$ is a resonance state of H_2 . This process may, in principle, proceed also when H_2 is initially in an excited electronic state.



Most of the studies of these processes have so far been performed for the reactions (121a), (121b).

4.4.1 Dissociative attachment on $H_2(X^1\Sigma_g^+; v)$

Experimental cross section measurements for dissociative electron attachment have been performed for both the $v = 0$ initial state [150] and $v = 0 - 4$ states [151]. A strong increase of DA cross section was observed with the increase of initial vibrational state. A large number of theoretical cross section calculations have been performed for the reactions (121a) (121b) employing the resonance theory [114] with local [152, 153], semi-local [111, 154] and non-local [155, 156] approximations for the interaction of negative ion state with the continuum. As mentioned in subsection 3.3, for internuclear distances $R \leq R_{s,u} \approx 3.0a_0$ the state $H_2^-(X^2\Sigma_u^+)$ becomes quasi-stationary (shape resonance) and is unstable against auto-detachment. Similarly, the state $H_2^-(B^2\Sigma_g^+)$ becomes quasi-stationary (Feshbach resonance) for $R \leq R_{s,g} = 4.9a_0$, where a_0 is the Bohr radius. The dissociative attachment process takes place only if, during the collision, the system survives in the resonant state before reaching the stabilization internuclear distance R_s . Since the time that the system spends in the decaying quasi-stationary state depends on the reduced mass of nuclei, the DA cross section exhibits a pronounced isotope effect [157]. This effect, however, diminishes for the high initial vibrational states of $H_2(X^1\Sigma_g^+; v)$.

Both local and non-local resonant theory calculations show that the contribution of DA channel via the $B^2\Sigma_g^+$ resonance [reaction (121b)] to the total DA rate coefficient is negligible for all initial v -states, except for the $v = 0$ and $v = 1$ states in the temperature range above ~ 3 eV [158]. However, the total DA rate coefficients for these two initial states are by one (for $v = 1$) or two (for $v = 0$) orders of magnitude smaller than that for $v = 2$. Theoretical calculations also show that the cross sections $\sigma_{DA}({}^2\Sigma_u^+)_v$ for the DA reaction (121a) show sharp peak immediately after the threshold and a fast (exponential) decrease with increasing the collision energy. Therefore, the following analytic fit has been proposed for $\sigma_{DA}({}^2\Sigma_u^+)_v$ [159]

$$\sigma_{DA}({}^2\Sigma_u^+)_v = \sigma_v^{(0)} \exp\left(-\frac{E - |E_{th}|_v}{E_0}\right) \quad (124)$$

where $\sigma_v^{(0)}$ is the peak cross section value for the initial vibrational state v at the threshold $E_{th,v}$, and $E_0 = 0.45$ eV. E and $E_{th,v}$ in Eq. (124) are also expressed in

4 Collision Processes of Electrons with Hydrogen Molecules

eV units, see Figure 27 on page 175. The value of thresholds $E_{th,v}$ and peak cross sections $\sigma_v^{(0)}$ for all initial $v = 0 - 14$ states of H_2 ($X^1\Sigma_g^+; v$) are given in Table 27.

It is to be mentioned that the binding energy of the loosely bound electron in H^- is 0.754 eV and lies below the energy of $v = 10$ vibrational level of H_2 ($X^1\Sigma_g^+$). The DA cross sections for $v \geq 10$ cannot be calculated within the local resonance theory and a non-local approach is necessary. The values $\sigma_v^{(0)}$ in Table 27 have been taken from non-local calculations [156, 158].

On the basis of analytic expression (124) for $\sigma_{DA}({}^2\Sigma_u^+)_v$, one can easily obtain the DA reaction rate coefficient in the form [15]

$$K_{DA}({}^2\Sigma_u^+)_v = 1.972\sigma_v^{(0)} \frac{T^{1/2}}{1 + T/E_0} e^{-\frac{|E_{th,v}|}{T}} \times \left[\frac{|E_{th,v}|}{T} + \frac{1}{1 + T/E_0} \right] (\times 10^{-8} \text{ cm}^3/\text{s}) \quad (125)$$

where T is expressed in eV units, and $\sigma_v^{(0)}$ in units of 10^{-16} cm^2 .

Apart from the $X^2\Sigma_u^+$ and $B^2\Sigma_u^+$ resonances, for which the parent H_2 states are $(1s\sigma_g)^2 X^1\Sigma_g^+$ and $(1s\sigma_g, 2p\sigma_u) b^3\Sigma_u^+$, respectively, many other H_2^- resonances have been observed [160] for which the parent state is one or more bound excited states of H_2 . The energies and widths of many of these resonance states have been calculated to a high accuracy [161] and can be used for calculation of dissociative attachment cross sections within the local potential approximation of resonance theory. However, such calculations have not been performed so far. The DA reactions proceeding via these states may produce either $H^- + H(1s)$ or $H^- + H(n \geq 2)$ products [reactions (122a) and (122b)]. The thresholds for these DA reactions are considerably higher than those proceeding via the $X^2\Sigma_u^+$ and $B^2\Sigma_g^+$ resonances.

4.4.2 Dissociative attachment on electronically excited H_2^* ($N^{1,3}\Lambda_\sigma$)

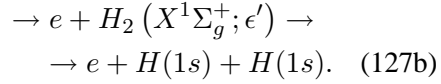
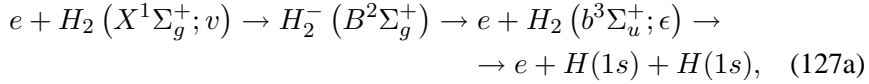
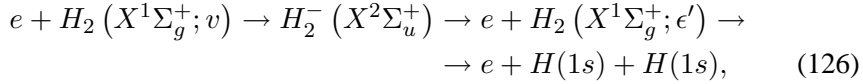
Dissociative attachment can, in principle, also take place on an electronically excited H_2 molecule, reaction (123), particularly when the excited state is a high Rydberg state, ($N \geq 4$). A total rate coefficient value of $\sim 6 \times 10^{-5} \text{ cm}^3/\text{s}$ has been suggested for DA on Rydberg H_2 molecules to explain some observations in laser produced hydrogen plasmas [162]. This extraordinary high value for K_{DA}^{Ryd} , although still controversial, has motivated construction of simple theoretical models for the process (123) [163]. More involved studies of this DA reaction would be obviously of considerable interest.

4.5 Dissociation and ionization of $H_2 (N^{1,3}\Lambda_\sigma)$ via resonant, doubly excited and auto-ionizing states.

4.5 Dissociation and ionization of $H_2 (N^{1,3}\Lambda_\sigma)$ via resonant, doubly excited and auto-ionizing states.

4.5.1 Dissociation of $H_2 ({}^1\Sigma_g^+; v)$ via H_2^- resonant states

The resonant states $H_2^- ({}^2\Sigma_g^+, {}^2\Sigma_u^+)$ formed in a slow electron collision with $H_2 (X^1\Sigma_g^+; v)$ provide the following channels for dissociation of H_2



Cross section calculations for the above dissociation processes have been performed within the local approximation of resonance theory (with semi-empirical parameters of complex potentials of ${}^2\Sigma_g^+$ and ${}^2\Sigma_u^+$ quasi-stationary states) [164], as well as within the non-local resonance theory [165] for $v = 0 - 12$ vibrational states of $H_2 (X^1\Sigma_g^+; v)$. These calculations show that the decay of $B^2\Sigma_g^+$ resonance takes place dominantly onto $b^3\Sigma_u^+$ state, and the cross sections of the channel (127b) are about two orders of magnitude smaller than those of channel (127a) for all v . The results of local and non-local resonance theory calculations agree well with each other, except in the case of lower v -states of the channel (126).

The rate coefficients of dissociation channels (126) and (127a) have been fitted to analytical expression [112]

$$\ln [K_{diss} ({}^2\Sigma_u^+, {}^2\Sigma_g^+)] = \frac{a_1}{T'^{a_2}} + \frac{a_3}{T'^{a_4}} + \frac{a_5}{T'^{2a_6}}, \quad T' = T/10^3, \quad (128)$$

where K_{diss} is expressed in cm^3/s , T in K , and the fitting coefficients a_i are given in Table 28 for $K_{diss} ({}^2\Sigma_u^+)$ and in Table 29 for $K_{diss} ({}^2\Sigma_g^+)$ (see Figures 28, 29 on page 175, 176, respectively). We note that the values of coefficients a_1 in Table 28 for the first few v -states ($v \leq 5$) were somewhat reduced with respect to those given in Ref. [112] in order to bring the rates for these states in conformity with the more accurate cross sections of Ref. [165]. The values of parameters a_i for $K_{diss} ({}^2\Sigma_g^+)$ in Table 29 are given for representative values of v only. The values of a_i for the other initial v -states can be obtained by interpolation.

As discussed at the end of sub-section 4.4.1, there are many H_2^- resonances energetically lying above the $B^2\Sigma_g^+$ resonance that can be excited at higher ($E \gtrsim 11eV$) collision energies [160, 161]. The non-radiative (auto-detachment) decay of

4 Collision Processes of Electrons with Hydrogen Molecules

these resonances to their parent states can lead, as in the case of $X^2\Sigma_u^+$ and $B^2\Sigma_g^+$ lowest resonances, to dissociation either to $H(1s)+H(1s)$ or to $H(1s)+H(n \geq 2)$ atoms. These dissociative processes have not been investigated so far. It should be, however, mentioned that the decay widths of these, higher lying resonances are about an order of magnitude smaller ($\lesssim 0.3eV$) than the widths of $X^2\Sigma_u^+$ and $B^2\Sigma_g^+$ resonances, and their contribution to dissociation may not be large.

4.5.2 Dissociation and ionization of H_2 via doubly excited states

Doubly excited electronic states of H_2 have been studied extensively both experimentally (via photo-ionization [166, 167]) and theoretically [168–170]. The series of states that involve the configurations $(2p\sigma_u, nl\sigma_g)(n \geq 2)$ are designated as $Q_1^1\Sigma_u^+$ -series, and those involving the $(2p\pi_u, nl\sigma_g)$ configurations are termed $Q_2^2\Pi_u$ -series [168]. The energies of $Q_1^1\Sigma_u^+$ doubly excited state lie below the energy of first excited state $B^2\Sigma_u^+(2p\sigma_u)$ of H_2^+ (and for $R \lesssim 4.5a_0$ above the $H_2^+(X^2\Sigma_g^+)$ ground state energy), while the energies of $Q_2^2\Pi_u$ -series lie below the energy of second excited $(2p\pi_u)^2\Pi_u$ state of H_2^+ (and for $R \gtrsim 1.2a_0$ above the energy of $H_2^+(^2\Sigma_u^+)$ state). The $Q_1^1\Sigma_u^+$ and $Q_2^2\Pi_u$ doubly excited states are dissociative auto-ionizing states for which the energies and decay widths have been calculated to high accuracy [169, 170]. The excitation of these states from the ground or an electronically excited bound state of H_2 , leads to the following processes

$$e + H_2(N^{1,3}\Lambda_\sigma) \rightarrow e + H_2^{**}(Q_1^1\Sigma_u^+) \rightarrow e + H_2^+(X^2\Sigma_g^+; v) + e \quad (129a)$$

$$\rightarrow e + H^+ + H(1s) + e \quad (129b)$$

$$\rightarrow e + H(1s) + H(n \geq 2) \quad (129c)$$

$$e + H_2(N^{1,3}\Lambda_\sigma) \rightarrow e + H_2^{**}(Q_2^1\Pi_u) \rightarrow e + H^+ + H(n \geq 2) + e \quad (130a)$$

$$\rightarrow e + H(2s) + H(n \geq 2) \quad (130b)$$

The process (129c) results from the survival of $Q_1^1\Sigma_u^+$ auto-ionizing states in the region $R \lesssim 4.5a_0$. For $R \gtrsim 4.5a_0$ the auto-ionizing width of these states vanishes. Similar is the situation with the channel (130b). Despite of the fact that parameters of auto-ionizing states $Q_1^1\Sigma_u^+$ and $Q_2^1\Pi_u$ are available as function of internuclear distance R , cross section calculations for the processes (129a), (129b), (129c) and (130a), (130b) have not been performed as yet. It is worthwhile to mention that the photo-ionization cross section from the ground state $X^1\Sigma_g^+(v=0)$ of H_2 shows that the non-dissociative channel (129a) accounts for about 95% of the total cross section [166, 167].

4.5.3 Auto-ionization and pre-dissociation of excited electronic states

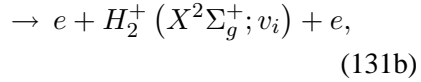
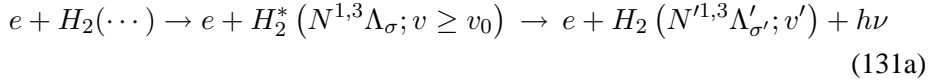
Singly excited bound electron state $(N^{1,3}\Lambda_\sigma; v)$ of H_2 , especially when N is high, may be subject to two decay processes: auto-ionization and pre-dissociation. Both

4.5 Dissociation and ionization of H_2 ($N^{1,3}\Lambda_\sigma$) via resonant, doubly excited and auto-ionizing states.

these processes result from the non-adiabatic coupling of electronic states induced by the kinetic energy operator of nuclear motion.

A Auto-ionization

When the vibrational energy of a singly excited bound electronic state ($N^{1,3}\Lambda_\sigma; v$) of H_2 becomes higher than the ionization energy of that state on its ground vibrational level, then the state becomes unstable against auto-ionization. In contrast to the case of doubly excited states of H_2 , or resonances H_2^- , where the configuration interaction with electronic continuum is responsible for the quasi-stationary character of the state, in the present case it is likely that the non-adiabatic coupling of electronic and nuclear motion is the principal mechanism for auto-ionization [171, 172]. Already the majority of singlet and triplet states with $N = 4$ (e.g., the O, B'', R, S singlets and k, p, r, s triplets) become auto-ionizing for $v \geq 4$. For the higher- N states, only a limited number of vibrational states remains stable against auto-ionization. The electron impact excitation of the states ($N^{1,3}\Lambda_\sigma; v > v_0$), where v_0 is the last stable vibrational state of $N^{1,3}\Lambda_\sigma$, thus, are subject to two competing decay processes: radiative decay to the lower states, and auto-ionization



where $H_2(\dots)$ may be either the ground or an excited electronic state of H_2 .

Radiative decay rates of $H_2^*(N^{1,3}\Lambda_\sigma)$ state are of the order of magnitude $10^7 - 10^8 s^{-1}$ and decrease as N^{-3} with increasing N . Calculations of auto-ionization rates $W_{AI}(N, v; v_i)$ for $(Np\sigma_u\Sigma_u^+; v)$ and $(Np\pi_u\Pi_u; v)$ excited states with $N = 4 - 10$ have been performed for different $v > v_0$ vibrational levels [172]. For a given value of v , $W_{AI}(N, v; v_i)$ decreases (approximately) as N^{-3} with increasing N , and decreases strongly with increasing the difference $|v - v_i|$. For a given N , however, W_{AI} increases with the increase of v . The typical maximum (for $|v - v_i| = 1$) values of W_{AI} for the states $N = 4 - 10$ are in the range $10^6 - 10^7 s^{-1}$ for $N = 4, 5$ to $10^{11} s^{-1}$, for $N = 9, 10$. The available auto-ionization rates for all H_2 Rydberg series are collected in Ref. [173].

B Pre-dissociation

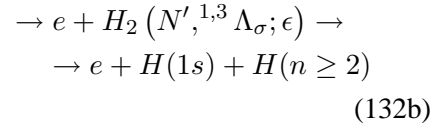
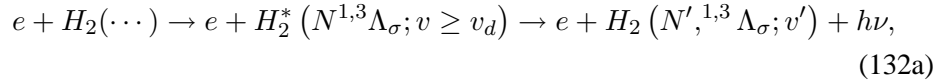
When the energy of a bound excited state ($N^{1,3}\Lambda_\sigma; v$) lies above the dissociation limit of the energetically nearest lower excited state ($N'^{1,3}\Lambda'_{\sigma'}$), (e.g., for $v \geq v_d$), the non-adiabatic coupling of the two electronic states due to nuclear motion can induce a transition ($N^{1,3}\Lambda_\sigma; v \geq v_d$) \rightarrow ($N'^{1,3}\Lambda'_{\sigma'}; \epsilon'$) leading to dissociation. The

4 Collision Processes of Electrons with Hydrogen Molecules

closer the energies of $(N^{1,3}\Lambda_\sigma; v > v_d)$ and $(N'^{1,3}\Lambda_\sigma; \epsilon)$ states, the stronger is the non-adiabatic coupling between them. Non-adiabatic coupling between considered states can be induced either by the rotational nuclear motion (rotational coupling) or radial (vibrational) nuclear motion (radial coupling). For the $(N\lambda\mu; ^{1,3}\Lambda_\sigma)$ and $(N'\lambda'\mu'; ^{1,3}\Lambda'_{\sigma'})$ molecular states these two couplings are subject to the selection rules: $\Delta\mu = 0, \Delta\sigma = 0$ for the radial coupling, and $\Delta\mu = \pm 1, \Delta\sigma = 0$ for the rotational coupling, where μ is the projection of angular momentum λ of excited electron on the internuclear axis. (Additional selection rules in the case of rotational coupling exist for the change of rotational quantum number [174]). The spin multiplicity of the state is also conserved in a non-adiabatic transition.

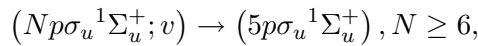
It should be mentioned that the excited states (of a given spin multiplicity) with the same principal quantum number N all have potential energy curves that lie very close (quasi-degenerate) to each other in the internuclear distance region of their repulsive parts. For $N \geq 4$, this is true also for any neighbouring $(N, N \pm 1)$ pairs of states. Therefore, the non-adiabatic transitions are expected to be strong between all the neighbouring states with $N \geq 3$ when they satisfy the selection rules.

The electron-impact excitation of a bound electronic state $(N^{1,3}\Lambda_\sigma; v > v_d)$ is subject to both pre-dissociation and radiative decay to the lower states,

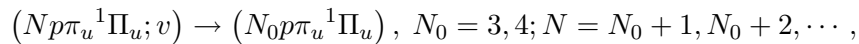


The pre-dissociation of many excited states (upon their electron-impact excitation) has been observed experimentally [119, 175, 176]. It has been found that $(D^1\Pi_u; v \geq 3)$ states rapidly pre-dissociate via the $B^1\Sigma_u^+$ state, with a pre-dissociation branching ratio of 55% for $v = 3$, 80% for $v = 6$ and 100% for $v \geq 8$ [119]. The states $(D'^1\Pi_u; v \geq 1)$ and $(B''^1\Sigma_u^+; v \geq 1)$ also rapidly pre-dissociate via $B^1\Sigma_u^+$, with the pre-dissociation branching ratio in the latter case being 90 – 100% already for $v = 1$ [119]. The pre-dissociation of $(d^3\Pi_u; v \geq 3)$ via $e^3\Sigma_u^+$ is also known to be fast [126].

Calculation of rates for



and



pre-dissociative transitions for $v \geq v_d$, have been performed in Ref. [172]. The results of these calculations show that the pre-dissociation rate $W_{PD}(N_0, N, v)$

4.6 The metastable ($c^3\Pi_u; v = 0$) state

does not change considerably with increasing v , but decreases rapidly when the difference $(N - N_0)$ increases. The pre-dissociation rates for $(N_0 + 1) \rightarrow N_0$ transitions are about $5 \times 10^9 s^{-1}$, $3 \times 10^{12} s^{-1}$ and $5 \times 10^{12} s^{-1}$ for $N_0 = 3, 4$ and 5 , respectively. Although not calculated in [172], one can nevertheless, plausibly assume (on the basis of the higher degree of energy quasi-degeneracy) that the rates of $N^{1,3}\Lambda_\sigma \rightarrow N^{1,3}\Lambda'_\sigma$ pre-dissociation transitions should be higher than those for the $N^{1,3}\Lambda_\sigma \rightarrow (N - 1)^{1,3}\Lambda'_\sigma$ transitions. The pre-dissociation rates for many H_2 Rydberg series can be found in Ref. [173].

In the case of $v_d \geq v_0$, when both pre-dissociation and auto-ionization are possible, pre-dissociation is normally the dominant decay channel. However, since $W_{PD}(N, v)$ is almost independent on v , whereas $W_{AI}(N, v)$ may significantly increase with v , there may be cases where the two decay channels effectively compete [172, 173].

It should be noted that the non-adiabatic coupling between the neighbouring quasi-degenerate molecular states is not limited only to the states with $v \geq v_d$. It may also take place for $v < v_d$, becoming a mechanism for excitation transfer, $(N^{1,3}\Lambda_\sigma; v) \rightarrow (N^{1,3}\Lambda'_\sigma; v')$. This process, obviously important for the distribution of excitation energy among the excited states, has not been studied as yet. The non-adiabatic coupling between a dissociating state ($N^{1,3}\Lambda_\sigma; \epsilon$) and a bound state ($N^{1,3}\Lambda'_\sigma; v'$) may impede the dissociation by populating that bound state (inverse pre-dissociation).

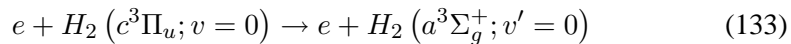
4.6 The metastable ($c^3\Pi_u; v = 0$) state

The state ($2p\pi_u, c^3\Pi_u; v = 0$) lies energetically below the $v = 0$ level of the ($2s\sigma_g, a^3\Sigma_g^+$) state, and there are no other triplet states of *gerade* symmetry lying energetically below it to which it can be optically coupled. This state is coupled to the ground $X^1\Sigma_g^+$ state by magnetic-dipole and electric-quadrupole interactions with a transition probability of $10^{-3} s$ [177]. Because of the large energy separation of ($c^3\Pi_u; v = 0$) and $b^3\Sigma_u^+$ states, their non-adiabatic coupling is extremely weak, and the predissociation decay of ($c^3\Pi_u; v = 0$) via $b^3\Sigma_u^+$ is not possible. The state ($c^3\Pi_u; v = 0$) is, therefore, metastable with a lifetime of $1ms$. The ($c^3\Pi_u; v \geq 1$) states are optically coupled to ($a^3\Sigma_g^+; v'$) states, but the corresponding transition probabilities are nevertheless small ($\sim 10^4 s^{-1}$) [177].

In a detailed description of radiative-collisional kinetics of H_2 processes in a plasma, it might be necessary to single-out the ($c^3\Pi_u; v = 0$) state and treat it as a separate plasma constituent [178]. Then, its collision processes with other plasma constituents have to be known. The most important of them are discussed below.

4.6.1 Electron-impact excitation from ($c^3\Pi_u; v = 0$)

The excitation cross section for the transition



4 Collision Processes of Electrons with Hydrogen Molecules

is expected to be very large in view of the small energy difference $\Delta E_{00} = 0.017$ eV between these two states. The cross section for reaction (133) has been calculated both in the first Born and distorted wave approximations [179], the latter being by a factor of about two larger than the Born results in the energy region of cross section maximum ($E_m \sim 5\Delta E_{00}$). The distorted wave cross section can be fitted to the expression

$$\sigma_{exc}(c^3\Pi_u; v=0 \rightarrow a^3\Sigma_g^+; v'=0) = \frac{2.08}{x^{1.20}} \left(1 - \frac{1}{x}\right)^{3.80} (\times 10^{-11} \text{cm}^2) \quad (134)$$

where $x = E/\Delta E_{00}$ (with E in eV). It has a maximum of $\simeq 1.3 \times 10^{-12}$ at $E \simeq 0.07$ eV, Figure 30 on page 176. The cross sections for $(c^3\Pi_u; v=0) \rightarrow (a^3\Sigma_g^+; v' \geq 1)$ transitions can be estimated from Eq. (134) by using there $x = E/\Delta E_{0v'}$, and multiplying it with the Franck-Condon factor $F_{0v'}$. The values of $F_{0v'}$, however, decrease very rapidly with v' prime; for $v' = 1, 2, 3$ they are 3.9×10^{-2} , 2.7×10^{-3} and 2.0×10^{-6} , respectively [177]. We note that the $a^3\Sigma_g^+$ state is radiatively coupled to the dissociating $b^3\Sigma_u^+$ state with a transition probability of $\sim 10^8 \text{s}^{-1}$.

The cross sections for electron-impact excitation transitions $(c^3\Pi_u; v=0) \rightarrow (h^3\Sigma_g^+; v)$, $(g^3\Sigma_g^+; v)$ have been calculated in Ref. [142]. Their maxima, of about $\sim 10^{-16} \text{cm}^2$, occur at $E \sim 4 - 6$ eV, and are, thus, for more than two orders of magnitude smaller than the cross section for $(c^3\Pi_u; v=0) \rightarrow (a^3\Sigma_g^+; v'=0)$ transition at these energies. The cross sections for other excitation transitions from $(c^3\Pi_u; v=0)$ are expected to be even smaller.

4.6.2 Ionization of $(c^3\Pi_u; v=0)$ state

There have been no cross section calculations for the ionization of $(c^3\Pi_u; v=0)$ state. A rough estimate of this cross section can be made by using the GBB model described in sub-section 4.3.2. At the energy of its maximum ($E \simeq 18 \text{eV}$), the GBB ionization cross section for the state $(c^3\Pi_u; v=0)$ is $\simeq 5.5 \times 10^{-16} \text{cm}^2$, and is ten times smaller than the value of cross section for the excitation reaction (133) at this energy. (As discussed in section 4.3.2, GBB model usually overestimates the ionization cross section.)

4.6.3 Electron attachment on $(c^3\Pi_u; v=0)$ state

There are several H_2^- resonances that energetically lie close to the potential energy curve of $c^3\Pi_u$ state, and for which this state alone, or in combination with other neighbouring states (such as $a^3\Sigma_g^+$, $B^1\Sigma_u^+$, $c^1\Pi_u$, E , $F^1\Sigma_g^+$), appears as a parent (co-parent) state [161]. The incident electron can temporarily be captured to these quasi-stationary states, which decay along the following channels

$$e + H_2(c^3\Pi_u; v=0) \rightarrow H_2^-(\dots) \rightarrow e + H(1s) + H(n \geq 2) \quad (135a)$$

$$\rightarrow H^- + H(n \geq 2) \quad (135b)$$

$$\rightarrow e + H_2(\bar{N}^{1,3}\bar{\Lambda}_\sigma) \quad (135c)$$

where $(\bar{N}^{1,3}\bar{\Lambda}_\sigma)$ is a co-parent (with $c^3\Pi_u$) state for the resonance H_2^- . In the quasi-classical approximation for the nuclear motion, and introducing an average value $\bar{\Gamma}$ for the resonance width, the cross section of reactions (135a), (135b), (135c) can be represented in the form [114, 157]

$$\sigma_\lambda = \sigma_0 \frac{\bar{\Gamma}}{E} P_\lambda(\bar{\Gamma}) \quad (136)$$

where σ_0 is a constant characterizing the electron "capture" to the H_2^- state and $P_\lambda(\bar{\Gamma})$ is the probability for the exit channel λ in Eq. (135a), (135b), (135c). For instance, for the dissociative attachment channel (135b), $P_\lambda = P_{da}$ is the survival probability of the resonance before the stabilization internuclear distance R_s (defined by $\Gamma(R \geq R_s) = 0$) is reached by the system, i.e.

$$P_{da} = \exp(-a\bar{\Gamma}) \quad (137)$$

where a is a constant that depends on the energy of resonant state. For the dissociation and relaxation processes (135a) and (135c), $P_\lambda = f_\lambda(1 - P_{da})$, with $f_\lambda((135a)) + f_\lambda((135c)) = 1$. The average values of $\bar{\Gamma}$, for the resonances connected with $c^3\Pi_u$ parent (or co-parent) state, are in the range 0.1 – 0.3 eV. With the typical values for a ($\sim 1a_0$) and σ_0 ($\sim a_0^2$), Eqs. (136) and (137) then give a dissociative attachment cross section ($\bar{\Gamma} = 0.2$ eV) $\sigma_{da} \simeq 4.58/E(\times 10^{-18} \text{ cm}^2)$. A similar value for σ_{da} was obtained in [180] by a more detailed analysis of the dominant ($\bar{\Gamma} = 0.3$ eV) H_2^- resonance based upon the $c^3\Pi_u$ state.

In conclusion, it appears that the excitation process (133) is the only important process which needs to be taken into account when including the metastable state ($c^3\Pi_u; v=0$) explicitly in the kinetics.

5 Collision Processes of Protons with Hydrogen Molecules

Collision processes of protons with hydrogen molecules have been much less studied than electron impact processes. At low collision energies, the dynamics of these processes is rather complex because of the coupling of electronic and nuclear motions. The presence of charge exchange channels in the $H^+ + H_2(N^{1,3}\Lambda_{\sigma}; v)$ collision system unavoidably introduces the vibrational states of H_2^+ ion into collisional dynamics. Moreover, for collision energies below $\approx 3 - 4$ eV the collision complex $[H^+ + H_2(v)]$ supports long-lived intermediary states that relax in

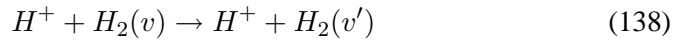
5 Collision Processes of Protons with Hydrogen Molecules

heavy-particle rearrangement (reactive collisions). Even when the H_2 molecule is in its ground electronic state, there appear strong non-adiabatic couplings between vibronic adiabatic states of the system. The $[H^+ + H_2(X^1\Sigma_g^+; v)]$ asymptotic configuration becomes energetically quasi-resonant with the asymptotic configuration $[H(1s) + H_2^+(X^2\Sigma_g^+; v')]$ for any $v \geq 4$ which results in series of strong couplings between all vibronic states of the system, including the $H_2(X^1\Sigma_g^+; \epsilon)$ and $H_2^+(X^2\Sigma_g^+; \epsilon')$ continua.

The existing experimental studies of collision processes in $H^+ + H_2$ system are related only to H_2 in its ground electronic and vibrational state, $(X^1\Sigma_g^+; v = 0)$, while theoretical studies include also vibrationally excited states of $H_2(X^1\Sigma_g^+)$. In the sub-sections that follow, we shall discuss the available cross section information for vibrational excitation, charge transfer, dissociation and ionization in proton collisions with $H_2(X^1\Sigma_g^+; v)$ only. When appropriate, however, we shall give some comments on the corresponding cross sections when H_2 is in an electronically excited state. For simplicity, we shall omit in reaction equations the spectroscopic symbols $(X^1\Sigma_g^+)$ and $(X^2\Sigma_g^+)$ for the ground electronic states of H_2 and H_2^+ , respectively.

5.1 Vibrational excitation

The vibrational excitation processes



have been studied experimentally [181, 182] only for the $v = 0$ initial vibrational state. Close-coupling theoretical cross section calculations have been performed by using the quantal infinite order sudden approximation (IOSA) for $v = 0$ state [183, 184], as well as for $v \geq 0$ states [185, 186], in the collision energy range from threshold to 100 eV (≈ 10 eV in [186]). While in Refs. [183–186], the expansion basis has been limited to $v, v' \leq 9$ states, in Ref. [186] all discrete vibrational states corresponding to the asymptotic configurations $H^+ + H_2(v)$ (15 states) and $H + H_2^+(v')$ (19 states), and a large number (about 850) discretized continuum states have been included in the expansion basis of the IOSA close-coupling scheme.

The cross sections for vibrational excitation show a structure with two maxima, the first of which appears immediately after the threshold. The second, much broader maximum appears at higher ($\approx 40 - 60$ eV) energies. The theoretical and experimental cross section data from Refs. [185, 186], and [181, 182], respectively, for the excitation transitions $v = 0 \rightarrow v' = 1 - 4$ can be fitted to the analytic expressions (see Figure 31 on page 177)

$$\sigma_{exc}(0 \rightarrow v') = \sigma^<(0 \rightarrow v') + \sigma^>(0 \rightarrow v') \quad (139)$$

5.1 Vibrational excitation

$$\sigma^{<}(0 \rightarrow v') = \frac{a_1 \exp(-a_2/E^{a_3}) \chi(E - E_{0v'})}{E^{a_4}} (\times 10^{-16} \text{ cm}^2) \quad (140a)$$

$$\sigma^{>}(0 \rightarrow v') = \frac{b_1 \exp(-b_2/E^{b_3})}{E^{b_4}(1 + b_5 E^{b_6})} (\times 10^{-16} \text{ cm}^2) \quad (140b)$$

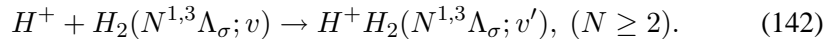
where E is in the proton impact (laboratory) energy (in eV units), $E_{0v'}$ is the threshold energy in the laboratory reference system ($E_{0v} = 1.5E_{th,cm}$), and $\chi(E - E_{0v}) = 1$ for $E \geq E_{0v}$, and $= 0$ for $E < E_{0v}$. The values of E_{0v} and fitting parameters a_i and b_i in Eqs. (140) are given in Table 30. In this table also given are the cross section fit parameters for the excitation of $v' = 5 - 7$ states. The b_i parameters for $\sigma^{>}(0 \rightarrow v' = 5 - 7)$ have been determined on the basis of observed scaling of $\sigma^{>}(0 \rightarrow v' \leq 4)$ cross sections. For the transitions $v = 0 \rightarrow v' \geq 8$, a rough estimate of the cross sections can be obtained by using the scaling relations

$$\begin{aligned} \sigma^{<}(0 \rightarrow v' \geq 8) &\approx \left(\frac{E_{exc,7}}{E_{exc,v'}} \right)^2 \sigma^{<}(0 \rightarrow 7; E') \\ \sigma^{>}(0 \rightarrow v' \geq 8) &\approx \frac{1}{12^{(v'-7)}} \sigma^{>}(0 \rightarrow 7; E') \end{aligned} \quad (141)$$

where $E' = (E_{exc,v'}/E_{exc,7})E$, and $E_{exc,v'}$ is the excitation energy of the v' vibrational state (see Table 23). The comparison of proton-impact vibrational excitation cross sections of $H_2(v = 0)$ with those of electron impact (via the H_2^- resonant states; see sub-section 4.1.1) shows that for a given $0 \rightarrow v'$ transition the $\sigma^{<}(0 \rightarrow v')$ cross section is more than an order of magnitude larger than the corresponding electron-impact cross section in the energy region below 10 eV. This difference increases for $E > 10$ eV, since the cross section component $\sigma^{<}(0 \rightarrow v')$ is absent in electron-impact vibrational excitation.

Proton impact excitation (and de/excitation) cross sections for higher initial vibrationally excited states of H_2 have not been published in the literature. Such cross sections have been, however, calculated within the IOSA close coupling formalism (see [185, 186]) for collision energies below ~ 10 eV. These data are stored in the Oak Ridge National Laboratory atomic database and can be accessed via Internet (see Ref. [19]). It appears that for a given value $|v' - v| = \Delta v$ of the change of initial vibrational state, the de-excitation cross section is comparable to (or larger than) the excitation cross section.

As mentioned in the introductory part of this section, no studies exist for the vibrational excitation of electronically excited states of H_2 by proton impact,



Theoretical description of this process at low collision energies would require simultaneous inclusion in the treatment of (at least) several electronic states (close in energy to $N^{1,3}\Lambda_\sigma$, together with their complete vibrational spectra. The solution of this problem is obviously beyond the presently available computational

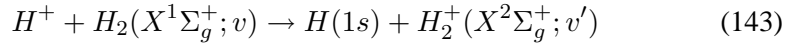
5 Collision Processes of Protons with Hydrogen Molecules

capabilities. Having in mind the remark that the cross sections for proton-impact de-excitation are comparable to those for excitation for a given amount of change Δv of initial vibrational state v , one can perhaps plausibly assume that the vibrational population of excited electronic states of H_2 is close to the Boltzmann distribution for a given plasma temperature and avoid the explicit consideration of collision processes of type (142) in the plasma kinetic modelling.

5.2 Charge transfer processes

5.2.1 Proton charge exchange with $H_2(X^1\Sigma_g^+; v)$

The charge transfer (or charge exchange) reactions



convert the atomic ions into molecular ones and, for $v \geq 4$, may play an important role in low-temperature plasma recombination. This is due to the facts that for $v \geq 4$ reactions (143) are exothermic (and quasi-resonant), and that dissociative electron recombination with H_2^+ is a much faster process (see sub-section 7.1) than the radiative and three-body recombination at low plasma temperatures (and not too high plasma densities).

There have been numerous experimental studies of the charge transfer process (143) with H_2 in its ground vibrational state (or with unknown distribution over the lower vibrationally excited states) and unspecified vibrational state of the H_2^+ product ion [187–190], covering the energy range from threshold to several hundreds keV. These studies are supplemented by a similarly large number of theoretical studies employing different models for the collision dynamics [186, 191–196]. The cross section for this process is, thus, considered to be well established with a high (10 – 20%) accuracy [11, 12]. State selective ($v \rightarrow v'$) cross section calculations for the reaction (143) have been performed in the low-energy region within the IOSA close-coupling formalism [186, 191, 192] ($E \lesssim 10$ eV) and by using the classical trajectory- surface-hopping (CTSH) method [195, 196] ($E \leq 20$ eV). For the initial $v = 1$ state, the total (summed over v') charge exchange cross section is also available from Ref. [193] in the energy range 50 eV - 4 keV. It should be noted that both the IOSA and CTSH methods can resolve the contribution of particle exchange channel in the state selective (or total) charge transfer cross section. This contribution becomes increasingly important with decreasing the collision energy below ~ 5 eV, especially for the higher excited states [195].

The vibronic non-adiabatic coupling affects the dynamics of charge transfer process only at relatively low collision energies (below $\sim 100 - 300$ eV); for energies $\sim 0.5 - 1$ keV, the collision dynamics is determined dominantly by the pure electronic couplings. This is reflected in the sensitivity of magnitude and energy behaviour of charge transfer cross section on initial (and final) vibrational state. This sensitivity is particularly pronounced for the initial vibrational states for which the reaction is endothermic ($v \leq 3$), and for slightly or moderately

exothermic channels ($v = 4 - 6$). As a consequence of the two mechanisms for the process, prevailing respectively at low and high energies, the cross sections for $v \leq 6$ exhibit a structure with two maxima. For $v \geq 6$, the cross sections attain a typical quasi-resonant ($v = 6 - 8$) or resonant ($v \geq 9$) energy behaviour. We shall now separately discuss the initial state ($v-$) and $v - v'$ resolved charge transfer cross sections .

A Initial v -state resolved cross sections

The total (summed over v') charge exchange cross section for a given initial vibrational state v , σ_v^{CX} , can be constructed by a critical assessment of all available experimental (for $v = 0$ only) and theoretical data. The theoretical data for $v \geq 1$ from Ref. [186, 192] (IOSA) and Ref. [195, 196] (CTSH) are generally consistent with each other, except for the first few v -states, for which preference must be given to the IOSA results. As mentioned earlier, for energies above 20 – 25 keV, the vibrational excitation of H_2 is not expected to play any role in the collision dynamics and all σ_v^{CX} cross sections should converge to that for $v = 0$ (known from experiments; see [11, 12]). Keeping in mind the above discussed two-maxima structure of σ_v^{CX} cross sections for $v \lesssim 6$, we represent σ_v^{CX} by the analytical expression

$$\sigma_v^{CX}(E) = \sigma_v^<(E) + \sigma_v^>(E), \quad (144)$$

$$\sigma_v^<(E) = a_1 E^{a_2} \left[1 - \left(\frac{E_{0v}}{E} \right)^{a_3} \right]^{a_4} \exp(-a_5 E^{a_6}) (\times 10^{-16} \text{ cm}^2), \quad (145a)$$

$$\sigma_v^>(E) = \frac{b_1 \exp(-b_2/E^{b_3})}{b_4 E^{b_5} + b_6 E^{b_7} + b_8 E^{b_9} + b_{10} E^{b_{11}}} (\times 10^{-16} \text{ cm}^2), \quad (145b)$$

where E is the proton impact (laboratory) energy (in eV units), E_{0v} is the threshold energy in the laboratory reference frame ($E_{0v} = 1.5E_{th,cm}$), and a_i and b_i are fitting parameters, see Figure 32 on page 177. The values of parameters a_i and b_i for initial states $v = 0 - 8$ are given in Table 31. For the $v \geq 9$ initial states, the cross sections $\sigma_v^{CX}(E)$ are given by

$$\sigma_{v \geq 9}^{CX}(E) = \frac{27.0 f(v)}{E^{0.033} + 9.85 \times 10^{-10} E^{2.16} + 1.66 f(v) \times 10^{-25} E^{5.25}} (\times 10^{-16} \text{ cm}^2) \quad (146)$$

$$f(v = 9) = 1, f(v \geq 10) = 1.97/(v - 8)^{1.23}. \quad (147)$$

The validity of analytical representations (144) -(147) for $\sigma_v^{CX}(E)$ extends from thermal (or threshold, for $v \leq 3$) to ~ 200 keV energies. The small negative values of parameter b_5 for $v = 4 - 8$ in Table 31 indicate the quasi-resonant character of these reactions, while the small positive value (0.033) of the corresponding term in the denominator of Eq. (146) indicates the pure resonant character of charge exchange reactions (143) for $v \geq 9$ at low collision energies.

5 Collision Processes of Protons with Hydrogen Molecules

B $v - v'$ resolved charge exchange cross sections

State selective ($v - v'$ resolved) charge transfer cross sections for reaction (143) have been calculated in Ref. [186] (IOSA) for all initial v -states, and in Ref. [196] (CTSH) for $v = 0 - 6$. These calculations cover the energy range from threshold to ~ 10 eV. The v' -populations of product H_2^+ ion for a given initial v

$$P_v(v') = \frac{\sigma_{vv'}^{CX}}{\sigma_v^{CX}} \quad (148)$$

are different for endothermic ($v \leq 3$) and exothermic ($v \geq 4$) charge exchange reactions. For endothermic reactions, $P_v(v')$ weakly depends on collision energy (at least in the energy interval covered by the calculations) and is close to the v' -distribution of Franck-Condon factors, $F_{vv'}$. For exothermic reactions, $P_v(v')$ exhibits a sharp peak at the v' level which energetically is in (quasi-) resonance with the initial v -level. The quasi-resonant condition is defined by the equality (or near-equality) of dissociation energies of v and v' levels,

$$E_v^{diss}(H_2) \approx E_{v'_0}^{diss}(H_2^+). \quad (149)$$

The distribution $P_v(v')$ rapidly decreases with the departure of v' from the quasi-resonant level v'_0 . The values of $E_v^{diss}(H_2)$ are given in Table 32. In this table are also given the quasi-resonant v'_0 levels and the values of corresponding "resonant energy defects", $\Delta E_{v,v'_0} = |E_v^{diss}(H_2) - E_{v'_0}^{diss}(H_2^+)|$. The distribution $P_v(v')$ has a Gaussian form (centered at $v' = v'_0$), and shows a (relatively weak) dependence on collision energy E : with increasing E the distribution broadens and, consequently, its peak value decreases. $P_v(v')$ can, therefore, be represented in the form

$$P_v(v') = \frac{A}{E^{1/4}} \exp \left[-a \frac{\Delta E_{vv'}}{E^{1/2}} \right] \quad (150)$$

where A and a are constants (A is the normalization constant), E is the collision energy and $\Delta E_{v,v'} = |E_v^{diss}(H_2) - E_{v'}^{diss}(H_2^+)|$. It should be noted that the exponent in Eq. (150) has the same form as the Massey exponent in the probability for inelastic transitions in slow atomic collisions [5, 6].

The calculated $\sigma_{vv'}^{CX}$ cross sections [186, 196] show that for $v \geq 4$, the population of v'_0 and $v'_0 \pm 1$ levels accounts for 90% of σ_v^{CX} for $E \lesssim 5$ eV, and about 80% for $E \sim 10$ eV.

5.2.2 Proton charge exchange with $H_2(N^{1,3}\Lambda_\sigma; v)$, $N \geq 2$

Charge exchange in proton collisions with electronically excited H_2 molecules have not been studied so far. Yet, the analogy with proton-excited hydrogen atom collisions (see sub-section 2.2.3) suggests that the charge exchange cross section in such collisions should be large. The electron binding energy of an electronically excited state ($N^{1,3}\Lambda_\sigma; v$) in its ground vibrational state ($v = 0$) is close

5.3 Proton impact dissociation of H_2

to the electron binding energy of the corresponding hydrogen atom excited state. For example, the binding energies of ($3^{1,3}\Lambda_\sigma, v = 0$) H_2 states are distributed in the interval 1.418 eV - 2.204 eV, while the binding energy of $n = 3$ hydrogen atom level is 1.512 eV. With increasing N , the spread of electron binding energies of ($N^{1,3}\Lambda_\sigma; v = 0$) states rapidly decreases and its centroid energy converges towards the energy of corresponding atomic n -level.

The achieved energy resonance for the high N ($v = 0$) and n levels is, however, destroyed when the ($N^{1,3}\Lambda_\sigma; v \geq 1$) states are considered. Thus, in general, the charge exchange problem in $H^+ + H_2(N^{1,3}\Lambda_\sigma; v)(N \geq 2)$ collisions reduces to the case of quasi-resonant charge exchange.

For rough estimates of the cross section of quasi-resonant charge exchange reactions one can make use of developed two or multi-state models of atomic collision theory [5, 6]. Additional assumptions (or approximations) can be adopted to account for the multitude of states within the N -manifold (having also different spin multiplicities), such as energy degeneracy, same electron exchange interactions, closure of Franck-Condon factors for $H_2(v) \rightarrow H_2^+(v')$ transitions when summed over v' , etc.

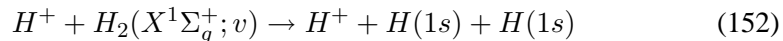
For the states with sufficiently high N (e.g., $N \geq 4$), one can also employ the classical over-barrier transition model (see sub-section 2.2.3), which, when adapted to the present (molecular) case, gives [see Eq. (45)]

$$\sigma_{CX}^{OBM}(N \geq 4) \simeq \frac{1.77N^{*4}}{1 + 0.42\tilde{E}^{0.2} + 0.52\tilde{E}^{0.5}} (\times 10^{-15} \text{ cm}^2) \quad (151)$$

where $\tilde{E} = N^{*2}E$ (in units of keV/amu), N^* is the effective principal quantum number defined by the relation $E_{N,v} = \frac{13.6}{N^{*2}}$ eV, where $E_{N,v}$ is the ionization energy of the ($N^{1,3}\Lambda_\sigma; v$) state. The validity of Eq. (151) is limited to $\tilde{E} \leq 5$ keV/amu. The cross section (151) is a sum over the vibrational levels of the H_2^+ product ion.

5.3 Proton impact dissociation of H_2

All experimental studies of proton impact dissociation of H_2 have been performed for the ground electronic and vibrational state of the H_2 molecule, and at high collision energies (see e.g., [12]). There have been, however, two recent theoretical studies of proton impact dissociation from vibrationally excited molecules



performed by the CTSH method [195] (for $E_{CM} < 20$ eV) and within IOSA close-coupling formalism [197] (for $E_{CM} \lesssim 10$ eV). Cross sections have been reported for all $v = 0 - 14$ initial states. The quantum-mechanical study of reaction (152) [197] has revealed that the promotion of the system into the vibrational continuum is due to a number of series of non-adiabatic couplings, connecting pair-wise the

5 Collision Processes of Protons with Hydrogen Molecules

adiabatic vibrionic states and extending to the continuum. This study has also showed that the dissociation can take place both in the H_2 and H_2^+ vibrational continuum, i.e. that the dissociative charge transfer process is an equally important dissociation channel in this reaction.

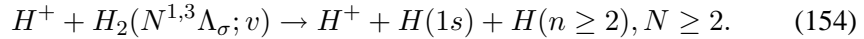
The dissociation cross sections of Ref. [195] and [197] are consistent with each other, except for the lower v -levels, for which preference should be given to the quantal results. Differences between the two sets of calculations also exist in the threshold energy region, where, again, preference must be given to the quantal calculations [197]. (The threshold energies for reactions (152) are given in Table 32, denoted there as $E_v^{diss}(H_2)$).

The dissociation cross sections σ_v^{diss} , derived from the data in Refs. [195, 197] can be represented by the following analytical expression

$$\sigma_v^{diss}(E) = \frac{a_1}{E^{a_2}} \left[1 - \left(\frac{E_{0v}}{E} \right)^{a_3} \right]^{a_4} (\times 10^{-16} \text{ cm}^2) \quad (153)$$

where E is the proton impact energy in the laboratory reference frame, expressed in eV units, and E_{0v} is the corresponding threshold energy ($E_{0v} = 1.5E_v^{diss}(H_2)$), see Figure 33 on page 178 for some selected initial v states. The values of fitting parameters a_i are given in Table 33 for $v = 0-6, 8, 10, 12$ and 14 . For $v = 7, 9, 11$ and 13 , $\sigma_v^{diss}(E)$ can be obtained by interpolation. We note that the validity of analytical representation (153) for σ_v^{diss} is limited to $E \lesssim 20 - 30$ eV, since it represents only the data from Refs. [195, 197].

There have been no attempts so far to determine, or estimate, the cross sections of reactions

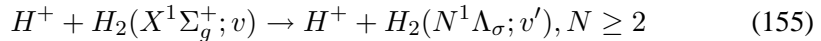


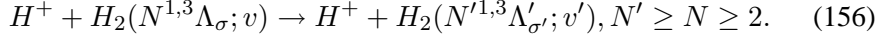
In view of the strong competing charge exchange process, however (see preceding sub-section), one can expect that the cross section of reaction (154) is small at low collision energies (at least with respect to the corresponding charge exchange cross section). More precise cross section estimates for this process, especially for $N = 2, 3$, would be, nevertheless, desirable.

5.4 Proton impact electronic excitation and ionization of H_2

5.4.1 Electronic excitation

SO far no studies have been performed for proton impact electronic excitation process of H_2

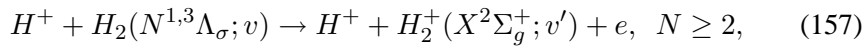




Like in case of proton-hydrogen atom excitation collisions, the cross sections for reactions (155) at low collision energies ($E \lesssim 200 - 300$ eV) should be adiabatically small for all v , and the role of these processes in the plasma kinetics can be neglected. The cross sections of excitation transition between electronically excited states, particularly those for $N' = N$, or $\Delta N = (N' - N) \ll N, N'$, may, however, be large. In absence of any quantitative information on these cross sections, one can adopt for their rough estimate the semi-empirical expression (38) of sub-section 2.2.1 for the proton-excited hydrogen atom excitation cross section. The principal quantum numbers n and m of the initial and final electronic state, appearing in Eqs. (38-39), have to be replaced by the effective principal quantum numbers N^* and N'^* of the states $(N^{1,3}\Lambda_\sigma; v)$ and $(N'^{1,3}\Lambda'_{\sigma'}; v')$ defined in terms of their respective ionization potentials. This procedure should be increasingly better justifiable with increasing N .

5.4.2 Ionization processes

The proton-impact ionization of H_2 in its ground electronic and vibrational state has been subject of several experimental [12, 190, 198] and theoretical [199] studies. The cross section maximum for this process (with a magnitude of $\simeq 2.0 \times 10^{-16} \text{ cm}^2$) appears at energies around $\sim 50 - 70$ keV, and for energies below ~ 200 eV the cross section attains values smaller than $1.0 \times 10^{-18} \text{ cm}^2$, further decreasing with the decrease of energy [11, 12]. This process, therefore, can be neglected in the low-temperature plasma kinetics. However, in view of the n^4 -scaling of proton-impact ionization cross sections of excited hydrogen atoms (see sub-section 2.2.2), one can expect the ionization cross sections of electronically excited molecules to be large, and the processes



should be taken into consideration in the plasma collisional kinetics. No cross section estimates have been performed for these processes. A rough estimate of the total (summed over v') proton-impact ionization of $H_2(N^{1,3}\Lambda_\sigma; v)$ can be obtained by using the expressions 40, or (42) of sub-section 2.2.2, by replacing n there with the effective principal quantum number N_v^* of the considered $(N^{1,3}\Lambda_\sigma; v)$ state.

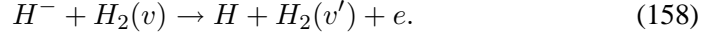
6 Collision Processes of H^- , H and H_2 with Hydrogen Molecules

In this section we shall consider mainly collision processes involving H_2 in its ground electronic state, $X^1\Sigma_g^+$, and, therefore, omit its state specification in reaction symbolics. In sub-section 6.4, some remarks will be given on the processes involving electronically excited H_2 .

6.1 Collisions of H^- with H_2

6.1.1 Electron detachment

The most important inelastic process of H^- ion with H_2 at low collision energies is the electron detachment



The cross section for this reaction for $v = 0$ (summed over all final v') has been measured for energies from threshold to the MeV region [104, 200] and also calculated [201] in the energy range $\sim 5 - 200$ keV/amu. The cross section shows a broad maximum (of magnitude $\sim 1 \times 10^{-15} \text{cm}^2$) in the range 2-8 keV. The reaction (158) at low collision energies proceeds most probably by electron capture into $H_2^-(X^2\Sigma_u^+)$ resonant state, followed by a rapid auto-detachment, in view of the large width (see, e.g., [161]) of this resonance. The electron capture reaction to $^2\Sigma_u^+$ resonance is, however, endothermic by 2.18 eV, and, consequently, the detachment cross section decreases with decreasing the energy below ~ 1 keV. The observed experimental cross section can be represented in the following analytic form (Figure 34 on page 20)

$$\sigma_{v=0}^{det}(E) = \sigma_{v=0}^{<}(E) + \sigma_{v=0}^{>}(E) \quad (159a)$$

$$\sigma_{v=0}^{<}(E) = \frac{81.10 (\times 10^{-16} \text{cm}^2)}{E^{0.63} [1 + 2.03 \times 10^{-6} E^{1.95}]} \left\{ 1 - \exp \left[-0.057 \left(\frac{E}{2.18} - 1 \right)^{0.94} \right] \right\} \quad (159b)$$

$$\sigma_{v=0}^{>}(E) = \frac{1.22 \times 10^3 (\times 10^{-16} \text{cm}^2)}{E^{0.5} [1 + 6.91 \times 10^{-4} E^{0.40}]} \exp(-125.0/E^{0.663}) \quad (159c)$$

where the H^- impact energy E (in the laboratory reference frame) is in keV units.

The endothermicity of electron capture to $^2\Sigma_u^+$ resonance decreases with increasing the initial vibrational state of H_2 , and for $v = 5$ the reaction becomes exothermic. This means that with increasing v up to $v = 4$, the exponential factor in (159b) becomes increasingly weaker, and for $v \geq 5$ the cross section $\sigma_v^{det}(E)$ is expected to take the typical form of a charge exchange reaction [2, 5, 7]. It should be noted that for any initial vibrational state, the H_2 molecule after the electron detachment is left in vibrationally excited states with $v \geq 5$. We also note that resonant $H_2^-(X^2\Sigma_u^+)$ state supports a number of vibrational states [160, 161], that facilitates the electron capture in this state.

6.1.2 Other processes

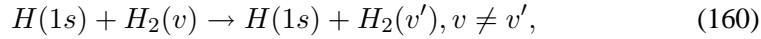
The electron detachment process at high ($\gtrsim 10 - 20$ keV) collision energies may also be accompanied by dissociation of $H_2(v)$. The cross section for this process

has, however, not been measured (or calculated) so far. In a low temperature plasma this process is not expected to play an important role.

6.2 Collisions of H with H_2

6.2.1 Vibrational excitation and de-excitation ($V - T$ transfer)

The processes of vibrational excitation and de-excitation (or $V - T$ transfer processes)



have been theoretically studied within the IOSA coupled channel formalism [185] (with $v, v' \leq 9, E_{CM} \lesssim 100$ eV), and by the classical trajectory method (CTM) [202] (all $v, v', E \lesssim 10$ eV), with the vibrational motion also treated classically in the latter case. When averaged over the rotational motion, the CTM results may have an accuracy sufficient for many applications. In Ref. [185] only the cross section results for $0 \rightarrow v'$ vibrational excitation, with $v' \leq 5$ have been displayed. The cross sections for other $v \rightarrow v'$ transitions ($v, v' \leq 9$) can be accessed via Internet (see Ref. [19]). The $0 \rightarrow v'$ ($v' \leq 5$) excitation cross sections of Ref. [185] can be fitted to the analytical expression

$$\sigma_{exc}(0 \rightarrow v') = \sigma_{exc}^{<}(0 \rightarrow v') + \sigma_{exc}^{>}(0 \rightarrow v') \quad (161)$$

$$\sigma_{exc}^{<}(0 \rightarrow v') = \frac{a_1}{E^{a_2}} \left[1 - \left(\frac{E_{0v'}}{E} \right)^{a_3} \right]^{a_4} (\times 10^{-16} \text{ cm}^2) \quad (162a)$$

$$\sigma_{exc}^{>}(0 \rightarrow v') = \frac{b_1 \exp(-b_2/E^{b_3})}{E^{b_4}(1 + b_5 E^{b_6})} (\times 10^{-16} \text{ cm}^2) \quad (162b)$$

where E is the H -atom impact (laboratory frame) energy in eV units, and parameters $E_{0v'}$, a_i and b_i are given in Table 34. See Figure 35 on page 179 for $v' = 1, 2, 3, 4$.

The vibrational excitation cross section for $v' = 1 - 3$ have similar structure as those for proton-impact excitation (see sub-section 5.1), while for $v' \geq 4$ the two-maxima structure is $\sigma_{exc}(0 \rightarrow v')$ for $H-H_2$ collisions disappears (see Table 34). The cross sections for $0 \rightarrow v' \geq 6$ excitation can be obtained from $\sigma_{exc}(0 \rightarrow 5)$ by using the observed scaling relationship

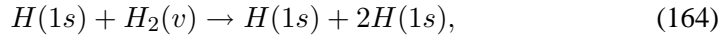
$$\begin{aligned} \sigma_{exc}(0 \rightarrow v' \geq 6; E) &= \left(\frac{E_{v'=5}^{exc}}{E_{v'}^{exc}} \right)^2 \sigma_{exc}(0 \rightarrow 5; E'), \\ E' &= \left(\frac{E_v^{exc}}{E_{v'=5}^{exc}} \right) E, \end{aligned} \quad (163)$$

6 Collision Processes of H^- , H and H_2 with Hydrogen Molecules

where $E_{v'}^{exc}$ is the excitation energy of the vibrational level v' (see Table 23).

A number of CTM de-excitation cross section in $H(1s) + H_2(v)$ collisions are reported in Refs. [112, 202]. Quasi-classical rate coefficients for vibrational excitation and de-excitation for all v, v' states in Eq. (160) are also available in Ref. [203]. The validity of CTM results is limited to collision energies below ~ 5 eV, and their reliability for lower- v, v' states can not be considered high.

6.2.2 Dissociation



has been studied by the classical trajectory method for all vibrationally states [202]. Additional studies can be found in Ref. [204].

The CTM rate coefficients $K_v^{diss}(T)$ of reactions (164) ($v = 0 - 14$), assuming a Boltzmann distribution of rotational states within a given v , taken from Ref. [205], can be represented the following analytic fit

$$\ln(K_v^{diss}) = -a_1 - \frac{a_2}{T^{a_3}[1 + a_4 T^{a_5}]}, \quad (165)$$

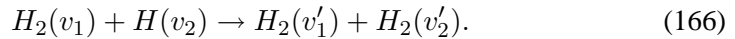
where T is expressed in Kelvin, and K_v^{diss} is in cm^3/s (Figure 36 on page 179). The fitting coefficients a_i are given in Table 35.

It is important to note that the rate coefficients for the reaction (164) are comparable (or larger for $v \lesssim 5$) to those of electron impact dissociation of $H_2(X^1\Sigma_g^+; v)$ via excitation of the dissociative $b^3\Sigma_u^+$ state, for plasmas in thermodynamic equilibrium [112]. Only when the electron temperature is significantly higher than the neutral gas temperature, the electron impact dissociation of H_2 becomes dominant.

6.3 $H_2 - H_2$ collisions

6.3.1 Vibrational ($V - V$) transfer

An efficient mechanism for redistribution of vibrational energy in a H_2 molecule in its ground electronic state is the vibrational- vibrational ($V - V$) energy transfer (or vibrational excitation transfer)



The process is most effective when total vibrational excitation energy in the system before and after the collision remains unchanged, i.e. when

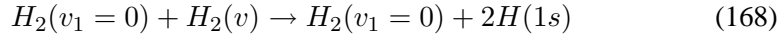
$$|v'_1 - v_1| \simeq |v'_2 - v_2|. \quad (167)$$

6.4 Collisions of H^- , H^* and H_2 with electronically excited H_2

The simplest model for calculation of $V - V$ transfer cross section is the Schwartz-Slawsky-Herzfeld (SSH) model [206], treating the process as energy transfer between two coupled oscillators. The classical trajectory method (CTM) has also been widely used for calculation of $V - V$ transfer cross sections (see, e.g., [207]). Complete sets of CTM $V - V$ transfer rate coefficients for all v_1, v_2 and v'_1, v'_2 combinations are currently available, the most elaborate being those of Ref. [208]. The CTM $V - V$ transfer data (as well as those from the SSH model) are usually valid for temperatures below $\sim 1 - 2$ eV. Their extension to higher temperatures can be made by using certain plausible arguments (e.g., their proportionally to the momentum transfer data).

6.3.2 Dissociation

There have been a number of CTM studies of dissociation process [112, 208]



at low collision energies. The rate coefficients for reactions (168) for a number of initial v -states are given in Ref. [112] in form of analytic fits. These fits can be unified in a compact form that also allows interpolation for all v . The unified form of rate coefficients of reactions (168), $v = 0 - 14$, is

$$K_v^{diss}(T) = K_0(v) \exp\left(-\frac{T_0(v)}{T}\right) (\times 10^{-10} \text{ cm}^3/\text{s}), \quad (169)$$

where

$$K_0(v) = 1.30 [1 + 0.023v + 1.93 \times 10^{-5}v^{4.75} + 2.85 \times 10^{-24}v^{21.60}] \quad (170a)$$

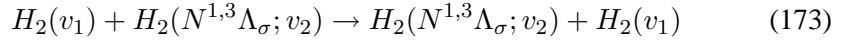
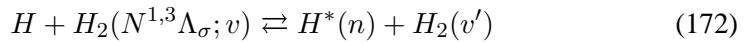
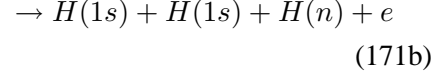
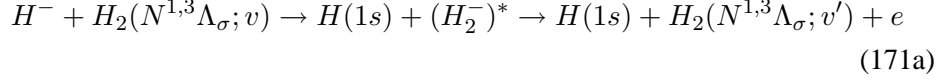
$$T_0(v) = (7.47 - 0.322v) \times 10^3, \quad (170b)$$

and T is expressed in Kelvin. The validity of Eq. (169) is limited to $T \lesssim 2 - 3 \times 10^4 \text{ K} (\lesssim 2 - 3 \text{ eV})$, see Figure 37 on page 180.

6.4 Collisions of H^- , H^* and H_2 with electronically excited H_2

The collision processes of H_2^-, H (or H^*) and H_2 with electronically excited H_2 molecules have not been studied so far. Although from the point of view of overall plasma (gas) kinetics such processes are less important than those involving ground state H_2 molecules, a due consideration for some of them must be given. The potentially important processes of electronically excited H_2 molecules with H^-, H and $H_2(X^1\Sigma_g^+; v)$ include

7 Collision Processes of H_2^+



The $(H_2^-)^*$ state in Eq. (171) is one of the higher resonances of H_2 [see, e.g., [160, 161]] that can be formed by electron capture during the course of a slow collision. The reactions (172) and (173) are molecular analogs of atomic excitation transfer process, considered in sub-section 2.3.1.

The energy resonance condition required for the efficiency of reaction (172) can be easily reached in the dense electronic-vibrational spectrum of colliding system.

7 Collision Processes of H_2^+

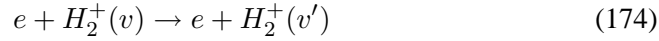
As discussed in several of previous sections, molecular hydrogen ions formed in a plasma by various collision processes are, generally, left in vibrationally excited states. When produced by electron impact ionization of a H_2 molecule in its ground electronic and vibrational state, the population of vibrational states of $H_2^+(v)$ is close to the distribution of Franck-Condon factors F_{0v} for the $H_2(v=0) \rightarrow H_2^+(v)$ transitions (see Table 25). Other processes usually produce $H_2^+(v)$ with other populations of vibrational states. Inelastic processes of H_2^+ in collisions with other plasma constituents show, in most cases, high sensitivity to the initial vibrational state of H_2^+ . Therefore, in the sub-sections that follow, the focus of our discussion will be on the collision processes of H_2^+ in a specific vibrational state. Only the ground electronic state ($1s\sigma_g; ^2\Sigma_g^+$) of H_2^+ is bound. Although the dissociation energy of $H_2^+(^2\Sigma_g^+; v=0)$ is only 2.645 eV, it supports 19 bound vibrational levels (the binding energies of which are given in Table 25).

The collision processes of $H_2^+(v)$ that will be discussed in this section will be those with electrons, H^- ions, H atoms and $H_2(v)$ molecules. Due to the strong Coulomb repulsion, collision processes of $H_2^+(v)$ with protons become important only at high (keV region) collision energies, and will be briefly discussed at the end of this section. The designation $X^2\Sigma_g^+$ of the electronic ground state of H_2^+ will normally be omitted in the reaction symbolics.

7.1 Collision processes with electrons

7.1.1 Vibrational excitation

Since $H_2^+(1s\sigma_g)$ ion is a non-polar system, its electron-impact vibrational excitation



can take place only due to the quadrupole and higher moments of its charge distribution. The cross section of reaction (174), therefore, cannot be large. The process (174) has been theoretically studied within the Coulomb-Born approximation (CBA) [209] and by the close-coupling method in the static-exchange approximation [210]. No experimental data have so far been reported (to the best of our knowledge) for this process.

Both mentioned theoretical treatments show that the cross sections for $v \rightarrow v' = v + 1$ transitions are at least an order of magnitude larger than for the $v \rightarrow v'$ with $v' \geq v + 2$. The CBA description of the process reveals in analytic form the dependencies of cross section on collision energy and parameters of initial and final vibrational state. For the dominant $v \rightarrow v + 1$ transition, the CBA cross section of reaction (174) is given by

$$\sigma_{vib}^{exc}(v \rightarrow v + 1) = \frac{(v + 1) A_0}{\Delta E_{v,v+1} E} (\times 10^{-16} cm^2) \quad (175)$$

where $\Delta E_{v,v+1} = |E_{v+1}^{exc} - E_v^{exc}| = |E_{v+1}^{diss} - E_v^{diss}|$, $E_v^{exc}(E_v^{diss})$ is the excitation (dissociation) energy of $H_2^+(v)$, and A_0 is a constant (within the CBA). The more involved close-coupling calculations [210] have shown that A_0 contains a weak energy dependence. When $\Delta E_{v,v+1}$ and E in Eq. (175) are expressed in units of eV, the quantity A_0 , determined from the close-coupling cross section results for $0 \rightarrow 1$ (and $1 \rightarrow 2$) transitions of Ref. [210], has the form

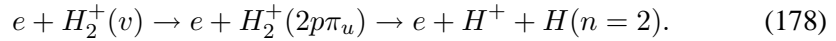
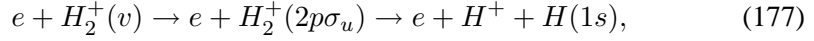
$$A_0 = 0.14E^{0.072} \quad (176)$$

The scaled cross section $\tilde{\sigma} = \sigma \cdot (\Delta E_{v,v+1})^2 / (v + 1)$ is shown in Figure 38 on page 180. We note that A_0 has been determined from the spin averaged singlet and triplet cross sections of Ref. [210] and it refers to $J = J' = 0$ initial (J) and final (J') rotational states. Inclusion of rotational states in the consideration introduces only a numerical factor in Eq. (175) [209]. We further note that the cross section σ_{vib}^{exc} , in both CBA and close-coupling static-exchange approximation, is finite at the threshold $E_{th} = \Delta E_{v,v+1}$. The values $\Delta E_{v,v+1}$ can be calculated from the values of E_v^{diss} given in Table 25.

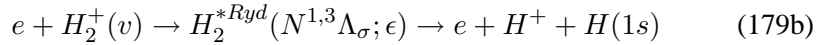
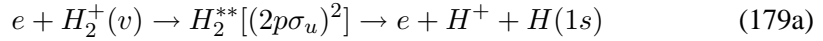
7 Collision Processes of H_2^+

7.1.2 Dissociative excitation

The simplest mechanism of dissociative excitation (DE) of $H_2^+(X^2\Sigma_g^+; v)$ ion by electron impact is its excitation to the two lowest dissociative excited states, $(2p\sigma_u; ^2\Sigma_u^+)$ and $(2p\pi_u; ^2\Pi_u)$,



In view of the large energy thresholds of these reactions for the low-lying v -states ($E_{th}(2p\sigma_u; v=0) \simeq 15.2\text{eV}$, $E_{th}(2p\pi_u; v=0) \simeq 19.0\text{eV}$), this mechanism should become operative only at high collision energies [except for the highest v -states in the case of reaction (177)]. On the other hand, recent total cross section measurements of dissociative excitation of $H_2^+(v)$ ion having a Franck-Condon population of vibrational states (or close to it), [211], have shown that DE reaction has very large ($\sim 10^{-14}\text{cm}^2$) cross sections even at energies as low as $\sim 0.01\text{eV}$. This indicates that at low collision energies the reaction takes place by electron capture into the doubly excited dissociative H_2 state $(2p\sigma_u)^{21}\Sigma_g^+$, or into a number of auto-ionizing dissociative Rydberg states of H_2 lying below the $2p\sigma_u$ state of H_2^+ ion. All these states auto-ionize in the continuum of the H_2^+ ion. The main low-energy mechanisms for DE reaction of H_2^+ ions are, thus,



The part of H^{**} and H^{*Ryd} populations that survive the auto-ionization in the H_2^+ continuum dissociates in the vibrational continuum of H_2 , producing two neutral atoms, $H(1s)$ and $H(n \geq 2)$. Thus, the DE and dissociative recombination (DR) processes at low collision energies are governed by the same dynamical mechanisms, and are complementary (or competing) to each other. The DR process will be considered in the next sub-section.

A Total DE cross section

There have been several cross section measurements of total DE cross section of H_2^+ ion by electron impact [211–214], covering the energy range from $\sim 0.01\text{eV}$ to $\sim 2000\text{eV}$. In the overlapping energy regions, the measured cross sections agree well with each other. Theoretical cross section calculations have also been performed in the first Born approximation assuming that direct mechanisms (177), (178) as responsible for the process [215], and by employing the multichannel quantum defect theory (MQDT) [216]. These calculations were performed for each individual initial vibrational state of H_2^+ . When weighted with the corresponding

7.1 Collision processes with electrons

Franck-Condon populations of initial v -levels the sum of theoretical v -selective cross sections of Ref. [215] agrees well with experimental data for $E \gtrsim 20$ eV. The corresponding sum of v -selective cross sections of Ref. [216], however, do not show such agreement.

The experimental data for total DE cross section can be represented by the analytic expression

$$\sigma_{DE}^{tot}(E) = \frac{13.2 \ln(e + 2.55 \times 10^{-4} E)}{E^{0.31} (1 + 0.017 E^{0.76})} (\times 10^{-16} \text{cm}^2) \quad (180)$$

where E is the center-of-mass energy (in eV units), and $e = 2.71828 \dots$. This expression represents the data well within their experimental uncertainty ($\sim 20\%$), but its validity cannot be extended much beyond the energy range of original data (0.01 eV - 2000 eV). See Figure 39 on page 181.

We note that the dominant contribution to the total DE cross section (159) comes from the capture and direct excitation mechanisms involving the $2p\sigma_u$ state (represented by Eqs. (179) and (177), respectively). A minor contribution to σ_{DE}^{tot} , however, give the analogous mechanisms involving the $2p\pi_u$ state. (The doubly excited dissociative $Q_2^2\Pi_u$ states, involved in a process similar to Eq. (179a), were discussed in sub-section 4.5.2). There have been no theoretical studies of DE process proceeding via the electron capture to the $Q_2^2\Pi_u$ state. Such studies have, however, been performed for the direct excitation mechanism, reaction (178). The corresponding total cross section (averaged over the Franck-Condon population of $H_2^+(v)$ states) be represented by the analytic expression [11]

$$\sigma_{DE}(2p\pi_u) = 1.36 \left(\frac{E_0}{E} \right)^{1.04} \ln(E/E_0) (\times 10^{-16} \text{cm}^2) \quad (181)$$

where $E_0 = 14.4$ eV, and collision energy is in eV units. The $\sigma_{DE}(2p\pi_u)$ cross section is about an order of magnitude smaller than σ_{DE}^{tot} given by Eq. (180) in the energy region above ~ 20 eV. The validity of analytic fit (181) extends up to a few keV.

B DE cross sections for individual vibrational levels

Dissociative excitation cross sections for $H_2^+(v)$, calculated in Ref. [215] and [216], considerably disagree with each other, particularly for higher v . At low collision energies (≤ 10 eV), the MQDT data of Ref. [216] should be considered more reliable. While the Born approximation results for v -selective cross sections monotonically increase with increasing v (predicting cross sections of the order of 10^{-14}cm^2 for $v \sim 16-18$ at $E \lesssim 40$ eV), the MQDT cross sections monotonically increase up to $v = 9$ and then begin to decrease. In the region close to the threshold (the dissociation energy of the level) they also show an oscillatory structure (with decreasing amplitude when v increases).

7 Collision Processes of H_2^+

The MQDT v -selective DE cross sections, available for energies below ~ 13 eV [216, 217], can be fitted to the analytic expression (after averaging over the near-threshold oscillations)

$$\sigma_{DE}(v) = \frac{a_1}{E^{0.805}} \left[1 - \left(\frac{E_v^{diss}}{E} \right)^{a_2} \right]^{a_3} (\times 10^{-16} cm^2) \quad (182a)$$

where collision energy E is in eV units, and the fitting parameters a_i are given in Table 36. (The values of dissociation energies E_v^{diss} are given in Table 25). The cross sections for $v = 5, 7, 13$, and 15, not presented in Table 36, can be obtained by interpolation.

As mentioned in part A of this sub-section, the sum of MQDT cross sections (182a), weighted with a Franck-Condon population of v -levels, does not reproduce the experimental total cross section at a given energy, represented by Eq. (180). However, the mutual ratios of $\sigma_{DE}(v)$ cross sections, determined by the collision dynamics, should remain valid. Therefore, the cross sections $\sigma_{DE}(v)$ have to be re-normalized for any collision energy by the condition

$$\sum_v F_{FC}(v) \sigma_{DE}(v; E) = \sigma_{DE}^{tot}(E) \quad (182b)$$

where $F_{FC}(v)$ is the Franck-Condon factor for $H_2(v=0) \rightarrow H_2^+(v)$ transition given in Table 25. (Instead of using Franck-Condon factors in Eq. (182a) one can, alternatively, use the experimental von Busch-Dunn distribution of v -state populations, Ref. [148], also given in Table 25.) This re-normalization affects only the constants a_1 in Eq. (182a) which, for a given energy, are all changed by the same factor. For $E = 1eV, 5eV$ and 10 eV, the value of this factor is 1.12, 2.73 and 4.18, respectively.

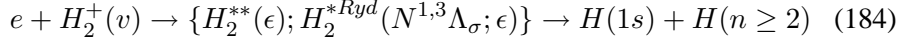
The Born approximation results of Ref. [215] for the $\sigma_{DE}(v)$ cross sections of direct excitation reactions (177) and (178) can be analytically represented by the Bethe-Born formula

$$\sigma_{DE}^{BB}(v) = \frac{0.88}{V_{rel}^2} (A_v \ln V_{rel} + B_v) (\times 10^{-16} cm^2), \quad (183)$$

where V_{rel} is the relative collision velocity expressed in atomic units (a.u.) ($E(eV) = 13.60V_{rel}^2(a.u.)$), and the coefficients A_v and B_v for excitation of $2p\sigma_u$ and $2p\pi_u$ states are given in Table 37. It should be noted that Eq. (183) is valid also for proton impact excitation of dissociative states $2p\sigma_u$ and $2p\pi_u$ states from individual $H_2^+(v)$ levels. (The laboratory proton energy is related to $V_{rel}(a.u.)$ as $E_p(keV) \simeq 25V_{rel}^2(a.u.)$).

7.1.3 Dissociative recombination

In view of its importance for the recombination of low-temperature plasmas, dissociative recombination (DR) process



has been subject to many experimental [218–222] and theoretical [216, 223–225] studies in the past. There also exist several excellent recent reviews on the results of this research [217, 226–228]. The process takes place by direct capture of incident electron on a doubly excited state of H_2 , such as $(2p\sigma_u, np\sigma_u)^1\Sigma_g^+$, $(2p\sigma_u, np\pi_u)^{1,3}\Pi_g$, etc., (direct resonant mechanism [229]), or by vibrational (or rotational) excitation of $H_2^+(1s\sigma_g; ^2\Sigma_g^+)$ and simultaneous capture of the electron on a dissociative auto-ionizing Rydberg state $[(1s\sigma_g, nl\lambda_\sigma)^{1,3}\Lambda_\sigma; \epsilon]$ of H_2 (indirect mechanism [230]). The energy position of the lowest doubly excited $(2p\sigma_u)^{21}\Sigma_g^+$ state of H_2 is such that one of the dissociated atoms is in an excited, $n \geq 2$, state. The strong mutual interaction of many doubly excited and core-excited Rydberg states, as well as their interactions with the continuum, give rise to a complex structure of DR cross section in certain energy regions (resonances). Because the DR process involves direct coupling of bound-state and continuum nuclear wave-functions, its cross section is fairly sensitive to the initial vibrational (and rotational [231]) state of H_2^+ ion. An important aspect of the DR process is also the distribution of dissociated excited atoms over the n -levels [220, 221, 223].

A Total DR cross section

The total experimental cross section of reaction (184), with a distribution of initial vibrational state corresponding to that which results from $H_2^+(v)$ production by electron impact on $H_2(v = 0)$ (see Table 25), is known with high (10 – 15%) accuracy in the energy range $\sim 0.01 - 3eV$ [218, 219, 221].

The extension of total DR cross section σ_{DR}^{tot} to higher energies can be achieved by using the most accurate presently available (up to 11 eV) theoretical v -selective cross sections of Ref. [216] (see also [225]), averaging over the "experimental" population of initial H_2^+v -levels of Ref. [148] (see Table 25), and normalizing the obtained result to the experimental data in the region $E \lesssim 1$ eV. The so determined total DR cross section in the energy range 0.01 – 10 eV can be represented by the analytic fit

$$\begin{aligned} \sigma_{DR}^{tot}(E) = 17.3 \left\{ \frac{1}{E^{0.665}(1 + 1.10E^{0.512} + 0.011E^{3.10})} + \right. \\ \left. + 0.133 \exp[-0.35(E - 6.05)^2] \right\} (\times 10^{-16} cm^2) \quad (185) \end{aligned}$$

where the collision energy is in eV units (see Figure 40 on page 181). The second term in Eq. (185) originates from well pronounced resonance structures in the v -selective theoretical cross sections, over which an averaging was performed. (The experimental data of Ref. [219] on σ_{DR}^{tot} also show somewhat less pronounced resonance structures in the region 0.1-3 eV. The fitting expression (185) is an average also over these resonances). It is to be noted that the increase of σ_{DR}^{tot} with

7 Collision Processes of H_2^+

decreasing the energy does not strictly follow the E^{-1} Wigner's law for break-up reactions [232]. However, in the energy range $\sim 0.05 - 3$ eV, σ_{DR}^{tot} does have an E behaviour very close to E^{-1} . Beyond the gross resonance around $E \simeq 6$ eV, σ_{DR}^{tot} begins rapidly to decrease with increasing E as result of the competition with the DE channels. The physical origin of the gross resonance in the region around $E \simeq 6$ eV is the excitation of $(2p\sigma_u, np\sigma_u)$ and $(2p\sigma_u, np\pi_u)$ ($n \geq 3$) auto-ionizing states of H_2 (see, e.g., [233]).

B DR cross sections for individual initial vibrational states of $H_2^+(v)$

Dissociative recombination of electrons with H_2^+ ion in a specific initial vibrational state v has been studied mainly theoretically [216, 223, 225, 234, 235]. In the semi-classical description of the process, employing only the $(2p\sigma_u)^{21}\Sigma_u^+$ doubly excited state, even an analytical expression for the cross section $\sigma_{DR}(v)$ for a given initial vibrational state of H_2^+ has been obtained [223]. In view of the crude approximations involved in such a treatment, the obtained result on $\sigma_{DR}(v)$ can be regarded, however, only as qualitative.

The most detailed theoretical study of DR process for individual $H_2^+(v)$ initial states has been performed in Ref. [216] by using the MQDT approach and including a large number of doubly excited and dissociative Rydberg states of H_2 . The cross sections calculated in Ref. [216] (shown only in the energy range 0.25 eV-11 eV) exhibit resonance structures both at low and high energies, with those at higher energies being more pronounced. The cross sections for $v \leq 7$ also exhibit a broad peak-structure in the energy region above ~ 2 eV, associated with the excitation of higher doubly excited states of H_2 . The sum of individual $\sigma_{DR}(v)$ cross section of Ref. [216], averaged over the Franck-Condon population of initial v -states (or "experimental" v -population of Ref. [216]), does not quite coincides with experimental total cross section in the overlapping energy region ($E \leq 3$ eV). By normalizing this sum to experimental data for σ_{DR}^{tot} , and averaging over the resonance structures (except for the broad gross resonance for $v \leq 7$ in the region $E \sim 2 - 10$ eV), the individual v -selective cross sections $\sigma_{DR}(v)$ of Ref. [216] can be represented by the analytic expression

$$\sigma_{DR}(v) = A \left\{ \frac{1}{E^{0.665} (1 + 1.1E^{0.512} + aE^\alpha)} + b \exp[-\beta(E - E_c)^2] \right\} (186)$$

$(\times 10^{-16} \text{ cm}^2)$

where E is expressed in eV units, and parameters A, a, α, b, β , and E_c are given in Table 38, see also Figure 41 on page 182. It can be seen from this table that the position E_c of the gross resonance structure shifts towards smaller energies with increasing v . The half-width of this structure generally decreases with increasing v and so does its relative amplitude. Equation (186) shows that the low-energy behaviour of $\sigma_{DR}(v)$ is the same for all v , reflecting the fact that the direct DR mechanism (mediated by electron capture to $(2p\sigma_u)^{21}\Sigma_g^+$ state) is common for all initial v -states at these collision energies.

7.1 Collision processes with electrons

It is interesting to note that for $E \lesssim 1$ eV $\sigma_{DR}(v)$ generally increases (for a given energy) with increasing v up to $v = 9, 10$, and then decreases with the further increase of v (a behaviour similar to that of $\sigma_{DE}(v)$; see the preceding subsection). It is also noteworthy that for a Franck-Condon population of initial states, dominant contribution (about 75%) to the total DR cross section give the states with $v = 4 - 10$.

C n -distribution of excited dissociation products

The distribution of excited $H(n)$ products in reaction (184) has been studied both experimentally (with an “experimental” distribution of v -levels in H_2^+) [220, 221] and theoretically [216, 223, 234]. The experimental observations show that for $E \gtrsim 1$ eV $n = 3$ is the mostly populated level of excited dissociation products [220], and that the contribution of $n \geq 10$ states to the total DR cross section is only about 3% for collision energies in the range 0.01-1 eV [221]. The theoretical studies confirm these findings.

As mentioned earlier, the position of potential energy curves of $H_2^+(1s\sigma_g; ^2\Sigma_g^+)$ and $H^{**}[(2p\sigma_u)^{21}\Sigma_g^+]$ is such that the $n = 1$ level cannot be populated in reaction (184). On the other hand, the $n = 2$ reaction channel is exothermic for any initial v -state. The channels for production of excited atoms in $n \geq 3$ states for a given initial v -state of H_2^+ , however, exhibit thresholds at energies given by

$$E_v^{th}(n \geq 3) = (1 - E_v^{exc}) + [E_H(n = 3) - E_H(n)] \quad (187)$$

where (all energies are in eV) $E_H(n) = 13.598/n^2$ and $E_v^{exc} = E_{v=0}^{diss} - E_v^{diss}$ is the excitation energy of the level v (see Table 25). The values of $E_v^{th}(n)$ are given in Table 39 for $n = 3 - 11$ and all v -states.

For a given value of n , $E_v^{th}(n)$ decreases and at a certain level $v = v_0$ the n -production channel becomes exothermic for all $v \geq v_0$. The reaction exothermicities of (v, n) channels are also shown in Table 39.

The MQDT calculations of Ref. [216] provide state-selective cross sections $\sigma_{DR}(v \rightarrow n)$ for reaction (184) for all v and $n = 2 - 5$ in the energy range 0.25-11 eV. This reference also provides the total cross section for all $n \geq 6$ states for a given v . As function of energy, $\sigma_{DR}(v \rightarrow n)$ cross sections show resonant structures, particularly pronounced for $E \gtrsim 1$ eV (and taking form of pseudo-regular oscillations for $v \geq 4$, with an amplitude decreasing with the increase of v).

After averaging over these structures (except for $v \leq 3$), the relative contributions of individual (v, n) channels to the total $\sigma_{DR}(v)$ cross section ,

$$P_v(n) = \frac{\sigma_{DR}(v \rightarrow n)}{\sigma_{DR}(v)}, \quad (188)$$

are given in Table 40 for $v = 0 - 5, v = 10$ and a selected number of collision energies. As evident from this table, the values of $P_v(n)$ tend to become invariant

7 Collision Processes of H_2^+

of v and n for collision energies well above the threshold $E_v^{th}(n)$. Therefore, the $P_n(v)$ distributions for $v \geq 6$ can be taken to be the same as that for $v = 10$ given in Table 40 for energies above the corresponding thresholds.

The contribution of $n \geq 6$ levels to $\sigma_{DR}(v)$ is given in Table 40 in form of a sum, $\tilde{P}_v(\sum n \geq 6)$. The extraction of individual contributions of $n(\geq 6)$ levels to $\sigma_{DR}(v)$ from $\tilde{P}_v(\sum n \geq 6)$ can be achieved by taking into account that for $n \gg 1$ the $P_v(n)$ distributions behave as $P_v(n) \sim n^{-3}$ (see, e.g., [223]). One should keep, however, in mind that with increasing n for a given initial v , $E_v^{th}(n)$ increases (see Table 39), and for a given collision energy only the levels $n \leq n_0$, satisfying the condition $E_v^{th}(n) \leq E$, are exothermic. This leads to a finite number of n states that contribute to $\tilde{P}_v(\sum n \geq 6)$ for a given E . (For instance, for $v = 1$ and $E = 2$ eV, only the $n = 6, 7$ states contribute to $\tilde{P}_v(\sum n \geq 6)$). The use of n^{-3} distribution law then gives for the populations $P_v(n \geq 6)$ the following expression

$$P_v(n \geq 6) = \frac{\tilde{P}_v(\sum n \geq 6)}{\xi_6(3) - \xi_{n_0}(3)} \left(\frac{1}{n}\right)^3, \quad (189)$$

where $\xi_n(3)$ is the Riemann ξ -function. When n_0 is very large (high v and/or E), $\xi_{n_0}(3) \gg \xi_6(3)$, and Eq. (189) becomes

$$P_v(n \geq 6) \simeq \frac{\tilde{P}_v(\sum n \geq 6)}{3.54} \left(\frac{6}{n}\right)^3. \quad (190)$$

Without much loss of accuracy, for the case of high v and E one can also use the simple scaling

$$P_v(n \geq 6) \simeq P_v(n = 5) \left(\frac{5}{n}\right)^3 \quad (191)$$

(which may, however, violate to some extent the unitarity $\sum_n P_v(n) = 1$).

D Relation of $\sigma_{DR}(v \rightarrow n)$ with state selective associative ionization of $H + H(n)$

The principle of detailed balance relates the cross sections of reaction (184) and its inverse reaction, state-selective associative ionization. i.e.,

$$n^2(\mu v_{rel})^2 \sigma_{AI}^{(J)}(n \rightarrow v) = E \sigma_{DR}^{(J)}(v \rightarrow n) \quad (192)$$

where μ is the reduced mass of $(H + H^{(+)})$ system, v_{rel} is the relative velocity of $H + H(n)$ colliding (or receding) particles, and J is the total angular momentum of the system. For large values of J (i.e. large rotational quantum numbers j in

7.1 Collision processes with electrons

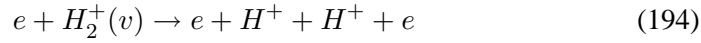
$H_2^+(v, j)$), the use of quasi-classical approximation in Eq. (192), and summing over J (integration over impact parameters), gives [223]

$$\sigma_{AI}(n \rightarrow v) \approx \frac{0.442}{n^2} E R_x^2 \sigma_{DR}(v \rightarrow n) (\times 10^{-16} \text{ cm}^2), \quad (193)$$

where $R_x \simeq 2.80a_0$ is the internuclear distance at which the H_2^+ potential energy curve intersects that of $H^{**}[(2p\sigma_u)^{21}\Sigma_g^+]$ doubly excited state, and a_0 is the Bohr radius. Equation (193) accounts only for the contribution of $(2p\sigma_u)^2$ auto-ionizing state to the AI/DR process and is, therefore, valid for $E \lesssim 1$ eV where the formation of this intermediary state provides the main reaction mechanism. On the other hand, the use of quasi-classical approximation is justified only at relatively high energies when the nuclear motion can be treated classically. Thus, the energy region in which Eq. (193) is valid is rather limited, particularly for the lower v .

7.1.4 Dissociative ionization

The process of dissociative ionization (DI)



has been experimentally studied in the energy range 20-950 eV, with $H_2^+(v)$ having an "experimental" v -distribution [236]. No theoretical studies of this reaction have been reported so far. Reaction (194) proceeds via excitation of the repulsive ionic state ($H^+ + H^+ + e$), which in the Franck-Condon region of $H_2^+(v=0)$ lies 29.84 eV above the energy of the $v=0$ level. The experimental cross section suggests a threshold of about 15 eV for reaction (194), an indication for a significant contribution from highly excited $H_2^+(v)$ states.

The measured total DI cross section of Ref. [236] can be represented by the analytical fit function (with an accuracy much higher than experimental uncertainties, $\pm 10\%$)

$$\sigma_{DI}^{tot}(E) = \frac{7.39}{E} \ln(0.18E) \left\{ 1 - \exp \left[-0.105 \left(\frac{E}{15.2} - 1 \right)^{1.55} \right] \right\} (\times 10^{-16} \text{ cm}^2) \quad (195)$$

where collision energy E is expressed in eV. The threshold energy of 15.2 eV in Eq. (195) corresponds to the $v=18$ level of $H_2^+(v)$, see also Figure 42 on page 182.

We note that $\sigma_{DI}^{tot}(E)$ has a broad maximum around $E \simeq 100$ eV of magnitude $\simeq 1.7 \times 10^{-17} \text{ cm}^2$. The σ_{DI}^{tot} cross section is, thus, considerably smaller than the cross section for dissociative excitation of H_2^+ by electron impact.

The thresholds ΔE_v for DI reactions in Eq. (194) for individual v levels (defined as the vertical electron transition energy from the outermost turning point of

7 Collision Processes of H_2^+

the v level to the potential curve of repulsive ($H^+ + H^+$) state) are distributed between 15.2 eV ($v = 18$) and 27.0 eV ($v = 0$) (see Table 41). Since the cross section $\sigma_{DI}(v)$ for a v -selective DI process is inversely proportional to ΔE_v , the variation of magnitudes of $\sigma_{DI}(v)$ with v is within a factor of two (for energies above all thresholds, $E \gtrsim 30$ eV). i.e. relatively weak. Assuming that the ΔE_v^{-1} dependence of $\sigma_{DI}(v)$ contains its main v -dependence, an approximate expression can be obtained for $\sigma_{DI}(v)$ (by using the closure relation for Franck-Condon densities)

$$\sigma_{DI}(v, E) = \frac{A}{\Delta E_v} \sigma_{DI}^{tot}(E), \quad A = \left(\sum_v 1/\Delta E_v \right)^{-1}, \quad (196)$$

where the constant A ensures proper normalization. The sum over v in the constant A includes all open v -channels for a given collision energy. When $E > \Delta E(v = 0)$, $A = 1.044$.

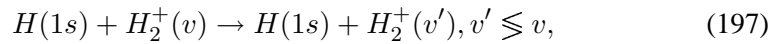
The values of ΔE_v are given in Table 41. For reference, we give in this table also the excitation energies E_v^{exc} of v -levels in $H_2^+(v)$.

7.2 Collisions of $H_2^+(v)$ with H Atoms

The cross sections of collision processes of $H_2^+(v)$ with $H(n)$ involving specific initial and final states from the discrete spectrum are related to those of corresponding (inverse) processes in $H^+ + H_2(N^{1,3}\Lambda_\sigma; v)$ collision system (considered in Section 5) by detailed balance principle. However, the cross section information given in Section 5 for $H^+ + H_2(N^{1,3}\Lambda_\sigma; v)$ collision processes often relates to the total cross sections (i.e. state-selective cross sections summed over all initial or final states, or both), and the detailed balance principle either cannot be used, or would require detailed additional considerations of collision dynamics. Therefore, in the present section we shall review the available cross section information on the most important collision processes of $H_2^+(v)$ with H atoms: vibrational excitation, charge exchange and dissociation. Most of the existing studies of these processes involve the H atom in its ground state.

7.2.1 Vibrational excitation and de-excitation of $H_2^+(v)$

The processes of vibrational excitation and de-excitation



have been theoretically studied recently within the IOSA vibronic close-coupling formalism in the C.M. collision energy range from threshold to ~ 8 eV [186]. The form and magnitude of excitation cross sections $\sigma^{exc}(0 \rightarrow v')$ for $v = 0, v' = 1 - 18$ displayed in Ref. [186] are similar to those of corresponding excitation cross sections in the $H^+ + H_2(v)$ collision system, except that the near-threshold peak, present in the latter case, is absent in $H + H_2^+(v)$ excitation cross sections.

7.2 Collisions of $H_2^+(v)$ with H Atoms

The cross sections $\sigma^{exc}(0 \rightarrow v')$ for $H + H_2^+(v = 0)$ collisions rapidly decrease with increasing v' at a given collision energy: for $E \simeq 3 - 4$ eV $\sigma^{exc}(0 \rightarrow 18)$ is three orders of magnitude smaller than $\sigma^{exc}(0 \rightarrow 1)$. The magnitude and energy behaviour of $\sigma^{exc}(0 \rightarrow v')$ cross sections in the C.M. energy region below 7 eV are illustrated by the cross section values given in Table 42 for a selected number of v' states and collision energies. Interpolations in this table can be made with respect to both v' and E . The $\sigma^{exc}(0 \rightarrow v')$ cross section rise sharply to their values shown in the table as soon as the excitation channel becomes open (see Table 41 for excitation energies $E_{0 \rightarrow v'}^{exc}$).

The sharp decrease of $v \rightarrow v'$ excitation cross section with increasing the difference $(v' - v)$, observed in Table 42, is a consequence not only of the increased energy difference between the v and v' levels but also (and even more so) of the increase of the number of intermediary non-adiabatic transitions ($v \rightarrow v_1 \rightarrow v_2 \rightarrow \dots \rightarrow v'$) involved in reaching the level v' from v . In addition, with increasing the initial v , the strength of non-adiabatic coupling between two consecutive v -states usually decreases [186, 197]. Although not published in the literature, the state-to-state excitation cross sections $\sigma^{exc}(v \rightarrow v')$ have been calculated for all (v, v') pairs in the energy region up to ~ 8 eV (see Ref. [19]).

The cross sections for vibrational de-excitation in $H(1s) + H_2^+(v)$ collisions ($v' < v$ in Eq. (197)) have also been calculated within the close-coupling IOSA scheme for energies below ~ 8 eV [186], but published results are available only for the sum

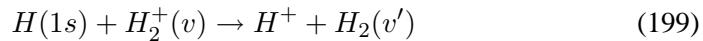
$$\sigma^{dp}(v) = \sum_{v'} [\sigma^{exc}(v \rightarrow v') + \sigma^{de-exc}(v \rightarrow v')], \quad (198)$$

i.e. for the depopulation cross section of H_2^+ v -level by $H(1s)$ impact. The magnitude and energy behaviour of $\sigma^{dp}(v)$ cross sections are illustrated by the cross section values given in Table 43 for a number of v -states and collision energies. As evident from this table $\sigma^{dp}(v \geq 1)$ cross sections are considerably larger than $\sigma^{dp}(v = 0)$. This indicates that $v' \rightarrow v$ de-excitation cross sections are significantly larger than those for $v \rightarrow v'$ excitation (which follows also from the principle of detailed balance).

7.2.2 Charge exchange

A Charge exchange with $H(1s)$

The state-selective charge exchange reaction



has been theoretically studied in Ref. [186] by the IOSA close-coupling method in the energy range below ~ 8 eV, but cross section data have been reported in that reference only for $v = 0$ and $v' = 1 - 8$. (The other cross section data

7 Collision Processes of H_2^+

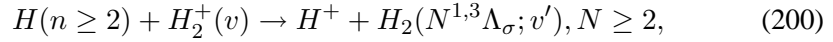
can be accessed via Internet; see Ref. [19]). The cross sections of reaction (199) can also be obtained from those for the inverse reaction, considered in sub-section 5.2, by using the detailed balance principle. As discussed in sub-section 5.2.1, reaction (199), as well as its inverse reaction, has the largest cross section at a given collision energy when the initial and final state are (quasi-) resonant in energy [see Eq. (149)]. The quasi-resonant vibrational levels of $H_2^+(v)$ and $H_2(v')$ are given in Table 32. For collision energies sufficiently far from the reaction thresholds, the cross sections $\sigma_v^{CX}(v')$ of reaction (199) rapidly [exponentially, see Eq. (150)] decrease with increasing of the energy difference $\Delta E_{vv'}$ between the v and v' levels. In the threshold region, $\sigma_v^{CX}(v')$ is, of course, strongly affected by reaction exo-(endo)-thermicity.

The magnitude and energy behaviour of the cross sections $\sigma_{v=0}^{CX}(v')$ for $v' = 0 - 7$ are illustrated in Table 44 (based upon the data from Ref. [186]). As observed from this table, the quasi-resonant $v = 0, v' = 4$ channel is by far the strongest charge exchange channel for $E \gtrsim 1$ eV. The next most populated v' levels, $v' = 3$ and $v' = 5$, have cross sections more than an order of magnitude smaller than $\sigma_{v=0}^{CX}(v' = 4)$ at energies above ~ 1.5 eV.

There exists a single total cross section measurement for reaction (199) in the (laboratory) energy range 100 eV- 22.5 keV [237]. The total cross section exhibits a broad maximum in the region 2-4 keV of magnitude of 10^{-15} cm^2 .

B Charge exchange with $H(n \geq 2)$

The charge exchange reaction



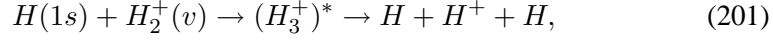
has a quasi-resonant character for $N \simeq n$ and should have large cross sections at low collision energies. As discussed in sub-section 5.2.2 in connection with inverse reaction to (200), the energy resonance defects already for $n = N = 3 (v = v' = 0)$ are small (and lie in the interval 0.09-0.69 eV). By varying the v and v' levels in the entrance and exit reaction channels, the conditions for a near (or accidentally exact) resonance can be met. With increasing both n and N , the near-resonance conditions are, obviously, more easily achieved.

The cross sections for quasi-resonant charge exchange reactions at low collision energies can be roughly (within a factor smaller than two) estimated by the well established two-state models of atomic collision theory [5, 6]. For sufficiently high excited atoms ($n \geq 4$), the classical over-barrier transition model can also be used to estimate the total (summed over v and v') cross section of reaction (200) (see Eq. (45) in sub-section 2.2.3).

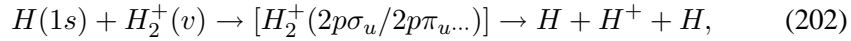
7.2.3 Dissociation

The process of $H_2^+(v)$ dissociation by $H(1s)$ impact proceeds at low collision energies by promotion of adiabatic vibronic states of $(H_3^+)^*$ collision complex to the continuum via series of non-adiabatic couplings

7.2 Collisions of $H_2^+(v)$ with H Atoms



and at higher energies by excitation of dissociative $(2p\sigma_u)^2\Sigma_u$, or $(2p\pi_u)^2\Sigma_u$ states of H_2^+ ,



i.e. as dissociative excitation. Theoretical studies of the process (201) have been performed recently within the IOSA close-coupling formalism [197], while the dissociative excitation (202) has been studied [215] within the first Born approximation. Both these studies have provided cross sections for the process for specific initial vibrationally excited states of H_2^+ . Experimental cross section measurements for $H_2^+(v)$ dissociation by H atoms, with $H_2^+(v)$ having an "experimental" v -distribution, have been performed only at high energies (keV region) [238, 239]. However, the separation of $H^+ + 2H$ channel from other H^+ production channels in $H_2^+ + H$ collisions, such as $H + 2H^+ + e$, $3H^+ + 2e$, has been achieved only in Ref. [239].

The σ_v^{diss} cross sections calculated in Refs. [197] and [215] show a strong dependence of σ_v^{diss} on v : with increasing v from $v = 0$ to $v = 18$, the cross sections increase by about two orders of magnitude. The σ_v^{diss} cross sections in Ref. [197] are given in the C.M. energy range from threshold to about 6-8eV. Their energy behaviour is similar to that of dissociative cross section for $H^+ + H_2(v)$ collision system. Table 45 gives the values of these cross sections for a selected number of initial v -states and collision energies. The v -dependence of σ_v^{diss} is monotonic for higher v , and the cross sections for the v -levels missing in Table 45 can be obtained by interpolation. The data of this table can be safely extrapolated to about 10-15 eV, keeping in mind that the cross sections for $v \lesssim 7$ levels should also reach their maxima in the energy region 8-12 eV (as do the higher v cross sections at lower energies). The Born cross sections of Ref. [215] become reliable at energies above ~ 1 keV (for $v = 18$) – 5 keV (for $v = 0$), and no smooth connection can be established between the data from Refs. [197] and [215] in the intermediate energy region.

It should be mentioned that for any initial state v , reaction (201) contains two channels: a direct dissociative channels, in which the $H^+ + H$ dissociation fragments originate from the initial H_2^+ ion, and a charge transfer dissociative channel, in which the electron from the incident H atom is first captures by H_2^+ , followed by dissociation (via promotion to the continuum) of resulting $H_2(v)$. These two channels have approximately equal contribution to the total low energy dissociation cross section. It should be also noted that at higher collision energies, dissociative excitation may involve not only the $2p\sigma_u$ and $2p\pi_u$ states of H_2^+ , but also its higher $np\lambda_u$ excited states.

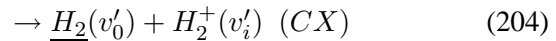
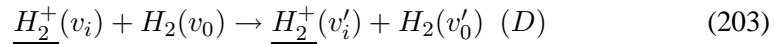
7.3 Collisions of H_2^+ with H_2

Collision processes of $H_2^+(v_i)$ ions with $H_2(v_0)$ are very sensitive to the state of vibrational excitation of both collision partners. For a fixed v_0 level in H_2 , the variation of v_i in H_2^+ ion can make the reaction energy defect to vary from negative (endothermic) to positive (exothermic) values, resulting in significant differences in the corresponding cross sections. And *vice versa*: for a fixed value of v_i , the reactions with $H_2(v_0)$ will be exothermic for certain values of v_0 , and endothermic for others. In most experiments neither the vibrational distribution of $H_2^+(v_i)$ nor that of $H_2(v_0)$ are precisely known; that results in significant differences in the measured total cross sections. Even if $H_2(v_0)$ can be prepared to be in its ground vibrational state, the uncertainty in the population of $H_2^+(v_i)$ levels still remains (except in certain dedicated state-selective experiments). The v_i -population distribution depends on the method of formation of H_2^+ ion: if it is electron-impact ionization of $H_2(v_0 = 0)$, then it depends on the energy of ionizing electrons; if it is formed by a charge exchange of $H_2(v_0 = 0)$ on a certain ion, then $H_2^+(v_i)$ is produced with a quite different v_i -distribution that depends again on the collision energy. In Penning type ion sources, $H_2^+(v_i)$ can be produced from dissociation of H_3^+ ions, with a v_i -distribution that is different from those of already mentioned methods, and that depends on the gas temperature of the source. Therefore, the experimental total cross section for a given collision process of H_2^+ with H_2 (even $H_2(v_0 = 0)$) always reflects the specific (but unknown) v_i -distribution of the ion, which is the origin of the differences in cross section results of different experiments.

With all this in mind we shall review below the available cross section information for vibrational excitation, charge exchange, dissociation and H_3^+ formation processes in $H_2^+ + H_2$ collisions, with inclusion also the results of theoretical studies of these processes, as well as of some state-selective studies.

7.3.1 Vibrational excitation (de-excitation) and charge transfer

Due to the nuclear symmetry of colliding system, the processes of vibrational excitation (and de-excitation) and charge transfer in $H_2^+(v_i) + H_2(v_0)$ collisions are mutually connected



When $v_0 = 0$, reaction (203) corresponds to direct (D) vibrational excitation; otherwise it describes the vibrational transfer process. The charge exchange (CX) reaction (204), even for $v_0 = 0$, produces vibrationally excited $H_2(v'_0)$ and $H_2^+(v'_i)$.

The direct and charge exchange channel, (203) and (204), are experimentally distinguished by monitoring the fast (underlined) or slow reaction products.

Starting with the seminal work of Ref. [240], there have been several theoretical studies of state-selective processes (203) and (204) for H_2 in its ground vibrational state, $v_0 = 0$, [241, 242] for a number of ion impact energies in the range 1 eV – 5 keV, and for initial vibrational states of the H_2^+ ion $v_i = 0 - 5$. (If $H_2^+(v_i)$ are produced by electron impact ionization of $H_2(v_0 = 0)$, the vibrational states $v_i = 0 - 5$ account for 85% of the total $H_2^+(v_i)$; see Table 25.) v_i -selective (total in v'_0 and v'_i) experimental cross sections for charge exchange reaction (204) for $v_i = 0 - 4$ have been reported for a number of selected ion energies in the range 8-1000 eV [243–246]. The total cross section of charge exchange reaction (204) (with unknown v_i distribution of H_2^+) has been measured by many authors and covers the ion energy range from 1 eV to ~ 150 keV [247–252]. A critical assessment of all these data has been performed in Refs. [12] and [253].

A Vibrational excitation cross sections

Vibrationally excited H_2^+ ions in collisions with $H_2(v_0 = 0)$ are produced either by the direct mechanism, reaction (203) (with $v_i = v_0 = 0$), or as result of charge exchange process, reaction (204). Combining the available theoretical (Ref. [240]) and experimental (Ref. [246]) data, the cross section for $v_i = 0 \rightarrow v'_i = 1$ direct excitation (d-exc) has been derived in Ref. [253] in the ion energy range from threshold to 10 keV. This cross section can be represented by the following analytic expression

$$\sigma_{v_i}^{d-exc}(0 \rightarrow 1) = \frac{5.75 \exp[-20.5/(E - 1.032)^{1.20}]}{E^{0.29}(1 + 2.58 \times 10^{-4} E^{0.874})} (\times 10^{-16} \text{ cm}^2), \quad (205)$$

where the ion (laboratory) energy is in eV. See Figure 43 on page 183. The calculations of Ref. [242] indicate that the cross section $\sigma_{v_i}^{CX-exc}(0 \rightarrow 1)$ via charge exchange process (CX excitation) in the ion energy range 16 eV-800 eV is, on average, by a factor 3.7 larger than the cross section $\sigma_{v_i}^{d-exc}(0 \rightarrow 1)$. These calculations (considered to be the most involved ones) further indicate that the CX-excitation cross section for $v_i = 0 \rightarrow v'_i = 2$ transition is by a factor of about 5 smaller than $\sigma_{v_i}^{CX-exc}(0 \rightarrow 1)$ for energies below in ~ 40 eV. This is a result of the increased strong mixing of many reaction channels with the increase of collision energy. Since direct excitation channels for $v_i = 0 \rightarrow v'_i \geq 2$ transitions are also strongly mixed with many charge exchange channels, the observed ratio $\sigma_{v_i}^{CX-exc}(0 \rightarrow 2)/\sigma_{v_i}^{CX-exc}(0 \rightarrow 1)$ can be expected to approximately hold also for $\sigma_{v_i}^{d-exc}(0 \rightarrow 2)/\sigma_{v_i}^{d-exc}(0 \rightarrow 1)$.

The excitation (and de-excitation) cross sections of vibrationally excited H_2^+ ions ($v \geq 1$) will be discussed in the following part B of this sub-section, together with the state-selective electron capture.

B State-selective charge transfer and associated excitation (de-excitation)

As mentioned earlier, the state-selective processes associated with charge transfer reaction (204) have been studied only for $v_0 = 0$. Most of experimental studies

have been state-selective only with respect to the initial vibrational state of $H_2^+(v_i)$ with no resolution of vibrational states of the products [243, 245, 246, 254, 255]. The only v_i -selective charge transfer absolute cross section measurements have so far been performed for $v_i = 0$ and $v_i = 1$ in Ref. [254] in the ion (laboratory) energy range 8-400 eV. The measured cross sections $\sigma_{v_i}^{CX}$ (total with respect to (v'_i, v'_0) product channels) agree well with theoretical predictions [242], and for a number of ions impact energies they are given in Table 46. The cross sections show maxima in the region around 16 eV, for $v_i = 1$, and 35 eV, for $v_i = 0$, in contrast to the expectations based upon the simple two-state resonant charge transfer theory [1–3, 5–8]. This indicates the strong multi-state coupling in the system in this collision energy range. Relative measurements of $\sigma_{v_i}^{CX}$ have been performed for $v_i = 0 - 4$ [244], $v_i = 0 - 5$ [243] and $v_i = 0 - 10$ [255] for a selected number of collision energies. The results of these measurements are generally in good agreement with each other. The ratios of the cross sections $\sigma_{v_i}^{CX}$ and $\sigma_{v_i=0}^{CX}$ taken from Ref. [244] and Ref. [255] (the later normalized on those of Ref. [244]) for a number of ion impact energies are given in Table 47. (We note that the levels $v_i = 0 - 10$ comprise about 99% of the population of all $H_2^+(v_i)$ ions produced by electron impact ionization of $H_2(v_0 = 0)$). The ratios $\sigma_{v_i}^{CX}/\sigma_{v_i=0}^{CX}$ are continuous functions of v_i for a given energy with a maxima at $v_i \simeq 1 - 2$ when $E_{lab} \lesssim 30$ eV. Their energy variation for $E_{lab} \lesssim 100$ eV is also smooth and an interpolation procedure can be used to obtain $\sigma_{v_i}^{CX}/\sigma_{v_i=0}^{CX}$ from the data in Table 47 for ion impact energies below 100 eV. At higher collision energies, the number of reaction channels becomes large for any initial state v_i , and the variation of $\sigma_{v_i}^{CX}/\sigma_{v_i=0}^{CX}$ with v_i is weaker, as seen in Table 47 for $E_{lab} = 400$ eV.

Theoretical studies of reaction (204) by a close-coupling formalism are able to provide cross sections for any of the (v'_i, v'_0) reaction product channels. Such cross section calculations have been performed for $v_0 = 0$ and a selected number of v_i [240–242] within a semi-classical formulation of the collision dynamics. The cross section of a particular channel $(v_i, v_0 = 0) \rightarrow (v'_i, v'_0)$ of charge transfer reaction (204) strongly depends on the channel energy defect, $\Delta E_{v_i}(v'_i, v'_0)$, and the overlap of vibrational wave-functions of initial and final states. The later becomes important at collision energies above ~ 100 eV, and attains a decisive role at energies above $\sim 1 - 2$ keV [241]. The channel energy defects are proportional to the difference $\Delta N = N' - N$, $N' = v'_i + 2v'_0$ and $N = v_i + 2v_0$. Levels with $\Delta N = 0$ are in energy resonance (or near resonance), and their cross sections at low energies are (generally) much larger than for the channels with $\Delta N \neq 0$. The strictly resonant charge transfer channel is, of course, that with $v'_i = v_i$ and $v'_0 = v_0$.

Theoretical calculations of Ref. [242] have proved to be very successful in predicting the ratios of initial-state-selective total cross sections, $\sigma_{v_i}^{CX}$. In that reference, the fully state-selective charge transfer cross sections, $\sigma_{v_i}^{CX}(v'_i, v'_0)$, have been calculated for $v_i = 0 - 5$ for ion impact energies 16, 32, 400 and 800 eV. The fractional contributions of these cross sections to the total $\sigma_{v_i}^{CX}$ cross section,

$$f_{v_i}(v'_i, v'_0) = \frac{\sigma_{v_i}^{CX}(v'_i, v'_0)}{\sigma_{v_i}^{CX}} \quad (206)$$

for the ion energies of 16 eV and 32 eV are given in Tables 48 and 49, respectively. As it can be noticed from these tables, the contribution of $\Delta N = 0$ channels to $\sigma_{v_i}^{CX}$ is substantial for the lower values of v_i , but it decreases with increasing v_i . This decrease is faster for $E_{lab} = 32$ eV than for $E_{lab} = 16$ eV. The (v'_i, v'_0) channels in these tables with $v'_0 = 0$ describe the CX excitation ($v'_i > v_i$) or de-excitation ($v'_i < v_i$) of H_2^+ ion. The channels with $v'_i = v_i$ and $v'_0 \geq 1$ describe the CX excitation of neutral molecule. Other charge exchange channels are a kind of CX $V - V$ transfer.

C Total charge transfer cross section

Although the charge exchange reaction of H_2^+ and H_2 possesses nuclear and charge symmetry in the entrance and exit channels, its total cross section does not show the typical energy behaviour of symmetric resonant charge transfer reactions (logarithmic increase of the cross section with decreasing the collision velocity in the energy region below $\sim 10 - 20$ keV). The reason is the strong coupling of many quasi-resonant and non-resonant $(v_i, v_0) \rightarrow (v'_i, v'_0)$ channels with the resonant one ($v'_i = v_i, v_0 = v'_0$) and the coupling with the strong nuclear rearrangement channel, $H_2^+ + H_2 \rightarrow H_3^+ + H$, at C.M. energies below $\sim 2 - 3$ eV.

Most of the total cross section measurements of $H_2^+ + H_2$ charge exchange reaction [247–252] have been performed in the ion impact energy range above ~ 5 eV, with the exception of that in Ref. [251] where the cross section extends down to 1 eV. The cross sections of Refs. [251] and [256] show a sharp decrease for $E_{lab} \lesssim 4$ eV, attributed to the coupling with the competing H_3^+ formation channel (see subsection 7.3.3). The total CX cross section measured in Ref. [251] at $E_{lab} = 1$ eV is $\simeq 3.0 \times 10^{-16} \text{ cm}^2$. On the other hand, the measured thermal rate coefficient for $H_2^+ + H_2$ charge exchange reaction is $6.4 \times 10^{-10} \text{ cm}^3/\text{s}$ [257], indicating a cross section value of $2.89 \times 10^{-15} \text{ cm}^2$ for $E_{lab} = 0.052$ eV. Therefore, in the ion energy region below ~ 1 eV, the total CX cross section has to start to increase again with decreasing the collision energy. It should be also noted that in the region 500-1000 eV, the total cross section exhibits a mild minimum. In general, the measured total cross sections from various sources are in good mutual agreement in the energy regions of their overlap ($E_{lab} \gtrsim 5 \text{ eV}$).

The energy dependence of total cross section σ_{CX}^{tot} for $H_2^+ + H_2$ charge exchange reaction, in the ion impact energy range from thermal to $\sim 150 - 200$ keV, can be represented by the analytic expression (with an accuracy well within the experimental uncertainties, $\pm 10\%$)

$$\sigma_{CX}^{tot}(E) = \sigma_{CX}^{<}(E) + \sigma_{CX}^{>}(E) \quad (207a)$$

7 Collision Processes of H_2^+

$$\sigma_{CX}^<(E) = \frac{6.59}{E^{0.5}(1 + 2.29E^{1.78})} + \quad (207b)$$

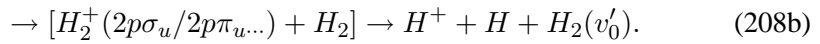
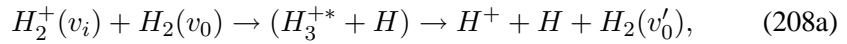
$$+ \frac{12.85 \exp(-1.84/E^{1.55})}{E^{0.0673}(1 + 2.60 \times 10^{-3}E^{0.97} + 1.63 \times 10^{-10}E^{2.76})} (\times 10^{-16} \text{ cm}^2)$$

$$\sigma_{CX}^>(E) = \frac{11.38 \exp(-61.80/E^{0.54})}{1 + 8.21 \times 10^{-10}E^{2.08} + 3.80 \times 10^{-26}E^{5.15}} (\times 10^{-16} \text{ cm}^2) \quad (207c)$$

where $E = E_{lab}$ is in eV units (see Figure 44 on page 183). The first term in Eq. (207c) describes the cross section behaviour in the thermal energy region, while the exponential function in the second term of $\sigma_{CX}^<$ accounts for the cross section decrease (down to $\sim 1 \text{ eV}$) due to the competition with H_3^+ formation process. We should note that in Refs. [253] and [258] no account was taken of the large cross section values in the thermal region, and their recommended σ_{CX}^{tot} cross section continues to decrease with the decrease of energy below $\sim 1 \text{ eV}$. The σ_{CX}^{tot} cross section of Ref. [11] does take into account its thermal energy values, but the decrease in the region 1-5 eV due to competing H_3^+ formation channel was accounted for much more conservatively, in view of the trend of other experimental results (for instance those of Ref. [259]) in the energy range 5-10 eV. The $\sigma_{CX}^>$ term, Eq. (207c), describes appropriately the high energy part of the CX cross section.

7.3.2 Collision induced dissociation of $H_2^+(v_i)$

The collision induced dissociation (CID) of $H_2^+(v_i)$ in collisions with $H_2(v_0)$ can proceed via two mechanisms,



The first mechanism is operative at low ($\lesssim 8 \text{ eV}$) collision energies, whereas the second one (dissociative excitation, DE) is effective at higher (above $\sim 15 - 20 \text{ eV}$) energies. The formation of intermediate excited H_3^+ complex in this collision system has been demonstrated in classical trajectory- surface hopping (TSH) calculations [260]. On the other hand, the observed angular distribution of dissociation protons at high collision energies confirms that the excitation of repulsive $2p\sigma_u, 2p\pi_u, \dots$ states of H_2^+ is the operating mechanism at these energies [261].

Reaction (208) has been subject of many experimental [250–252, 255, 259, 261–266] and one theoretical study [260]. Determination of the total cross section of reaction (208), with $H_2^+(v_i)$ having an unknown distribution over v_i , has been the main focus of experimental investigations. However, there have been both measurements [255] and calculations [260] of the cross sections of reaction (208) for H_2^+ in specific initial vibrational states v_i . In all these studies, the H_2 molecule was in its ground vibrational state, $v_0 = 0$.

A Total CID cross section

The low-energy total cross section of reaction (208) is sensitive to the initial state population distribution of $H_2^+(v_i)$ and the results of different measurements may differ by a factor as high as two (cf., e.g., Refs. [251] and [259]). In the high-energy experiments, the measured fast- H^+ ion production cross section contains a significant contribution from the dissociative ionization of H_2^+ in the region above ~ 10 keV, that has to be subtracted [261, 262]. The state of the target after the collision is usually left undetermined (see, however, [250]).

In this situation, a conservative approach (followed, e.g., in Ref. [253]) would be to determine a "lower bound" of the total CID cross section based upon reliable experimental data. The cross sections from Refs. [251, 252, 265] have provided a basis for implementing such an approach in Ref. [253]. The σ_{CID}^{tot} cross section recommended in Ref. [253], extended beyond 10 keV with the data from Ref. [252] (after subtraction of the dissociative ionization contribution to the fast- H^+ production cross section, see e.g., [261]) and its modification in the region below 10 eV by the use of original cross section values of Ref. [251], has been adopted in the present work. This (modified) cross section can be represented by the analytic expression

$$\sigma_{CID}^{tot}(E) = \sigma_{CID}^{<}(E) + \sigma_{CID}^{>}(E) \quad (209a)$$

$$\sigma_{CID}^{<}(E) = \frac{4.05}{E^{0.653}} \exp\left[-\frac{3.15}{(E-2.0)^{1.65}}\right] \quad (\times 10^{-16} \text{ cm}^2), \quad (209b)$$

$$\sigma_{CID}^{>}(E) = \frac{0.139E^{0.318} \exp(-680/E^{2.10})}{1 + 2.75 \times 10^{-12} E^{2.65} + 9.04 \times 10^{-23} E^{4.65}} \quad (\times 10^{-16} \text{ cm}^2), \quad (209c)$$

where E is the ion impact (laboratory) energy in eV units (see Figure 45 on page 184). Other low-energy experimental data (e.g., from Ref. [259]) can be accommodated in this expression by increasing the coefficient 4.05 in Eq. (209b) by a factor of two. The reliability of $\sigma_{CID}^{>}$ cross section above $\sim 30 - 40$ keV, however, is not very high.

B CID cross sections for individual initial v_i states

The cross sections $\sigma_{v_i}^{CID}$ for the individual excited states of $H_2^+(v_i)$ in reaction (208) have been experimentally determined in Ref. [255] for $v_i = 0 - 10$ at ion impact energies $E_{lab} = 8, 12, 16$ and 32 eV. These cross sections are given in Table 50. From the values in this table it is observed that $\sigma_{v_i}^{CID}$ have, on average, a linear dependence on v_i and are virtually independent on ion energy in the considered energy range. The claimed accuracy of $\sigma_{v_i}^{CID}$ cross sections of Ref. [255] is $\sim 30\%$.

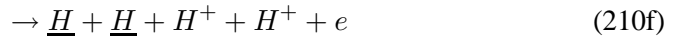
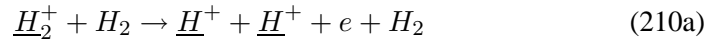
The TSH calculations of $\sigma_{v_i}^{CID}$ in Ref. [260] for $v_i = 0, 3$ and 6 for $E_{lab} = 8$ and 16 eV, and $v_i = 0 - 7$ for $E_{lab} = 12$ eV, give somewhat higher values than

7 Collision Processes of H_2^+

those of Ref. [255], but confirm the linear v_i -dependence and the weak energy dependence of $\sigma_{v_i}^{CID}$. It is, however, unclear how far beyond the considered energy range these dependencies of $\sigma_{v_i}^{CID}$ can be extended.

C Other collision induced dissociative processes

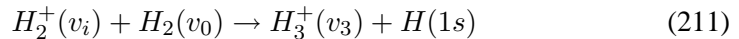
Apart from the induced dissociation described by Eq. (208), there are several other dissociative processes that can take place in high energy $H_2^+ + H_2$ collisions. These include (we omit the vibrational state labels)



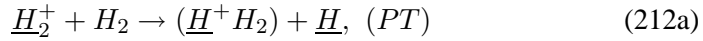
where the "fast" products are underlined. Coincident registration of all reaction products is infeasible, and in most cases composite (inclusive) cross sections for particle (ion, atom, or electron) production are measured. The cross section for dissociation ionization process (210a) has been, however, determined experimentally [262] in the ion energy range above 30 keV. The fast-H atom-production cross section has been measured in [252] for $E_{lab} \geq 3$ keV; it is by a factor 2-3 larger than the fast- H^+ -ion production cross section in this energy region. The slow- H^+ -ion production cross section has also been measured in the ion energy range 5 – 50 keV [250] with values significantly smaller than the fast- H^+ production cross section. All "particle production" inclusive cross sections of dissociative processes (210) attain their maxima (of the order of 10^{-16} cm^2) at ion kinetic energies in the range $\sim 20 - 100 \text{ keV}$, and show a trend of rapid decrease with decreasing the energy.

7.3.3 H_3^+ ion formation

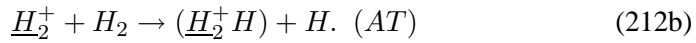
The process



has been subject of numerous experimental [251, 259, 267–274] and theoretical [260, 275–277] studies. Most of experimental studies have been devoted to determination of total cross section of H_3^+ ion formation (with unspecified initial and final vibrational state distributions), but in a few of them [271–273], the v_i -dependence of the cross section for a number of collision energies (in the range $E_{CM} = 0.04 - 15$ eV) and for $v_0 = 0$ has been investigated. Theoretical studies have been performed within the classical trajectory surface hopping (TSH) method and have produced not only total and initial (v_i) state-selective cross sections [275, 277], but also cross sections corresponding to the two particle exchange channels of reaction (211) [260, 276] : the proton transfer channel



and the atom transfer channel



The H_3^+ molecular ion has two vibrational modes: a symmetric stretch mode and a degenerate (asymmetric plus bend) mode. The asymmetric stretch vibrational states can make dipole transitions to the ground symmetric stretch states and have lifetimes in the millisecond range [278]. The symmetric stretch states can decay to the ground state only via electric quadrupole transitions. Dipole transitions from symmetric to asymmetric states are, however, possible, which renders their lifetime in the millisecond range as well. The symbol v_3 in Eq. (211) refers to the symmetric stretch vibrational states of H_3^+ .

The population of vibrational states of H_3^+ resulting from reaction (211) with $v_i = v_0 = 0$ at thermal energies has been analyzed in Ref. [279] and the results are given in Table 51. The excitation energies of vibrational states of H_3^+ are also given in this table (taken from Ref. [279]). A more refined treatment of vibrational spectrum of H_3^+ ion can be found in [276, 278]. We note that the dissociation energy of H_3^+ is 4.51 eV, i.e. H_3^+ is more stable than H_2^+ .

A State-selective cross sections

For $v_i = v_0 = 0$, the reaction (211) is exothermic by 1.73 eV with a thermal rate coefficient of $2.11 \times 10^{-9} \text{ cm}^3/\text{s}$ [274]. Its cross section $\sigma^{H_3^+}(v_i = v_0 = 0)$ has been experimentally determined in the energy region below 15 eV [271–273]. Theoretical calculations [275–277] support the experimental data for $E_{CM} \lesssim 5$ eV, but at higher energies the TSH cross sections decrease faster than the experimental ones. The $\sigma^{H_3^+}(v_i = v_0 = 0)$ cross section increases with decreasing the energy as $E_{CM}^{-0.48}$ for $E_{CM} \lesssim 1 \text{ eV}$, and shows a rapid decrease when the energy increases above $E_{CM} \sim 2$ eV. A similar energy behaviour is observed in the total cross sections with undetermined v_i and v_0 initial state distributions. The rapid decrease of $\sigma^{H_3^+}$ for $E_{CM} \gtrsim 2$ eV is associated with the competing CID process.

7 Collision Processes of H_2^+

The available experimental and theoretical data on $\sigma^{H_3^+}(v_i = v_0 = 0)$ can be represented by the analytic expression

$$\sigma^{H_3^+}(v_i = v_0 = 0) = \frac{17.76(\times 10^{-16} \text{cm}^2)}{E^{0.477}(1 + 0.0291E^{3.61} + 1.53 \times 10^{-5}E^{6.55})} \quad (213)$$

where E is the C.M. energy in eV units. This cross section has a correct thermal energy limit, and describes the original data well within their inherent uncertainties. See Figure 46 on page 184.

The ratio

$$f(v_i) = \frac{\sigma^{H_3^+}(v_i, v_0 = 0)}{\sigma^{H_3^+}(v_i = v_0 = 0)} \quad (214)$$

has been experimentally determined for $v_i = 1 - 4$ [273] at a number of C.M. energies between 0.04 eV and 15 eV, and shows a smooth behaviour that allows reliable extrapolation. (Note that $v_i = 0 - 4$ states account for 77% of the $H_2^+(v_i)$ population; see Table 25.)

The values of $f(v_i)$ from Ref. [273], extrapolated up to $v_i = 10$, are given in Table 52 for twelve energies from the range 0.04 eV-15 eV. The smooth energy behaviour of $f(v_i)$ allows reliable interpolation along the energy scale. It is to be noted in Table 52 that for $E_{CM} \leq 0.5$ eV and $E_{CM} \gtrsim 10$ eV, $f(v_i) \leq 1$, whereas for $0.5 \text{ eV} < E_{CM} < 10 \text{ eV}$, $f(v_i) \geq 1$ for the lower v_i values. The suppression of $\sigma^{H_3^+}(v_i \geq 1, v_0 = 0)$ with respect to $\sigma^{H_3^+}(v_i = v_0 = 0)$ in the region $E_{CM} \leq 0.5 \text{ eV}$ is due to competition with the strong charge exchange channel, while its suppression for $E \gtrsim 10$ eV (and even at lower energies for the high v_i states) is due to competition with the CID channel.

There have been no experimental or theoretical studies so far for the state-selective H_3^+ formation process with $v_0 \geq 1$. For the most populated $v_i = 1 - 3$ levels of H_2^+ , however, reaction (211) becomes endothermic for $v_0 \gtrsim 5 - 3$, resulting in a decrease of H_3^+ formation cross section with respect to $\sigma^{H_3^+}(v_i = v_0 = 0)$. The merged and crossed beams experiments on H_3^+ formation [267, 268], in which the H_2 beam is produced by charge exchange with H_2^+ and is, therefore, vibrationally excited, indeed give total H_3^+ formation cross sections that are by a factor 0.7-0.8 smaller than $\sigma^{H_3^+}(v_i = v_0 = 0)$.

Apart from the earlier mentioned determination of $P(v_3)$ populations of $H_3^+(v_3)$ vibrational states for the $v_i = v_0 = 0$ case of reaction (211) at thermal energies [279] (see Table 51), only a single theoretical TSH study is available [276] in which $P(v_3)$ has been investigated for $v_i = 3, v_0 = 0$ and $E_{CM} = 0.11, 0.46$ and 0.93 eV. This study indicates that $P(v_3)$ has a significant v_i dependence, but its variation in the considered energy is relatively weak.

B Total cross sections

The total cross section for H_3^+ ion formation, summed over v_i and v_3 , but for

the initial $v_0 = 0$ state, is obtained as

$$\sigma^{H_3^+}(v_i \text{ all}; v_0 = 0) = \sum_{v_i=0}^{18} f(v_i) P_{H_2^+}(v_i) \sigma^{H_3^+}(v_i = v_0 = 0) \quad (215)$$

Where $f(v_i)$ is given by Eq. (214), and $P_{H_2^+}(v_i)$ is the initial population of $H_2^+(v_i)$ states (see Table 25). The values of $f(v_i)$ from Table 52 can further be extrapolated to $v_i \geq 11$, but in view of small values of $P_{H_2^+}(v_i)$ for $v_i \geq 11$, the terms with $v_i \leq 10$ in the sum of Eq. (215) account for about 99% of the total cross section. In the energy range $0.5 \text{ eV} \lesssim E_{CM} \lesssim 10 \text{ eV}$, where for the lower v_i $f(v_i) > 1$, the total cross section $\sigma^{H_3^+}(v_i \text{ all}; v_0 = 0)$ is larger than $\sigma^{H_3^+}(v_i = v_0 = 0)$, in accordance with experimental data obtained by the ion beam gas cell method [269, 270], in which $H_2^+(v_i)$ are produced by electron-impact ionization of $H_2(v_0 = 0)$.

As discussed in the preceding sub-section, the total section

$$\sigma_{H_3^+}^{tot}(v_i \text{ all}; v_0 \text{ all}) = \sum_{v_i=0}^{18} \sum_{v_0=0}^{14} f(v_i) P_{H_2^+}(v_i) P_{H_2}(v_0) \sigma^{H_3^+}(v_i = v_0 = 0) \quad (216)$$

is expected to be somewhat smaller than $\sigma^{H_3^+}(v_i \text{ all}; v_0 = 0)$ due to appearance of endothermic channels in Eq. (211) for certain pairs v_i, v_0 of initial states. ($P_{H_2}(v_0)$ in Eq. (216) is the population of v_0 state of $H_2(v_0)$.) The total merged (crossed) beams H_3^+ formation cross sections of Refs. [267, 268] indicate that the reduction factor

$$\kappa(E_{CM}) = \frac{\sigma_{H_3^+}^{tot}(v_i \text{ all}; v_0 \text{ all})}{\sigma^{H_3^+}(v_i = v_0 = 0)} \quad (217)$$

lies in the range $\kappa(0.02 \text{ eV}) \simeq 0.78$ to $\kappa(3 \text{ eV}) \simeq 0.67$.

C Proton and atom transfer cross sections

In certain plasma modelling studies it is important to distinguish between the proton and atom transfer H_3^+ formation channels, (212a) and (191b), respectively. The TSH cross section calculations for these reaction channels have been performed for $v_i = v_0 = 0$ and $v_i = 3, v_0 = 0$ cases in the C.M. energy range 0.25-5.0 eV [276]. The relative contribution of proton transfer (PT) and atom transfer (AT) channels to H_3^+ ion formation cross section are given in Table 53 [276]. Similar calculations have been extended in Ref. [261] up to 8 eV. Table 53 shows that at low ($\lesssim 1 \text{ eV}$) energies, the PT and AT contributions to H_3^+ formation cross section are approximately equal, but at higher energies the AT contribution dominates. These findings are in agreement with the experimental studies of PT and AT reactions



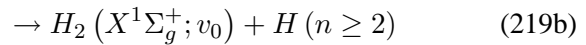
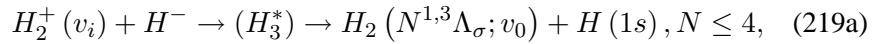
performed in Ref. [280].

7.4 Collisions of $H_2^+(v_i)$ with H^-

The collision dynamics of $H_2^+(v_i) + H^-$ system at low energies is dominated by the strong attractive Coulomb interaction in the entrance channel. The energy of $\{H_2^+(v_i = 0) + H^-\}$ state at infinite separations R between H_2^+ and H^- ions lies 0.754 eV below the energy of $\{H_2^+(v_i = 0) + H(1s)\}$ state, and 1.08 eV above the energy of $\{H_2(v_0 = 0) + H^+\}$ state. With decreasing R , the potential energy curve of ionic state $\{H_2^+(v_i = 0) + H^-\}$, therefore, intersects (in a diabatic approximation) the potential energies of all covalent $\{H_2^*(N^{1,3}\Lambda_{\sigma'}, v_0) + H(1s)\}$ ($N \leq 4$) and $\{H_2(X^1\Sigma_g^+; v_0) + H^*(n \geq 2)\}$ states. The non-adiabatic coupling of initial ionic state with the covalent states (having the same symmetry as the ionic state) results in electron capture reactions during a $H_2^+ + H^-$ collision. The adiabatic energy curve of the $\{H_2^+(v_i = 0) + H^-\}$ state, as function of $H_2^+ - H$ distance R (and at a fixed distance $\rho = 1.65a_0$ between two of the protons, corresponding to the equilibrium distance of equilateral H_3 systems; a_0 is the Bohr radius), has a minimum at $R \simeq 3.6 - 3.8a_0$, and intersects the potential energy curve of H_3^+ ion at $R \simeq 2.6a_0$ [281]. In the region $R \leq 2.6a_0$ the $\{H_2^+(v_i = 0) + H^-\}$ state becomes an auto-ionizing (resonant) state that can decay either forming a vibrationally excited H_3^+ ion (associative detachment) or producing $H_2^+ + H(1s)$ (or $H_2 + H^+$ at higher collision energies) fragments (non-associative detachment). Before entering the $H_3^+ + e$ continuum, the potential curve of resonant $\{H_2^+(v_i = 0) + H^-\}$ state diabatically intersects (for the second time) the potential energy curves of all states of the H_3 system, except those of the first excited and of the dissociative ground state. The excited states of H_3 system are loosely bound and unstable against pre-dissociation. The first excited state of H_3 , although of different symmetry (2B_2) than the resonant $\{H_2^+(v_i = 0) + H^-\}$ state (2A_1) is, nevertheless, coupled with it and can be significantly populated during the $H_2^+(v_i = 0) + H^-$ collision. This state asymptotically correlates to the $H_2(b^3\Sigma_u^+) + H$ configurations and its population leads to production of three $H(1s)$ atoms.

7.4.1 $H_2^+ - H^-$ mutual neutralization

The mutual ion-ion neutralization (or recombination) processes:



have not been studied in detail so far. There has been only one total cross section measurement of reaction (219) at three energies in the keV region [282] indicating that the cross section for this reaction (at these energies) is close to that of the $H^+ + H^-$ collision system. A recent theoretical attempt to estimate the cross section of reaction (219) within a multichannel Landau-Zener model [283] has failed due to an inappropriate treatment of channel dynamics and coupling interactions.

On general theoretical grounds (see [5, 6]), one should expect that mutual neutralization cross section of $H_2^+(v_i)$ and H^- ions in the energy region below ~ 1

7.4 Collisions of $H_2^+(v_i)$ with H^-

keV should be large and comparable to that for the $H^+ - H^-$ system (see subsection 3.2.1). For the electron capture in reactions (219), the most important are the (avoided) potential energy crossings R_x of initial ionic state with the final channel states at the large $H_2^+ - H$ distances, R . The crossings of $N \geq 4$ and $n \geq 4$ channels in Eqs. (219a),(219b) are distributed at $R \gtrsim 80a_0$, where the ionic-covalent coupling is too weak (see, e.g., [284]). For the states with $(N, n) = 2$ and $(N, n) = 3$, these crossings are distributed in the regions $\delta R_{2,x} = 8 - 11 a_0$ and $\delta R_{3,x} = 19 - 40 a_0$, respectively, where the ionic-covalent coupling can induce strong transitions (in analogy with the case of $H^+ - H^-$ system; see [93,94,284]). The large density of available charge exchange (covalent) channels within each $(N, n) = 2, 3$ group of states, particularly when the vibrational v_0 -states are taken into account, provides ample compensation for the reduction of coupling matrix element due to its multiplication with the Franck-Condon factor for the $v_i \rightarrow v_0$ transition.

A rough estimate of the total mutual neutralization cross section for reactions (219a,219b), summed over v_0 -states, can be obtained by using the absorbing sphere model (ASM) [285]. The application of this model can be justified by the high density of available charge exchange states within each $N^{1,3}\Lambda_\sigma$ vibrational manifold. The cross section for charge exchange reaction (219a) within this model for $N = 2, 3$ states is, respectively, given by

$$\begin{aligned}\sigma_{CX,2}^{(ASM)}(v_i; 2^{1,3}\Lambda_\sigma) &= \pi R_{2x}^2 S_2(E), \\ \sigma_{CX,3}^{(ASM)}(v_i; 3^{1,3}\Lambda_\sigma) &= \pi [R_{3x}^2 S_3(E) - R_{2x,max}^2]\end{aligned}\quad (220)$$

where R_{2x} and R_{3x} are the crossing points (in a_0 units) of corresponding ionic and covalent states, and $R_{2x,max}$ is the largest of $R_{2,x}$ crossings. The factors $S_2(E)$ and $S_3(E)$, that depend on collision energy E , are the survival probabilities of the system in the covalent state $\{H_2(N^{1,3}\Lambda_\sigma) + H(1s)\}$ in the region $R \leq R_{Nx}$ against pre-dissociation to states $N' \neq N$, or decay in the H_3^+ continuum (after the second interaction of covalent state with the $\{H_2^+(v_0) + H^-\}^2 A_1$ resonant state at small R). The crossing point R_{Nx} is related to the vibrational energy $E_{H_2^+}^{exc}(v_i)$, ionization energy $I_{H_2}(N^{1,3}\Lambda_\sigma; v_0 = 0)$ and electron affinity $EA(H^-)$ ($=0.754$ eV) by

$$R_{Nx}(a_0) = \frac{27.2}{E_{H_2^+}^{exc}(v_i) + I_{H_2}(N^{1,3}\Lambda_\sigma; v_0 = 0) - EA(H^-)}\quad (221)$$

where all energies in Eq. (221) are expressed in eV.

Relations similar to Eqs. (220-221) can be written also for charge exchange channel (198b). If one sets $S_2 = S_3 = 1$ in Eq. (220), the total cross sections for mutual neutralization, $\sigma_{MN,2}^{(ASM)}$ and $\sigma_{MN,3}^{(ASM)}$ in the $N = 2$, and $N = 3$ channels are determined only by the values of R_{Nx} , Eq. (221).

In order to estimate the magnitudes of $\sigma_{MN,2}^{(ASM)}$ and $\sigma_{MN,3}^{(ASM)}$, we take the mean values $\bar{R}_{2x} (= 9.24a_0)$ and $\bar{R}_{3x} (= 25.5a_0)$ for R_{2x} and R_{3x} from the intervals

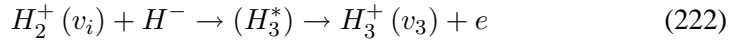
7 Collision Processes of H_2^+

δR_{2x} and δR_{3x} mentioned above. The resulting cross sections are $\sigma_{MN,2}^{(ASM)} \simeq 7.5 \times 10^{-15} \text{cm}^2$ and $\sigma_{MN,3}^{(ASM)} \simeq 5.0 \times 10^{-14} \text{cm}^2$. These values are of the same order of magnitude as those for $\sigma_{MN}(n=2)$ and $\sigma_{MN}(n=3)$, respectively, of the reaction $H^+ + H^- \rightarrow H(n) + H(1s)$ in the energy range 1-10 eV (see sub-section 3.2.1).

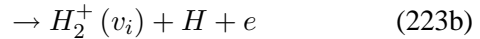
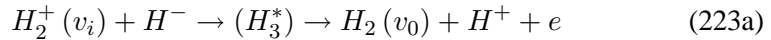
As we shall see in the next sub-section, the total electron detachment (associative and non-associative) cross section in the $H_2^+ + H^-$ collision system is not very large ($\sim 5 \times 10^{-17} \text{cm}^2$ in the energy region 1-5 eV), which indicates that the population of resonant $H_3^*(^2A_1)$ by the non-adiabatic couplings of this and covalent states at small $H_2^+ - H^-$ distances ($2.6 a_0 \leq R \lesssim 4a_0$), and its decay in the H_3^+ , $(H_2 + H^+)$ and $(H_2^+ + H)$ continua is not very strong. Therefore, continuum decay processes do not affect significantly the survival of charge exchange (covalent) states in the region $R < R_{Nx}$, and, consequently, the total mutual ion-ion neutralization cross section. However, the pre-dissociation of H_3^* bound excited states, as well as their coupling with the resonant state at $R > 2.6 a_0$, can significantly affect the above estimates for $\sigma_{MN,2}^{(ASM)}$ and $\sigma_{MN,3}^{(ASM)}$. It should also be mentioned that even some of the asymptotic states in reaction (219a) are pre-dissociating states (such as $D^1\Pi_u(v_0)$ and $d^3\Pi_u(v_0)$ for $v_0 \geq 3$). Furthermore $N=2,3$ gerade triplet states are radiatively coupled with the dissociative $b^3\Sigma_u^+$ state. This indicates that $H_2^+ - H^-$ mutual neutralization can lead to significant dissociation to neutral atoms.

7.4.2 Associative and non-associative detachment

The associative detachment (AD) reaction



has been experimentally studied [85, 286] and its total cross section (summed over v_i and v_3) is known in the collision (C.M.) energy range 0.07-10 eV. As discussed earlier, reaction (222) results from the decay of resonant $H_3^*(^2A_1)$ state in the H_3^+ continuum for $H_2^+ - H^-$ distances $R \leq 2.6 a_0$ [281]. Other decay modes of $H_3^*(^2A_1)$ resonance in the region $R < 2.60 a_0$, the non-associative reactions



have, however, not been studied as yet.

The potential curve of 2A_1 resonant $\{H_2^+(v_i=0) + H^-\}$ state intersects the H_3^+ potential energy curve at the position ($R = 2.6 a_0$) on the right from its minimum ($R \simeq 1.5a_0$), which energetically corresponds to the $v_3=3$ vibrational level [281]. This indicates that the levels $v_3 \gtrsim 3$ are predominantly populated in reaction (222). For $v_i \geq 1$, the v_3 -distribution of H_3^+ in reaction (222) is shifted upward for the amount of excitation energy $E_{H_2^+}^{exc}(v_i)$.

The measured total cross section of associative detachment reaction (222) can be represented by the analytic expression

$$\sigma_{AD}^{\text{det}} = \frac{0.38 \times 10^{-16} \text{ cm}^2}{E^{0.782} (1 + 0.039E^{2.62})} \quad (224)$$

where the collision (C.M.) energy is expressed in eV. The $E^{-0.782}$ (close to E^{-1} !) behaviour of σ_{AD}^{det} at energies below ~ 1 eV reflects the dominant role of attractive Coulomb interaction in the entrance reaction channel (see for more detail Refs. [86,286]). The fast decrease of σ_{AD}^{det} for $E \gtrsim 3$ eV indicates that the non-associative detachment reactions (223), competing with (201), become dominant decay modes of the H_3^* resonance at these energies. See Figure 47 on page 185.

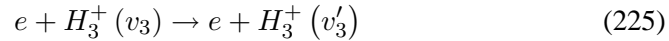
8 Collision Processes of H_3^+

The collision processes of H_3^+ ions with e, H, H_2 and H^- have been relatively little investigated compared to the processes of other charged particles of a low-temperature hydrogen plasma. Exception is the process of dissociative $e + H_3^+$ recombination that received much attention in last two decades because of several conflicting experimental results on its rate coefficient, and because of its fundamental importance in astrophysics (see sub-section 8.1.2 and Refs. [287,288]). In the present section we review the available cross section information for collision processes of H_3^+ with other constituents of a low temperature hydrogen plasma and emphasize the lack of such information for some important processes.

8.1 Collision processes of H_3^+ with electrons

8.1.1 Vibrational excitation

The electron impact vibrational excitation of $H_3^+(v_3)$



has not been studied so far. The transitions between the (symmetric stretch) v_3 states of H_3^+ can take place only via the electric quadrupole interaction, and in the Coulomb-Born approximation (CBA) the cross section for predominant $v_3 \rightarrow v_3 + 1$ transition is given (in analogy with the $e + H_2^+(v)$ case; see sub-section 7.1.1) by [209]

$$\sigma_{vib}^{exc}(v_3 \rightarrow v_3 + 1) = \frac{3 \times 0.284}{\omega k^2} (v_3 + 1) \left(\frac{\partial Q_2}{\partial \rho} \right)_{\rho_0}^2 (\pi a_0^2) \quad (226)$$

where ω is the v_3 -vibrational spacing in $H_3^+(v_3)$ ($\omega = 0.372$ eV; see Table 51), k is the electron wave number, Q_2 is the electric quadrupole moment of H_3^+ related to the charge displacement along one of its three internal internuclear distances ρ , and

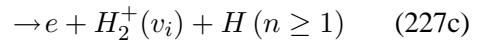
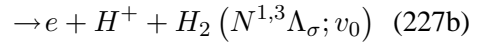
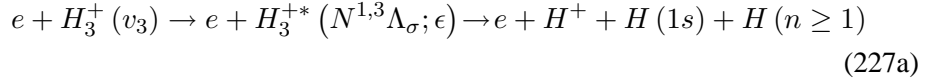
8 Collision Processes of H_3^+

its derivative is evaluated at the equilibrium distance ρ_0 ($= 1.65 a_0$) of equilateral geometry (D_{3h} symmetry) of H_3^+ . The factor 3 in Eq. (226) takes into account the three internuclear distances in H_3^+ ; the energies ω and $k^2 (= 2E_{el})$ are expressed in atomic units (1 a.u. of energy = 27.2 eV) and a_0 ($= 0.529 \text{ \AA}$) is the Bohr radius. The electric quadrupole moment $Q_2(\rho)$ for H_3^+ has been calculated in Ref. [289]. The cross section σ_{vib}^{exc} given by Eq. (226) is summed over the rotational states of v_3 and $(v_3 + 1)$ vibrational levels.

For the dipole allowed electron impact transitions between the symmetric stretch v_3 states and asymmetric stretch \tilde{v}_3 states of H_3^+ , a general CBA cross section formula, analogous to Eq. (226), is available in Ref. [209]. It relates σ_{vib}^{exc} to the derivative of dipole moment $Q_1(\rho)$ at the equilibrium distance ρ_0 , which is also available from Ref. [289].

8.1.2 Dissociative excitation

In the Franck-Condon region of ground vibrational state of H_3^+ ion, all electronic excited states of this ion have repulsive character in the D_{3h} geometries [290]. Only some of them exhibit bound character at large bond distances with a shallow potential well. A vertical Franck-Condon transition from the lower v_3 -states ($v_3 \lesssim 6 - 7$) of ground electronic state $^1A'$ of H_3^+ to any of the electronic excited states of this ion leads to dissociation of H_3^+ . The electron-impact dissociative excitation of H_3^+ ion can result in several dissociation channels



The total cross section of proton production reactions (227a) and (227b) has been measured in the energy range from threshold ($\simeq 15$ eV) up to ~ 600 eV [291], while the total cross section of reaction (227c) has been measured only in the region 14.75 eV (threshold) to $\simeq 30$ eV [292]. The initial vibrational state of H_3^+ in these experiments was claimed to be $v_3 = 0$ (this claim being supported by the observed threshold energies corresponding to vertical transitions from $H_3^+(v_3 = 0)$ state to specific electronic excited states of H_3^+). The total cross section for proton production reactions (227a) and (227b) shows weak structures above $E \simeq 19.25$ eV, indicating that several excited states of H_3^+ ion contribute to the cross section. Similar, but much more pronounced structures were observed in the cross section for the reaction (227c) [292].

With an accuracy exceeding the experimental uncertainties, the total H^+ production cross section in reactions (227a) and (227b) can be represented by the

8.1 Collision processes of H_3^+ with electrons

analytic expression

$$\sigma_{DE}^{(H^+)} = \frac{82.56}{E^{0.521}} \left[1 - \left(\frac{15.0}{E} \right)^{5.15} \right] \exp \left\{ - \frac{50.32}{E^{1.177} (1 + 1.019 \times 10^{-14} E^{7.462})} \right\} \quad (228)$$

$(\times 10^{-16} \text{ cm}^2)$

where E is the collision energy in eV units (see Figure 48 on page 185). Experimental resolution of the contributions of channels (227a) and (227b) to the cross section $\sigma_{DE}^{(H^+)}$ has not been made, but the potential energy curves of excited electronic states of H_3^+ [290] indicate that for $E \gtrsim 20$ eV the $\sigma_{DE}^{(H^+)}$ cross section is dominated by the reaction channel (227a) with $n = 1$.

The cross section of reaction (227c) in the energy interval 14.75 - 32 eV, in which it has been measured [292], shows sharp resonant structures, typical for the processes proceeding via formation of intermediary resonances (H_3^*). The mean value of this cross section, averaged over the resonant structures, is about $0.3 \times 10^{-16} \text{ cm}^2$, i.e. more than an order of magnitude smaller than $\sigma_{DE}^{(H^+)}$ in the energy interval 16 - 32 eV. Since in the energy region above ~ 20 eV dominant contribution to $\sigma_{DE}^{(H^+)}$ gives the dipole allowed transition to the first excited singlet $^1E'$ state of H_3^+ , which is a dissociative state producing two $H(1s)$ atoms, it follows that dominant electron-impact dissociative excitation channel for H_3^+ above 20 eV is (227a) with $n = 1$. A polynomial fit to $\sigma_{DE}^{(H^+)}$ cross section is given also in Ref. [11].

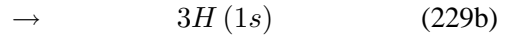
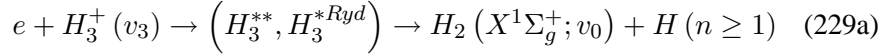
8.1.3 Dissociative recombination (DR)

Contrary to the case of $e + H_2^+(v_i)$ dissociative recombination (DR), where the diabatic potential energy curve of doubly excited $(2p\sigma_u)^2$ resonant state of H_2 intersects the potential energy curve of H_2^+ ion at the energy position of $v_i = 0$ vibrational state, and thereby ensures the effectiveness of "direct" DR mechanism (see sub-section 7.1.3), in the case of $e + H_3^+(v_3)$ collision system, as mentioned earlier, the potential energy curve of 2A_1 resonant state of H_3 intersects the potential curve of ground electronic state of H_3^+ at the energy position of its $v_3 = 3$ vibrational level. This circumstance strongly suppresses the effectiveness of direct DR mechanism for the $e + H_3^+(v_3 = 0)$ collision system at thermal energies, and was taken as a basis for interpretation of the small observed values of thermal DR rate coefficient ($K_{DR}(300K) \lesssim 10^{-10} \text{ cm}^3/\text{s}$) in flowing afterglow / Langmuir probe (FALP) experiments [293]. At the same time, this argument was used to question the complete vibrational relaxation of $H_3^+(v_3)$ ion in the stationary afterglow [294], merged beams [295, 296] and infrared spectroscopy [297] DR experiments, reporting thermal DR rate coefficient of $1 - 2 \times 10^{-7} \text{ cm}^3/\text{s}$ and claiming

8 Collision Processes of H_3^+

complete vibrational relaxation of $H_3^+(v_3)$. The multi-pass merged beams experiments performed on ion storage rings [298,299], in which the H_3^+ ions are certainly vibrationally fully relaxed ($v_3 = 0$), also give values for the thermal DR rate coefficient of H_3^+ of $1 - 2 \times 10^{-7} \text{ cm}^3/\text{s}$. The question then arises about the reaction mechanism producing such high thermal values for K_{DR} of $H_3^+(v_3 = 0)$.

The $e + H_3^+(v_3)$ DR reaction has two principal dissociation channels,



where H_3^{**} is a doubly excited (resonant) state and H_3^{*Ryd} is a (core excited) pre-dissociating (possibly also auto-ionizing) Rydberg state that provides an "indirect" mechanism for DR. Most of DR cross section measurements have been performed for "cold" ($v_3 \leq 1$) H_3^+ ions [295, 296, 298, 299], covering the collision energy range from $\sim 0.001 \text{ eV}$ to 30 eV . There are also cross section measurements with H_3^+ vibrationally excited [300], with a v_3 -population distribution corresponding to that given in Table 51. In all these experiments only the total cross section for the two DR channels, (229a) and (229b), has been measured.

There are only two theoretical (total) cross section calculation of DR reaction (229) with $v_3 = 0$. In one of them [301], only the contribution from the direct DR mechanism (with inclusion of four H_3^{**} states) was considered by employing the wave packet propagation method on potential energy surfaces of H_3 (two-dimensional dynamics). These calculations have reproduced the broad resonant feature in the DR cross section observed in the energy region around 10 eV . The other calculation [302], performed within a "hybrid" wave packed-multichannel quantum defect method in the energy range below 1 eV , has included the contributions from both direct and indirect DR mechanisms. It was shown that the cross section obtained with the direct DR mechanism alone is four to five orders smaller than the experimental cross section in this region. Adding the contribution from the indirect DR mechanism reduces this difference to two orders of magnitude. Only quite recently, in a three-dimensional treatment of collision dynamics (involving inclusion of new types of kinetic couplings, such as Jahn-Teller interactions) [303], an agreement of theoretical and experimental cross section results in the low energy region has been reached.

A Total cross section and channel branching ratios for $H_3^+(v_3 = 0)$ DR

As mentioned earlier, the total DR cross section results from storage ring experiments with $H_3^+(v_3 = 0)$ agree well with each other (see also discussions in [228] and [287]) and cover the collision energy range from $\sim 5 \times 10^{-4} \text{ eV}$ to $\sim 30 \text{ eV}$. The total cross section from the CRYRING storage ring experiment [298] can be represented by the following analytic expression

$$\sigma_{DR}^{tot}(v_3 = 0) = \sigma_{DR}^L(v_3 = 0) + \sigma_{DR}^H(v_3 = 0) \quad (230)$$

8.1 Collision processes of H_3^+ with electrons

$$\sigma_{DR}^L = \frac{3.00 (\times 10^{-16} \text{ cm}^2)}{E^{0.725} (1 + 4.45E^{1.20})} \quad (231a)$$

$$\frac{1}{\sigma_{DR}^H} = \frac{1}{\sigma^<} + \frac{1}{\sigma^>} \quad (231b)$$

$$\sigma^< = 0.0646E^{1.478} (\times 10^{-16} \text{ cm}^2) , \sigma^> = \frac{634.22}{E^{2.605}} (\times 10^{-16} \text{ cm}^2) \quad (231c)$$

where E is the relative collision energy in eV.

This cross section is plotted in Figure 49 on page 186. σ_{DR}^L describes the low-energy part of the cross section. The departure of its $E^{-0.725}$ behaviour in the low energy limit (for $E \lesssim 0.1$ eV) from the E^{-1} Wigner law is a reflection of complex dynamical mechanisms governing the DR process in this region [302, 303]. σ_{DR}^H term in Eq. 230 describes the broad resonant feature in $\sigma_{DR}(v_3 = 0)$ in the region around $E \simeq 10$ eV.

The relative contributions of reaction channels (229a) and (229b) to the total cross section $\sigma_{DR}^{tot}(v_3 = 0)$ as function of energy have been measured in both single-pass [304] and multi-pass (storage ring) [305] merged beams experiments. The storage ring data cover a broader energy range and they are given in Table 54 for a number of collision energies in the range 0.003 – 25 eV. This table shows that for $E \lesssim 0.3$ eV, the branching ratios of the channels (229a) and (229b) are practically constant, with average values of 0.24 and 0.76, respectively. At the collision energy of $\simeq 0.35$ eV (close to the threshold for excitation of first vibrational state of H_3^+ ; see Table 51, the branching ratio of two-body dissociation channel begins to increase rapidly, reaching a maximum of 0.65 at $E = 5$ eV. The two-body dissociation branching ratio exhibits resonance structures at $E \simeq 1$ eV and $E \simeq 13.6$ eV, corresponding to the thresholds for $H_2 + H$ ($n = 2$) and $H_2 + H^+ + e$ dissociation channels. For $E \gtrsim 14$ eV, the three-body dissociation channel ((229b)), completely dominates the DR process.

B Quantum state distribution of DR reaction products

The quantum states of products of DR reaction (229) with $v_3 = 0$ have been theoretically investigated in [306] under the assumption that the process is dominated by the direct mechanism (via the 2A_1 resonant state in C_{2v} geometry). The threshold energies for the lower dissociation channels of reaction (229) with $v_3 = 0$, calculated in Ref. [306], are given in Table 55. It should be noted that the exothermic $H_2(b^3\Sigma_u^+) + H(1s)$ channel in Table 55 promptly produces three $H(1s)$ atoms. The thresholds in Table 55 are given for the H_2 -fragments in their ground vibrational states. It is, however, very likely, that the large potential energy of H_3^{**} state is, to a significant extent, distributed over the vibrational (and rotational) degrees of freedom, so that the values in Table 55 represent the upper limits of corresponding thresholds. For collision energies above $\simeq 0.37$ eV, when $H_3^+(v_3)$ can be vibrationally excited by the incident electron, the DR process can also proceed via

8 Collision Processes of H_3^+

core-excited Rydberg states of H_3 , and the distribution of available total energy in the system over the possible dissociation channels is quite different. The inclusion of Jahn-Teller couplings to properly describe the DR process at low energies also leads to different populations of dissociation channels. The question of quantum state distribution of products from reaction (229) for different collision energies at the present remains open.

C Total DR cross section for $H_3^+(v_3 \geq 0)$

There have been two merged-beams cross sections measurements of reaction (229) with both cold ($v_3=0$) and vibrationally excited ($v_3 \geq 0$) H_3^+ ions in the energy range 0.01 – 0.8 eV [300]. The excited H_3^+ ions have been produced in $H_2^+ + H_2$ collisions and their vibrational population should have been that given in Table 51.

The measured total cross section $\sigma_{DR}^{tot}(v_3 = 0)$ and $\sigma_{DR}^{tot}(v_3 \geq 0)$ in the energy range 0.01 – 0.8 eV are mutually related by

$$\sigma_{DR}^{tot}(v_3 \geq 0) = R(E)\sigma_{DR}^{tot}(v_3 = 0), \quad (232)$$

where

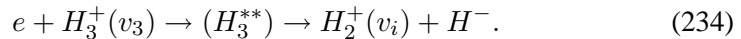
$$R(E) = \frac{9.02}{E^{0.173}}. \quad (233)$$

It should, however, be noted that the merged-beams cross section $\sigma_{DR}^{tot}(v_3 = 0)$ of Ref. [300] is by a factor of about three lower than the storage ring cross section of Ref. [298], represented by Eqs. (230 - 231), in the overlapping energy range. Nevertheless, one can plausibly assume that the ratio $R(E)$ given by Eq. (233) should retain its validity. Moreover, the ratio of other merged-beams total cross sections $\sigma_{DR}^{tot}(v_3 \geq 0)$, that are available in a broader energy range (0.001 - 5 eV; see e.g., [227, 296]) also satisfy the relation (212).

The contribution of individual v_3 states to $\sigma_{DR}^{tot}(v_3 \geq 0)$ has not been investigated as yet. The crossing of potential energy curve of $H_3^{**}(^2A_1)$ resonant state with that of ground state H_3^+ ion at the position of its $v_3=3$ level could suggest that, at least at energies above ~ 5 -6 eV, $\sigma_{DR}(v_3 = 3)$ should give the main contribution to $\sigma_{DR}^{tot}(v_3 \geq 0)$. On the other hand, the cross section measurements of Ref. [300] with successively cooled $H_3^+(v_3)$ ions indicate that, in the energy region below ~ 1 eV, the contribution of different v_3 states to $\sigma_{DR}^{tot}(v_3 \geq 0)$ is fairly uniform.

8.1.4 Ion-pair formation

An alternative decay channel for the resonant state $H_3^{**}(^2A_1)$ formed during the $e + H_3^+(v_3)$ collision is the ion-pair formation process



8.2 Collision processes of H_3^+ with H

The asymptotic limit ($R \rightarrow \infty$) of $H_3^{**}(^2A_1)$ resonant state is just the $H_2^+(v_i) + H^-$ configuration, as mentioned earlier. In order to reach this asymptotic limit in the course of dissociation, the system formed in $^2\Lambda_1$ resonant state must pass (twice!) through the regions of strong interaction with the covalent $H_2(N^{1,3}\Lambda_\sigma; v_0) + H(1s)$ and $H_2(X^1\Sigma_g^+; v_0) + H(n)$ states having $N, n \leq 4$. These couplings divert the dissociation flux into the covalent DR channels and, as result, the $H_2^+(v_i) + H^-$ dissociation channel is populated very weakly.

When $v_3 = v_i = 0$, the energy threshold for reaction (234) is 4.51 eV [306].

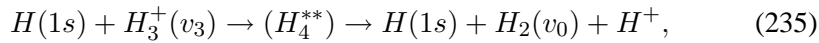
The cross section of ion-pair formation reaction (234) has been measured with both cold ($v_3 = 0$) [307,308] and $H_3^+(v_3 \geq 0)$ ions having the v_3 -distribution as in Table 51 [308]. The ion-pair formation cross section for $v_3=0$ ions has a maximum of $\sim 2 \times 10^{-18}$ cm² at $E_m \simeq 8$ eV. The cross section for $H_3^+(v_3 \geq 0)$ ions is about two times larger than for $H_3^+(v_3 = 0)$ with a threshold at $\simeq 2$ eV. Thus, the cross section for ion-pair formation in the energy range below ~ 30 eV is about two orders of magnitude smaller than the DR cross section, and the process (234) can be excluded from the plasma kinetics studies.

8.2 Collision processes of H_3^+ with H

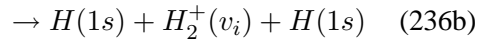
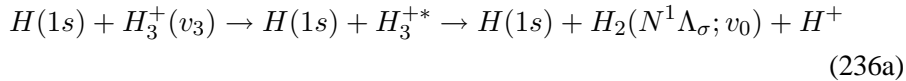
Collision processes of H_3^+ ions with hydrogen atoms have not been studied so far. However, some of these processes should exhibit significant cross sections, and their experimental and theoretical study should not pose serious difficulties. Below, we give a qualitative discussion of two such processes: dissociation and dissociative charge exchange.

8.2.1 H_3^+ dissociation

The dissociation of $H_3^+(v_3)$ in collisions with ground state H atoms may proceed via two mechanisms (in analogy with the $H + H_2^+$ case; see sub-section 7.2.3): promotion of adiabatic vibrionic states of H_4^{**} collision complex to the H_3^+ dissociation continuum,



and by direct excitation of excited electronic states of H_3^+ (dissociative excitation)



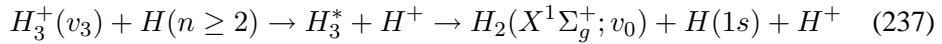
These processes can take place also when H is in an excited state. The process (235) is expected to have large cross sections ($\sim 10^{-16} - 10^{-15}$ cm²) in the collision energy region below ~ 10 eV, especially for vibrationally excited H_3^+ ions. Dissociative excitation processes (236) have thresholds in the energy region above

8 Collision Processes of H_3^+

~ 15 eV, depending on the vibrational excitation of $H_3^+(v_3)$. As mentioned earlier, in the Franck-Condon regions of lower vibrational states ($v_3 \lesssim 6 - 7$) of $H_3^+(v_3)$, all excited states of H_3^+ are dissociative. The first excited state of H_3^+ to which a dipole allowed transition is possible is the ${}^1E'$ fully dissociative state that lies 19.2 eV above the $H_3^+({}^1A_1'; v_3 = 0)$ ground state [290] and dissociates to $H_2(X^1\Sigma_g^+) + H^+$. When $v_3 \simeq 10$, the threshold for this transition is, however, reduced to about 15 eV. The next singlet excited state of H_3^+ , ${}^1A_2''$, is only 3 eV higher than ${}^1E'$ in the Franck-Condon region of $H_3^+({}^1A_1'; v_3)$. The calculation of the cross section for dissociative excitation of $H_3^+({}^1A_1'; v_3)$ in the first Born approximation, requires only knowledge of the dipole moments for the low-energy corresponding ground-to-excited singlet state transitions. The calculation of the cross section for reaction (235), however, requires determination of the adiabatic (discrete and continuous) vibronic spectrum of H_4^+ system, and solving of a large set of coupled equations (obtained e.g., within the IOSA description of collision dynamics), in analogy with the $H(1s) + H_2^+(v_i)$ case (see sub-section 7.2.3).

8.2.2 Dissociative charge transfer

The dissociative electron capture reaction



should also proceed with a large cross section at low collision energies. The formation of long-lived excited states of H_3^* (such as the np^2A_2'' states) for experimental studies of properties and dynamics of H_3^* Rydberg states [309], is standardly achieved by a H_3^+ charge exchange reaction at (1 - 1.5 keV) with Cs atoms [310]. It has been shown in Ref. [311] that np^2A_2'' states with $n=2, 3$ pre-dissociate to the vibrationally highly excited $n'p^2E'$ states, which further pre-dissociate to the dissociative ground state of H_3 [$\rightarrow H_2(X^1\Sigma_g^+) + H(1s)$]. For $H(n = 2, 3)$, the electron capture step in reaction (237) takes place at appropriately large ion-atom distances which ensures large total cross sections ($\sim 10^{-16} - 10^{-15}$ cm²) at collision energies below a few keV. It should be noted that the Rydberg state pre-dissociation dynamics may lead also to population of exit reaction channels involving electronically excited H_2 and H neutrals.

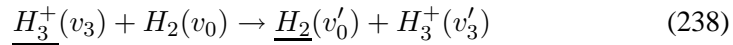
8.3 $H_3^+ - H_2$ collisions

The experimental studies of collision processes of H_3^+ ions with H_2 at both low and high collision energies are difficult because of many competing channels. Most often, inclusive cross sections are provided for a group of processes producing a specific common product ("particle production" cross sections). Theoretical studies of $H_3^+ + H_2$ collision processes are meeting the same channel complexity problem, in addition to the quantum-chemistry structural problem for this many-particle

collision system. Below we discuss the available experimental cross section information for the most important $H_3^+ - H_2$ processes. It should be noted that the vibrational energy of H_3^+ and H_2 in the experiments with these systems is largely undefined, which introduces significant uncertainties in the measured cross sections and differences between the results of various authors.

8.3.1 Proton transfer reaction

The proton transfer reaction (the “fast” particle is underlined)



can proceed very efficiently at low ($\lesssim 5$ eV) collision energies, provided the initial vibrational states of H_3^+ and H_2 ensure its exothermicity. For $v_0 = 0$ and $v_3 = 0$, reaction (238) is exothermic by 0.46 eV, but already for $v_0 = 1$ and $v_3 = 0$ it is endothermic by 0.16 eV. When H_3^+ is vibrationally excited, reaction (238) with $v_0 = 0$ becomes increasingly more exothermic and its efficiency in the thermal energy region increases. The thermal rate coefficient K_{PT} for reaction (238), with unspecified population of v_3 and v_0 states, has been measured [312] and has values in the range $(0.3 - 0.7) \times 10^{-9}$ cm³/s. It should be noted, however, that some authors have reported much smaller values of this rate coefficient for $v_3 = 1$ and $v_3 = 2$ [313].

The cross section of reaction (238) has been measured in the collision energy range above 3 eV [314]. For relative collision energies in the interval 3 - 8 eV its values are of the orders of magnitude 10^{-16} cm², but it decreases rapidly with increasing the collision energy. Connecting this cross section with the values derived from the thermal rate coefficients reported in Refs. [312], gives the following analytic expression

$$\sigma_{PT}^{(H_3^+ - H_2)} = \frac{A}{E^\alpha(1 + bE^\beta + cE^\gamma)} \quad (\times 10^{-16} \text{ cm}^2) \quad (239)$$

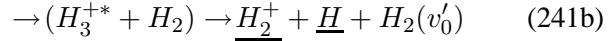
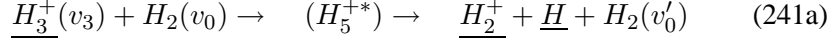
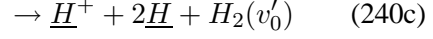
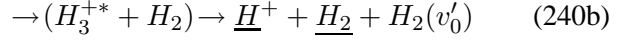
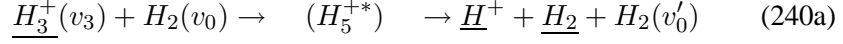
where E is the relative collision energy in eV. The cross section is shown on Figure 50 on page 186. The values of the fitting parameters in Eq. (239) for $K_{PT} = 0.3 \times 10^{-9}$ cm³/s, and for $K_{PT} = 0.7 \times 10^{-9}$ cm³/s, as well as for their average value 0.45×10^{-9} cm³/s are given in Table 56.

8.3.2 Collision induced dissociation of H_3^+

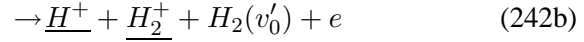
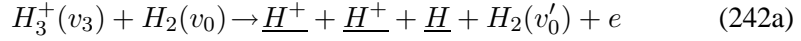
Collision induced dissociation (CID) of $H_3^+(v_3)$ in collisions with $H_2(v_0)$ can proceed either through formation and dissociation of an intermediate excited complex, H_5^{+*} , or by direct excitation of some of dissociative excited states of H_3^+ . The first mechanism is effective at low collision energies ($E_{CM} \lesssim 20 - 30$ eV), while the second one (dissociative excitation, DE) at high energies. Since H_3^+ can dissociate to both $H^+ + H_2$, $H_2^+ + H$ and $H^+ + 2H$ fragments, the following CID processes

8 Collision Processes of H_3^+

should be distinguished:



The thresholds for reaction channels (240a) and (241a), when $v_3 = v_0 = 0$, are 4.32 eV and 6.16 eV, respectively, whereas those for reaction channels (240b, 240c) and (241b) are above 15 eV (see sub-section 8.1.2). The cross sections for reactions (240) and (241) at collision (C.M.) energies below 120 eV have been measured in Refs. [314,315]. In the regions $E_{CM} \lesssim 100$ eV, for reactions (240) and $E_{CM} \lesssim 50$ eV, for reactions (241), the CID channels via formation and decay of intermediary complex (H_5^{+*}) are dominant processes and almost completely determine the $\underline{H^+}$ - and $\underline{H_2^+}$ -ion production cross sections, respectively. At the higher collision energies, where the DE channels (240b, 240c) and (241b) become more effective CID channels, contributions to the $\underline{H^+}$ - and $\underline{H_2^+}$ -ion production cross section give also the dissociative ionization processes



At these high energies, the target H_2 molecule may also be dissociated. The inclusive cross sections for processes for fast- $\underline{H^+}$ and fast- $\underline{H_2^+}$ production in $H_3^+ + H_2$ collisions have been measured in [252, 261, 263, 266] in the collision (C.M.) energy region above 800 eV. These cross sections can be smoothly connected with those of Ref. [314] for $E_{CM} \leq 120$ eV. Using the data of Refs. [252] and [314], the fast- H^+ and fast- H_2^+ ion production cross sections can be represented (with an accuracy well within the original data uncertainties) by the analytic expressions:

$$\sigma_{CID}(\underline{H^+}) = \sigma_{CID}^<(\underline{H^+}) + \sigma_{CID}^>(\underline{H^+}) \quad (243a)$$

$$\begin{aligned} \sigma_{CID}^<(\underline{H^+}) &= \frac{18.5 \exp(-54.5/E^{1.65})}{E^{0.63} (1 + 4.66 \times 10^{-6} E^{1.93})} \times \\ &\times \left[1 - \left(\frac{4.32}{E} \right)^{2.32} \right]^{4.06} (\times 10^{-16} \text{ cm}^2) \end{aligned} \quad (243b)$$

$$\sigma_{CID}^>(\underline{H^+}) = \frac{3.84 \exp(-44.2/E^{0.48})}{1 + 7.49 \times 10^{-11} E^{1.85} + 7.55 \times 10^{-28} E^{4.60}} (\times 10^{-16} \text{ cm}^2) \quad (243c)$$

$$\sigma_{CID}(\underline{H}_2^+) = \sigma_{CID}^<(\underline{H}_2^+) + \sigma_{CID}^>(\underline{H}_2^+) \quad (244a)$$

$$\sigma_{CID}^<(\underline{H}_2^+) = \frac{17.35 \exp[-5.35/(E - 6.16)^{1.65}]}{E^{1.08}(1 + 1.32 \times 10^{-8} E^{3.26})} \quad (244b)$$

($\times 10^{-16} \text{ cm}^2$)

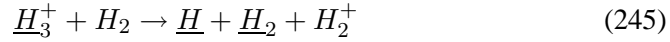
$$\sigma_{CID}^>(\underline{H}_2^+) = \frac{9.68 \times 10^{-3} E^{0.602} \exp(-1.39 \times 10^4/E^{2.57})}{1 + 7.95 \times 10^{-6} E^{1.25} + 1.03 \times 10^{-12} E^{2.62}} \quad (244c)$$

($\times 10^{-16} \text{ cm}^2$)

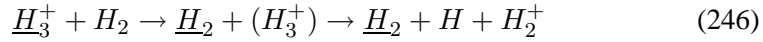
where the collision (C.M.) energy is expressed in eV units. The cross sections are shown in Figures 51 and reffig50 on page 187, respectively. The experimental cross sections of Ref. [252] for $\underline{H}^+ -$ and $\underline{H}_2^+ -$ ion production extend to $E_{CM} \simeq 50$ keV and $E_{CM} \simeq 40$ keV, respectively, and beyond these energies the analytic fits are less reliable.

8.3.3 Dissociative electron capture and fast H_2 production

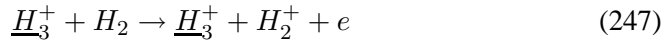
The dissociative charge transfer reaction



produces a slow H_2^+ ion and fast \underline{H} and \underline{H}_2 products. Slow H_2^+ ions are produced also in the dissociative proton transfer reaction at low collision energies



and direct target ionization at high energies



Besides in reactions (245) and (246), the fast H_2 products are produced also in collision induced processes (240) and non-dissociative proton transfer reaction (238) (the latter being effective for $E_{CM} \lesssim 10$ eV only).

The cross section for slow- H_2^+ ion production in $H_3^+ + H_2$ collisions has been measured in Refs. [314] and [316] in the energy region below $E_{CM} \simeq 150$ eV, and the two sets of results agree well with each other in the overlapping energy range (down to $E_{CM} \simeq 12$ eV). The cross section for fast- H_2 production has been measured in Ref. [252] in the C.M. energy range 2.0-50 keV, and these data can be smoothly be connected with those of Refs. [314, 316] in the region $E_{CM} \simeq 150$ eV. Below $\simeq 10$ eV, the slow- H_2^+ production cross section rapidly decreases with decreasing energy, indicating that reactions (245) and (246) with

8 Collision Processes of H_3^+

another rearrangement reaction (see next sub-section). The inclusive slow- H_2^+ /fast- H_2 cross section from Refs. [252, 314, 316] can be represented by the analytic expression

$$\sigma_{incl}(H_2^+/\underline{H}_2) = \sigma_{incl}^<(H_2^+/\underline{H}_2) + \sigma_{incl}^>(H_2^+/\underline{H}_2) \quad (248a)$$

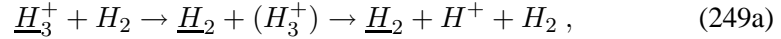
$$\sigma_{incl}^<(H_2^+/\underline{H}_2) = \frac{1.977 \exp(-9.64 \times 10^5/E^{6.15})}{E^{0.518}(1 + 1.68 \times 10^{-7}E^{2.41})} (\times 10^{-16} \text{cm}^2) \quad (248b)$$

$$\sigma_{incl}^>(H_2^+/\underline{H}_2) = \frac{8.22 \times 10^{-2} E^{0.462} \exp\left[-\frac{29.78}{E^{1.012}} \left(1 + \frac{5.15}{E}\right)\right]}{1 + 8.20 \times 10^{-6} E^{1.16} + 1.85 \times 10^{-18} E^{3.84}} (\times 10^{-16} \text{cm}^2) \quad (248c)$$

where the collision (C.M.) energy is expressed in eV units. See also Figure 53 on page 188. For $E_{CM} > 50$ keV, the reliability of the analytic fit (248) for $\sigma_{incl}(H_2^+/\underline{H}_2)$ is lower.

8.3.4 Slow H^+ production processes

Slow H^+ ion production in $\underline{H}_3^+ + H_2$ collisions can occur in the following processes



The dissociative proton transfer reaction (249a) should be the dominant slow- H^+ production channel at collision energies below $\sim 10 - 15$ eV, while dissociative charge transfer and dissociative ionization reactions, (249b) and (249c), respectively, should dominate for $E_{CM} \gtrsim 30$ eV.

The inclusive cross section for slow H^+ -ion production has been measured in Ref. [314] in the energy range below $E_{CM} \simeq 120$ eV. The cross section has maximum at $E_{CM} \sim 6 - 8$ eV (of $\sim 1.5 \times 10^{-16} \text{cm}^2$), and drops sharply at lower and higher energies. The cross section passes through a minimum (at $E_{CM} \sim 50 - 60$ eV, with a value $\sim 0.25 \times 10^{-16} \text{cm}^2$) and then starts to increase slowly with increasing the energy. The contribution of dissociative proton transfer channel (249a) can be, thus, unambiguously separated out from the total slow- H^+ production cross section of Ref. [314], and can be represented by the analytic expression

8.4 Collision processes of H_3^+ with H^-

$$\sigma_{PT}^{diss}(H^+) = \frac{70.32}{E^{1.782}} \exp \left[-\frac{198.8}{E^{3.26}(1 + 3.71 \times 10^{-13} E^{14.2})} \right] (\times 10^{-16} \text{ cm}^2) \quad (250)$$

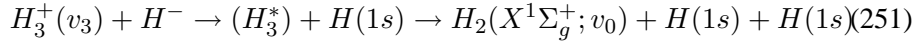
where the collision (C.M.) energy is expressed in eV units, see Figure 54 on page 188.

8.4 Collision processes of H_3^+ with H^-

Collision processes of H_3^+ with H^- have not been studied so far either experimentally or theoretically. The Coulomb attraction in the entrance channels, however, ensures that some of these processes proceed with large cross sections at low collision energies. Below we briefly discuss two such processes.

8.4.1 Dissociative mutual neutralization

The dissociative electron capture (mutual neutralization) reaction

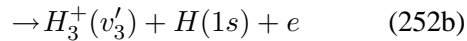
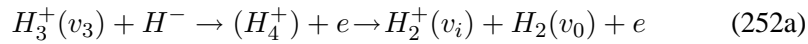


is initiated by electron capture to certain of bound H_3^* excited states at large $H_3^+ - H^-$ distances and then proceeds via predissociation of that state down to the ground dissociative state of H_3 . The predissociative dynamics may also leads to other excited neutral products.

Since the potential energy curve of initial ionic state in reaction (251) exhibits (avoided) crossings with the potential energy curves of all covalent $H_3^* + H(1s)$ states asymptotically lying for 0.754 eV below the $H_3^+ + H$ continuum edge, the number of intermediate electron capture channels of reaction (251) is expected to be large. The distribution of favourable (avoided) crossings (in the range $R_x \sim 10 - 40a_0$, a_0 is the Bohr radius) is also expected to be large, ensuring a cross section of reaction (251) of order of magnitude $10^{-15} - 10^{-14} \text{ cm}^2$ for collision energies below $\sim 1 \text{ keV}$.

8.4.2 Dissociative electron detachment

Another reaction in $H_3^+ + H^-$ collisions for which the cross section is expected to be large at collision energies below $\sim 10 \text{ eV}$ is the dissociative electron detachment



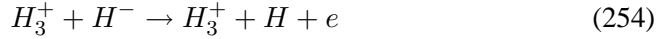
The associative detachment step of this reaction leads to formation of H_4^+ which is unstable against the $H_2^+ + H_2$ dissociation, and has a very shallow potential well of

9 Concluding Remarks

0.02 eV in the $H_3^+ + H(1s)$ exit channel [317]. The total electron detachment cross section of reactions (252) is determined by the first, associated detachment step, which involves formation and decay of an auto-ionization state H_4^{**} . According to the simple semiclassical analysis of associative detachment processes given in Refs. [85, 86], the total associative detachment cross section is given by

$$\sigma_{ADet}^{tot} = \pi a_0^2 \frac{R^* P_{ai}}{E} \quad (253)$$

where R^* is the $H_3^+ - H^-$ distance at which the auto-ionizing state H_4^{**} crosses the continuum edge, P_{ai} is the probability for auto-ionization for $R \leq R^*$, and E is the collision (C.M.) energy. (R^* and E in Eq. (253) are expressed in atomic units). The expression (253) is valid as long as the competing direct (non-associative) detachment becomes a more important H^- destruction process. The analogy with the $H_2^+ + H^-$ system (and other $A^+ + B^-$ systems) [86] suggests that this happens at $E_{CM} \simeq 2 - 3$ eV. For $E_{CM} \gtrsim 2 - 3$ eV, the E^{-1} decrease of σ_{ADet}^{tot} becomes much stronger (see Eq. (224) in sub-section 7.4.2). The non-associative detachment reaction



has also not been studied as yet.

9 Concluding Remarks

In the present work we have reviewed the most important collision processes taking place in a low-temperature hydrogen plasma. The plasma temperature was assumed to be in the range from about 0.01 eV (thermal region) to several hundreds eV, with particle composition containing $e, H^+, H, H^-, H_2, H_2^+$ and H_3^+ . The plasma and neutral particle densities were assumed to be not too high (below $\sim 10^{15} \text{ cm}^{-3}$) so that processes of formation of heavier complexes (such as H_5^+) were excluded from the consideration. The considered collision processes of above particles between themselves included not only their ground states but also their excited electronic (in the case of H and H_2) and vibrational (in the case of H_2, H_2^+ and H_3^+) states in both the entrance and exit reaction channels. The present work, therefore, is an attempt to construct the basic reaction scheme of a coupled collision-radiative (CR) model for atomic and molecular hydrogen with inclusion of vibrational kinetics. Only the collisional part of such a CR model has been, however, addressed in the framework of the present work. The information on radiative transition probabilities of excited electronic states of H and H_2 can be found in [318] and [319], respectively.

For the vast majority of considered collision processes of the constituents of a low-temperature hydrogen plasma, including those involving electronically and/or

vibrationally excited states, the cross section information is available in the literature. We have performed a critical assessment of this information and provided a "preferred" cross section for each considered reaction for use in hydrogen plasma studies. Each selected cross section has correct physical behaviour in its low- (or threshold) and high-energy limit. Only for a limited number of reactions, we have used the polynomial cross section fits from Refs. [11] and [112].

The cross section information provided in the present work, however, is still incomplete to establish a self-consistent collisional kinetic scheme for the coupled H/H_2 CR model. While appropriate cross section scaling relationships allow to extend the available cross section information for majority of considered processes to transitions involving the high atomic or molecular electronic states, for many state-selective processes involving vibrationally excited H_2 , H_2^+ and H_3^+ species the necessary basic cross section information is still missing. This is particularly true for the $v-v$ selective and exit-channel-resolved processes involving formation and destruction of $H_3^+(v_3)$ ion. Furthermore, a significant part of the available energy (kinetic plus potential) in molecular particle rearrangement processes is distributed to the rotational degrees of freedom of reacting products. The processes involving rotationally excited states in a low temperature plasma, therefore, may play a significant role in the overall plasma kinetics, but have not been included in the present work.

In many low-temperature hydrogen plasma studies, and particularly in the neutral particle transport kinetic codes, not only the cross section (or rate coefficient) for a specific reaction is required, but also information on angular and energy distribution of reaction products. In the present work we have refrained from providing such information for the considered collision processes. For many of these processes, however, such information is given in Ref. [11].

Finally, we note that the cross section database presented in this work cannot be in its entirety used for studies of hydrogen plasmas containing the heavier hydrogen isotopes (deuterium and tritium). While the identity of electronic structure of hydrogenic (atomic or molecular) isotopes ensures equality of the cross sections of processes involving a transition between two electronic states, the collision processes involving the vibrational states, an intermediary quasi-stationary state (such as the dissociative attachment or dissociative recombination), or formation of an long-lived intermediary complex (e.g., in low-energy particle rearrangement processes), usually show a significant isotopic dependence of the cross section. The mass dependent vibrational energy spectrum of different molecular isotopes is obviously related to the exothermicity of particle (proton or atom) transfer reactions and, thereby, can dramatically influence the cross section magnitude at low collision energies. (A survey of the cross sections for charge exchange and particle transfer processes between hydrogenic isotopomers is given in [320]). The time that the collision system spends on a decaying auto-ionizing or predissociating state also depends on the reduced mass of the system, which strongly affects the survival probabilities of the system on that state and, consequently, the probabilities of the reaction channels. Cross sections for isotope most sensitive processes of

9 Concluding Remarks

dissociative electron attachment and dissociative recombination (and excitation) for heavier hydrogenic isotopomers are given in Ref. [158] and Ref. [216], respectively. Information on predissociation rates of excited electronic states of a number of hydrogen isotopomers is given in Ref. [172].

References

- [1] N.F. Mott and H.S.W. Massey, "The Theory of Atomic Collisions", (Oxford Univ. Press, Oxford, 1965)
- [2] B.H. Bransden, "Atomic Collision Theory", (Benjamin, New York, 1970)
- [3] R.E. Johnson, "Introduction to Atomic and Molecular Collisions", (Plenum Press, New York, 1982)
- [4] I.I. Sobelman, L.A. Vainstein, and E.A. Yukov, "Excitation of Atoms and Broadening of Spectral Lines", (2nd ed., Springer-Verlag, Berlin, 1998)
- [5] B.M. Smirnov, "Asymptotic Methods in Theory of Atomic Collisions", (Atomizdat, Moscow, 1973) [In Russian]
- [6] E.E. Nikitin and S. Ya. Umanskii, "Theory of Slow Atomic Collisions", (Springer-Verlag, Berlin, Heidelberg, 1984).
- [7] M.R.C. McDowell and J.P. Coleman, "Introduction to the Theory of Ion-Atom Collisions", (North Holland, Amsterdam, 1970)
- [8] M.S. Child, "Molecular Collision Theory", (Academic Press, New York, 1976)
- [9] W.H. Miller, "Dynamics of Molecular Collisions", (Plenum Press, New York, 1976)
- [10] R.D. Levine and R.B. Bernstein, "Molecular Reaction Dynamics", (Oxford Univ. Press, Oxford, 1974)
- [11] R.K. Janev, W.D. Langer, K. Evans, and D.E. Post, "Elementary Processes in Hydrogen-Helium Plasmas" (Springer-Verlag, Berlin-Heidelberg, 1985).
- [12] C.F. Barnett et al., "Atomic Data for Controlled Fusion Research"; Vol. I ORNL-5206 (1977); Vol. II: ORNL-5207 (1980) (Oak Ridge National Laboratory, Oak Ridge, Tenn., USA); and: "Atomic Data for Fusion", ORNL Report No. ORNL-6086 (1990)
- [13] R.K. Janev and J.J. Smith, *At. Plasma-Mater. Interact. Data Fusion*, **4**, 1 (1993)
- [14] E.L. Freeman and E.M. Jones, "Atomic Collision Processes in Plasma Physics Experiments: I" UKAEA Rept. No. CLM-R137 (Culham Laboratory, Abingdon, England, 1974); and: E.M. Jones,

References

- “Atomic Collision Processes in Plasma Physics Experiments: II”. UKAEA Rept. No. CLM-R175 (Culham Laboratory, Abingdon, England, 1977).
- [15] R. Celiberto, R.K. Janev, A. Laricchimta, M. Capitelli, J.M. Wadehra, and D.E. Atems, *At. Data Nucl. Data Tables* **77**, 161 (2001).
- [16] *Atom. Plasma-Mater. Interact. Data Fusion*, Vol. **2** (1992), Vol. **5** (1995), Vol. **9** (2001), Vol. **10** (2002).
- [17] *Physica Scripta*, Topical issue, **T96** (2002)
- [18] <http://www-amdis.iaea.org> (IAEA atomic and molecular database)
- [19] <http://www-cfadc.phy.ornl.gov> (ORNL atomic database)
- [20] <http://www.idealibrary.com/links/doi/10.1006/adnd.2000.0850/dat>
- [21] L.C. Johnson, *Astrophys. J.* **174**, 227 (1972).
- [22] J. Callaway and M.R.C. McDowell, *Comm. At. Mol. Phys.* **31**, 19 (1983)
- [23] D.J.T. Morrison and M.R.H. Rudge, *Proc. Phys. Soc.* **89**, 45, (1966)
- [24] M.I. Chibisov, *Opt. Spectrosk.* **27**, 9 (1969) [in Russian]
- [25] J. Callaway et al., *Phys. Rev. A* **36**, 2576 (1987); *ibid.* **A 43**, 5175 (1991)
- [26] J. Hata, L.A. Morgan and M.R.C McDowell, *J. Phys. B*, **13**, L347 (1980)
- [27] K.M. Aggarwal, K.A. Berrington, P.G. Burke et al., *J. Phys. B* **24**, 1385 (1991)
- [28] C.T. Whelan, M.R.C. McDowell and P.W. Edmunds, *J. Phys. B* **20**, 1587 (1987); and: P.W. Edmunds et al., *ibid.* **16**, 2553 (1983)
- [29] L. Vriens and A.H.M. Smeets, *Phys. Rev. A* **22**, 940 (1980)
- [30] M.B. Shah, D.S. Elliot and H.B. Gilbody, *J. Phys. B* **20**, 3501, (1987); and: W.L. Fite and R.T. Brackmann, *Phys. Rev.* **112**, 1141 (1958)
- [31] A.J. Dixon, A. von Engel and M.F.A. Harrison, *Proc. Roy. Soc. (London) A* **343**, 333 (1975)
- [32] H.H. Coller, Inaugural Dissertation, Universität Zürich (1969)

-
- [33] H.L. Kyle and K. Omidvar, Phys. Rev. **176**, 164 (1968)
- [34] K. Omidvar, Phys. Rev. **140**, 126 (1965)
- [35] A.E. Kingston, J. Phys. B **1**, 559 (1968)
- [36] V.P. Shelvelko, personal communication (1993)
- [37] K. Takayanagi and H. Suzuki, "Cross Sections for Atomic Processes", Vol. 1 (Institute of Plasma Physics, Nagoya University, Nagoya, Japan, 1978).
- [38] R.K. Janev and H. van Regemorter, Astron. Astrophys. **37**, 1 (1974)
- [39] I.I. Sobelman, "Atomic Spectra and Radiative Transitions" (Springer-Verlag, Berlin-Heidelberg, 1981)
- [40] M. Abramowitz and I. Stegun, "Handbook of Mathematical Functions" (National Bureau of Standards, Washington DC, 1972)
- [41] L.P. Pitaevskii, Sov. Phys.-JETP **15**, 919 (1962); A.V. Gurevich and L.P. Pitaevskii, *ibid.* **19**, 870 (1964)
- [42] T.G. Morgan, J. Geddes and H.B. Gilbody, J.Phys. B **6**, 2118 (1973)
- [43] Y.P. Chang and W.L. Fite, Phys. Rev. A **16**, 933 (1977)
- [44] M. Kimura and W.R. Thorson, Phys. Rev. A **24**, 1780 (1981)
- [45] T.G. Winter and C.D. Lin, Phys. Rev. A **29**, 567 (1984)
- [46] R.K. Janev and P.S. Krstic, Phys. Rev. A **46**, 5554 (1992)
- [47] H.J. Lüdde and R.M. Dreizler, J.Phys. B **15**, 2703 (1982)
- [48] W. Fritsch and C.D. Lin, Phys. Rev. A **27**, 3361 (1981)
- [49] R. Shakeshaft, Phys. Rev. A **18**, 1930 (1978)
- [50] E. Fitchard, A.L. Ford and J.F. Reading, Phys. Rev. A **16**, 1325 (1977)
- [51] S. Saxena, G.P. Gupta and C.K. Mathur, J.Phys. B **17**, 3743 (1984)
- [52] H.J. Lüdde and R.M. Dreizler, J.Phys. B **22**, 3243 (1989)
- [53] C.R. Mandal, M. Mandal and S.C. Mukherjee, Phys. Rev. A **42**, 1787 (1990)
- [54] T.Kondow, R.J. Girnius, Y.P. Chong and W.L. Fite, Phys. Rev. A **10**, 1167 (1974)

References

- [55] R.A. Young, R.F. Stebbings and J.W. McGowan, Phys. Rev. **171**, 85 (1968); R.F. Stebbings et al., Phys. Rev. **138**, A1312 (1965)
- [56] K.H. Schartner, D. Detleffsen and B. Sommer, Phys. Lett. A **136**, 55 (1989)
- [57] J.T. Park, J.E. Adlag, J.M. George and J.L. Peacher, Phys. Rev. A **14**, 608 (1976)
- [58] A.M. Ermolaev, J.Phys. B **23**, L45 (1990)
- [59] C.O. Reinhold, R.E. Olson and W. Fritsch, Phys. Rev. A **41**, 4837 (1990)
- [60] R. Shakeshaft, Phys. Rev. A **14**, 1626 (1976)
- [61] J.G. Lodge, I.C. Percival and D. Richards, J. Phys. B **9**, 239 (1976)
- [62] M.B. Shah and H.B. Gilbody, J. Phys. B **14**, 2361 (1981); and: M.B. Shah et al., *ibid.*, **21**, 2455 (1988)
- [63] S. Yu. Ovchinnikov, Phys. Rev. A **42**, 3865 (1990)
- [64] P.D. Fainstein, V.H. Ponce and R.D. Rivarola, J.Phys. B **23**, 1481 (1990)
- [65] R.E. Olson, J. Phys. B **13**, 483 (1980).
- [66] J.E. Bayfield, Phys. Rev. **185**, 109 (1969)
- [67] W.L. Fite, A.C.H. Smith and R.F. Stebbings, Phys. Rev. **119**, 663 (1960); W.L. Fite et al., Proc. Roy. Soc. (London) **A268**, 527 (1962); W.L. Fite et al., Phys. Rev. **112**, 1161 (1958)
- [68] P. Hvelplund and A. Andersen, Physica Scripta **26**, 375 (1982)
- [69] J.H. Newman, J.D. Cogan, D.L. Zigler et al., Phys. Rev. A **25**, 2976 (1982)
- [70] W. Schwab, G.B. Batista, E. Justiniano et al., J.Phys. B **20**, 2825 (1987)
- [71] V.A. Belyaev, B.G. Brezhnev and E.M. Evastov, Sov. Phys.-JETP **25**, 777 (1967)
- [72] D.R. Bates and R.H.G. Reid, J.Phys. B **2**, 851 (1962)
- [73] V. Malaviya, J.Phys. B **3**, 1492 (1970)
- [74] J. Eichler, Phys. Rev. A **23**, 984 (1981)

-
- [75] D. Belkic, R. Gayet and A. Salin, Phys. Rep. **56**, 279 (1979) and: At. Data Nucl. Data Tables **51**, 59 (1992)
- [76] F. Decker and J. Eichler, J.Phys. B **22**, 3023 (1989)
- [77] R.K. Janev, C.J. Joachain and N.N. Nedeljkovic, Phys. Rev. A **29**, 2463 (1984)
- [78] P.S. Krstic, R.K. Janev and D.R. Schultz, J. Phys. B **36**, xxx (2003)
- [79] T. Watanabe, Phys. Rev. **138**, A1573 (1965); H. Nakamura and M. Matsuzawa, J. Phys. Soc. Japan **22**, 248 (1967)
- [80] E.L. Duman, B.M. Smirnov and M.I. Chibisov, Zh. Eksp. Teor. Fiz. **33**, 314 (1967) [Engl. transl.: Sov. Phys.-JETP **26**, 210 (1968)]; M.I. Chibisov, Dokl.Akad.Nauk SSSR, **180**, 1094 (1968) [Engl. transl.: Sov. Phys.-Doklady **13**, 583 (1968)]
- [81] M.I. Chibisov, Zh. Eksp. Teor. Fiz. **70**, 2087 (1976) [in Russian]
- [82] R.K. Janev and A.A. Mihajlov, Phys. Rev. A **20**, 1890 (1979); ibid **21**, 819 (1980).
- [83] M.R. Flannery, J. Phys. B **5**, 334 (1972); ibid. **4**, 892 (1971); Ann. Phys. (N.Y.) **61**, 465 (1970)
- [84] X. Urbain, A.Cornet, F. Brouillard et al., Phys. Rev. Lett. **66**, 1685 (1991)
- [85] A.Naji, K. Olamba, J.-P. Chenu et al., J. Phys. B **31**, 2961 (1998)
- [86] F. Brouillard and X. Urbain, Physica Scripta T**96**, 86 (2002)
- [87] T.A. Jacobs, R.R.Giedt and N.Cohen, J. Chem. Phys. **47**, 54 (1967).
- [88] A.E. Orel, J. Chem. Phys. **87**, 314 (1987);
- [89] F.H.M. Faisal and A.K. Bhatia, Phys. Rev. A **5**, 2144 (1972)
- [90] B. Peart, D.S. Walton and K.T. Dolder, J. Phys. B **4**, 88 (1971).
- [91] S. Szucs, M. Karemera, M. Terao et al., J. Phys. B **17**, 1613 (1984); B. Peart, M.A. Bennett and K. Dolder, J. Phys. B **18**, L439 (1985)
- [92] W. Schön, S. Krüdener, F. Melchert et al., J. Phys. B **20**, L759 (1987)
- [93] F. Borondo, A. Macias and A. Riera, Chem. Phys. Lett. **100**, 63 (1983); and: R. Shingal and B.H. Bransden, J. Phys. B **23**, 1203 (1990)

References

- [94] D. Fussen and C. Kubach, *J. Phys. B* **19**, L31 (1986); and: V. Sidis, C. Kubach and D. Fussen, *Phys. Rev. Lett.* **47**, 1280 (1981); and: A.M. Ermalaev, *J. Phys. B* **21**, 100 (1988)
- [95] K.L. Bell, A.E. Kingston and P.J. Madden, *J. Phys. B* **11**, 3977 (1978); and: R. Gayet, R.K. Janev and A. Salin, *J. Phys. B* **6**, 993 (1973)
- [96] B. Peart, R.Grey and K.T. Dolder, *J. Phys. B* **9**, 3074 (1976)
- [97] W. Schön, S. Krüdener, F. Melchert et al., *Phys. Rev. Lett.* **59**, 1565 (1987)
- [98] G. Poulaert, F. Brouillard, W. Claeys et al., *J. Phys. B* **11**, L671 (1978)
- [99] X. Urbain, A. Giusti-Suzor, D. Fussen et al., *J. Phys. B* **19**, L273 (1986)
- [100] D.G. Hummer, R.F. Stebbings, W.L. Fite et al., *Phys. Rev.* **119**, 668 (1960)
- [101] M.A. Huels, R.L. Champion, L.D. Doverspike et al., *Phys. Rev. A* **41**, 4809 (1990)
- [102] A. Dalgarno and M.R.C. McDowell, *Proc. Phys. Soc. (London) A* **69**, 615 (1956); and: R.K. Janev and D.M. Davidovic, *Phys. Rev.* **186**, 89 (1969)
- [103] J.N. Bardsley, *Proc. Phys. Soc. (London) A* **91**, 300 (1967)
- [104] J. Geddes, J.Hill, M.B. Shah et al., *J. Phys. B* **13**, 319 (1980)
- [105] V.A. Esaulov, *J. Phys. B* **13**, 4039 (1980)
- [106] J.C. Browne and A. Dalgarno, *J. Phys. B* **2**, 885 (1969); and: R.K. Janev and A.R. Tancic, *J. Phys. B* **4**, 215 (1971); and: D. Fussen and W. Claeys, *J. Phys. B* **17**, L89 (1984)
- [107] R.J. Bieniek, *J. Phys. B* **13**, 4405 (1980); and: R.J. Bieniek and A. Dalgarno, *Astrophys. J.* **228**, 635 (1979)
- [108] W.K. Trail, M.A. Morrison, W.A. Isaaks et al., *Phys. Rev. A* **41**, 4868 (1990)
- [109] G.J. Schulz, *Phys. Rev.* **135**, 988 (1964)

-
- [110] H. Ehrhardt, L. Langhaus, F. Linder et al., Phys. Rev. **173**, 222 (1968); and: M.Allan, J. Phys. B **18**, L451 (1985); and: M.J. Brunger, S.J. Buckmann, D.S. Newman et al., J. Phys. B **24**, 1435 (1991); and: A. Klonover and U. Kaldor, J. Phys. B **12**, 3797 (1979); and: F. Linder and H. Schmidt, Z. Naturf. **26a**, 1603 (1971)
- [111] D.E. Atems and J.M. Wadehra, Phys. Rev. A **42**, 5201 (1990); and: R. Celiberto and J.M. Wadehra, quoted in Ref. [112].
- [112] M. Capitelli, R. Celiberto, F. Esposito et al., Plasma Sources Sci. Technol. **11**, A7 (2002); and: R. Celiberto et al., Physica Scripta **T96**, 32 (2002)
- [113] S. Mazevet, M.A. Morrison and R.K. Nesbet, J. Phys. B **31**, 4437 (1998); and S. Mazevet, M.A. Morrison, O. Boydstum et al., Phys. Rev. A **59**, 477 (1999); and: F. Robicheaux, Phys. Rev. A **43**, 5946 (1991)
- [114] J.N. Bardsley, J. Phys. B **1**, 349 (1968); and: T. F. O'Malley, Phys. Rev. **150**, 14 (1966)
- [115] S.J. Buckmann and A.V. Phelps, JILA Report No. 27 (1985) (Joint Institute for Laboratory Astrophysics, Boulder, Colorado, May 1985); and: J.P. England, M.T. Elford and R.W.Crompton, Austr. J. Phys. **41**, 573 (1988)
- [116] J.R. Hiskes, J. Appl. Phys. **51**, 4592 (1980); *ibid.* **70**, 3409 (1991)
- [117] R. Celiberto, M.Capitelli and U.T. Lamanna, Chem. Phys., **183**, 101 (1994)
- [118] M.A. Khakoo and S. Trajmar, Phys. Rev. A **34**, 146 (1986); and: S.K. Srivastava and S.Jensen, J. Phys. B **10**, 3341 (1977)
- [119] J.M. Ajello, D.E. Shemansky, T.L. Kwok, and Y.L. Yung, Phys. Rev. A **29**, 636 (1984); and: D.E. Shemansky, J.M. Ajello and D.T. Hall, Astrophys. J., **296**, 765 (1985)
- [120] F.J. de Heer and J.D. Cariere, J.Chem. Phys. **55**, 3829 (1971)
- [121] G.P. Arrighini, F. Biondi and C. Guidotti, Molec. Phys. **41**, 1501 (1980); and: J.Marx et al., J.Phys. (Paris) **46**, 1667 (1985)
- [122] R. Celiberto and T. Rescigno, Phys. Rev. A. **47**, 1939 (1993); and: R. Celiberto et al., *ibid.* A. **50**, 4778 (1994); and: *ibid.* A. **54**, 432 (1996); and: *ibid.* A. **60**, 2091 (1999)
- [123] L. Mu-Tao, R.R. Lucchese and V. McKoy, Phys. Rev. A. **26**, 3240 (1982)

References

- [124] R. Celiberto, M.Capitelli and R.K.Janev, Chem. Phys. Lett. **256**, 575 (1996)
- [125] R. Celiberto, A. Laricchiuta, U.T. Lamanna et al., Phys. Rev. A. **60**, 2091 (1999)
- [126] S. Chung, C.C. Lin and E.T.P. Lee, Phys. Rev. A **12**, 1340 (1975)
- [127] R.W. Nichols, J.Phys. B **1**, 1192 (1968); M. Carvajal et al., Phys. Rev. A. **59**, 3462 (1999)
- [128] J. Geiger et al., Z. Naturforschung A **21**, 626 (1966)
- [129] R.J. Spindler, J. Quant. Spectrosc. Radiat. Transfer **9**, 597, 627, 1041 (1969)
- [130] A.C. Allison and A. Dalgarno, J. Quant. Spectrosc. Radiat. Transfer **9**, 1543 (1969)
- [131] V. Brems, Chem. Phys. **238**, 85 (1998)
- [132] R.I. Hall and L.Andric, J.Phys. B **17**, 3815 (1984); and: M.A. Khakoo and J.Segura, J.Phys. B **27**, 2355 (1994)
- [133] H.Nishimura and A. Danjo, J.Phys. Soc. Jpn. **55**, 3031 (1986)
- [134] T. Rescigno and B.I.Schneider, J.Phys. B **21**, L691 (1988)
- [135] M.A.P. Lima, T.L. Gibson and V. McKoy, Phys. Rev. A. **38**, 4527 (1988)
- [136] D.T. Stibbe and J. Tennyson, Astrophys. J. Lett. **513**, L147 (1999); New J. Phys. **1**, 21 (1998); C.S. Trevisan and J. Tennyson, J. Phys. B **34**, 2935 (2001)
- [137] S.Chung and C.C. Lin, Phys. Rev. A. **17**, 1874 (1978)
- [138] T. Rescigno, C.W. McCurdy, V. McKoy et al., Phys. Rev. A. **13**, 216 (1976)
- [139] R. Celiberto, M.Cacciatore, M.Capitelli et al., Chem. Phys. **133**, 355 (1989)
- [140] M. Gryzinski, Phys. Rev. A **138**, 305, 322, 336 (1965).
- [141] E. Bauer and C.D. Bratky, J. Chem. Phys. **43**, 2466 (1965).
- [142] A. Laricchiuta, R. Celiberto and R.K. Janev, (2003 submitted, Phys. Rev. A)

-
- [143] B. Adamczyk, A.J.H. Boerboom, B.L. Schram and J. Kistemaker, *J. Chem. Phys.* **44**, 4640 (1966).
- [144] A. Crowe and J.W. McConkey *J.Phys. B* **6**, 2088 (1973)
- [145] D. Rapp and P. Englander-Golden, *J. Chem. Phys.* **43**, 1464 (1965); and: D. Rapp et al., *J. Chem. Phys.* **42**, 4081 (1965); and: S.J.B. Corrigan, *J.Chem. Phys.* **43**, 4381 (1965)
- [146] H.C. Straub, P. Renault, B.G. Lindsey et al., *Phys. Rev. A.* **54**, 2164 (1996)
- [147] R. Celiberto, P. Cives, M. Cacciatore, et al., *Chem. Phys. Lett.* **169**, 69 (1990); and: R. Celiberto et al., *Chem. Phys.* **140**, 209 (1990)
- [148] F. von Busch and G.H. Dunn, *Phys. Rev. A.* **5**, 1726 (1972); and: N.P.F.B. van Asselt et al., *Chem. Phys.* **5**, 429 (1974); and: J.B. Ozenne et al., *Chem. Phys.* **16**, 75 (1976); and: Y.Weijun et al., *Z. Phys. D* **28**, 87 (1993)
- [149] R. Celiberto, M. Capitelli and R.K.Janev, *Chem. Phys. Lett.* **278**, 154 (1997)
- [150] G.J. Schulz and R.K. Asundi, *Phys. Rev.* **158**, 25 (1967)
- [151] M. Allan and S.F. Wong, *Phys. Rev. Lett.* **41**, 1791 (1978)
- [152] J.M. Wadehra and J.N. Bardsley, *Phys. Rev. Lett.* **41**, 1795 (1978)
J.M. Wadehra, *Phys. Rev. A* **29**, 106 (1984).
- [153] J.M. Wadehra, in "Production and Neutralisation of Negative Ions and Beams", ed.: K. Prelec, AIP Conference Proceedings, No. 111, p. 46 (AIP, New York, 1984)
- [154] J.N. Bardsley and J.M. Wadehra, *J. Chem. Phys.* **78**, 2227 (1983)
- [155] C. Mündel and W. Domke, *J.Phys. B* **17**, 3593 (1984); and: C. Mündel et al., *Phys. Rev. A.* **32**, 181 (1985)
- [156] Y. Xu, G.A. Gallup and I.I. Fabrikant, *Phys. Rev. A.* **61**, 052705 (2000); and: Y. Xu et al., *Phys. Rev. A.* **63**, 014703 (2001)
- [157] Yu. N. Demkov, *Phys. Lett.* **15**, 235 (1965)
- [158] I.I. Fabrikant, J.M. Wadehra and Y. Xu, *Physica Scripta*, **T96**, 45 (2002).
- [159] J.M. Wadehra; quoted in Ref. [15]

References

- [160] J. Comer and F.H. Read, *J.Phys. B* **4**, 368 (1971); and: G. Joyez et al., *J.Phys. B* **6**, 2427 (1973); and: A. Weingartshofer et al., *J.Phys. B* **8**, 1552 (1975)
- [161] D.T. Stibbe and J. Tennyson, *J.Phys. B* **31**, 815 (1998); *ibid.* **30**, L301 (1997); *ibid.* **29**, 4267 (1996)
- [162] L.A. Pinnaduwege, W.X. Ding, D.L. McCorcle et al., *J. Appl. Phys.* **85**, 7064 (1999); P.G. Datskos, L.A. Pinnaduwege, and J.F. Kielkopf, *Phys. Rev. A* **55**, 4131 (1997).
- [163] M. Capitelli, R. Celiberto, A. Eletskii, and A. Laricchiuta, *Atom. Plasma-Mater. Interact. Data Fusion*, **9**, 47 (2001).
- [164] D.E. Atems and J.M. Wadehra *J.Phys. B* **26**, L759 (1993); and: J.M. Wadehra, quoted in Ref. [112]
- [165] Y. Xu, A.K. Kazansky and I.I. Fabrikant, *Phys. Rev. A* **63**, 014703 (2001)
- [166] C. Backx, G.R. Wight and M.J. van der Wiel, *J.Phys. B* **9**, 315 (1976); and: C.J. Latimer et al., *J.Chem. Phys.* **102**, 722 (1995), and references therein
- [167] K. Ito, R.I. Hall and M.Ukai, *J. Chem. Phys.* **104**, 8449 (1996); and: C.J. Latimer et al., *J. Phys. B*, **29**, 6113 (1996); and: Z.X. He et al., *J. Chem. Phys.* **103**, 3912 (1995)
- [168] F. Martin, *J.Phys. B* **32**, R197 (1999), and references therein
- [169] I. Sanchez and F. Martin, *J. Chem. Phys.* **106**, 7720 (1997); *ibid.* **110**, 6702 (1999)
- [170] J. Tennyson, *At. Data Nucl. Data Tables* **64**, 253 (1996)
- [171] R.S. Berry *J. Chem. Phys.* **45**, 1228 (1966)
- [172] R.S. Berry and S.E. Nilsen, *Phys. Rev. A* **1**, 383, 395 (1970); *ibid.* **4**, 865 (1971)
- [173] M. Glass-Maujean, *At. Data Nucl. Data Tables* **30**, 301 (1984).
- [174] G. Herzberg, "Molecular Spectra and Molecular Structure", 2nd ed. (Van Nostrand, Princeton, N.J., 1950)
- [175] M. Misakian and J.C. Zorn, *Phys. Rev. A* **6**, 2181 (1972), and references therein
- [176] P.M. Guyon, J. Breton and M. Glass-Maujean, *Chem. Phys. Lett.* **68**, 314, 320 (1979); M. Rothschild et al., *Phys. Rev. A* **23**, 206, (1981)

-
- [177] R.P. Freis and J.R. Hiskes, *Phys. Rev. A*, **2**, 573 (1970)
- [178] D.A. Erwin and J.A. Kunc, *IEEE Trans. Plasma Sci.* **PS-11**, 266 (1983)
- [179] T. Rescigno and A. Orel; quoted in Ref. [178]
- [180] C. Bottcher and B.D. Buckley, *J. Phys. B* **12**, L497 (1979)
- [181] V. Herman, H. Schmidt and F. Linder, *J. Phys. B* **11**, 493 (1978)
- [182] F. Linder, in: "Electronic and Atomic Collisions" (Invited talks of 11th ICPEAC), Eds.: N. Oda and K. Takayanagi (North Holland, Amsterdam, 1980)
- [183] C.F. Giese and W.R. Gentry, *Phys. Rev. A*, **10**, 2156 (1974)
- [184] R. Schinke and P. McGuire, *Chem. Phys.* **31**, 391 (1978); and: R. Schinke, *ibid.* **24**, 379 (1977); and: R. Schinke, *J. Chem. Phys.* **72**, 3909, 3916, (1980)
- [185] P.S. Krstic and D.R. Schultz, *J. Phys. B* **32**, 2451 (1999).
- [186] P.S. Krstic, *Phys. Rev. A* **66**, 042717 (2002).
- [187] M.G. Holliday, J.T. Muckerman and L. Friedman, *J. Chem. Phys.* **54**, 1058 (1971)
- [188] W.H. Cramer, *J. Chem. Phys.* **35**, 836 (1961); and: D.W. Koopman, *Phys. Rev.* **154**, 79 (1967)
- [189] M.V. Gealy and B. Van Zyl, *Phys. Rev. A*, **36**, 3091 (1987); and: T. Kusakabe et al., *Phys. Rev. A*, **62**, 062714 (2000)
- [190] M.B. Shah, P. McCallion and H.B. Gilbody, *J. Phys. B* **22**, 3983 (1989); and: V.V. Afrosimov et al., *Sov. Phys. JETP* **29**, 648 (1969); and: G.W. McClure, *Phys. Rev.* **148**, 47 (1966)
- [191] Z.H. Top and M. Baer, *Chem. Phys.* **25**, 1 (1977); and: *J. Chem. Phys.* **66**, 1363 (1977)
- [192] P.S. Krstic, D.R. Schultz and R.K. Janev, *Physica Scripta* **T96**, 61 (2002).
- [193] D. Elizaga, L.F. Errea, J.D. Gorfinkiel et al., *J. Phys. B*, **33**, 2037 (2000); and: L.F. Errea et al., *J. Phys. B*, **30**, 3855 (1997)
- [194] W. Fritsch and C.D. Lin, *Phys. Rev.* **29**, 3039 (1984); and: R. Schinagal and C.D. Lin, *Phys. Rev. A*, **40**, 1302 (1989)

References

- [195] A. Ichihara, O. Iwamoto and R.K. Janev, *J. Phys. B* **33**, 4747 (2000).
- [196] A. Ichihara, O. Iwamoto, and K. Yokoyama, *Atom. Plasma-Mater. Interact. Data Fusion* **9**, 193 (2001).
- [197] P.S. Krstic and R.K. Janev, *Phys. Rev. A*, **67**, 022709, (2003).
- [198] B.S. Nesbitt, M.B. Shah, C.F.C. O'Rourke et al., *J. Phys. B* **33**, 637 (2000)
- [199] C. Illescas and A. Riera, *Phys. Rev. A*. **60**, 4546 (1999); and: D. R. Schultz et al., *Physica Scripta* **T62**, 69 (1996)
- [200] M.S. Huq, L.D. Doverspike and R.L. Champion, *Phys. Rev. A*. **27**, 2831 (1983); and: J.S. Risley and R. Geballe, *Phys. Rev. A*. **9**, 2485 (1974); and: G.I. Dimov and V.G. Dudnikov, *Sov. Phys.- Tech. Phys.* **11**, 919 (1967); and: A.C. Whittier, *Can. J. Phys.* **32**, 275 (1954)
- [201] D.R. Bates and J.C.G. Walker, *Proc. Phys. Soc.* **90**, 333 (1967)
- [202] F. Esposito, C. Gorse and M.Capitelli, *Chem. Phys. Lett.* **303**, 636 (1999); and: F. Esposito and M.Capitelli, *At. Plasma-Mater. Interact. Data Fusion* **9**, 65 (2001); and: H.R. Mayne, *Chem. Phys. Lett.* **66**, 487 (1979); and: H.R. Mayne and J.P. Toenies, *J. Chem. Phys.* **75**, 1794 (1981)
- [203] E. Garcia and A. Lagania, *Chem. Phys. Lett.* **123**, 365 (1986); and: A. Lagania and E. Garcia, "Quasiclassical Rate Coefficients for $H + H_2$ Reactions", (University of Perugia, Italy, 1996)
- [204] J.E. Dove and M.E. Mandy, *Int. J. Chem. Kin.* **18**, 893 (1986)
- [205] K. Hassouni, M. Capitelli, F. Esposito, A. Ciquel, *Chem. Phys. Lett.* **340**, 322 (2001)
- [206] R.N. Schwartz, I. Slawsky, and K.F. Herzfeld, *J. Chem. Phys.* **20**, 1591 (1952).
- [207] M. Capitelli, C.M. Ferreira, B.F. Gordiets, A.I. Osipov, eds. "Plasma Kinetics in Atmospheric Gases", (Springer-Verlag, Berlin, 2000)
- [208] A. Celallos, E. Garcia, A. Rodrigues, et al., *Chem. Phys. Lett.*, **305**, 276 (1999)
- [209] R.F. Boikova and V.D. Ob'edkov, *Sov. Phys.- JETP* **27**, 772 (1968).
- [210] W.D. Robb and L.A. Collins, *Phys. Rev. A* **22**, 2474 (1980); and: B.K. Saprall and J. Tennyson, *Mon. Not. Roy. Astron. Soc.* **236**, 909 (1993)

- [211] F.B. Yousif and J.B.A. Mitchell, *Z. Phys. D* **34**, 195 (1997)
- [212] B. Peart and K.T. Dolder, *J. Phys. B* **5**, 860, 1554 (1972).
- [213] G.H. Dunn and B. Van Zyl, *Phys. Rev.* **154**, 40 (1967)
- [214] D.F. Dance, M.F.A. Harrison, R.D. Rundel et al., *Proc. Phys. Soc.* **92**, 577 (1967)
- [215] J. M. Peek, *Phys. Rev.* **140**, 11 (1965); *ibid.* **154**, 52 (1967); and: J.M. Peek and T.A. Green, *Phys. Rev.* **183**, 202, (1969).
- [216] H. Takagi, *Physica Scripta* **T96**, 52 (2002).
- [217] J.B.A. Mitchell, *At. Plasma-Mater. Interact. Data Fusion* **9**, 97 (2001).
- [218] B. Peart and K.T. Dolder, *J. Phys. B* **7**, 236 (1974); *ibid.* **8**, 1570 (1975).
- [219] D. Auerbach, R. Cacak, R. Caudano et al., *J.Phys. B* **10**, 3797 (1977)
- [220] R.A. Phaneuf, D.H. Crandall and G.H. Dunn, *Phys. Rev. A.* **11**, 528 (1975); and: M.Vogler and G.H. Dunn, *Phys. Rev. A.* **11**, 1983 (1975)
- [221] J.B.A. Mitchell, F.B. Yousif, P.J.T. van der Donk et al., in “Dissociative Recombination: Theory, Experiment and Applications”, edited by B.R. Rowe et al. (Plenum Press, New York, 1993), p87
- [222] M. Larsson, L. Brostrom, M. Carlson et al., *Physica Scripta* **51**, 354 (1995); and: M. Larsson, M. Carlson, H. Danared et al., *J. Phys. B* **27**, 1397 (1994)
- [223] C. Bottcher, *J. Phys. B* **9**, 2899 (1976); and: C. Bottcher and K. Docken, *J. Phys. B* **7**, L5 (1974)
- [224] I.F. Schneider, O. Dulieu and A. Giusti-Suzor, *J.Phys. B* **24**, L289 (1991)
- [225] N. Nakashima, H. Takagi and H. Nakamura, *J. Chem. Phys.* **86**, 726 (1987)
- [226] J.B.A. Mitchell, *Phys. Rep.* **186**, 215 (1990).
- [227] J.B.A. Mitchell, in R.K. Janev, ed., “Atomic and Molecular Processes in Fusion Edge Plasmas” (Plenum Press, New York, 1995), p225.
- [228] I.F. Schneider and A. Suzor-Weiner, *Contrib. Plasma Phys.* **42**, 6 (2002).

References

- [229] D. R. Bates, Phys. Rev. **77**, 718 (1951) **78**, 492(1951)
- [230] J.N. Bardsley J.Phys. B **1**, 365 (1968)
- [231] H. Takagi, J.Phys. B **26**, 4815 (1993)
- [232] E.P. Wigner, Phys. Rev. **73**, 1002 (1948).
- [233] P. Forck, M. Grieser, D. Habs et al., Phys. Rev. Lett. **70**, 426 (1993)
- [234] V.P. Zhdanov and M.I. Chibisov, Sov. Phys. -JETP **47**, 38 (1978)
- [235] M.I. Chibisov, J.B.A. Mitchell, P.J.T. Van der Donk et al., Phys. Rev. A **56**, 443 (1997)
- [236] B. Peart and K.T. Dolder, J. Phys. B **6**, 2409 (1973).
- [237] W.L. Fite, R.T. Brackmann and W.R. Snow, Phys. Rev. **112**, 1161 (1958)
- [238] G.W. McClure, Phys. Rev. **153**, 182 (1967)
- [239] P.C.E McCartney, C. McGrath, J.W. McConkey et al., J.Phys. B **32**, 5103 (1999)
- [240] D.R. Bates and R.H.G. Reid, Proc. Roy. Soc. (London) A **310**, 1 (1969)
- [241] T.F. Moran, M.R. Flannery and D.L. Albritton, J. Chem. Phys. **62**, 2869 (1975); and: T.F. Moran and M.R. Flannery. J.Chem. Phys. **66**, 370, (1977)
- [242] C.-Y. Lee and A.E. DePristo, J. Chem. Phys. **80**, 1116 (1984)
- [243] F.M. Campbell, R. Browning and C.J. Latimer, J.Phys. B **14**, 3493 (1981)
- [244] C.L. Liao, C.X. Liao and C.Y. Ng, J. Chem. Phys. **81**, 5672 (1984)
- [245] S.K. Cole, T. Baer, P.-M. Guyon et al., Chem. Phys. Lett. **109**, 285 (1984)
- [246] C.L. Liao and C.Y. Ng, J. Chem. Phys. **84**, 197 (1986)
- [247] J.B.H. Stedeford and J.B. Hasted, Proc. Roy. Soc. (London) A **227**, 466 (1955); and: W.H. Cramer and A.B. Marcus, J. Chem. Phys. **32**, 186 (1960); and: D.W. Koopman, Phys. Rev. **154**, 79 (1967)
- [248] O. Hollricher, Z. Phys. **187**, 41 (1965)

-
- [249] H. L. Rothwell, B.V. Zyl and R.C. Amme, *J. Chem. Phys.* **61**, 3851 (1974)
- [250] C.J. Latimer, R. Browning and H.B. Gilbody, *J.Phys. B* **2**, 1055 (1969)
- [251] T.F. Moran and J.R. Roberts, *J. Chem. Phys.* **49**, 3411 (1968).
- [252] G.W. McClure, *Phys. Rev.* **130**, 1852 (1963)
- [253] A.V. Phelps, *J. Phys. Chem. Ref. Data* **19**, 653 (1990).
- [254] C.-Y. Lee, A.E. DePristo, C.-L. Liao et al., *Chem. Phys. Lett.* **116**, 534 (1985)
- [255] P.M. Guyon, T. Baer, S.K. Cole et al., *Chem Phys.* **119**, 145 (1988).
- [256] W.H. Cramer, *J. Chem. Phys.* **35**, 836 (1961)
- [257] Z. Karpas, V. Anicich and W.T. Huntress, *J. Chem. Phys.* **70**, 2877 (1979)
- [258] H. Tawara, Y. Itikawa, Y. Itoh et al. "Atomic data involving hydrogen relevant to edge plasmas", Institute of Plasma Physics, Nagoya University, Report No. IPPJ-AM-46 (1986).
- [259] D.W. Vance and T.L. Bailey, *J. Chem. Phys.* **44**, 486 (1986)
- [260] C.W. Eaker and G.C. Schatz, *J. Chem. Phys.* **89**, 6713 (1988)
- [261] G.W. McClure, *Phys. Rev.* **140**, A769 (1965)
- [262] J. Guidini, *Comp. Rend. Acad. Sci. (Paris)*, **253**, 829 (1961)
- [263] N.V. Fedorenko, V.V. Afrosimov, R.N. Il'in et al. *Sov. Phys.- JETP* **18**, 342 (1964); and: R.N. Il'in et al., *Sov. Phys.- JETP* **19**, 817 (1964)
- [264] A. Schmid, *Z. Phys.* **161**, 550 (1961)
- [265] E.S. Zhurkin, V.A. Kaminskii, M.V. Tikhomirov et al., *Sov. Phys.- Techn. Phys.* **18**, 259 (1973)
- [266] J.F. Williams and D.N.F. Dunbar, *Phys. Rev.* **149**, 62 (1966)
- [267] C.F. Giese and W.B. Maier II, *J. Chem. Phys.* **39**, 739 (1963)
- [268] R.H. Neynaber and S.M. Trujillo, *Phys. Rev.* **167**, 63 (1968)
- [269] W.R. Gentry, D.J. McClure and C.H. Douglass, *Rev. Sci. Instrum.* **46**, 367 (1975)

References

- [270] L.T. Specht, K.D. Forster and E.E. Muschlitz, *J. Chem. Phys.* **63**, 1582 (1975)
- [271] I. Koyano and K. Tanaka, *J. Chem. Phys.* **72**, 4858 (1980)
- [272] D. van Pijkeren, E. Bottjes, J. van Eck et al., *Chem. Phys.* **91**, 293 (1984)
- [273] J.D. Shao and C.Y. Ng, *J. Chem. Phys.* **84**, 4317 (1986)
- [274] T.M. Bowers, D.D. Elleman and J. King, *J. Chem. Phys.* **50**, 4787 (1969)
- [275] J.R. Stine and J.T. Muckerman, *J. Chem. Phys.* **65**, 3975 (1976); *ibid.* **68**, 185 (1978); and: J.T. Muckerman, *Theor. Chem.* **6**, 1 (1981)
- [276] C.W. Eaker and G.C. Schatz, *J. Chem. Phys.* **89**, 2612 (1985)
- [277] C.W. Eaker and G.C. Schatz, *Chem. Phys. Lett.* **127**, 343 (1986)
- [278] G.D. Carney and R.N. Porter, *J. Chem. Phys.* **65**, 3547 (1976); and: B. Dinelli, S. Miller and J. Tennyson, *J. Molec. Spectrosc.* **153**, 718 (1992); and: J. Tennyson and J.R. Henderson, *J. Chem. Phys.* **91**, 3815 (1989)
- [279] V.G. Anicich and J.H. Futrell, *Int. J. Mass Spectrom. Ion Processes*, **55**, 189 (1983/1984)
- [280] S.L. Anderson, F.A. Houle, D. Gerlich et al., *J. Chem. Phys.* **75**, 2153 (1981)
- [281] K.C. Kulander and M.F. Guest, *J. Phys. B* **12**, L501 (1979); H.H. Michels and R.H. Hobbs, *Astrophys. J.* **286**, L27 (1984).
- [282] B. Peart and M.A. Bennett, *J. Phys. B* **19**, L321 (1986)
- [283] M.J.J. Eerdem, M.C.M. van de Sanden, D.K. Otorbaev et al., *Phys. Rev. A* **51**, 3369 (1995).
- [284] M.I. Chibisov and R.K. Janev, *Phys. Reports* **106**, 3 (1988); and: R.K. Janev, *J. Chem. Phys.* **64**, 1891 (1976)
- [285] R.K. Janev, L.P. Presnyakov and V.P. Shevelko, "Physics of Highly Charged Ions", (Springer-Verlag, Berlin-Heidelberg, 1985)
- [286] A. Naji, K. Olamba, J.-P. Chenu et al., *J. Phys. B* **31**, 4887 (1998)
- [287] M. Larsson, *Phil. Trans. Roy. Soc. (London)* **A358**, 2433 (2000)
- [288] A. Dalgarno, *Adv. At. Mol. Opt. Phys.* **32**, 57 (1994)

-
- [289] G.D. Carney and R.N. Porter, *J. Chem. Phys.* **60**, 4251 (1974)
- [290] D. Talbi and R.P. Saxon, *J. Chem. Phys.* **89**, 2235 (1988); and: L.J. Schaad and W.V. Hicks, *ibid.* **61**, 1934 (1974); and: K. Kawaoka and R.F. Borkman, *ibid.* **54**, 4234 (1971)
- [291] B. Peart and K.T. Dolder, *J. Phys. B* **8**, L143 (1975); and: *ibid.* **B7**, 1567 (1974)
- [292] F.B. Yousif, P.J.T. Van der Donk, M.Orakzai et al., *Phys. Rev. A* **44**, 5653 (1991).
- [293] N.G. Adams, D. Smith and E. Alge, *J. Chem. Phys.* **81**, 1778 (1984); and: D. Smith and N.G. Adams, *J. Chem. Soc. Faraday Trans. II* **83**, 149 (1987)
- [294] M.T. Leu, M.A. Biondi and R. Johnsen, *Phys. Rev. A* **8**, 413 (1973); and: J.A. McDonald, M.A. Biondi and R. Johnsen, *Plant. Space Sci.* **32**, 651 (1984)
- [295] B. Peart and K.T. Dolder, *J. Phys. B* **7**, 1567 (1974); *ibid* **7**, 1948 (1974)
- [296] D. Auerbach, R. Cacak, R. Caudano et al., *J.Phys. B* **10**, 3797 (1977); and: J.W. McGowan, P.M. Mul, V.S. D'Angelo et al., *Phys. Rev. Lett.* **42**, 373 (1979); and: J.B.A. Mitchell, J.L. Forand, C.T. Ng et al., *Phys. Rev. Lett.* **51**, 885 (1983); and: F.B. Yousif, M. Rogelstadt and J.B.A. Mitchell, in: "Atomic and Molecular Physics: 4th US/Mexico Symposium", Eds. I. Alvarez et al. (World Scientific, Singapore, 1995), p343
- [297] T.Amano, *Astrophys. J.* **329**, L121 (1988); and: *J. Chem. Phys.* **92**, 6492 (1990); and: M. Feher, A. Rohrbacher and J.P. Maier, *J. Chem. Phys.* **185**, 357 (1995)
- [298] M. Larsson, H. Danared, J.W. Mowat et al., *Phys. Rev. Lett.* **70**, 430 (1993)
- [299] T. Tanabe et al., in: "Dissociative Recombination: Theory, Experiment and Applications", Eds. M. Larsson et al., (World Scientific, Singapore, 2000), p.170
- [300] P. Van der Donk, F.B. Yousif and J.B.A. Mitchell, *Phys. Rev. A* **43**, 5971 (1991); and: H. Hus, F.B. Yousif, A. Sen et al., *Phys. Rev. A* **38**, 658 (1988)
- [301] A.E. Orel and K.C. Kulander, *Phys. Rev. Lett.* **71**, 4315 (1993)

References

- [302] I.F. Schneider, A.E. Orel and A. Suzor-Weiner, Phys. Rev. Lett. **85**, 3785 (2000)
- [303] V. Kokoouline and C.H. Greene, Phys. Rev. Lett., **90**, 133201 (2003)
- [304] J.B.A. Mitchell, J.L. Forand, C.T. Ng et al., Phys. Rev. Lett. **51**, 885 (1983)
- [305] S. Datz, G. Sundström, Ch. Biedermann et al., Phys. Rev. Lett. **74**, 896 (1995)
- [306] K.C. Kulander and M.F. Guest, see Ref. [281]
- [307] B. Peart, R.A. Forest and K.T. Dolder, J.Phys. B **12**, 3441 (1979)
- [308] F.B. Yousif, P.J.T. Van der Donk and J.B.A. Mitchell, J. Phys. B **26**, 4249 (1993).
- [309] C. Bordas and H. Helm, Phys. Rev. A **45**, 387 (1992); and: C. Bordas, L.J. Lembo and H. Helm, Phys. Rev. **44**, 1817 (1991); and: P.C. Cosby and H. Helm, Phys. Rev. Lett. **61**, 298 (1988)
- [310] G.I. Gellene and R.F. Porter, J. Chem. Phys. **79**, 5975 (1983)
- [311] C. Bordas and H. Helm, Phys. Rev. **43**, 3645 (1991)
- [312] J.K. Kim, L.P. Threard and W.T. Huntress, Int. J. Mass. Spectrom. Ion Phys. **15**, 223 (1974); and: L.P. Threard and W.T. Huntress, J. Chem. Phys. **60**, 2840 (1974); and: T. Terao and R.A. Black, J. Chem. Phys. **73**, 3884 (1969); and: D.L. Smith and J.H. Futrell, Chem. Phys. Lett. **40**, 229 (1976)
- [313] C.R. Blakley, M.L. Vestal and J.H. Futrell, J. Chem. Phys. **66**, 2392 (1977)
- [314] B.L. Peko and R.L. Champion, J. Chem. Phys. **107**, 1156 (1997)
- [315] G. Lange, B. Huber and K. Wiesemann, Z. Phys. A**281**, 21 (1977)
- [316] B.A. Huber, U. Schultz and K. Wiesemann, Phys. Lett. **79A**, 58 (1980)
- [317] L.R. Wright and R.F. Borkmann, J. Chem. Phys. **77**, 1938 (1982); and: R. Polak, Chem. Phys. **16**, 535 (1976); R.D. Poshusta and D.F. Zetik, J. Chem. Phys. **58**, 118 (1973)
- [318] W.L. Wiese, M.V. Smith and B.M. Glennon, "Atomic Transition Probabilities", Vol. 1 (National Bureau of Standards, Washington, D.C., 1966); see also Refs. [4] and [21]

- [319] A.C. Allison and A. Dalgarno, *At. Data* **1**, 284 (1970); and: A. Dalgarno, G.Herzberg and T.L. Stephens, *Astrophys. J. Lett.* **162**, L49 (1975); and: M. Glass-Maujean, P. Quadrelli and K. Dressler, *At. Data Nucl. Data Tables*, **30**, 273 (1984); *ibid.* **30**, 310 (1984); and: H. Abgrall et al., *Astron. Astrophys. Suppl. Ser.* **101**, 273, 323 (1993); *J. Mol. Spectrosc.* **157**, 512 (1993); and: M. Glass-Maujean, et al., *Phys. Rev. A* **28**, 2868 (1983); *Chem. Phys.* **80**, 4355 (1984); and: A. Abgrall et al., *Can. J. Phys.* **72**, 856 (1994); and: T.L. Stephens and A. Dalgarno, *J. Quant. Spectrosc. Radiat. Transfer* **12**, 569 (1972); A. Abgrall et al., *Phys. Rev. A* **42**, 1835 (1990); *Astron. Astrophys.* **253**, 525 (1992); and: W.H. Smith and R. Shevalier, *Astrophys. J.* **177**, 835 (1972); and: T.L. Kwok et al., *Phys. Rev. A* **36**, 1962 (1986); and: S.L. Guberman and A. Dalgarno, *Phys. Rev. A* **45**, 2784 (1992); and: T.L. Kwok, A. Dalgarno, and A. Poser, *Phys. Rev. A* **34**, 1962 (1986)
- [320] F. Linder, R.K. Janev and J. Botero, in: "Atomic and Molecular Processes in Fusion Edge Plasmas", Ed. R.K. Janev (Plenum Press, New York, 1995), p225; and: J.G. Wang and P.C. Stancil, *Physica Scripta* **96**, 72 (2002)

10 Tables

Transition	$1s \rightarrow 2s$	$1s \rightarrow 2p$	$1s \rightarrow n = 2$
a	0.114	0.114	0.228
b	0.0575	0.129	0.1865
c	0.1795	0.323	0.5025
A_0	0.00	4.5146	4.4979
A_1	0.88606	0.43563	1.4182
A_2	-2.7990	-17.995	-20.877
A_3	5.9451	45.247	49.735
A_4	-7.6948	-42.229	-46.249
A_5	4.4152	15.446	17.442

Table 1: Values of parameters a, b, c and A_i in Eq. (4) for the cross sections of $1s \rightarrow 2l$ transitions.

Transition	$1s \rightarrow 3s$	$1s \rightarrow 3p$	$1s \rightarrow 3d$	$1s \rightarrow n = 3$	$1s \rightarrow n = 4$	$1s \rightarrow n = 5$
$\Delta E(eV)$	12.09	12.09	12.09	12.09	12.75	13.06
α	0.77920	0.14606	0.35496	0.38277	0.41844	0.45929
A_0	0.00	0.77738	0.00	0.75448	0.24300	0.11508
A_1	0.17663	0.014194	0.13527	0.42956	0.24846	0.13092
A_2	-0.42600	-0.34362	0.19672	-0.58288	0.19701	0.23581
A_3	0.18342	0.50609	-0.10712	1.0693	0.00	0.00
A_4	0.99615	0.00	0.00	0.00	0.00	0.00

Table 2: Values of threshold energies (ΔE) and parameters α and A_i in Eq. (5) for excitation cross section $\sigma(1s \rightarrow 3l; n)$, $n = 3, 4, 5$.

Initial state	$1s$	$2s$	$2p$	$n = 2$	$n = 3$
$I_n(eV)$	13.6	3.4	3.4	3.4	1.511
A_0	0.18450	0.20901	0.13197	0.14784	0.058463
A_1	-0.032226	-0.16481	0.033285	0.0080871	-0.051272
A_2	-0.034539	0.13873	0.21332	-0.062270	0.85310
A_3	1.4003	0.73025	1.0058	1.9414	-0.57014
A_4	-2.8115	-0.34957	-0.83918	-2.1980	0.76684
A_5	2.2986	0.00	0.29989	0.95894	0.00

Table 3: Values of threshold energy (I_n) and fitting parameters A_i in Eq. (14) for ionization cross sections of $1s, 2l$ and $n = 2, 3$ states.

a_i	$1s \rightarrow 2s$	$1s \rightarrow 2p$	$1s \rightarrow n = 2$
a_1	10.082	33.777	34.433
a_2	9.5185(-4)*	62.880	8.5476
a_3	0.60403	9.8099	7.8501
a_4	-2.7993	-11.310	-9.2217
a_5	8.7513(-3)	1.6317(-2)	1.8020(-2)
a_6	12.125	1.5817	1.6931
a_7	1.1038(-6)	4.3511(-3)	1.9422(-3)
a_8	3.1597	2.5564	2.9068
a_9	45.483	48.717	44.507
a_{10}	-	0.49512	0.56870

* $a(-X) = a \times 10^{-X}$

Table 4: Values of parameters a_i in Eq. (29) for proton-impact $1s \rightarrow 2s, 2p$, and $1s \rightarrow n = 2$ excitation cross sections for $H(1s)$.

b_i	$1s \rightarrow n = 3$	$1s \rightarrow n = 4$	$1s \rightarrow n = 5$	$1s \rightarrow n = 6$
b_1	6.1950	2.0661	1.2449	0.63771
b_2	5.5162(-3)*	5.1335(-4)	3.0826(-4)	3.2949(-4)
b_3	0.29114	0.28953	0.31063	0.25757
b_4	-4.5264	-2.2849	-2.4161	-2.2950
b_5	6.0311	0.11528	0.024664	0.050796
b_6	-2.0679	-4.8970	-6.3726	-5.5986
b_7	35.773	34.975	32.291	37.174
b_8	0.54818	0.91213	0.21176	0.39265

* $a(-X) = a \times 10^{-X}$

Table 5: Values of parameters b_i in Eq. (30) for the cross section of proton-impact excitation of $H(1s)$ for $n = 3, 4, 5, 6$ levels.

10 Tables

c_i	$2 \rightarrow 3$	$2 \rightarrow 4$	$2 \rightarrow 5$
c_1	1247.5	190.59	63.494
c_2	0.068781	0.073307	0.077953
c_3	0.521176	0.54177	0.53461
c_4	-1.2722	-1.2894	-1.2881
c_5	11.319	11.096	11.507
c_6	2.6235	2.9098	4.3417

Table 6: Values of fitting parameters c_i in Eq. (32) for proton-impact excitation cross sections $\sigma_{exc}(2 \rightarrow 3, 4, 5)$ of $H^*(n = 2)$.

c_i	$3 \rightarrow 4$	$3 \rightarrow 5$	$3 \rightarrow 6$
c_1	394.51	50.744	18.264
c_2	0.013597	0.014398	0.013701
c_3	0.16565	0.31584	0.31711
c_4	-0.8949	-1.4799	-1.4775
c_5	21.606	19.416	18.973
c_6	0.62426	4.0262	2.9056

Table 7: Values of fitting parameters c_i in Eq. (35) [with reference to (32)] for proton-impact excitation cross sections $\sigma_{exc}(3 \rightarrow 4, 5, 6)$ of $H^*(n = 3)$.

b_i	$n = 1$	$n = 2$	$n \geq 3$
b_1	2.016 (-3)*	3.867(-3)	1.1167(-2)
b_2	3.7154	1.800	1.6314
b_3	3.9890(-2)	7.1120(-3)	7.1516(-3)
b_4	3.1413 (-1)	5.2740(-3)	1.2217(-2)
b_5	2.1254	1.5908	1.4822
b_6	6.3990 (+3)	6.9575(+3)	3.3458(+3)
b_7	6.1897 (+1)	1.2944(+2)	1.2247(+2)
b_8	9.2731 (+3)	2.5440(+5)	5.5455(+2)

* $a(\pm) = a \times 10^{\pm X}$

Table 8: Values of parameters b_i in Eq. (40) for the proton-impact ionization cross sections of $H(n)$ for $n = 1, 2$ and $n \geq 3$.

A_i	$n = 1$	$n = 2$	$n = 3$	$n \geq 4$
A_1	3.2345	9.2750(-1)*	3.7271(-1)	2.1336(-1)
A_2	2.3588(+2)*	6.5040(+3)	2.7645(+6)	1.0000(+10)
A_3	2.3713	2.0699(+1)	1.4857(+3)	1.3426(+6)
A_4	3.8371(-2)	1.3405(-2)	1.5720(-3)	1.8184(-3)
A_5	3.8068(-6)	3.0842(-6)	3.0842(-6)	3.0842(-6)
A_6	1.1832(-10)	1.1832(-10)	1.1832(-10)	1.1832(-10)

$$* a(\pm X) = a \times 10^{\pm X}$$

Table 9: Values of parameters A_i in Eq. (44) for the total charge exchange cross section in $H^+ + H(n)$ collisions.

a_j	$n = 2$	$n = 3$
a_0	-3.49880888(+1)*	-3.11479336(+1)
a_1	2.15245051(-1)	-7.73020527(-1)
a_2	-2.35628664(-2)	5.49204378(-2)
a_3	5.49471553(-2)	-2.73324984(-3)
a_4	5.37932888(-3)	-1.22831288(-3)
a_5	-6.05507021(-3)	4.35049828(-4)
a_6	9.99168329(-4)	-6.21659501(-5)
a_7	-6.63625564(-5)	4.12046807(-6)
a_8	1.61228385(-6)	-1.039784996(-7)

$$* a(\pm X) = a \times 10^{\pm X}$$

Table 10: Values of fit coefficients a_j in Eq. (63) for the charge exchange cross sections of $H^+ + H^- \rightarrow H(n = 2, 3) + H$ reactions.

a_j	$H + H + e$	$H_2 + e$
a_0	-3.61799082(+1)*	-3.44152907(+1)
a_1	1.16615172	-3.39348209(-1)
a_2	-1.41928602(-1)	5.66591705(-2)
a_3	-1.11195959(-2)	-9.05150459(-3)
a_4	-1.72505995(-3)	7.66060418(-4)
a_5	1.59040356(-3)	-4.27126462(-5)
a_6	-2.53196144(-4)	-1.57273749(-7)
a_7	1.66978235(-5)	2.57607677(-7)
a_8	-4.09725797(-7)	-1.20071919(-8)

$$* a(\pm X) = a \times 10^{\pm X}$$

Table 11: Values of fitting coefficients a_j in Eq. (71) for the cross sections of $H + H + e$ and $H_2 + e$ production in $H^- + H$ collisions.

10 Tables

v'	a_1	a_2	a_3	a_4	a_5	a_6
0	-7.5980	-0.15006	-2.3448	1.0147	-8.0412	7.9813(-2)
1	-13.327	-8.7148(-2)*	-6.0249	1.2828	-8.8773	0.12732
2	-17.564	-5.4436(-2)	-17.117	0.80536	-4.3441	0.19250
3	-19.333	-5.3110(-2)	-22.534	0.80910	-3.5290	0.19760
4	-19.251	-6.7406(-2)	-30.152	0.81438	-2.4330	0.10814
5	-20.750	-6.4240(-2)	-32.227	0.92195	-3.5451	0.10243
6	-22.792	-5.5113(-2)	-33.789	0.98888	-3.3806	0.11688
7	-24.228	-5.0631(-2)	-36.382	0.98940	-2.8794	0.13049
8	-25.958	-4.3967(-2)	-39.417	1.0190	-3.0842	0.16320
9	-27.240	-3.9953(-2)	-42.249	1.0115	-2.7728	0.19473
10	-26.890	-4.6593(-2)	-48.900	0.90022	-0.59724	8.9765(-2)

* $a(-X) = a \times 10^{-X}$

Table 12: Values of fitting parameters a_i in Eq. (75) for the rate coefficients of $H_2(0 \rightarrow v')$ excitation via the H_2^- ($X^2\Sigma_u, B^2\Sigma_g$) states (from [112]).

v'	a_1	a_2	a_3	a_4	a_5	a_6
0	-22.103	2.5142(-2)*	-121.13	1.0583	-6.5889	0.28729
1	-124.80	1.0277	-21.196	1.2299(-2)	-3.4388	0.27455
2	-121.35	1.0563	-22.642	2.4069(-2)	-6.3281	0.28896
3	-22.128	1.9256(-2)	-122.46	1.0473	-5.4407	0.28314
4	-22.173	1.9497(-2)	-122.48	1.0471	-5.4929	0.27790
5	-22.492	2.1828(-2)	-121.60	1.0545	-6.1702	0.28867
6	-21.554	1.2471(-2)	-124.34	1.0319	-4.1247	0.25525
7	-125.50	1.0231	-21.043	6.3836(-3)	-3.6812	0.20980
8	-20.325	-1.1112(-3)	-127.61	1.0059	-1.9403	0.16030
9	-20.849	2.8543(-3)	-127.24	1.0081	-1.8860	0.19505
10	-127.78	1.0030	-21.011	4.0391(-3)	-0.85698	0.27961
11	-21.164	4.7984(-3)	-127.39	1.0061	-1.0805	0.31177
12	-126.69	1.0117	-21.471	7.0803(-3)	-1.3133	0.39423
13	-118.82	1.0733	-25.050	3.6964(-2)	-8.4809	0.33128
14	-25.411	3.5353(-2)	-118.77	1.0739	-8.6323	0.33313

* $a(-X) = a \times 10^{-X}$

Table 13: Values of fitting parameters a_i in Eq. (75) for the rate coefficients of $H_2(0 \rightarrow v')$ excitation via the H_2^* ($B^1\Sigma_u, C^1\Pi_u$) excited electronic states (from [112]).

Conf.	$Ns\sigma_g$	$Np\sigma_u$	$Np\pi_u$	$Nd\sigma_g$	$Nd\pi_g$	$Nd\delta_g$
Symm.	Σ_g^+	Σ_u^+	Π_u	Σ_g^+	Π_g	Δ_g
N	Singlets					
2	EF(2s)	B(2p)	C(2p)			
3	HH(3d)	B'(2s)	D(3d)	GK(2p)	I(2p)	J(3d)
4	O(3p)	B''(3s)	D'(4p)	P(3d)	R(3p)	S(4f)
N	Triplets					
2	a(2s)	b(1s)	c(2p)			
3	h(2p)	e(2s)	d(3p)	g(3s)	i(2p)	j(3d)
4	o(?)	f(2p)	k(3d)	p(3d)	r(3d)	s(4d)

Table 14: Electronic configuration ($1s\sigma_g, Nl\mu_\sigma$) and symmetry of lowest excited states of H_2 . (In parenthesis is given the nl -state of the one excited H atom in the dissociation limit.)

	$B^1\Sigma_u$	$B'^1\Sigma_u$	$B''^1\Sigma_u$	$C^1\Pi_u$	$D^1\Pi_u$	$D'^1\Pi_u$
$\Delta E(eV)$	12.754	14.85	15.47	13.29	14.996	15.555
α	0.550	0.550	0.550	0.552	0.552	0.552
A_1	3.651(-2)*	6.827(-3)	2.446(-3)	3.653(-2)	8.913(-3)	3.872(-3)
A_2	-0.8405	-0.1572	-5.631(-2)	-0.8398	-0.2049	-8.902(-2)
A_3	1.2365	0.23122	6.2846(-2)	1.2368	0.30178	0.13110
A_4	2.5236	0.47191	0.16908	2.8740	0.70126	0.30464

* $a(-X) = a \times 10^{-X}$

Table 15: Values of parameters α and A_i in Eq. (80) for the cross sections of dipole allowed transitions $X^1\Sigma_g^+(v=0) \rightarrow ^1\Sigma_u, ^1\Pi_u$ in H_2 .

	$EF^1\Sigma_g^+$	$HH^1\Sigma_g^+$	$GK^1\Sigma_g^+$	$I^1\Pi_g$
$\Delta E(ev)$	13.13	14.98	14.816	14.824
α	2.71	2.71	2.75#	2.80
A_1	0.8322	2.913(-2)*	1.43(-2)#	5.409(-2)

* $a(-X) = a \times 10^{-X}$

Estimate

Table 16: Values of parameters α and A_1 in Eq. (81) for the cross sections of symmetry-forbidden transitions $X^1\Sigma_g^+(v=0) \rightarrow EF^1\Sigma_g^+, HH^1\Sigma_g^+, GK^1\Sigma_g^+, I^1\Pi_g$ in H_2 .

10 Tables

	$X^1\Sigma_g^+ \rightarrow B^1\Sigma_u^+$	$X^1\Sigma_g^+ \rightarrow C^1\Sigma_u^+$
a_1	0.9754	1.1106
a_2	0.3708	0.8921
a_3	-0.2800	-0.2019
a_4	0.5479	0.6545
v	$\Delta E_{XB}(R_v^t)(eV)$	$\Delta E_{XC}(R_v^t)(eV)$
0	11.61	12.28
1	10.75	11.61
2	10.13	11.12
3	9.62	10.81
4	9.19	10.53
5	8.81	10.30
6	8.48	10.12
7	8.21	9.97
8	7.97	9.86
9	7.80	9.80
10	7.68	9.78
11	7.64	9.79
12	7.70	9.88
13	7.94	10.01
14	9.11	10.21

Table 17: Values of fitting parameters a_i , and of transition energies $\Delta E_{X\Lambda}$, in Eqs. (84), (85) for $X^1\Sigma_g^+(v) \rightarrow B, C^1\Sigma_u^+$ transitions.

	$X \rightarrow B'$		$X \rightarrow B''$		$X \rightarrow D$		$X \rightarrow D'$	
	v=0	v=1	v=0	v=1	v=0	v=1	v=0	v=1
$\Delta E_{X\Lambda}(R_v^t)(eV)$	14.85	13.09	14.99	13.35	15.67	13.86	15.66	14.04
b_1	0.1688	0.1937	0.3226	0.3696	0.0651	0.0746	0.1256	0.1471
b_2	1.2433	1.3554	0.4512	0.6749	1.1633	1.2327	0.7526	0.7778
b_3	0.8581	0.9300	-0.2770	-0.3478	0.8448	0.8157	-0.1110	-0.2842
b_4	1.0069	0.9659	0.5916	0.7568	1.1140	1.0515	0.5811	0.6728

Table 18: Values of $\Delta E(R_{0,1}^t)$ and parameters b_i in Eq. (86) for $X^1\Sigma_g^+(v = 0, 1) \rightarrow N^1\Lambda_u$ excitation cross sections.

C_i	$X \rightarrow B'$	$X \rightarrow B''$	$X \rightarrow D$	$X \rightarrow D'$
C_1	0.00	0.00	2.93(-3)	1.10(-4)
C_2	0.00	0.00	2.25	3.60
C_3	2.00	-2.01(-1)	1.00	5.50(-1)
C_4	0.00	0.00	2.00(-1)	2.6(-1)
C_5	1.10	1.10	1.00	1.00
C_6	-1.30(-1)*	-1.30(-1)	0.00	0.00
C_7	1.94(-2)	1.26(-2)	0.00	0.00
C_8	7.0(-1)	5.0(-1)	0.00	0.00
C_9	2.42(-2)	3.44(-2)	0.00	0.00
C_{10}	-3.21(-3)	-5.40(-3)	0.00	0.00
C_{11}	-1.08(-4)	-9.20(-5)	0.00	0.00
C_{12}	1.36(-4)	2.55(-4)	0.00	0.00

* $a(-X) = a \times 10^{-X}$

Table 19: Values of parameters C_i in the Eq. (89) related to excitation cross sections for $X(v) \rightarrow N^1\Lambda_u$ transitions.

v	$X \rightarrow B$	$X \rightarrow B'$	$X \rightarrow B''$	$X \rightarrow C$	$X \rightarrow D$	$X \rightarrow D'$
0	0.22	3.02	0.14	0.48	0.083	0.042
1	1.31	3.50	0.64	2.52	0.49	0.235
2	4.02	3.62	1.02	6.51	1.28	0.59
3	6.76	4.48	0.94	8.50	1.82	0.78
4	7.18	4.81	1.13	7.24	1.74	0.66
5	5.98	5.62	1.40	7.50	1.69	0.63
6	6.50	6.58	1.44	9.68	2.02	0.84
7	8.11	7.36	1.75	9.21	2.03	0.85
8	7.94	8.78	1.88	8.52	1.75	0.76
9	6.68	9.57	1.63	9.80	1.90	0.85
10	6.23	10.35	1.51	9.79	2.01	0.84
11	6.22	9.41	1.15	8.51	1.74	0.70
12	5.42	7.48	0.46	7.51	1.35	0.55
13	3.61	3.07	0.15	6.08	0.94	0.40
14	1.82	1.48	0.073	5.89	0.58	0.20

Table 20: Values of dissociative excitation cross sections $\sigma_{exc}^{diss}(v)$ (in units of 10^{-18}cm^2) via dipole-allowed transitions $X^1\Sigma_g^+(v) \rightarrow N^1\Lambda_u$ ($N = 2 - 4$) in H_2 , at the collision energy $E = 40 \text{ eV}$ (from [15]).

10 Tables

v	$X \rightarrow B$	$X \rightarrow B'$	$X \rightarrow B''$	$X \rightarrow C$	$X \rightarrow D$	$X \rightarrow D'$
0	0.44	38.5	4.41	1.10	0.92	1.20
1	2.18	40.2	18.5	5.71	5.27	6.44
2	5.58	37.7	29.4	13.0	13.2	15.2
3	8.78	43.5	27.0	16.2	17.4	19.0
4	7.98	43.3	31.6	13.1	15.1	15.5
5	5.67	48.4	39.2	12.9	13.85	14.4
6	5.55	55.1	40.2	15.4	16.3	18.8
7	6.39	61.3	50.9	13.8	16.0	18.5
8	5.80	72.0	60.6	13.1	13.1	16.6
9	4.64	79.7	64.7	13.4	13.8	17.0
10	4.24	90.8	75.5	12.7	13.9	16.2
11	4.51	90.5	59.9	10.5	11.4	13.2
12	4.23	84.0	29.2	8.92	8.71	10.1
13	3.44	45.8	11.4	7.22	6.06	7.21
14	2.56	27.7	4.10	6.93	3.87	4.10

Table 21: Contributions (in %) of dissociative excitation process (79) to total excitation cross section for dipole-allowed transitions $X^1\Sigma_g^+(v) \rightarrow N^1\Lambda_u$ ($N = 2-4$) in H_2 , at $E = 40$ eV.

	$a^3\Sigma_g^+$	$b^3\Sigma_u^+$	$c^3\Pi_u$	$e^3\Sigma_u^+$	$d^3\Pi_u$
A	0.544	11.16	1.43	0.190	0.375
β	4.5	2.33	5.5	4.5	5.5
γ	1.55	3.78	1.65	1.60	1.75
ΔE (eV)	11.72	7.93	11.72	13.0	13.6

Table 22: Values of parameters A , β and γ in Eq. (95) and of threshold energies ΔE for triplet state excitation cross sections from $X\Sigma_g^+(v = 0)$ in H_2 .

v	$E_{exc,v}(eV)$	$\Delta E_v(eV)$
0	0.00	7.93
1	0.516	6.76
2	1.003	6.05
3	1.461	5.00
4	1.891	4.05
5	2.293	3.42
6	2.667	2.76
7	3.012	2.14
8	3.327	1.74
9	3.611	1.26
10	3.863	0.95
11	4.086	0.79
12	4.254	0.66
13	4.384	0.45
14	4.461	0.28

Table 23: Values of excitation energies $E_{exc}(v)$ of $H_2(X^1\Sigma_g^+; v)$ vibrational states and threshold energies, ΔE_v , for $X^1\Sigma_g^+(v) \rightarrow b^3\Sigma_u^+$ transitions in Eq. (96).

v	b_1	b_2	b_3	b_4	b_5	b_6
0	-11.565	-7.6012(-2)*	-78.433	0.74960	-2.2126	0.22006
2	-12.035	-6.6082(-2)	-67.806	0.72403	-1.5419	1.5195
2	-13.566	-4.3737(-2)	-55.933	0.72286	-2.3103	1.5844
3	-46.664	0.74122	-15.297	-2.2384(-2)	-1.3674	1.3621
4	-37.463	0.81763	-0.40373	-0.45851	-18.093	1.1460(-2)
5	-28.283	0.99053	-10.377	-8.5590(-2)	-11.053	6.7271(-2)
6	-23.724	1.0112	-2.9905	-0.24701	-17.931	3.4376(-2)
7	-19.547	1.0224	-1.7489	-0.31413	-19.408	2.8643(-2)
8	-15.937	1.0213	-10175	-0.38040	-20.240	2.4170(-2)
9	-12.712	1.0212	-0.60400	-0.44572	-20.766	2.1159(-2)
10	-0.40557	-0.49721	-9.9025	1.0212	-21.031	1.9383(-2)

* $a(-X) = a \times 10^{-X}$

Table 24: Values of fitting parameters in Eq. (97) for dissociation of $H_2(X^1\Sigma_g^+; v)$ via excitation of $b^3\Sigma_u^+$, $a^3\Sigma_g^+$ and $c^3\Pi_u$ states (from [112]).

10 Tables

v'	Ref. [148]	FC	$E_{H_2^+}^{diss}(v')(eV)$
0	0.119	0.092	2.645
1	0.190	0.162	2.374
2	0.188	0.176	2.118
3	0.152	0.155	1.877
4	0.125	0.121	1.651
5	0.075	0.089	1.440
6	0.052	0.063	1.243
7	0.037	0.044	1.059
8	0.024	0.030	0.890
9	0.016	0.021	0.734
10	0.0117	0.0147	0.593
11	0.0082	0.0103	0.465
12	0.0057	0.0072	0.351
13	0.00374	0.0051	0.252
14	0.00258	0.0036	0.168
15	0.00175	0.0024	0.100
16	0.00109	0.0016	0.0491
17	0.00056	0.0008	0.0170
18	0.00012	0.0002	0.0020

Table 25: Population factors $F_{0v'}$ of $H_2^+(v')$ levels by electron-impact transitions from $H_2(^1\Sigma_g^+; v = 0)$ derived from experiment [148] and calculated in Franck-Condon approximation (FC). $E_{H_2^+}^{diss}(v')$ is the dissociation energy of $H_2^+(v')$ level (in eV).

v	C_1	C_2	C_3	C_4	C_5	$\Delta E_v(eV)$
0	-2.1196(+2)*	1.0022	-20.350	-4.5201	1.0773 (-2)	30.6
1	-2.0518(+2)	0.99226	-19.905	-3.3364	1.1725(-2)	27.4
2	-1.9936(+2)	0.98837	-19.600	-3.0891	1.2838(-2)	25.2
3	-1.9398(+2)	0.98421	-19.457	-3.1386	1.3756(-2)	23.4
4	-1.8893(+2)	0.97647	-19.397	-3.2807	1.4833(-2)	21.9
5	-1.8422(+2)	0.96189	-19.310	-3.2609	1.6030(-2)	20.6
6	-1.7903(+2)	0.94593	-19.170	-3.0592	1.7254(-2)	19.6
7	-1.7364(+2)	0.93986	-19.052	-2.9880	1.8505(-2)	18.5
8	-1.6960(+2)	0.93507	-18.908	-2.7334	1.8810(-2)	17.6
9	-1.6664(+2)	0.92602	-18.723	-2.2024	1.8055(-2)	16.7
10	-1.6521(+2)	0.92124	-18.549	-1.6895	1.6245(-2)	16.0
11	-1.6569(+2)	0.93366	-18.479	-1.6311	1.5194(-2)	15.4
12	-1.6464(+2)	0.94682	-18.440	-1.7259	1.5304(-2)	14.8
13	-1.6071(+2)	0.95533	-18.405	-1.8938	1.6254(-2)	14.2

* $a(\pm X) = a \times 10^{\pm X}$

Table 26: Values of fitting coefficients C_i in Eq. (112) for ionization rate coefficient $K_{ion}^{diss}(^2\Sigma_g^+, ^1\Sigma_u^+)_v$, and values of transition energies, ΔE_v , for $^1\Sigma_g^+(v) \rightarrow ^2\Sigma_u^+$ in Eq. (111).

10 Tables

v	$E_{th,v}(eV)$	$\sigma_v^{(0)}(10^{-16} cm^2)$
0	3.72	3.22(-5)*
1	3.21	5.18(-4)
2	2.72	4.16(-3)
3	2.26	2.20(-2)
4	1.83	1.22(-1)
5	1.43	4.53(-1)
6	1.36	1.51
7	0.713	4.48
8	0.397	10.1
9	0.113	13.9
10	-0.139	11.8
11	-0.354	8.87
12	-0.529	7.11
13	-0.659	5.00
14	-0.736	3.35

* $a(-X) = a \times 10^{-X}$

Table 27: Values of threshold energies, $E_{th,v}$, and peak DA cross sections, $\sigma_v^{(0)}$, in Eq. (124) for $\sigma_{DA}(^2\Sigma_u^+(v))$.

v	a_1	a_2	a_3	a_4	a_5	a_6
0	-50.862	0.92494	-28.102	-4.5231(-2)*	0.46439	0.87950
1	-48.125	0.91626	-24.873	-4.9898(-2)	0.45288	0.87604
2	-41.218	0.96738	-23.167	-4.8546(-2)	-1.7222	0.19858
3	-37.185	0.96391	-21.264	-5.1701(-2)	-1.8121	0.19281
4	-35.397	0.85294	-18.452	-6.522(-2)	-0.56595	8.8997(-2)
5	-33.861	0.9301	-20.852	-3.016(-2)	5.561	0.45548
6	-23.751	0.9402	-19.626	-3.276(-2)	-0.3982	1.58655
7	-19.988	0.83369	-18.700	-3.552(-2)	-0.38065	1.74205
8	-18.278	0.8204	-17.754	-4.453(-2)	-0.10045	2.5025
9	-13.589	0.7021	-16.850	-5.012(-2)	-0.77502	0.3423
10	-11.504	0.84513	-14.603	-6.775(2)	-3.2615	0.13666

* $a(-X) = a \times 10^{-X}$

Table 28: Values of fitting parameters a_i in Eq. (128) for rate coefficient $K_{diss}(^2\Sigma_u^+)$ of reaction (126).

v	a_1	a_2	a_3	a_4	a_5	a_6
0	-15.760	-5.2659(-2)*	-84.679	1.0414	-8.2933	0.18756
3	-16.966	-4.41421(-2)	-53.814	0.96478	-1.8705	0.30887
6	-14.430	-5.8984(-2)	-33.755	0.90310	-1.4420	6.9051(-3)
9	-14.423	-5.4825(-2)	-16.684	0.88550	-1.6937	6.9260(-3)
12	-19.921	-9.2022(-3)	-46.095	0.62850	44.245	0.28407

* $a(-X) = a \times 10^{-X}$

Table 29: Values of fitting parameters a_i in Eq. (128) for rate coefficient $K_{diss}(^2\Sigma_g^+)$ of reaction (127a).

	$v' = 1$	$v' = 2$	$v' = 3$	$v' = 4$	$v' = 5$	$v' = 6$	$v' = 7$
$E_{0v'}(eV)$	0.774	1.5045	2.192	2.837	3.440	4.001	4.518
a_1	7.21	5.71	3.12	1.86	10.56	58.51	385.8
a_2	0.50	3.75	25.5	218.0	580.0	628.0	642.0
a_3	2.15	4.50	5.50	4.50	4.50	4.50	4.50
a_4	1.255	1.65	1.38	1.20	2.40	3.60	4.90
b_1	62.0	84.8	26.50	27.42	4.03	0.34	0.028
b_2	26.5	60.2	79.8	164.0	164.0	164.0	164.0
b_3	1.15	1.32	1.40	1.38	1.38	1.38	1.38
b_4	0.488	0.862	0.867	1.22	1.22	1.22	1.22
b_5	1.26(-7)*	8.55(-5)	9.50(-6)	8.5(-7)	8.5(-7)	8.5(-7)	8.5(-7)
b_6	1.74	1.05	1.45	1.67	1.67	1.67	1.67

* $a(-X) = a \times 10^{-X}$

Table 30: Values of $E_{0v'}$ and fitting parameters a_i and b_i in Eqs. (140a), (140b) for the cross section of $0 \rightarrow v'$ vibrational excitation .

10 Tables

	$v = 0$	$v = 1$	$v = 2$	$v = 3$	$v = 4$	$v = 5$	$v = 6$	$v = 7$	$v = 8$
E_{0v} (eV)	2.67	1.74	1.17	0.48	0.00	0.00	0.00	0.00	0.00
a_1	18.60	2.51	3.01	4.50	24.0	11.75	11.58	0.00	0.00
a_2	-1.66	-0.56	-0.63	-0.57	0.32	0.092	0.091	0.00	0.00
a_3	2.53	4.21	7.04	5.00	0.00	0.00	0.00	0.00	0.00
a_4	1.93	4.07	10.74	14.62	0.00	0.00	0.00	0.00	0.00
a_5	0.00	1.0(-5)	1.0(-5)	1.0(-5)	0.145	3.86(-3)	3.84(-3)	0.00	0.00
a_6	0.00	1.00	1.00	1.00	1.84	2.86	2.87	0.00	0.00
b_1	17.3	58.0	26.53	39.50	10.8	20.0	20.04	33.0	30.0
b_2	105.0	11.28	25.20	9.35	0.00	0.00	0.00	0.00	0.00
b_3	2.0	0.246	0.65	0.51	0.00	0.00	0.00	0.00	0.00
b_4	1.0(+4)*	1.00	1.00	1.00	1.00	1.00	1.00	1.00	1.00
b_5	-1.12	0.00	0.00	0.00	-0.297	-0.193	-0.192	-0.022	-0.017
b_6	3.64(-4)	3.92(-5)	1.56(-6)	5.32(-7)	2.92(-4)	1.36(-5)	1.34(-5)	1.22(-2)	1.87(-2)
b_7	0.90	1.11	1.45	1.60	0.76	1.15	1.15	0.36	0.375
b_8	5.03(-19)	4.95(-17)	5.50(-19)	3.52(-20)	4.93(-11)	4.46(-12)	4.46(-12)	6.51(-8)	9.0(-10)
b_9	4.00	3.65	4.00	4.25	2.35	2.61	2.61	1.78	2.18
b_{10}	5.87(-28)	3.88(-26)	8.50(-27)	3.50(-27)	2.62(-27)	4.31(-27)	4.31(-27)	3.25(-23)	1.85(-25)
b_{11}	5.50	5.20	5.30	5.40	5.50	5.50	5.50	4.86	5.25

* $a(\pm X) = a \times 10^{\pm X}$

Table 31: Values of E_{0v} and of fitting parameters a_i and b_i in Eqs. (145) for total v -selective charge transfer cross sections in $H^+ + H_2(v)$ collisions.

$v(H_2)$	$E_v^{diss}(H_2)(eV)$	$v_{0'}(H_2^+)$	$\Delta E_{vv_0'}(eV)$
0	4.478	-	-
1	3.962	-	-
2	3.475	-	-
3	3.017	-	-
4	2.587	0	0.058
5	2.185	2	0.067
6	1.811	3	0.066
7	1.466	5	0.026
8	1.151	6	0.092
		7	0.093
9	0.866	8	0.024
10	0.612	9	0.019
11	0.3995	12	0.049
12	0.224	13	0.028
13	0.0940	15	0.006
14	0.0171	17	0.0001

Table 32: Dissociation energies, $E_v^{diss}(H_2)$, of vibrational levels of H_2 , the quasi-resonant levels v_0' in $H_2^+(v')$ corresponding to the $H_2(v)$ levels and their resonance energy defect, $\Delta E_{vv_0'}$.

v	$E_{0v}(eV)$	a_1	a_2	a_3	a_4
0	6.717	7.52(+3)*	4.64	5.37	2.18
1	5.943	1.56(+3)	3.91	3.42	1.55
2	5.313	3.83(+2)	3.22	2.71	1.50
3	4.526	72.5	2.40	2.32	1.34
4	3.881	23.8	1.64	1.86	1.50
5	3.278	8.68	0.94	1.39	1.04
6	2.716	6.85	0.58	1.20	1.14
8	1.727	10.54	0.36	1.03	1.25
10	0.918	22.86	0.28	0.73	1.78
12	0.336	30.11	0.20	0.65	1.64
14	0.0257	33.92	0.15	0.58	2.08

* $a(+X) = a \times 10^X$

Table 33: Values of E_{0v} and fitting parameters a_i in Eq. (153) for proton-impact dissociation cross section of $H_2(v)$.

10 Tables

	$0 \rightarrow 1$	$0 \rightarrow 2$	$0 \rightarrow 3$	$0 \rightarrow 4$	$0 \rightarrow 5$
$E_{0v'}(eV)$	1.55	2.04	2.50	-	-
a_1	3.15	4.33	9.56	-	-
a_2	1.00	1.61	1.56	-	-
a_3	9.84	12.5	8.16	-	-
a_4	16.58	3.92	16.20	-	-
b_1	16.50	3.55	4.57	4.03	7.14
b_2	37.45	31.31	213.7	132.0	91.4
b_3	1.29	1.47	1.88	2.82	1.77
b_4	0.57	0.50	0.66	0.76	0.80
b_5	5.22(-4)*	3.25(-4)	1.45(-4)	4.31(-4)	2.54(-4)
b_6	0.94	0.96	1.13	1.12	1.12

* $a(-X) = a \times 10^{-X}$

Table 34: Values of parameters $E_{0v'}$, a_i and b_i in Eqs. (162) for vibrational $H_2(0 \rightarrow v')$ excitation by H -atom impact.

v	a_1	a_2	a_3	a_4	a_5
0	2.06964(+1)*	7.32149(+7)	1.74660	4.75874(+3)	-9.42775(-1)
1	2.05788(+1)	4.32679(+7)	1.68520	1.91812(+3)	-8.16838(-1)
2	2.05183(+1)	5.15169(+7)	1.73345	3.09006(+3)	-8.88414(-1)
3	2.04460(+1)	1.87116(+8)	1.87951	9.04442(+3)	-9.78327(-1)
4	2.03608(+1)	4.93688(+8)	1.99499	2.32656(+4)	-1.06294
5	2.02426(+1)	1.80194(+8)	1.92249	1.28777(+4)	-1.02713
6	2.00161(+1)	2.96945(+5)	1.31044	9.55214(+2)	-1.07546
7	1.98954(+1)	4.53104(+5)	1.37055	3.88065(+2)	-8.71521(-1)
8	1.97543(+1)	5.13174(+5)	1.39819	3.54272(+2)	-8.07563(-1)
9	1.97464(+1)	9.47230(+4)	1.24048	2.28283(+2)	-8.51591(-1)
10	1.95900(+1)	6.43990(+4)	1.22211	1.16196(+2)	-7.35645(-1)
11	1.94937(+1)	3.49017(+4)	1.20883	1.26329(+2)	-8.15130(-1)
12	1.90708(+1)	1.05971(+5)	9.91646(-1)	1.05518(+2)	-1.93837(-1)
13	1.89718(+1)	7.76046(+5)	7.84577(-1)	1.31409(+3)	-1.00479(-2)
14	1.87530(+1)	5.81508(+5)	7.35904(-1)	1.69328(+3)	4.47757(-3)

* $a(-X) = a \times 10^{-X}$

Table 35: Values of parameters a_i in Eq. (165) for the rate coefficient of H -impact dissociation of $H_2(v)$.

v	a_1	a_2	a_3
0	6.20	2.56	9.72
1	7.60	2.30	4.82
2	9.05	1.91	2.88
3	10.50	1.72	2.45
4	11.93	2.05	2.87
6	14.75	1.82	2.15
8	16.70	2.16	3.38
9	16.79	2.36	4.82
10	16.52	2.32	4.52
11	14.04	2.35	5.85
12	11.31	2.00	8.43
14	6.72	1.08	4.06
16	3.61	1.00	15.77
17	2.26	1.00	44.58
18	0.69	0.75	68.42

Table 36: Values of parameters a_i in Eq. (182a) for electron impact v -selective DE cross section of $H_2^+(v)$.

10 Tables

v	$2p\sigma_u$		$2p\pi_u$	
	A_v	B_v	A_v	B_v
0	3.10	1.96	2.79	0.007
1	3.45	2.61	2.91	0.058
2	3.84	3.40	3.04	0.111
3	4.28	4.34	3.16	0.166
4	4.79	5.48	3.27	0.221
5	5.35	6.87	3.38	0.277
6	6.00	8.55	3.49	0.334
7	6.74	10.6	3.59	0.391
8	7.61	13.2	3.68	0.448
9	8.61	16.4	3.75	0.504
10	9.82	20.6	3.82	0.558
11	11.26	25.9	3.88	0.612
12	13.1	33.2	3.94	0.666
13	15.4	43.3	4.00	0.722
14	18.4	58.2	4.05	0.778
15	22.8	82.1	4.11	0.835
16	30.0	126.0	4.17	0.892
17	43.9	234.0	4.22	0.945
18	91.8	782.0	4.29	0.969

Table 37: Values of coefficients A_v and B_v in Eq. (183) for $\sigma_{DE}(v)$ in Bethe-Born approximation (from Ref. [215]).

v	A	a	α	b	β	$E_c(eV)$
0	3.758	0.69	1.37	0.350	0.12	9.0
1	5.037	0.56	1.54	0.422	0.18	7.0
2	2.505	0.66	1.82	1.391	0.22	5.5
3	4.575	0.0025	3.12	1.292	0.28	4.5
4	16.72	0.011	3.12	0.443	0.66	3.5
5	34.04	0.026	3.14	0.199	0.60	2.5
6	28.32	0.018	3.14	1.708	0.80	2.0
7	52.83	0.056	3.14	0.269	0.85	1.5
8	85.23	0.17	2.96	-	-	-
9	133.43	0.43	2.85	-	-	-
10	114.37	0.41	2.84	-	-	-
11	92.04	0.71	2.52	-	-	-
12	66.71	0.52	2.58	-	-	-
13	50.65	0.39	2.68	-	-	-
14	37.58	0.38	2.58	-	-	-
15	28.86	0.37	2.56	-	-	-
16	21.29	0.40	2.56	-	-	-
17	10.46	0.37	2.55	-	-	-
18	3.16	0.44	2.50	-	-	-

Table 38: Values of parameters A, a, α, b, β and E_c in Eq. (186) for $\sigma_{DR}(v)$.

10 Tables

v	$n = 3$	$n = 4$	$n = 5$	$n = 6$	$n = 7$	$n = 8$	$n = 9$	$n = 10$	$n = 11$
0	1.00	1.661	1.967	2.133	2.233	2.298	2.343	2.375	2.399
1	0.729	1.390	1.696	1.862	1.962	2.027	2.072	2.104	2.128
2	0.473	1.134	1.440	1.606	1.706	1.771	1.816	1.848	1.872
3	0.232	0.893	1.199	1.365	1.465	1.530	1.575	1.607	1.631
4	0.006	0.667	0.973	1.139	1.239	1.304	1.349	1.381	1.405
5	-0.205	0.456	0.762	0.928	1.028	1.093	1.138	1.170	1.194
6	-0.402	0.259	0.565	0.731	0.831	0.896	0.941	0.973	0.997
7	-0.580	0.081	0.390	0.553	0.653	0.718	0.763	0.795	0.819
8	-0.755	-0.094	0.212	0.378	0.478	0.543	0.588	0.620	0.644
9	-0.911	-0.250	0.056	0.222	0.322	0.387	0.432	0.464	0.488
10	-1.052	-0.391	-0.085	0.081	0.181	0.246	0.291	0.323	0.347
11	-1.180	-0.519	-0.213	-0.047	0.053	0.118	0.163	0.195	0.219
12	-1.294	-0.633	-0.327	-0.161	-0.061	0.004	0.049	0.081	0.105
13	-1.393	-0.732	-0.426	-0.260	-0.160	-0.095	-0.050	-0.018	0.006
14	-1.477	-0.816	-0.510	-0.344	-0.244	-0.179	-0.134	-0.102	-0.078
15	-1.545	-0.884	-0.578	-0.412	-0.312	-0.247	-0.202	-0.170	-0.146
16	-1.596	-0.935	-0.629	-0.463	-0.363	-0.298	-0.253	-0.221	-0.197
17	-1.628	-0.967	-0.661	-0.495	-0.395	-0.330	-0.285	-0.253	-0.229
18	-1.643	-0.982	-0.676	-0.510	-0.410	-0.345	-0.300	-0.268	-0.244

Table 39: Threshold energies (in eV) for production of an $H(n \geq 3)$ atom from electron DR on $H_2^+(v)$. (The negative numbers indicate the exothermicities (in eV) of (v, n) DR channels).

$E(\text{eV})$	0.5	1.0	2.0	3.0	4.0	6.0	8.0	10.0
n	$v = 0$							
2	1.00	1.00	0.84	0.66	0.50	0.31	0.13	0.09
3	0.00	0.00	0.11	0.18	0.24	0.30	0.33	0.32
4	0.00	0.00	0.04	0.10	0.14	0.21	0.27	0.26
5	0.00	0.00	0.01	0.02	0.04	0.06	0.09	0.11
≥ 6	0.00	0.00	0.00	0.04	0.08	0.012	0.18	0.22
n	$v = 1$							
2	1.00	0.85	0.57	0.23	0.15	0.11	0.07	0.07
3	0.00	0.15	0.20	0.29	0.30	0.31	0.32	0.32
4	0.00	0.00	0.11	0.18	0.24	0.26	0.28	0.28
5	0.00	0.00	0.06	0.10	0.10	0.11	0.11	0.11
≥ 6	0.00	0.00	0.06	0.20	0.21	0.22	0.22	0.22
n	$v = 2$							
2	1.00	0.65	0.25	0.14	0.08	0.07	0.06	0.06
3	0.00	0.35	0.32	0.32	0.32	0.31	0.31	0.31
4	0.00	0.00	0.19	0.23	0.27	0.27	0.27	0.27
5	0.00	0.00	0.08	0.10	0.11	0.12	0.12	0.12
≥ 6	0.00	0.00	0.16	0.21	0.22	0.23	0.24	0.24
n	$v = 3$							
2	0.57	0.34	0.22	0.15	0.10	0.07	0.06	0.06
3	0.43	0.54	0.42	0.38	0.34	0.33	0.32	0.32
4	0.00	0.10	0.21	0.26	0.29	0.29	0.29	0.29
5	0.00	0.00	0.05	0.07	0.09	0.10	0.11	0.11
≥ 6	0.00	0.00	0.10	0.14	0.18	0.21	0.22	0.22
n	$v = 4$							
2	0.32	0.22	0.14	0.08	0.07	0.07	0.06	0.06
3	0.68	0.54	0.40	0.34	0.33	0.32	0.31	0.31
4	0.00	0.24	0.25	0.27	0.28	0.28	0.27	0.27
5	0.00	0.00	0.07	0.09	0.11	0.11	0.12	0.12
≥ 6	0.00	0.00	0.14	0.18	0.21	0.22	0.24	0.24

Table 40: Population of excited H atoms from $e + H_2^+(v) \rightarrow H(1s) + H(n \geq 2)$ DR process for $v = 0 - 5, 10$ and $E = 0.5, 1 - 4, 6, 8, 10$ eV.

10 Tables

Table 40 (continued):

Population of excited H atoms from $e + H_2^+(v) \rightarrow H(1s) + H(n \geq 2)$

DR process for $v = 0 - 5, 10$ and $E = 0.5, 1 - 4, 6, 8, 10$ eV.

$E(\text{eV})$	0.5	1.0	2.0	3.0	4.0	6.0	8.0	10.0
n	$v = 5$							
2	0.24	0.16	0.10	0.08	0.07	0.07	0.08	0.08
3	0.74	0.55	0.38	0.34	0.33	0.32	0.32	0.32
4	0.02	0.24	0.25	0.25	0.24	0.24	0.23	0.23
5	0.00	0.02	0.09	0.11	0.12	0.12	0.12	0.12
≥ 6	0.00	0.03	0.18	0.22	0.24	0.25	0.25	0.25
n	$v = 10$							
2	0.08	0.07	0.07	0.07	0.07	0.07	0.08	0.08
3	0.43	0.36	0.33	0.33	0.33	0.32	0.32	0.32
4	0.25	0.24	0.24	0.24	0.24	0.24	0.23	0.23
5	0.08	0.11	0.12	0.12	0.12	0.12	0.12	0.12
≥ 6	0.16	0.22	0.24	0.24	0.24	0.25	0.25	0.25

v	$E_v^{exc}(eV)$	$\Delta E_v(eV)$
0	0.000	27.0
1	0.271	25.9
2	0.527	25.0
3	0.768	23.95
4	0.994	22.95
5	1.205	22.2
6	1.402	21.6
7	1.586	21.2
8	1.755	20.6
9	1.911	20.0
10	2.052	19.7
11	2.180	19.3
12	2.294	18.9
13	2.393	18.6
14	2.477	17.4
15	2.545	16.6
16	2.596	16.0
17	2.628	15.5
18	2.643	15.2

Table 41: Excitation energies, E_v^{exc} , of $H_2^+(v)$ levels, and transition energies ΔE_v for DI reaction (194) .

10 Tables

v'	1 eV	2 eV	3 eV	4 eV	5 eV	6 eV	7 eV
1	1.21	1.45	1.52	1.62	2.0	2.6	3.4
2	0.34	0.28	0.34	0.47	0.68	0.9	1.2
3	0.83	5.2(-2)	6.4(-2)	0.15	0.25	0.34	0.43
4	6.4(-2)*	3.8(-2)	4.0(-2)	9.0(-2)	1.40	1.95	2.08
5	0.0	3.6(-2)	3.8(-2)	7.6(-2)	0.11	0.12	0.12
6	0.0	2.4(-2)	3.7(-2)	5.6(-2)	6.4(-2)	6.2(-2)	6.0(-2)
7	0.0	2.1(-2)	3.5(-2)	4.0(-2)	4.0(-2)	3.6(-2)	3.2(-2)
8	0.0	1.8(-2)	2.5(-2)	2.7(-2)	2.8(-2)	2.5(-2)	2.2(-2)
10	0.0	0.0	1.8(-2)	2.0(-2)	1.9(-2)	1.8(-2)	1.6(-2)
12	0.0	0.0	1.2(-2)	1.2(-2)	1.1(-2)	1.0(-2)	8.6(-3)
14	0.0	0.0	7.6(-3)	6.1(-3)	6.0(-3)	5.8(-3)	5.4(-3)
16	0.0	0.0	4.6(-3)	4.0(-3)	3.1(-3)	2.6(-3)	2.2(-3)
18	0.0	0.0	1.9(-3)	1.5(-3)	1.4(-3)	1.3(-3)	1.2(-3)

* $a(-X) = a \times 10^{-X}$

Table 42: Excitation cross sections $\sigma^{exc}(0 \rightarrow v')$, in units of 10^{-16}cm^2 , in $H + H_2^+(v = 0)$ collisions for a number of $0 \rightarrow v'$ transitions and center-of-mass collision energies 1, 2, 3, 4, 5, 6 and 7 eV (from Ref. [186]).

v	0.5eV	1.0eV	2.0eV	3.0eV	4.0eV	5.0eV	6.0eV	7.0eV
0	1.68	1.64	1.80	2.08	2.22	2.95	3.82	4.90
1	8.2	9.4	12.0	14.2	16.5	19.2	19.8	19.6
2	6.9	8.7	9.6	12.5	15.8	18.8	18.2	17.8
3	5.4	6.3	8.2	9.6	12.2	14.0	15.3	14.8 [†]
5	14.7	16.1	15.2	17.0	18.7	18.6	17.8	17.0
10	21.5	18.8	16.5	16.2	16.0	15.9	15.8 [†]	-
14	23.6	19.2	17.8	17.0	16.3	15.8	15.7 [†]	-
18	9.6	6.6	4.3	3.7	3.4	3.3	-	-

[†] Extrapolated values

Table 43: Depopulation cross sections in $H(1s) + H_2^+(v)$ collisions (in units of 10^{-16}cm^2) for a number of v -states and C.M. collision energies (Ref. [186]).

v'	0.2eV	0.5eV	1.0eV	1.5eV	2.0eV	3.0eV	4.0eV	5.0eV	6.0eV	7.7eV
0	3.6	0.95	0.22	7.7(-2)*	4.1(-2)	2.5(-2)	2.0(-2)	1.8(-2)	1.8(-2)	2.4(-2)
1	4.9	1.4	0.36	0.13	7.0(-2)	3.8(-2)	3.4(-2)	3.9(-2)	5.0(-2)	0.11
2	5.2	1.7	0.48	0.20	0.13	8.0(-2)	7.1(-2)	9.0(-2)	0.12	0.26
3	8.3	3.2	1.1	0.49	0.33	0.28	0.36	0.50	0.68	1.02
4	10.8	18.3	24.7	22.2	20.0	16.1	13.8	11.9	10.0	8.2
5	#	0.15	0.22	0.31	0.42	0.65	1.20	1.40	1.36	1.15
6	-	-	4.6(-2)	6.5(-2)	9.2(-2)	0.16	0.24	0.26	0.28	0.27
7	-	-	-	3.8(-2)	5.0(-2)	6.2(-2)	6.3(-2)	5.9(-2)	5.5(-2)	6.7(-2)

* $a(-X) = a \times 10^{-X}$

Charge transfer to $v' = 6, 7, 8$ levels is endothermic by 0.40, 0.78, and by 1.12 eV, respectively.

Table 44: Charge exchange cross sections (in units of 10^{-16}cm^2) of reaction (199) for $v = 0$ and $v' = 0 - 7$, for a number of center-of-mass collision energies (from [186]).

v	0.2eV	0.5eV	1.0eV	1.5eV	2.0eV	3.0eV	4.0eV	5.0eV	7.7eV
0	0.0#	0.0	0.0	0.0	0.0	3.8(-2)*	0.13	0.20	0.41
1	0.0	0.0	0.0	0.0	0.0	0.36	0.51	0.70	0.96
2	0.0	0.0	0.0	0.0	0.0	0.60	0.84	1.12	1.38
3	0.0	0.0	0.0	0.0	6.7(-2)	0.85	1.22	1.60	1.82
4	0.0	0.0	0.0	0.0	0.40	1.61	1.98	2.15	2.45
5	0.0	0.0	0.0	9.6(-2)	1.80	2.56	2.63	2.68	2.73
6	0.0	0.0	0.0	0.45	2.55	3.00	3.06	3.12	3.18
8	0.0	0.0	0.3	3.24	3.57	3.97	4.00	4.02	(3.98)†
10	0.0	0.0	2.45	5.34	6.26	6.20	6.14	6.00	(5.87)
12	0.0	1.28	9.8	10.0	10.2	10.0	9.7	9.3	(8.8)
14	2.25	7.5	17.0	18.2	17.7	17.2	16.7	16.3	(15.7)
16	18.0	26.8	35.7	37.0	37.8	38.6	37.6	36.4	(35.0)
18	68.7	70.2	67.4	65.1	63.7	60.1	56.6	52.2	(47.6)

Threshold ($= E_v^{exc}$) energies for individual v -channels are given in Table 41.

* $a(-X) = a \times 10^{-X}$

† Extrapolated value

Table 45: Dissociation cross sections (in units of 10^{-16}cm^2) of $H_2^+(v)$ by $H(1s)$ impact for various v -states and C.M. collision energies (from Ref. [197]).

10 Tables

$E_{lab}(eV)$	$\sigma_{v_i=0}^{cx}$	$\sigma_{v_i=1}^{cx}$	$\sigma_{v_i=1}^{cx}/\sigma_{v_i=0}^{cx}$
4	6.82 [†]	11.18 [†]	1.64
8	8.20	12.04	1.47
16	10.35	13.66	1.32
24	11.75	13.20	1.12
32	12.06	12.45	1.04
45	11.86	11.15	0.94
60	10.93	10.00	0.91
80	9.78	9.18	0.94
100	9.00	8.75	0.97
140	8.03	8.28	1.03
200	7.12	7.91	1.11
300	6.36	7.58	1.12
400	5.77	7.33	1.27

[†] Extrapolated values

Table 46: Selected values of $\sigma_{v_i=0}^{cx}$ and $\sigma_{v_i=1}^{cx}$ total charge transfer cross sections (in units of $10^{-16} cm^2$) for $H_2^+(v_i = 1, 2) + H_2(v_0 = 0)$ collisions in the ion (laboratory) energy range 4 – 400 eV (from Ref. [254]).

v_i	4eV	8eV	16eV	24eV	32eV	45eV	100eV	400eV
0	1.00	1.00	1.00	1.00	1.00	1.00	1.00	1.00
1	1.64	1.47	1.32	1.12	1.04	0.94	0.97	1.27
2	1.75	1.52	1.41	1.17	1.00	0.81	0.86 [†]	1.32
3	1.54	1.38	1.28	1.03	0.88	0.73	0.75 [†]	1.27
4	1.34	1.22	1.07	0.89	0.76	0.62	0.64 [†]	1.22
5	1.20	1.06	0.92	0.77	0.63	0.51	0.53 [†]	1.14 [†]
6	1.03	0.91	0.77	0.63	0.52	0.40	0.42 [†]	1.06 [†]
7	0.88	0.75	0.64	0.51	0.42	0.31	0.33 [†]	0.98 [†]
8	0.73	0.62	0.52	0.39	0.32	0.22	0.24 [†]	0.90 [†]
9	0.59	0.49	0.40	0.29	0.23	0.14	0.16 [†]	0.82 [†]
10	0.47	0.37	0.29	0.20	0.14	0.08	0.10 [†]	0.74 [†]

[†] Extrapolated values

Table 47: Total charge exchange cross section ratios $\sigma_{v_i}^{cx}/\sigma_{v_i=0}^{cx}$ for $H_2^+(v_i) + H_2(v_0 = 0)$ collisions for a selected number of ion (laboratory) energies (based upon Refs. [244] and [255]).

ΔN	$v_i = 0$		$v_i = 1$		$v_i = 2$		$v_i = 3$		$v_i = 4$		$v_i = 5$	
	(v'_i, v'_0)	f	(v'_i, v'_0)	f	(v'_i, v'_0)	f	(v'_i, v'_0)	f	(v'_i, v'_0)	f	(v'_i, v'_0)	f
-2					(0,0)	0.8	(1,0)	0.7	(2,0)	1.4	(3,0)	1.9
									(0,1)	0.3	(1,1)	1.2
-1			(0,0)	5.4	(1,0)	6.1	(2,0)	6.6	(3,0)	5.7	(4,0)	4.3
							(0,1)	2.4	(1,1)	5.4	(2,1)	7.1
											(0,2)	2.8
0	(0,0)	88.9	(1,0)	71.6	(2,0)	52.8	(3,0)	36.8	(4,0)	23.8	(5,0)	12.8
					(0,1)	13.6	(1,1)	13.8	(2,1)	14.4	(3,1)	14.6
									(0,2)	8.1	(1,2)	17.2
+1	(1,0)	6.7	(2,0)	6.4	(3,0)	5.8	(4,0)	5.1	(5,0)	4.4	(6,0)	3.3
			(0,1)	10.3	(1,1)	11.1	(2,1)	7.9	(3,1)	3.7	(4,1)	1.7
							(0,2)	8.4	(1,2)	10.6	(2,2)	8.1
											(0,3)	8.6
+2	(2,0)	1.1	(3,0)	0.9	(4,0)	1.7	(5,0)	1.2	(6,0)	1.6	(7,0)	0.9
	(0,1)	3.0	(1,1)	0.3	(2,1)	1.3	(3,1)	1.6	(4,1)	1.9	(5,1)	0.5
					(0,2)	3.2	(1,2)	5.7	(2,2)	2.4	(3,2)	1.0
									(0,3)	6.5	(1,3)	6.9

Table 48: Fractional contributions f (in %) of state-selective cross sections $\sigma_{v'_i}^{cx}(v'_i, v'_0)$ of charge exchange $H_2^+(v_i) + H_2(v_0 = 0) \rightarrow H_2(v'_0) + H_2^+(v'_i)$ to total cross section $\sigma_{v'_i}^{cx}$ at $E_{lab} = 16$ eV (based upon Ref. [242]). (The sum of f-values in a given column of the table is less than 100% due to neglected weak channels.)

10 Tables

ΔN	$v_i = 0$		$v_i = 1$		$v_i = 2$		$v_i = 3$		$v_i = 4$		$v_i = 5$	
	(v'_i, v'_0)	f	(v'_i, v'_0)	f	(v'_i, v'_0)	f	(v'_i, v'_0)	f	(v'_i, v'_0)	f	(v'_i, v'_0)	f
-2					(0,0)	1.4	(1,0)	1.6	(2,0)	2.2	(3,0)	1.6
									(0,1)	1.0	(1,1)	1.5
-1			(0,0)	12.5	(1,0)	12.0	(2,0)	9.7	(3,0)	7.4	(4,0)	4.4
							(0,1)	3.2	(1,1)	6.0	(2,1)	6.9
											(0,2)	5.1
0	(0,0)	78.7	(1,0)	44.4	(2,0)	30.3	(3,0)	21.0	(4,0)	14.6	(5,0)	8.2
					(0,1)	10.6	(1,1)	11.3	(2,1)	11.0	(3,1)	11.6
									(0,2)	6.8	(1,2)	15.1
+1	(1,0)	11.9	(2,0)	10.8	(3,0)	8.9	(4,0)	5.8	(5,0)	4.0	(6,0)	2.9
			(0,1)	23.6	(1,1)	15.2	(2,1)	9.7	(3,1)	4.2	(4,1)	2.2
							(0,2)	10.5	(1,2)	1.3	(2,2)	10.9
											(0,3)	8.2
+2	(2,0)	1.1	(3,0)	1.4	(4,0)	1.7	(5,0)	1.3	(6,0)	0.8	(7,0)	0.6
	(0,1)	6.4	(1,1)	1.9	(2,1)	2.7	(3,1)	2.9	(4,1)	1.6	(5,1)	0.8
					(0,2)	9.4	(1,2)	6.1	(2,2)	4.0	(3,2)	2.2
									(0,3)	10.0	(1,3)	6.2

Table 49: Fractional contributions f (in %) of state-selective cross sections $\sigma_{v_i}^{cx}(v'_i, v'_0)$ of charge exchange $H_2^+(v_i) + H_2(v_0 = 0) \rightarrow H_2(v'_0) + H_2^+(v'_i)$ reactions to total cross section $\sigma_{v_i}^{cx}$ at $E_{lab} = 32$ eV (based upon Ref. [242]).

v_i	8 eV	12 eV	16 eV	32 eV
0	0.6	0.8	1.1	1.1
1	0.7	1.7	1.3	1.4
2	1.6	1.8	1.8	2.1
3	2.4	2.4	2.2	2.5
4	2.9	2.9	2.6	2.7
5	4.0	4.4	3.7	2.8
6	4.4	4.3	3.9	5.3
7	5.2 [†]	5.5	4.7	5.4
8	6.1 [†]	6.3 [†]	4.5	5.5
9	6.8 [†]	7.0 [†]	4.7	6.9
10	7.5 [†]	(7.7)	4.9	7.1

[†] Extrapolation

Table 50: Values of $\sigma_{v_i}^{CID}$ cross sections (in units of $10^{-16} cm^2$) for $v_i = 0 - 10$ and selected ion impact (laboratory) energies (from Ref. [255]).

v_3	$P(v_3)$	$E_{v_3}^{exc}(eV)$
0	0.0341	0.00
1	0.0919	0.372
2	0.1601	0.744
3	0.2197	1.116
4	0.2303	1.488
5	0.1387	1.860
6	0.0796	2.232
7	0.0299	2.604
8	0.0109	2.976
9	0.0037	3.348
10	0.0010	3.720
11	0.0001	4.092

Table 51: Relative populations $P(v_3)$ of $H_3^+(v_3)$ arising from reaction (211) with $v_i = v_0 = 0$, and excitation energies $E_{v_3}^{exc}$ of $H_3^+(v_3)$ ion (after [279]).

10 Tables

v_i	0.04 eV	0.25 eV	0.5 eV	0.75 eV	1.0 eV	2.0 eV
1	0.94	0.98	1.00	1.01	1.075	1.27
2	0.89	0.965	0.995	1.02	1.10	1.40
3	0.865	0.95	0.990	1.01	1.11	1.49
4	0.84	0.935	0.985	0.99	1.115	1.47
5	0.825	0.925	0.980	0.97	1.11	1.44
6	0.805	0.915	0.975	0.94	1.10	1.39
7	0.79	0.905	0.970	0.91	1.09	1.34
8	0.77	0.895	0.965	0.88	1.08	1.29
9	0.76	0.885	0.960	0.85	1.07	1.24
10	0.75	0.875	0.955	0.82	1.06	1.19
v_i	3.0 eV	4.0 eV	5.0 eV	8.0 eV	10.0 eV	15.0 eV
1	1.46	1.23	1.17	1.13	1.01	0.97
2	1.59	1.245	1.14	1.06	0.93	0.89
3	1.57	1.175	1.035	0.93	0.82	0.78
4	1.46	1.075	0.925	0.81	0.72	0.68
5	1.33	0.99	0.835	0.72	0.62	0.59
6	1.21	0.90	0.74	0.63	0.54	0.50
7	1.09	0.82	0.67	0.55	0.47	0.43
8	0.99	0.74	0.60	0.48	0.41	0.37
9	0.89	0.67	0.53	0.415	0.36	0.31
10	0.79	0.61	0.46	0.35	0.31	0.26

Table 52: Values of $f(v_i)$ ratio, Eq. (214), for a number of collision (C.M.) energies ($v_i = 1 - 4$ from Ref. [273]; $v_i = 5 - 10$, extrapolation).

	$v_i = 0$		$v_i = 3$	
$E_{CM}(eV)$	f_{PT}	f_{AT}	f_{PT}	f_{AT}
0.25	0.56	0.44	0.58	0.42
0.50	0.55	0.45	0.52	0.48
1.0	0.52	0.48	0.44	0.56
3.0	0.36	0.74	0.47	0.53
5.0	0.15	0.85	0.28	0.72

Table 53: Relative contributions of proton (f_{PT}) and atom (f_{AT}) transfer channels to H_3^+ formation cross section for $v_i = 0$ and $v_i = 3$ in the collision (C.M.) energy range 0.25 – 5.0 eV (after [276]).

$E_{CM}(eV)$	$H_2 + H$	$3H$	$E_{CM}(eV)$	$H_2 + H$	$3H$
0.003	0.225	0.775	3.0	0.60	0.40
0.01	0.25	0.75	4.0	0.64	0.36
0.03	0.25	0.75	5.0	0.65	0.35
0.1	0.24	0.76	6.0	0.64	0.36
0.3	0.25	0.75	7.0	0.56	0.44
0.4	0.28	0.72	8.0	0.45	0.55
0.6	0.40	0.60	9.0	0.40	0.60
0.8	0.48	0.52	10.0	0.36	0.64
0.9	0.40	0.60	12.0	0.34	0.66
1.0	0.45	0.55	13.6	0.32	0.68
1.2	0.53	0.47	15.0	0.38	0.62
1.5	0.52	0.48	17.0	0.28	0.72
2.0	0.51	0.49	20.0	0.18	0.82
2.5	0.49	0.51	25.0	0.08	0.92

Table 54: Relative contributions of dissociation channels (229a) and (229b) to total DR cross section of $H_3^+(v_3 = 0)$ in the C.M. energy range 0.003-25 eV (after Ref. [305])

Reaction channel	$E_{th}^{C.M.}(eV)$
$H_2(X^1\Sigma_g^+) + H(1s)$	0.00
$H_2(b^3\Sigma_u^+) + H(1s)$	0.00
$H_2(X^1\Sigma_g^+) + H(n = 2)$	0.93
$H_2(B^1\Sigma_u^+) + H(1s)$	1.91
$H_2(c^3\Pi_u) + H(1s)$	2.42
$H_2(a^3\Sigma_g^+) + H(1s)$	2.48
$H_2(X^1\Sigma_g^+) + H(n = 3)$	2.80

Table 55: Energy thresholds, $E_{th}^{C.M.}$, for various exit channels of DR reaction (229) with $H_3^+(v_3 = 0)$ (after [306]).

10 Tables

	$K_{PT} = 0.3$	$K_{PT} = 0.45$	$K_{PT} = 0.7$
A	9.15	13.54	16.88
α	0.078	0.111	0.171
b	1.83(-2)*	0.145	0.125
β	2.71	1.66	1.88
c	6.15(-7)	1.45(-5)	1.33(-5)
γ	7.25	6.22	6.25

* $a(-X) = a \times 10^{-X}$

Table 56: Values of fitting parameters in Eq. (239) for proton transfer reaction (238) for three values of thermal rate coefficient K_{PT} (K_{PT} in units of $10^{-9}cm^3/s$)

11 Figures

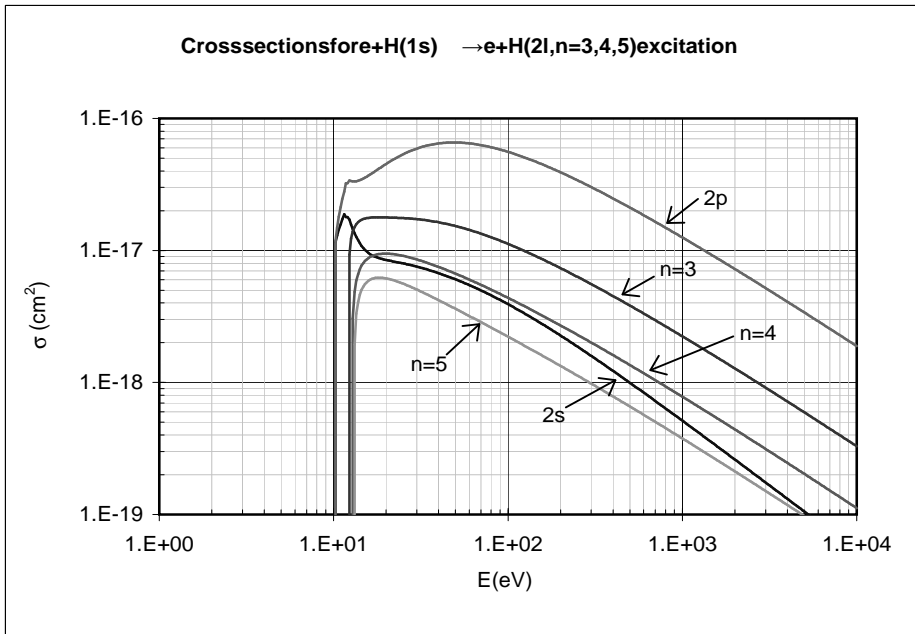


Figure 3: Electron impact excitation cross sections of $H(1s) : 1s \rightarrow 2s, 2p$, and $1s \rightarrow n = 3, 4, 5$, transitions, Eqs. (4,5), resp.

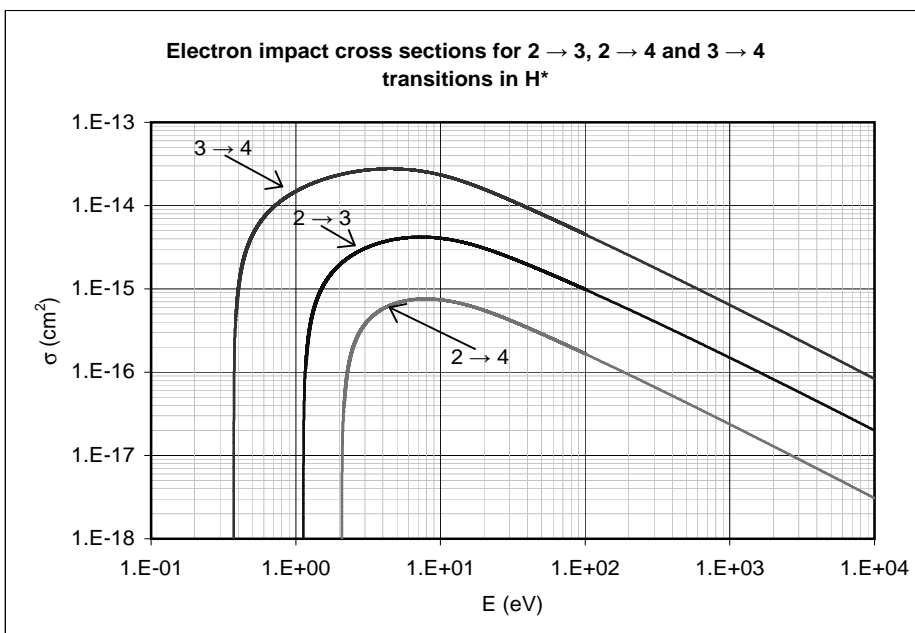


Figure 4: Electron impact excitation cross sections of $H(n) : n \rightarrow m$ transitions ($2 \rightarrow 3, 2 \rightarrow 4$ and $3 \rightarrow 4$), Eqs. (10-13).

11 Figures

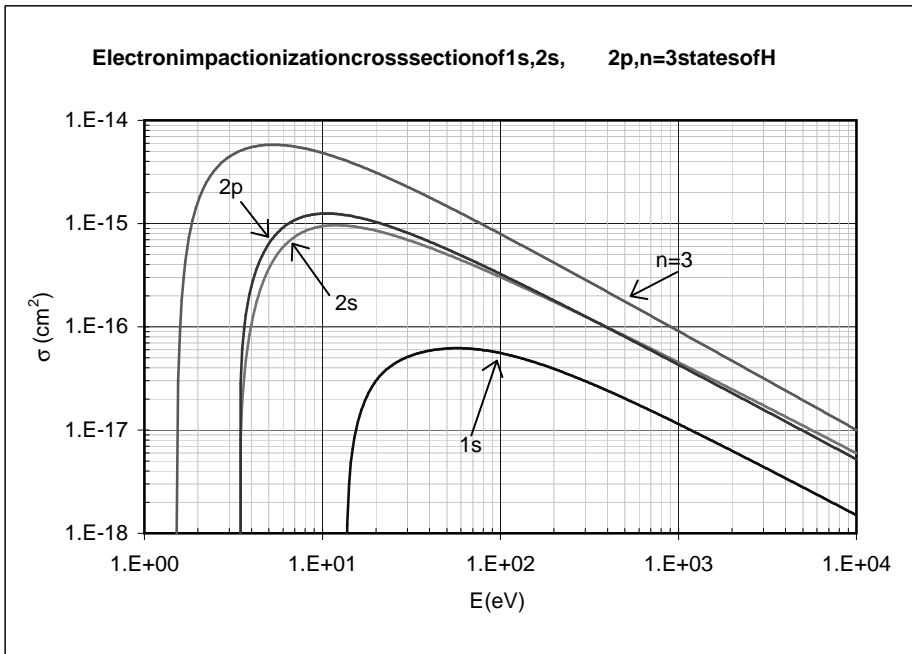


Figure 5: Electron impact ionization cross sections for 1s, 2s, 2p states and $n = 3$ level of atomic hydrogen, Eq. (14).

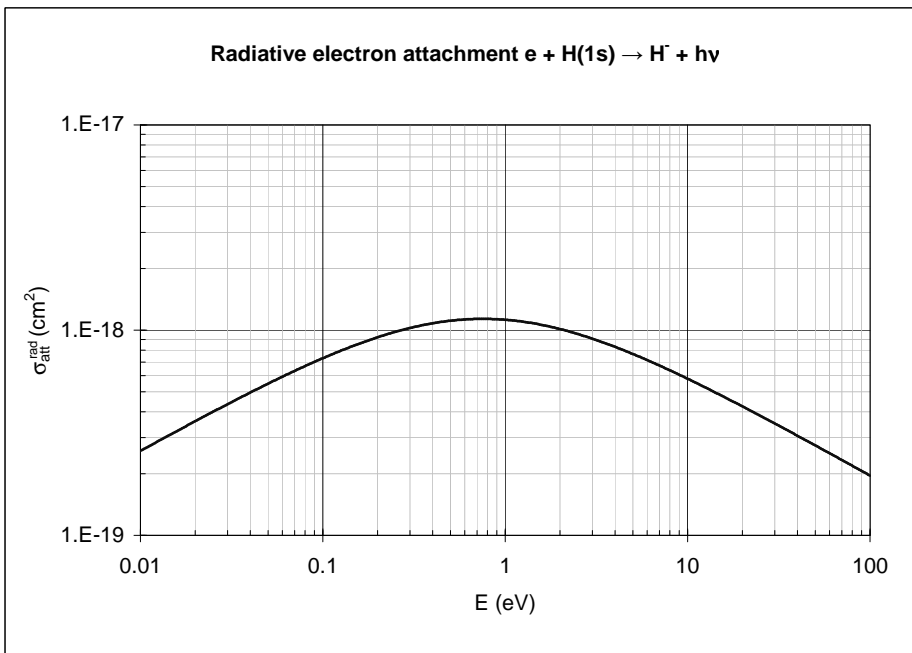


Figure 6: Cross section for radiative electron attachment on $H(1s)$, Eq. (18).

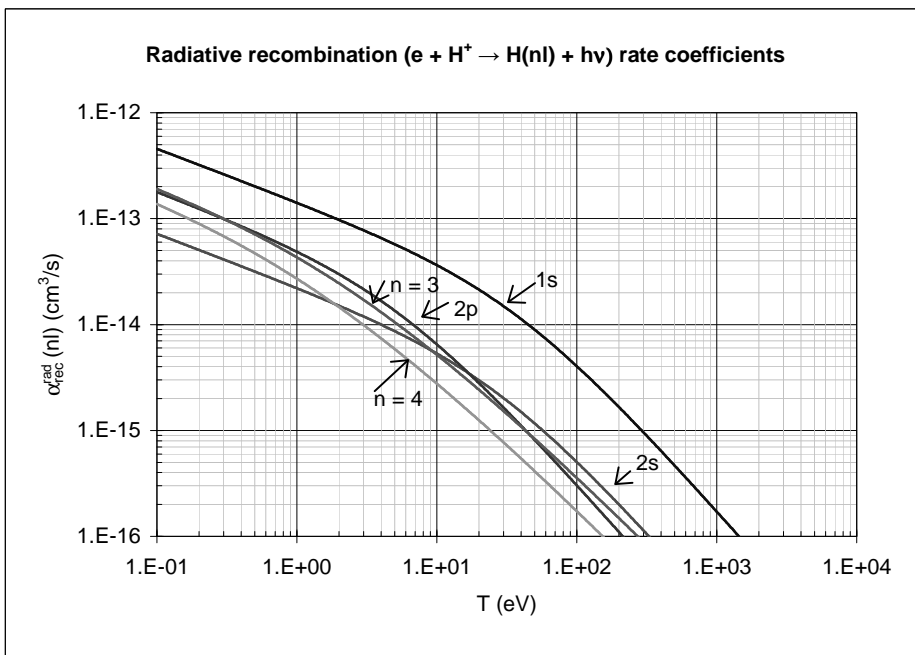


Figure 7: Rate coefficients for radiative $e + H^+$ recombination into $1s, 2s, 2p$ states and $n = 3, 4$ levels of hydrogen, Eqs. (21,22).

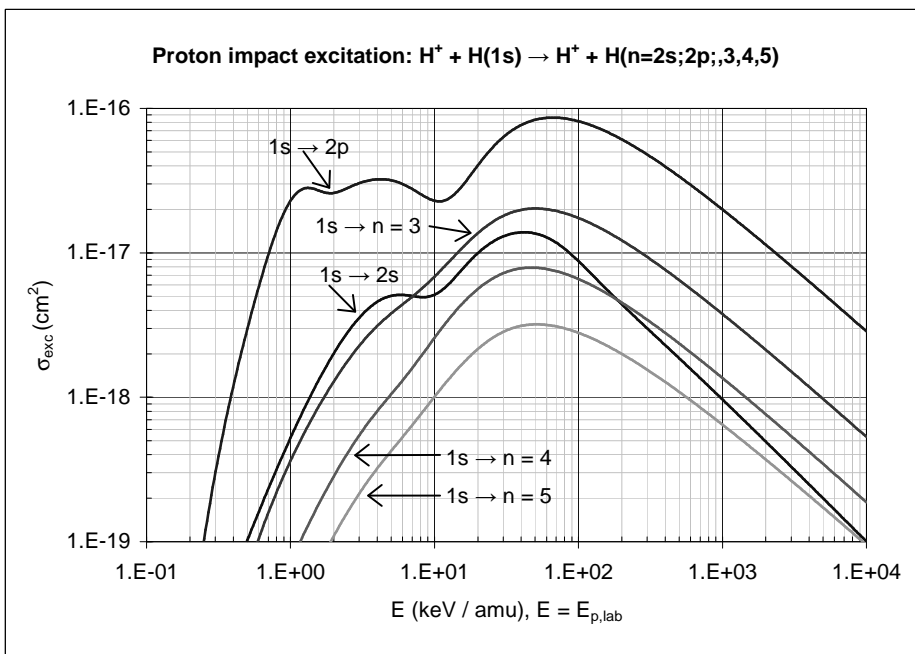


Figure 8: Proton impact excitation cross sections of $H(1s)$ to $2s$ and $2p$ states and $n = 3, 4, 5$ levels, Eqs. (29,30).

11 Figures

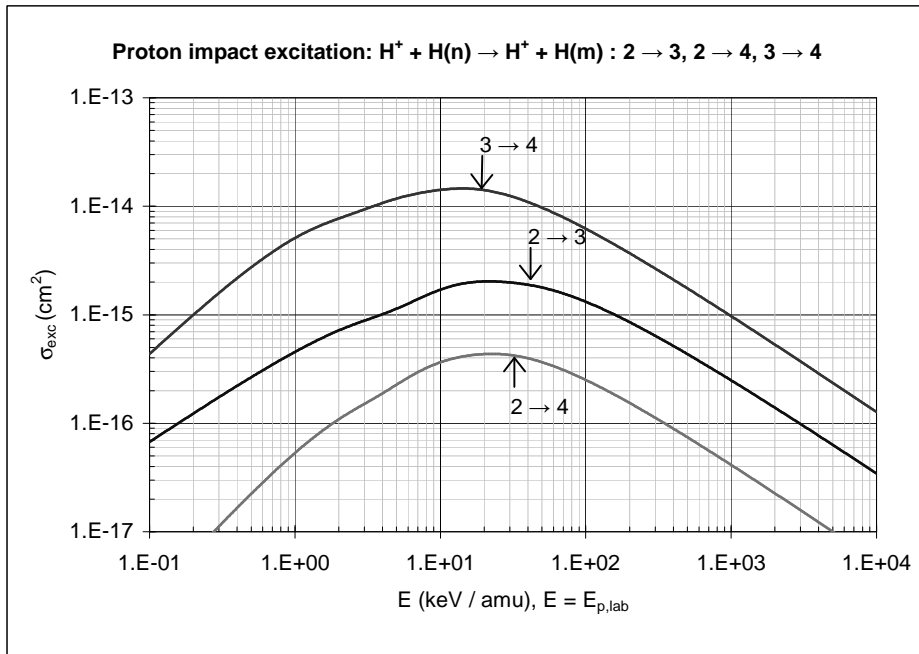


Figure 9: Proton impact excitation cross sections of $H(n) : n \rightarrow m$ transitions ($2 \rightarrow 3, 2 \rightarrow 4, 3 \rightarrow 4$), Eqs. (32-37).

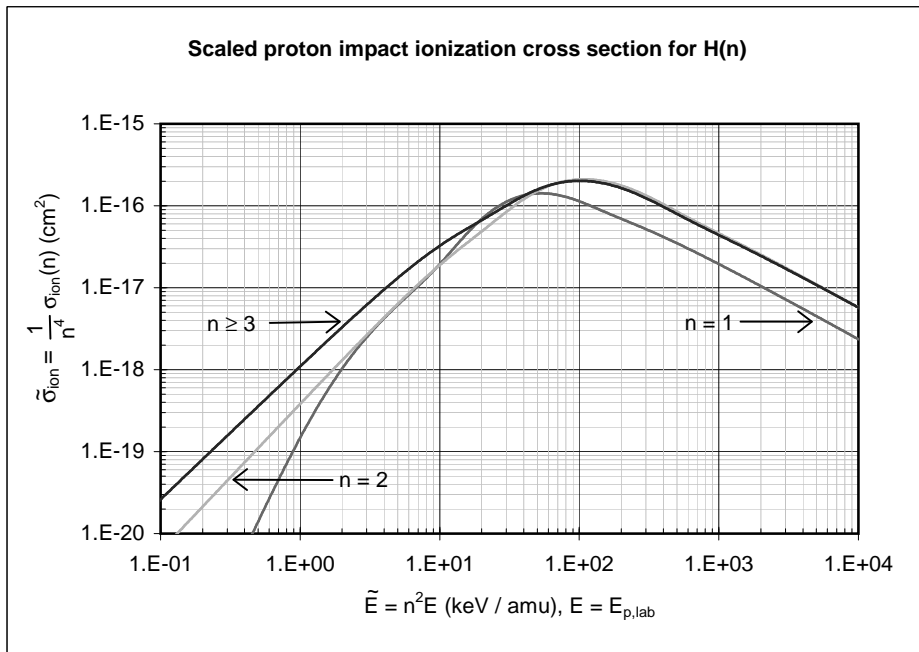


Figure 10: Scaled proton impact ionization cross section for $H(n) : n = 1s, n = 2$ and $n \geq 3$, Eq. (40).

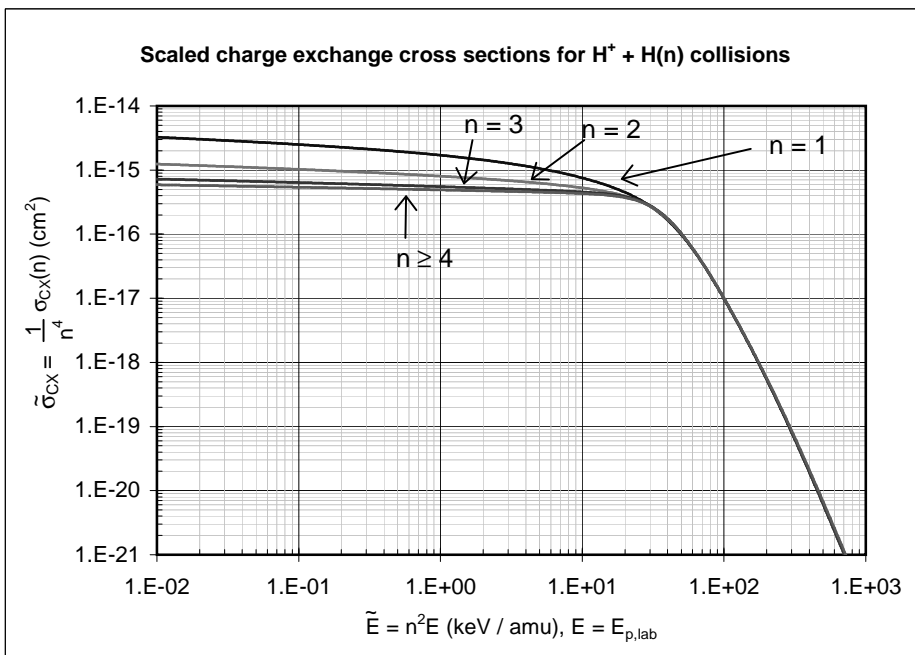


Figure 11: Scaled charge exchange cross section for $H^+ + H(n)$ collisions: $n = 1, 2, 3$ and $n \geq 4$, Eq. (44).

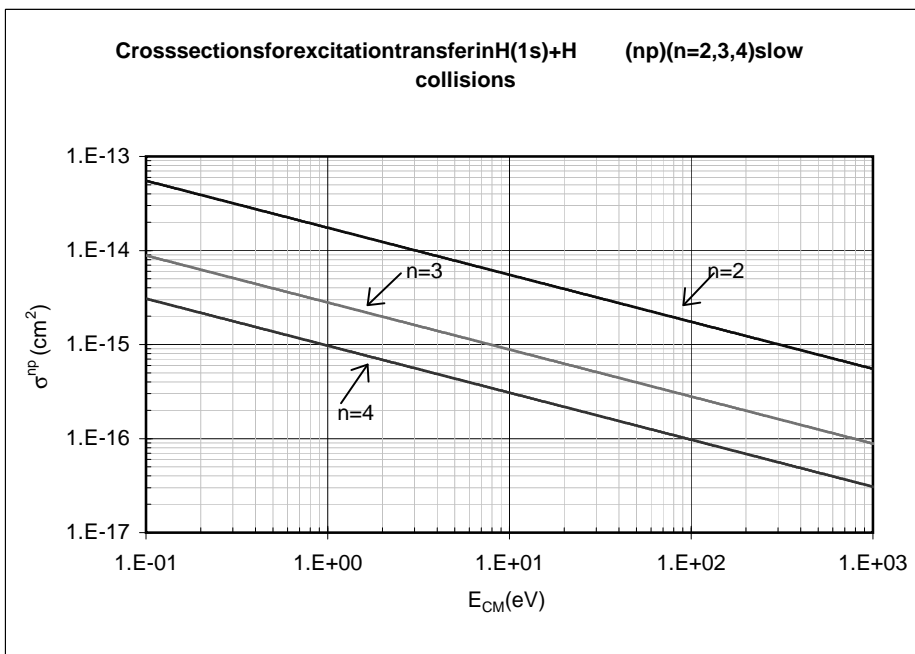


Figure 12: Cross section for excitation transfer in $H(1s) + H(np)$ collisions: $n = 2, 3, 4$, Eq. (53).

11 Figures

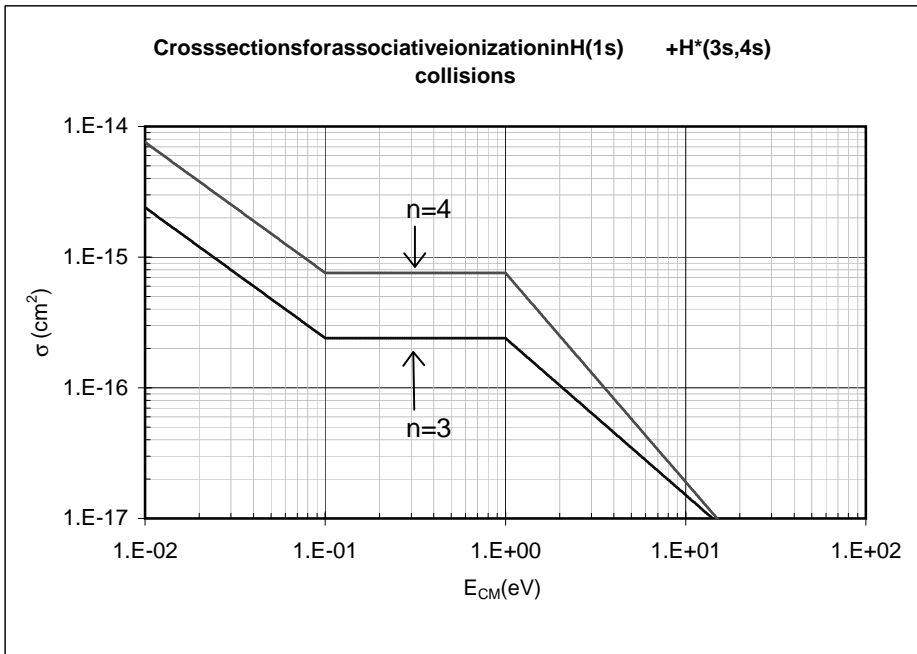


Figure 13: Cross sections for associative ionization in $H(1s) + H^*(3s), H^*(4s)$ collisions. [The sharp cross section changes at $E_{CM} = 0.1\text{eV}$ and $E_{CM} = 1\text{eV}$ are results of the approximate character of the analytic fit function, Eq. (55).]

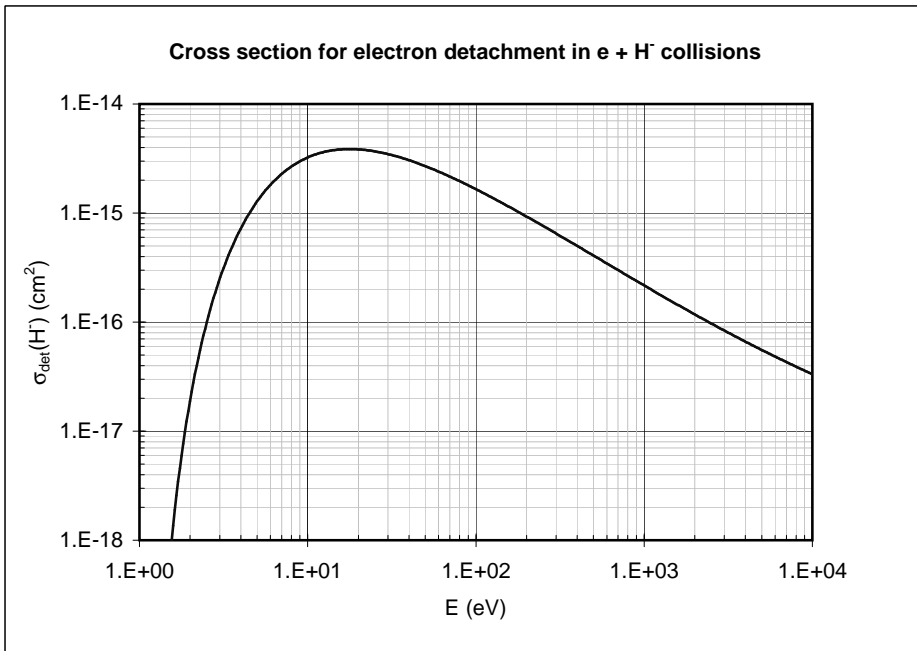


Figure 14: Cross section for electron detachment in $e + H^-$ collisions, Eq. (58).

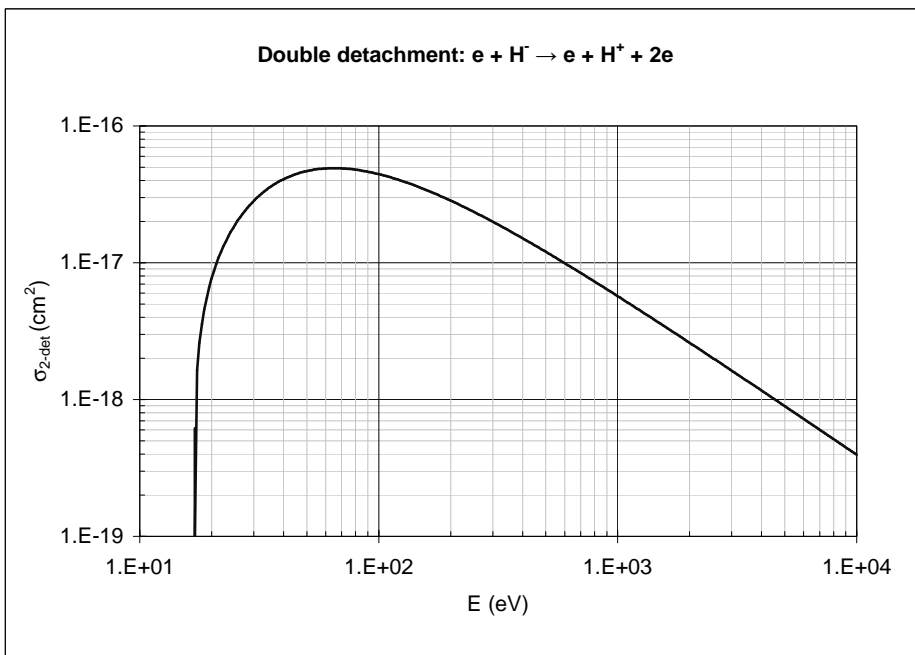


Figure 15: Cross section for “double detachment” reaction: $e + H^- \rightarrow e + H^+ + 2e$, Eq. (61).

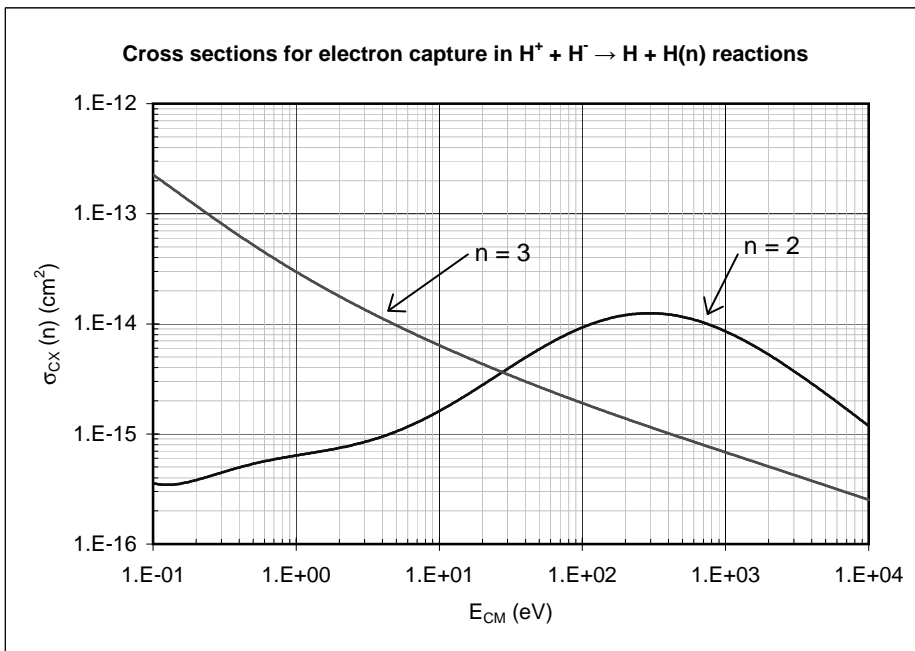


Figure 16: Cross section for electron capture into $n = 2$ and $n = 3$ levels in $H^+ + H^- \rightarrow H(n) + H$ mutual neutralization reaction, Eq. (63).

11 Figures

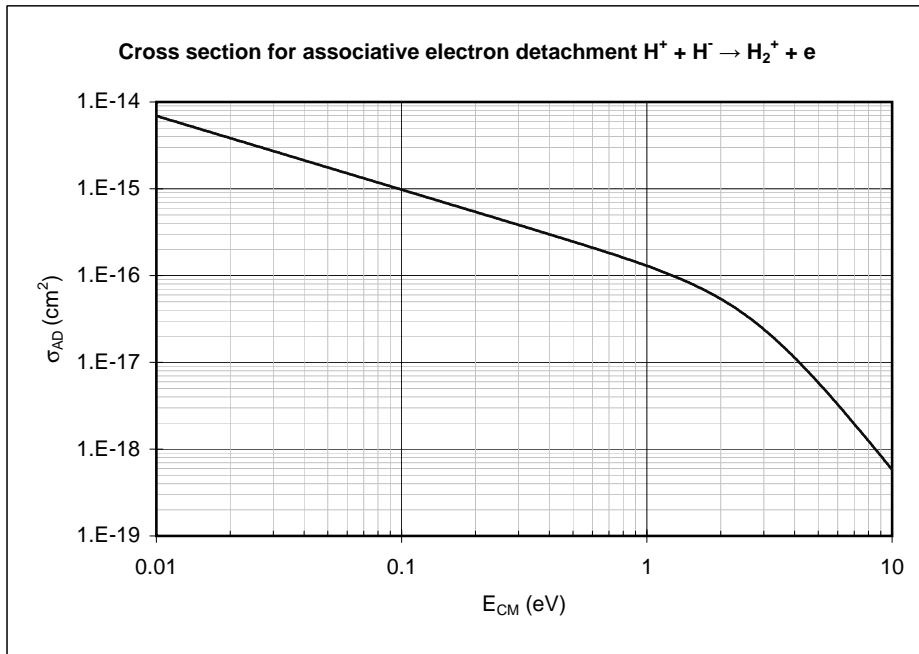


Figure 17: Cross section for associative electron detachment $H^+ + H^- \rightarrow H_2^+ + e$ reaction, Eq. (66).

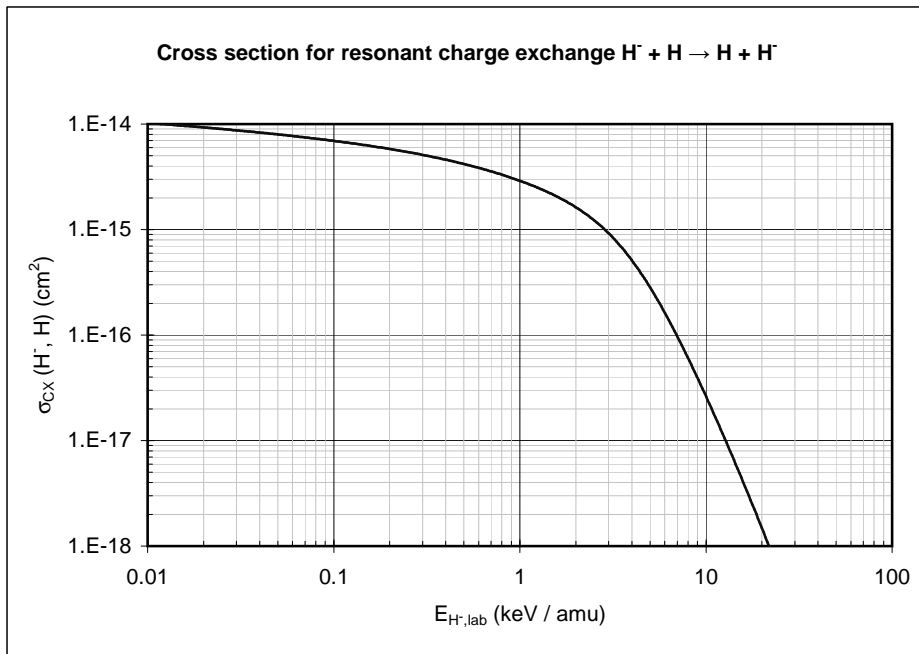


Figure 18: Cross section for resonant charge exchange reaction $H^- + H \rightarrow H + H^-$, Eq. (70).

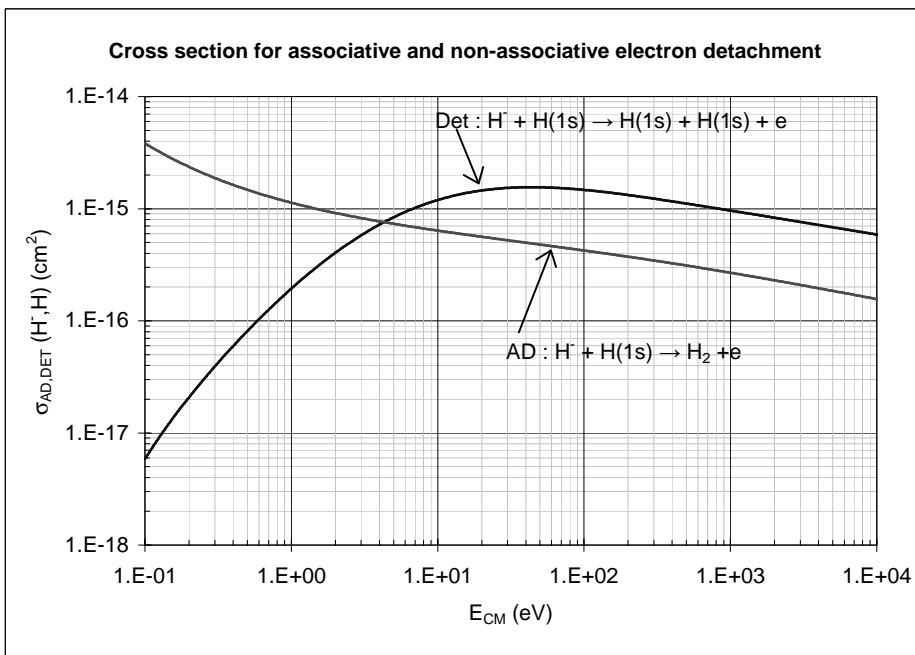


Figure 19: Cross section for associative (AD) and non-associative (Det) electron detachment in $H^- + H$ collisions, Eq. (71).

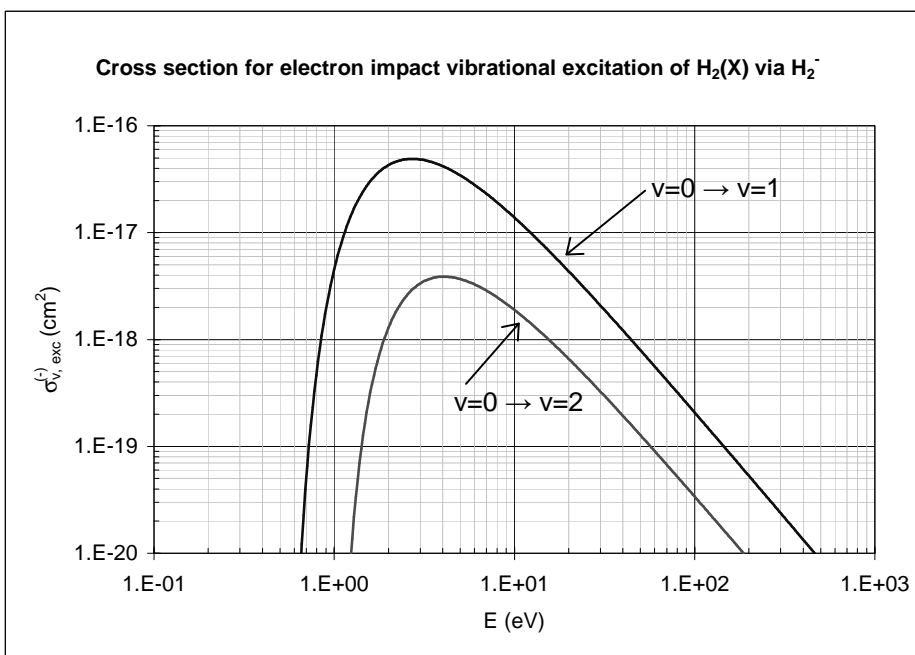


Figure 20: Cross section for electron impact vibrational excitation of $H_2(X^1\Sigma_g^+; v=0)$ to $v=1$ and $v=2$ states via the two lowest H_2^- resonant states, Eq. (74).

11 Figures

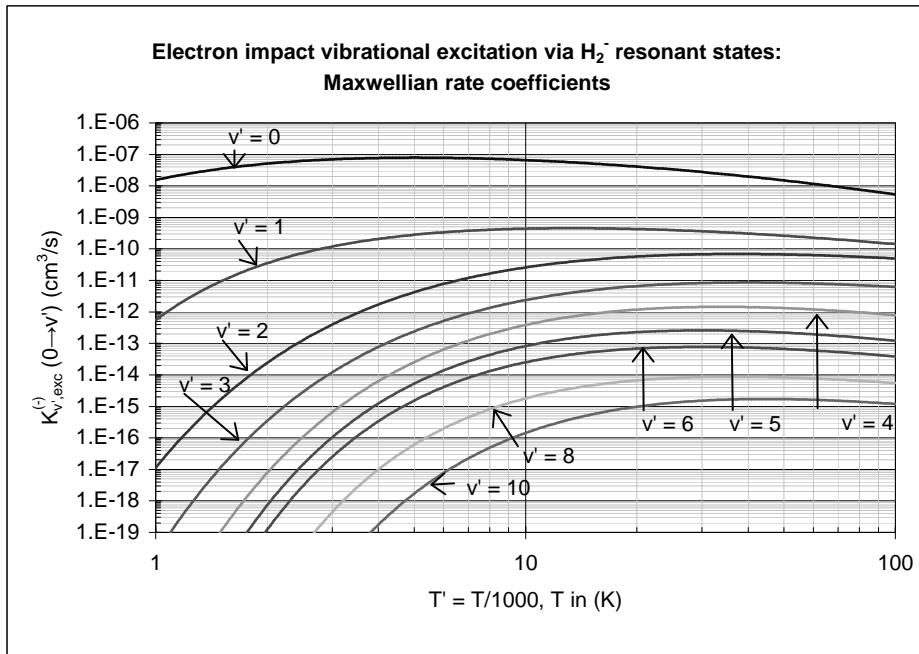


Figure 21: Rate coefficients for electron impact vibrational excitation of $H_2(X^1\Sigma_g^+; v=0)$ via the two lowest H_2^- resonant states, Eq. (75).

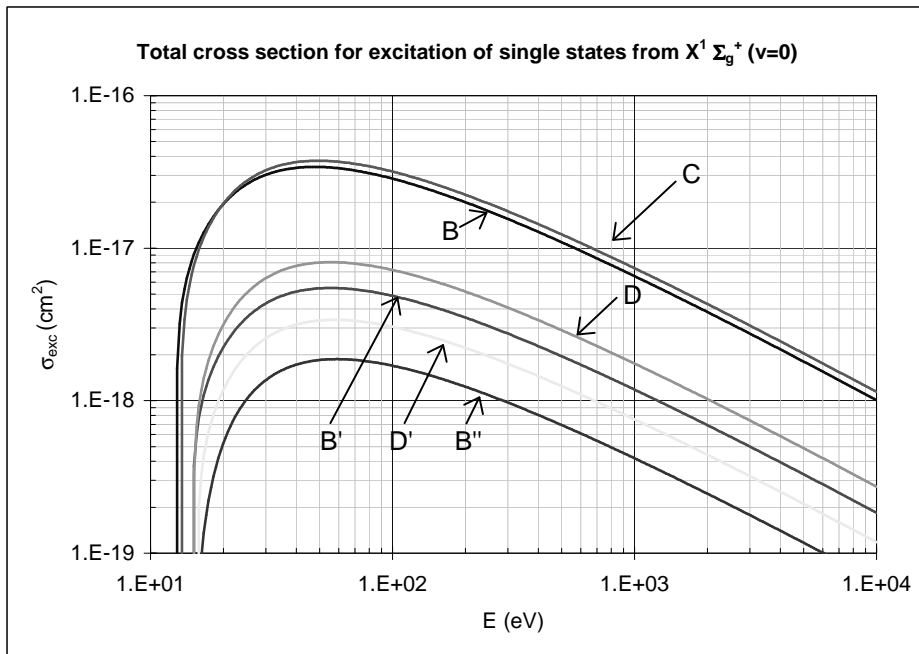


Figure 22: Total electron impact excitation cross sections of B, C, D, B', D', B'' singlet electronic states of H_2 from the $H_2(X^1\Sigma_g^+; v=0)$ ground state, Eq. (80).

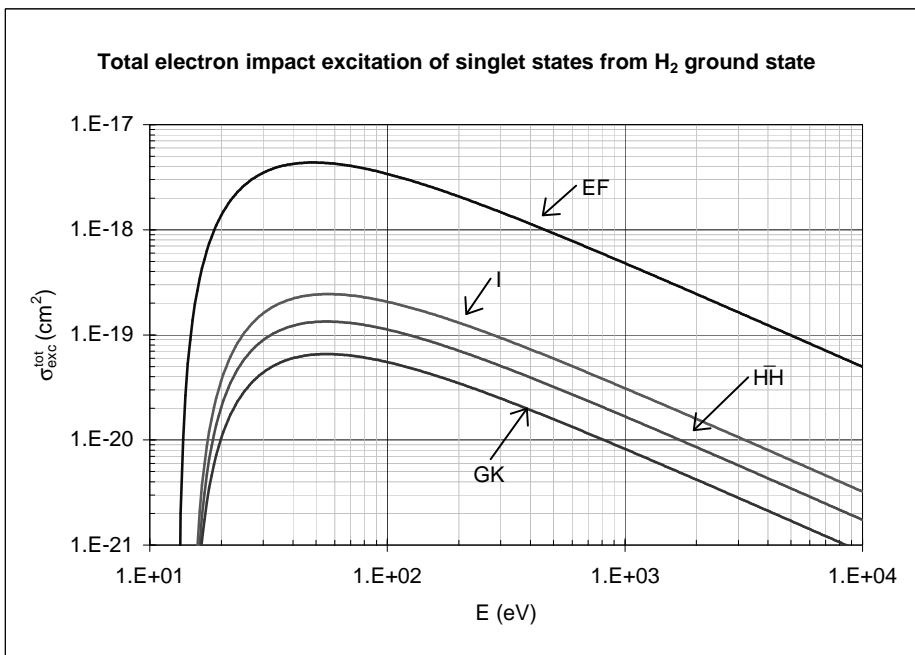


Figure 23: Total electron impact excitation cross sections of EF , I , HH and GK singlet electronic states of H_2 from the $H_2(X^1\Sigma_g^+; v=0)$ ground state, Eq. (81).

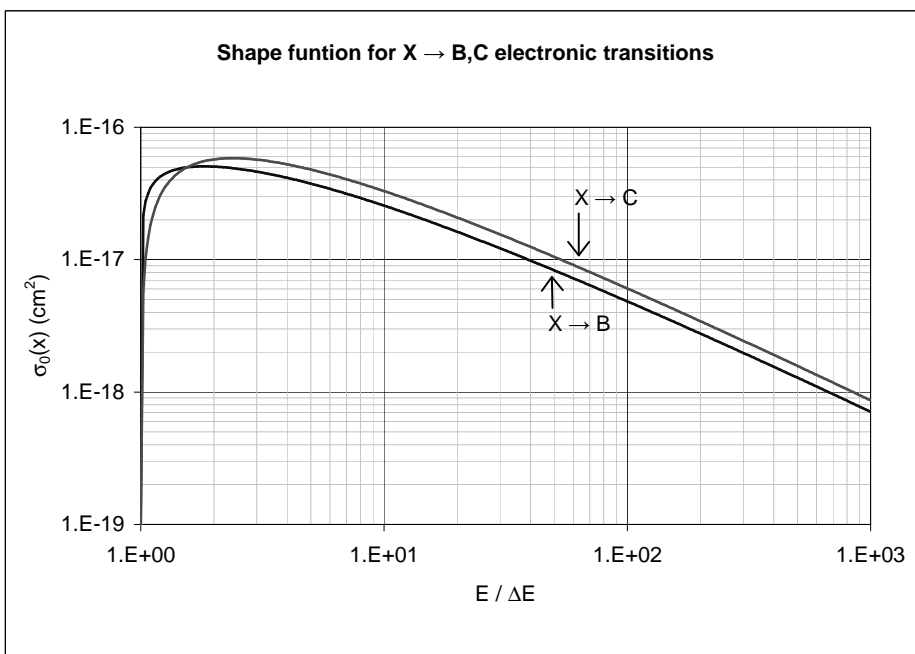


Figure 24: The "shape function" $\sigma_0(x)$, Eq. (85), for $X \rightarrow B$ and $X \rightarrow C$ electronic transitions, Eqs. (84,85).

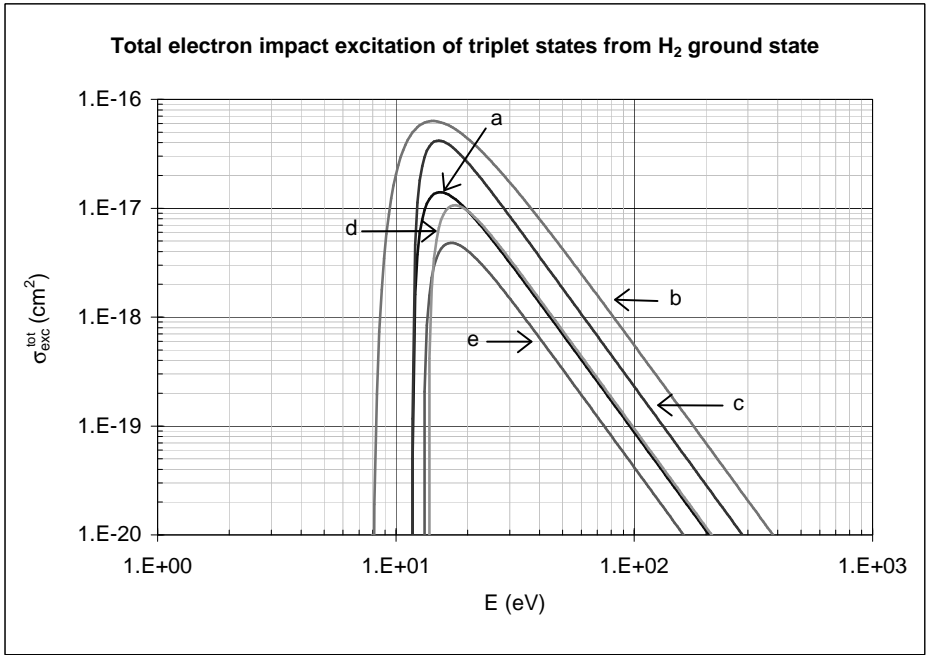


Figure 25: Total electron impact excitation cross section of a,b,c,d and e triplet states of H_2 from its ($X^1\Sigma_g^+; v = 0$) ground state, Eq. (95).

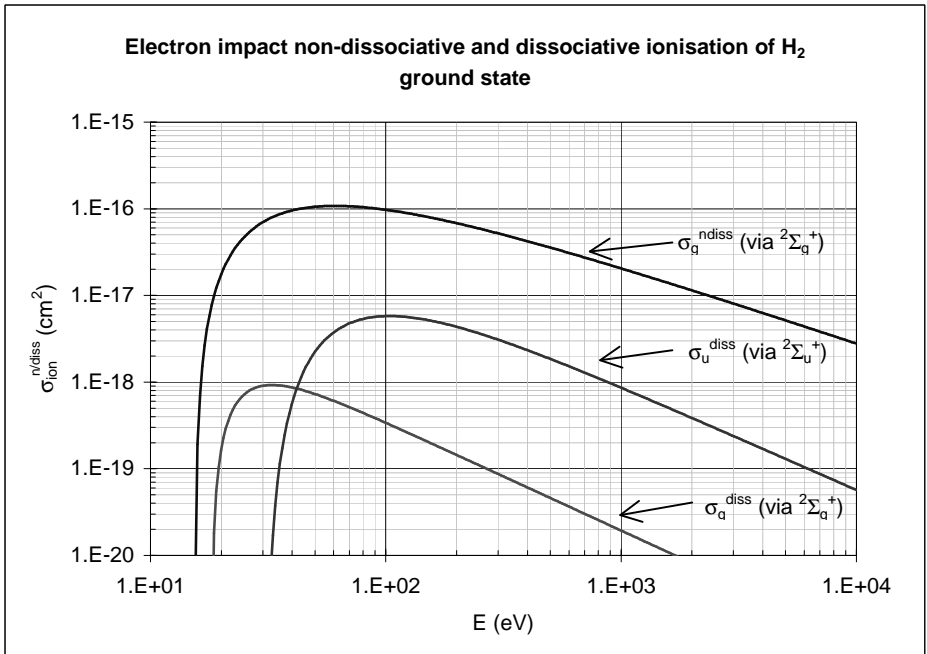


Figure 26: Cross sections for electron impact non-dissociative and dissociative ionization of $H_2(X^1\Sigma_g^+; v = 0)$ via transitions to $^2\Sigma_g^+$ and $^2\Sigma_u^+$ electronic states of H_2^+ , Eq. (106).

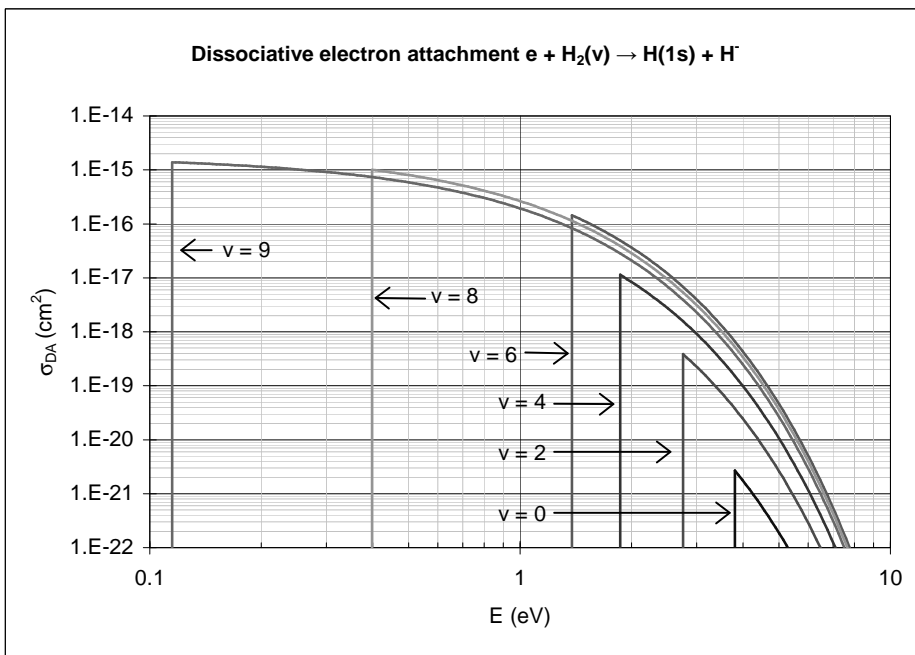


Figure 27: Cross sections for dissociative electron attachment reaction $e + H_2(X^1\Sigma_g^+; v) \rightarrow H_2^-(^2\Sigma_u^+) \rightarrow H(1s) + H^-$ for a number of initial vibrational states, Eq. (124).

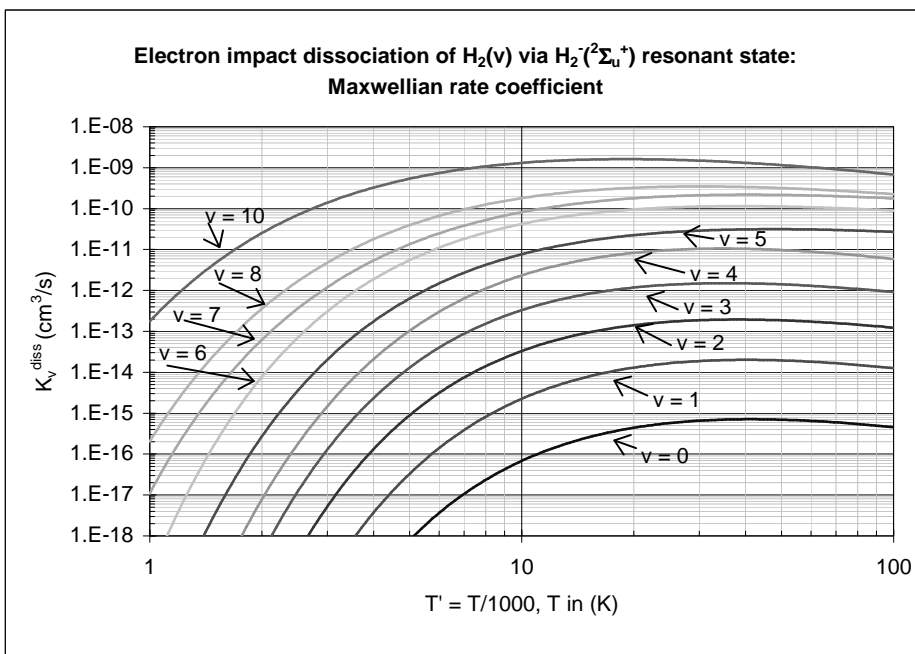


Figure 28: Rate coefficients for electron impact dissociation of $H_2(X^1\Sigma_g^+; v)$ via the $H_2^-(^2\Sigma_u^+)$ resonant state, Eq. (128).

11 Figures

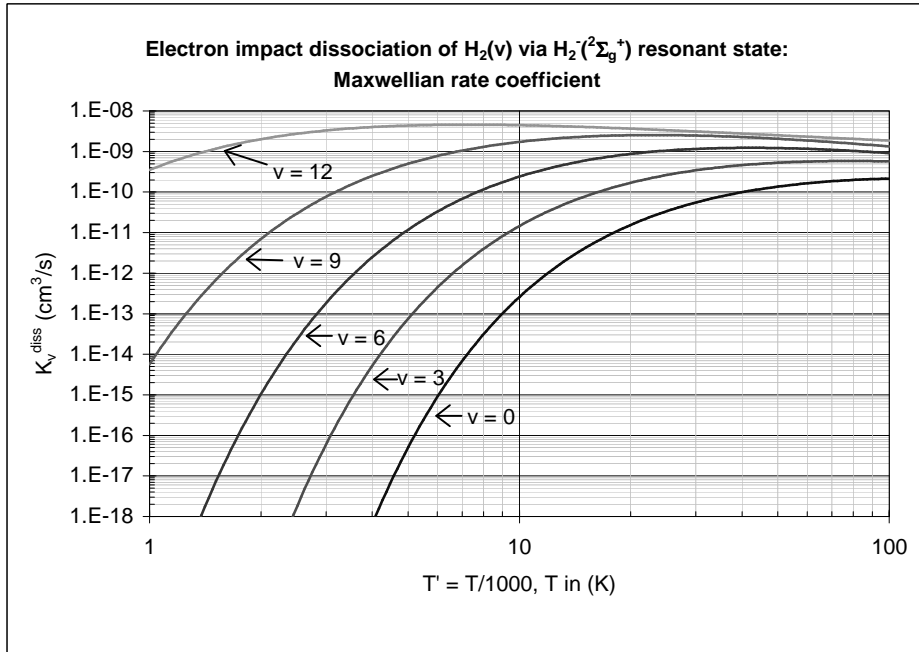


Figure 29: Rate coefficients for electron impact dissociation of $H_2(X^1\Sigma_g^+; v)$ via the $H_2(^2\Sigma_g^+)$ resonant state, Eq. (128).

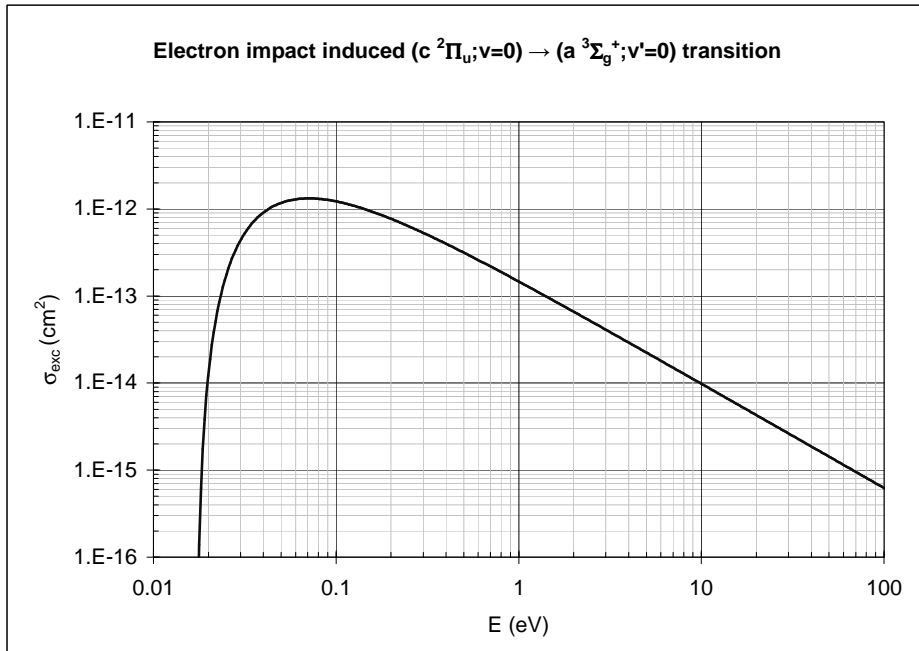


Figure 30: Cross section for the electron impact induced ($c^3\Pi_u; v = 0$) \rightarrow ($a^3\Sigma_g^+; v' = 0$) transition in H_2 in distorted wave approximation, Eq. (134).

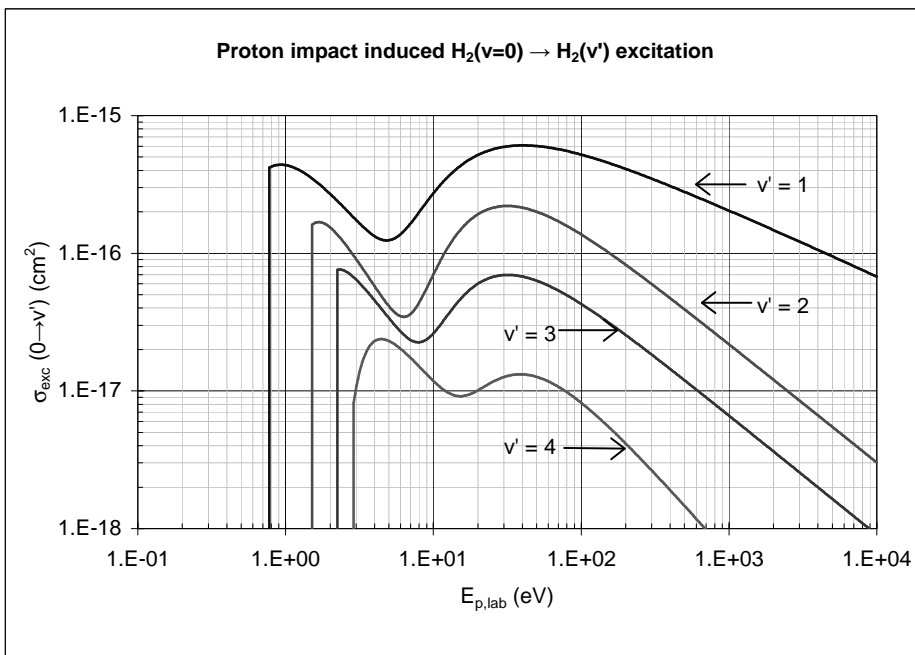


Figure 31: Cross sections for proton impact induced excitation $H_2(v=0) \rightarrow H_2(v')$ for $v' = 1, 2, 3$ and 4 , Eqs. (139,140)

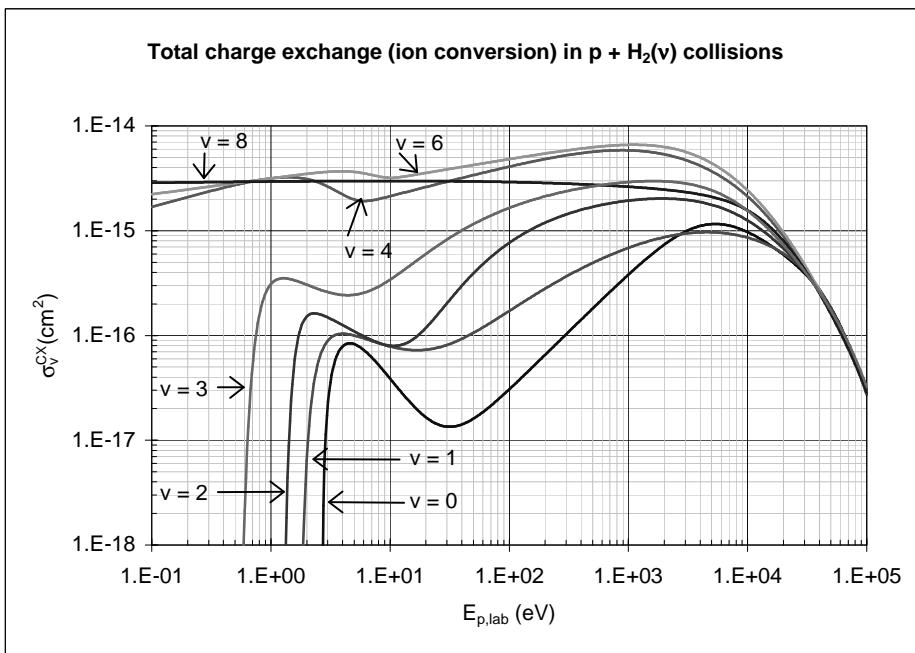


Figure 32: Total charge exchange cross sections in $H^+ + H_2(X^1\Sigma_g^+; v)$ collisions for a number of initial vibrational states v , Eqs. (144,145).

11 Figures

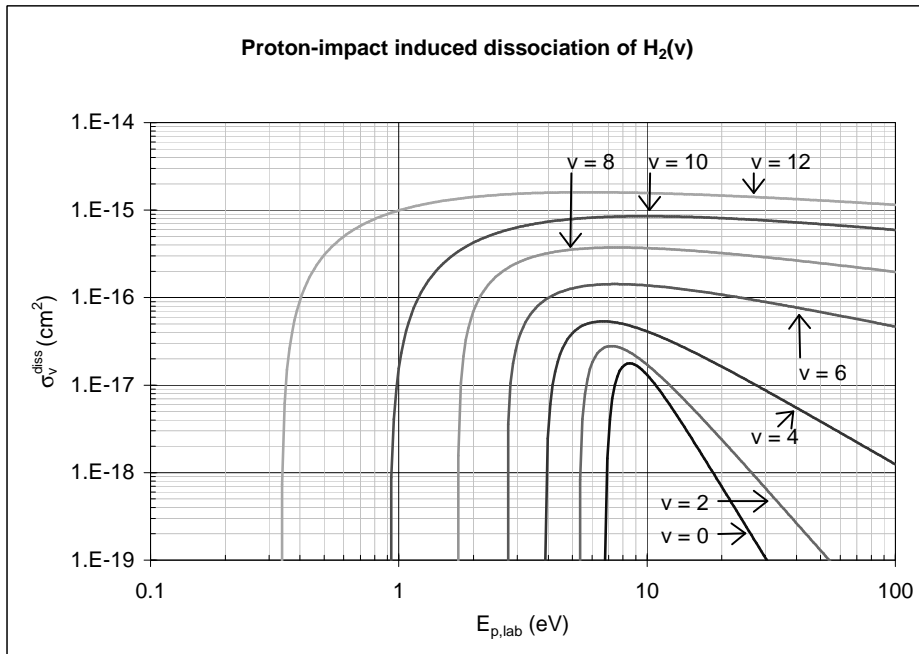


Figure 33: Cross sections for proton impact induced dissociation of $H_2(X^1\Sigma_g^+; v)$ for a number of initial vibrational states v , Eq. (153).

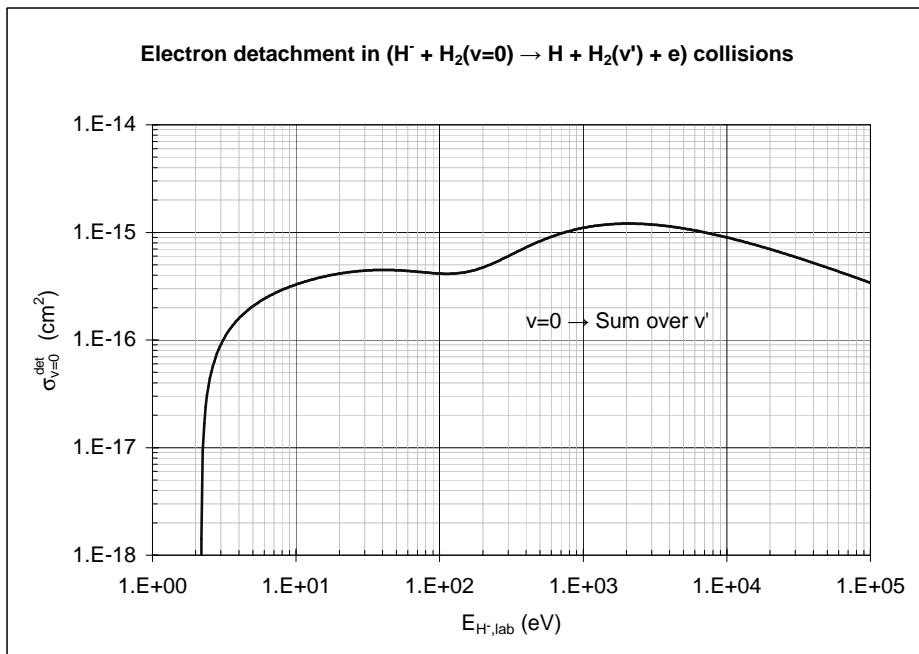


Figure 34: Cross section for electron detachment in $H^- + H_2(v = 0)$ collisions, Eqs. (159).

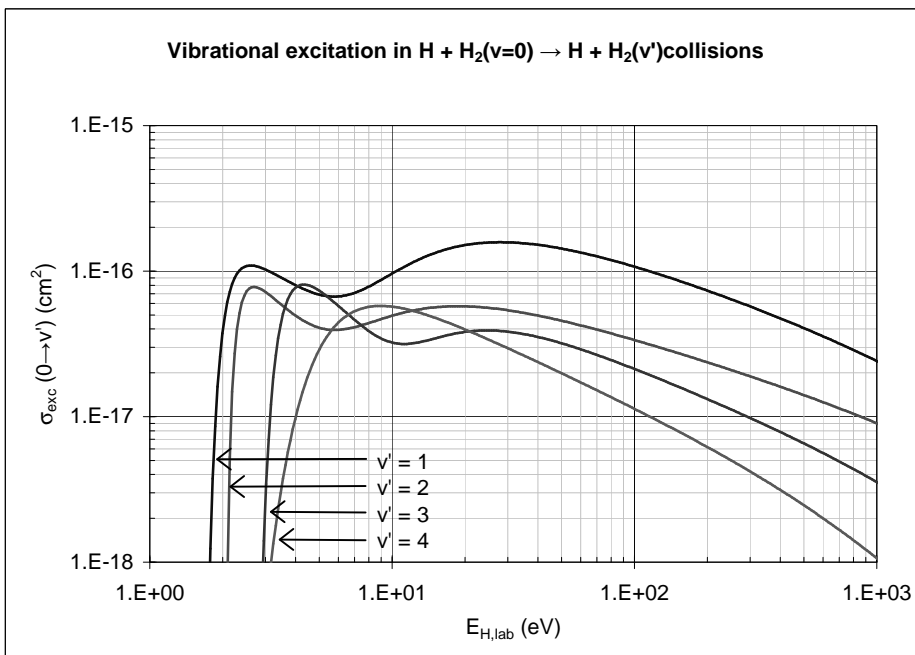


Figure 35: Vibrational excitation cross sections in $H + H_2(v = 0)$ collisions: $H_2(v = 0) \rightarrow H_2(v')$ transitions ($v' = 1 - 4$), Eqs. (161,162).

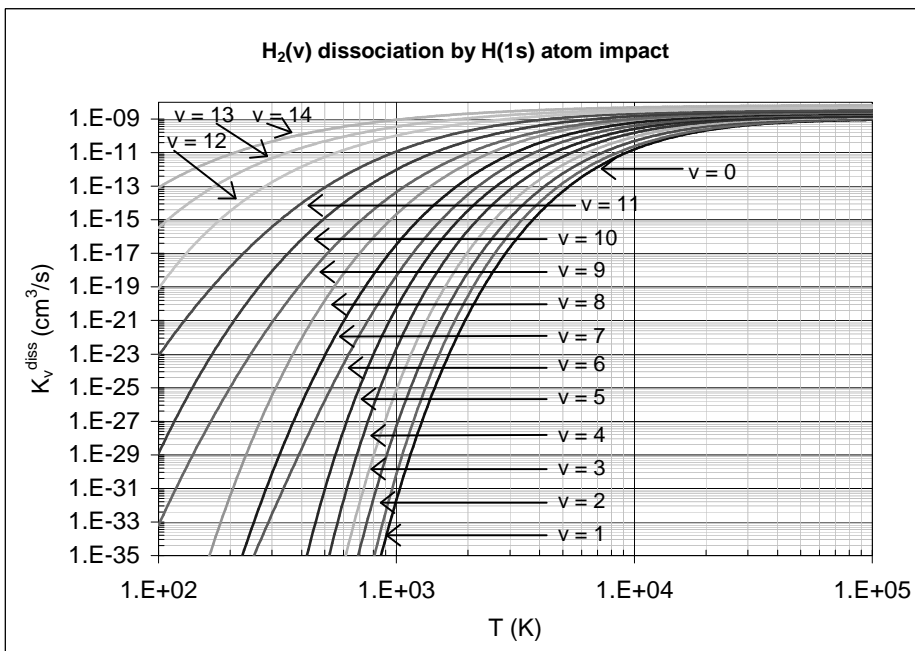


Figure 36: Rate coefficients for $H_2(v)$ dissociation in collisions with $H(1s)$ atoms, Eq. (165).

11 Figures

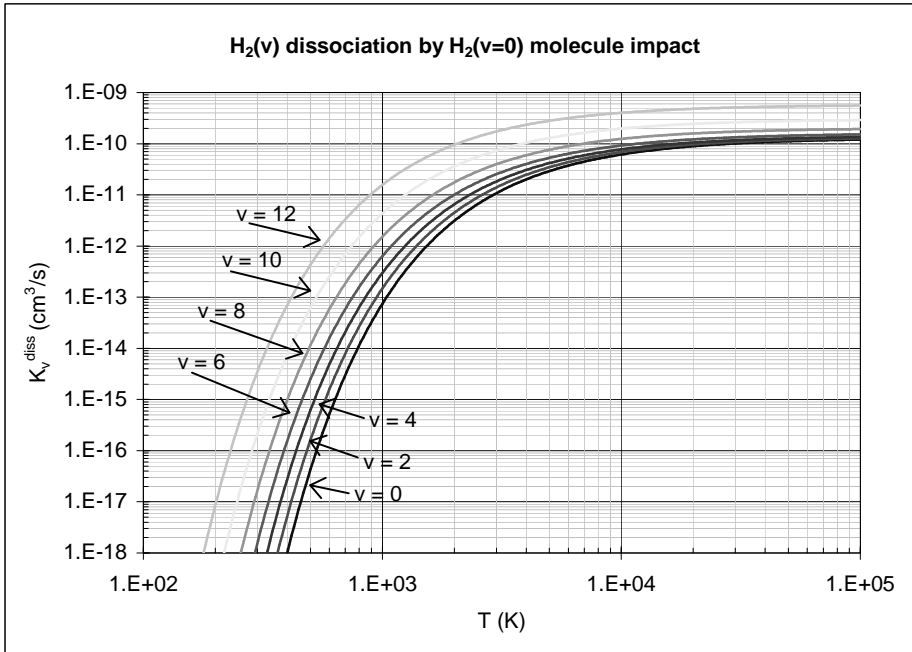


Figure 37: Rate coefficients for dissociation of $H_2(v)$ in collisions with $H_2(v = 0)$ molecules, Eqs. (169,170).

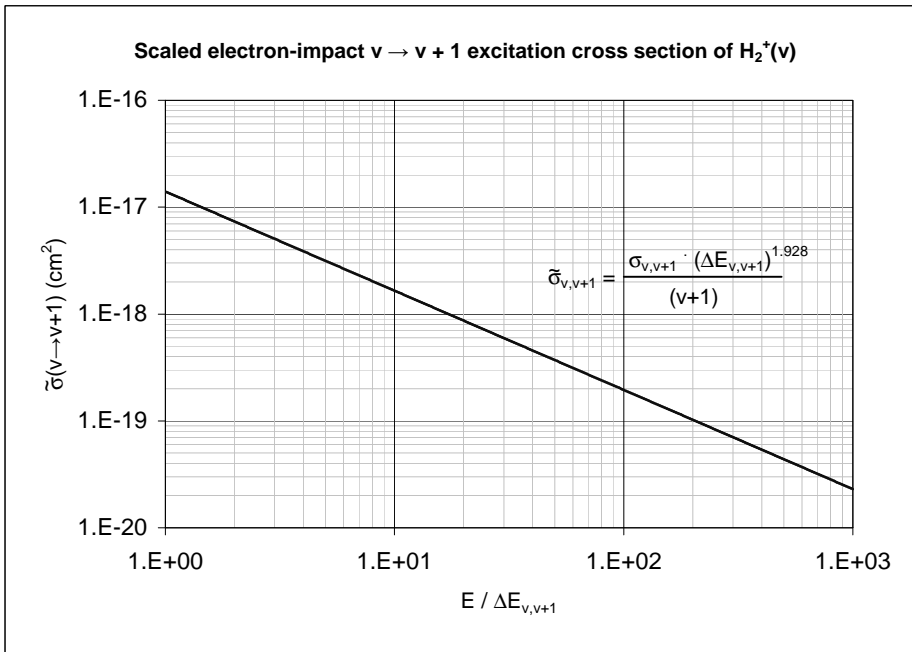


Figure 38: Scaled form of electron impact $v \rightarrow v + 1$ excitation cross section of $H_2^+(v)$, Eqs. (175,176).

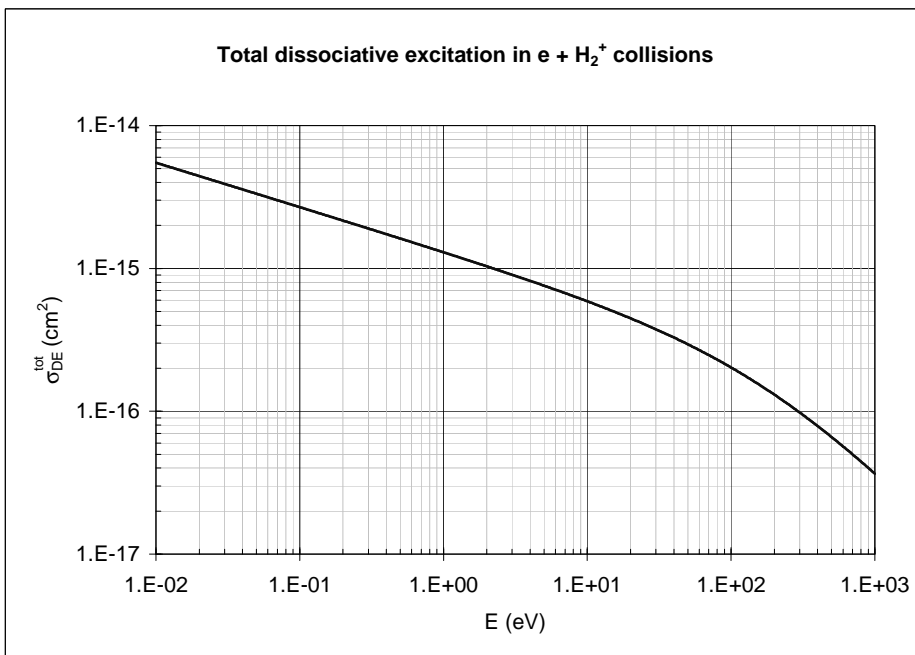


Figure 39: Cross section for total dissociative excitation in $e + H_2^+$ collisions, Eq. (180).

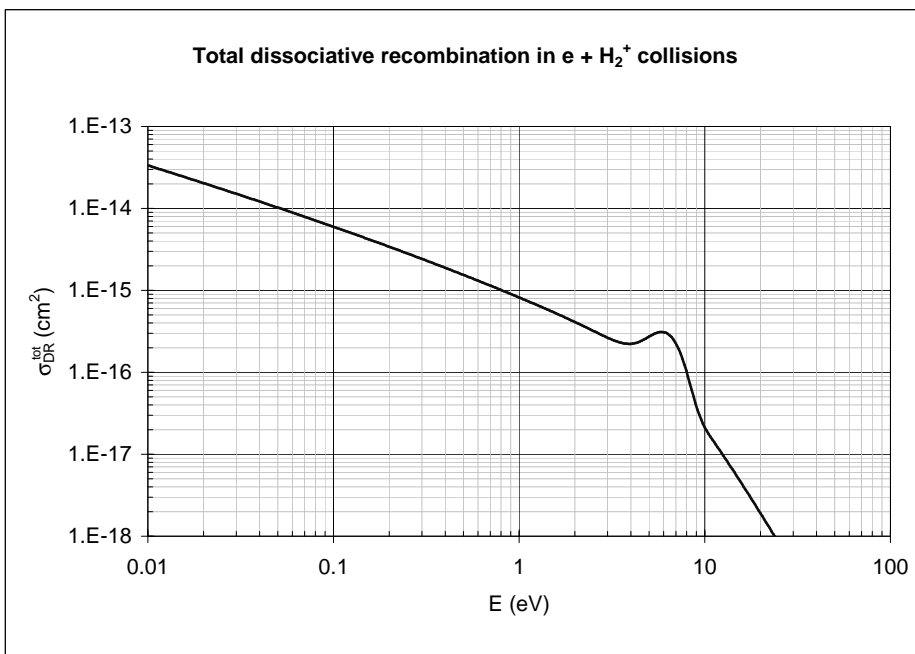


Figure 40: Total cross section for dissociative recombination in $e + H_2^+$ collisions (see text, Eq. (185)).

11 Figures

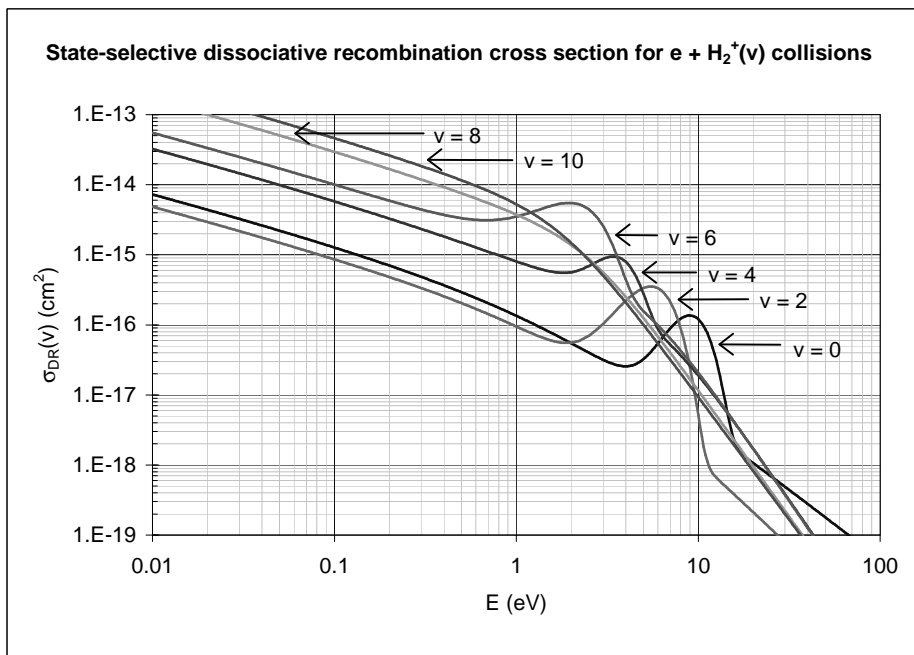


Figure 41: State-selective cross sections for dissociative recombination in $e + H_2^+(v)$ collisions, Eq. (186).

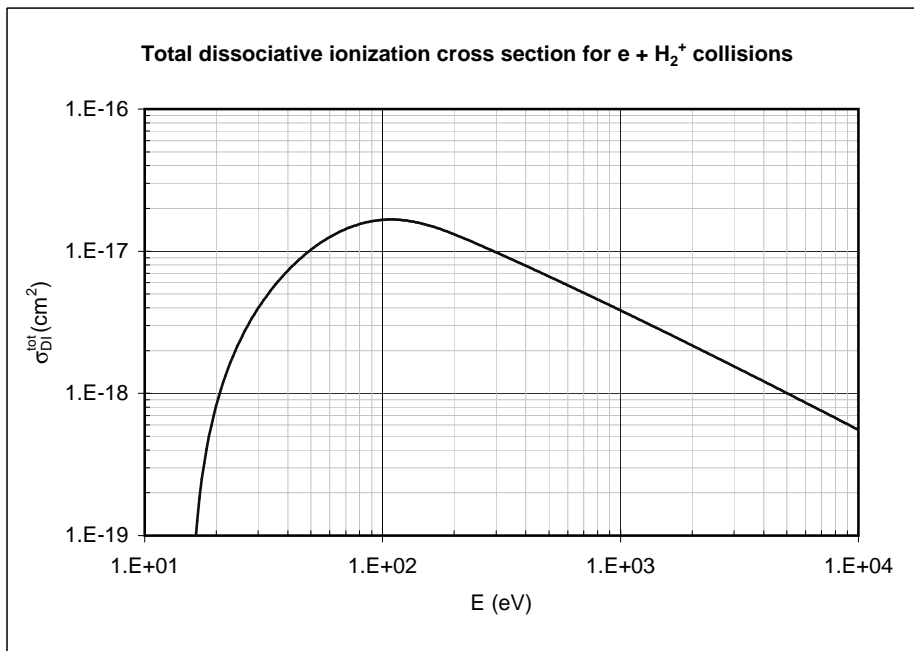


Figure 42: Total dissociative ionization cross section for $e + H_2^+$ collisions, Eq. (195).

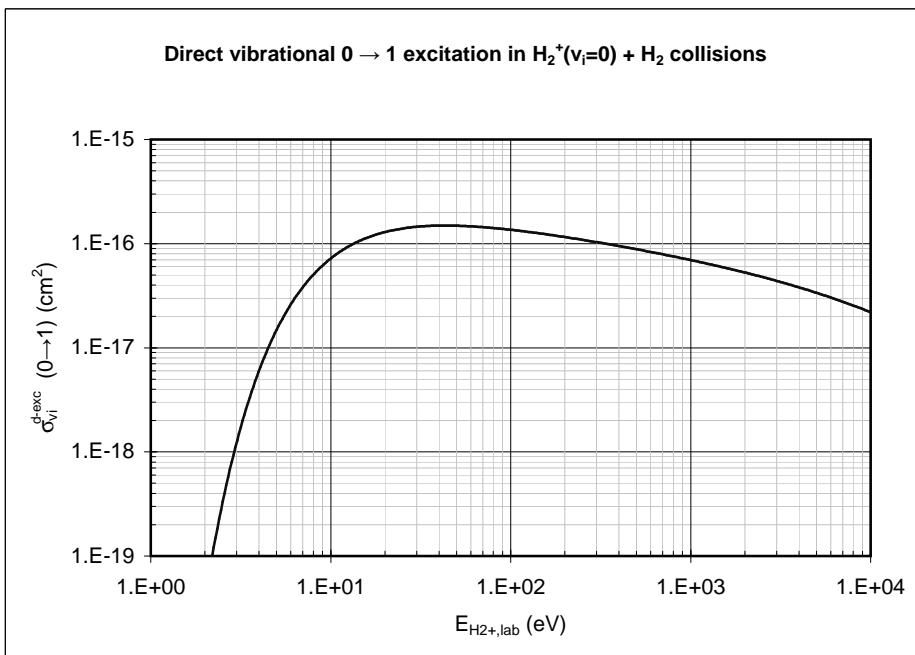


Figure 43: Cross section for direct vibrational $0 \rightarrow 1$ excitation of $H_2^+(v_i = 0)$ in collisions with ground state H_2 , Eq. (205).

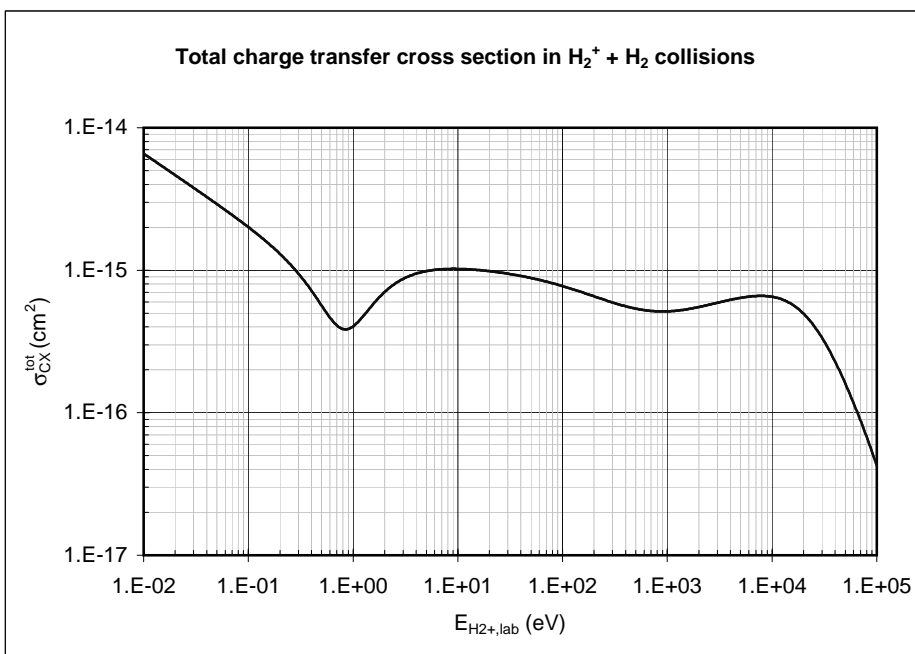


Figure 44: Total charge transfer cross section in $H_2^+ + H_2$ collisions, Eqs. (207).

11 Figures

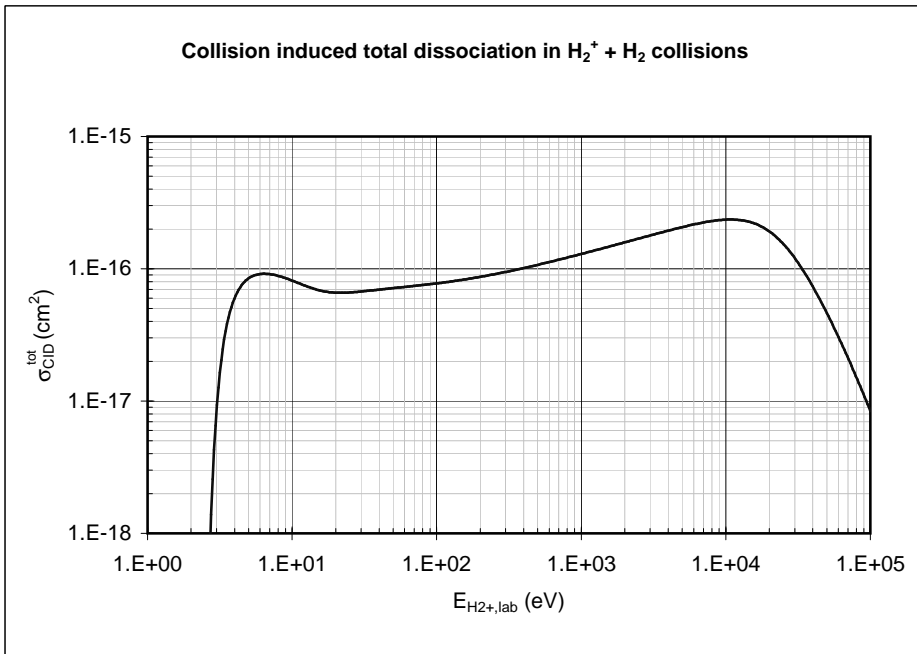


Figure 45: Total collision induced cross section of H_2^+ in collisions with $H_2(v_0 = 0)$, Eqs. (209).

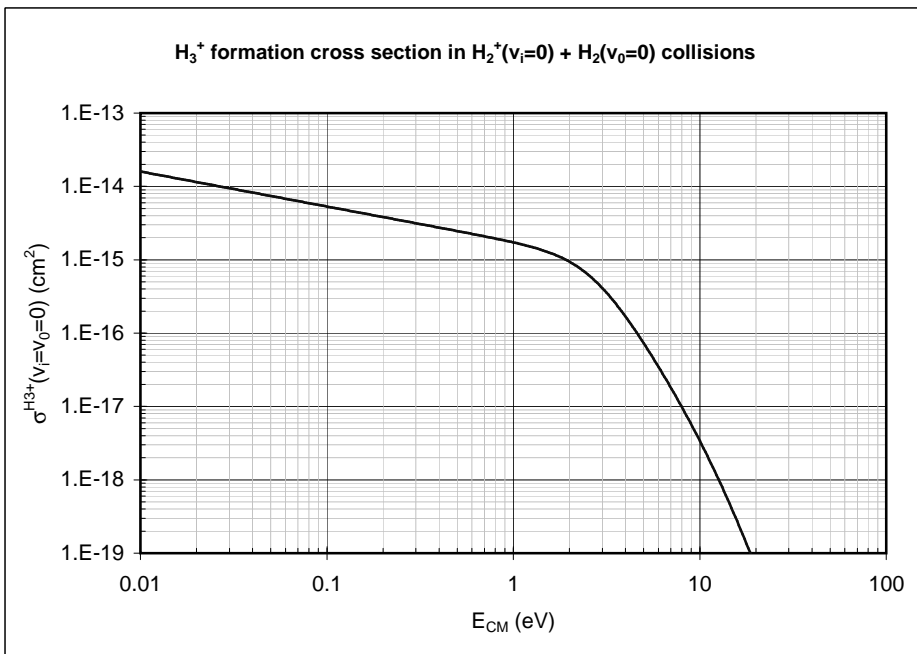


Figure 46: Cross section for H_3^+ formation in collisions of $H_2^+(v_i = 0)$ and $H_2(v_0 = 0)$, Eq. (213).

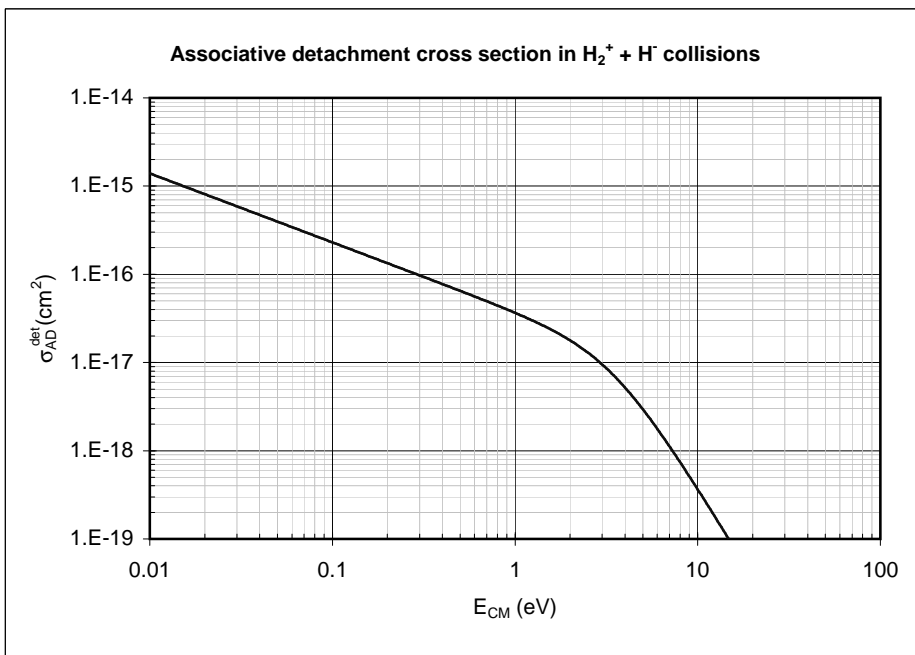


Figure 47: Associative detachment cross section in $H_2^+ + H^-$ collisions, Eq. (224).

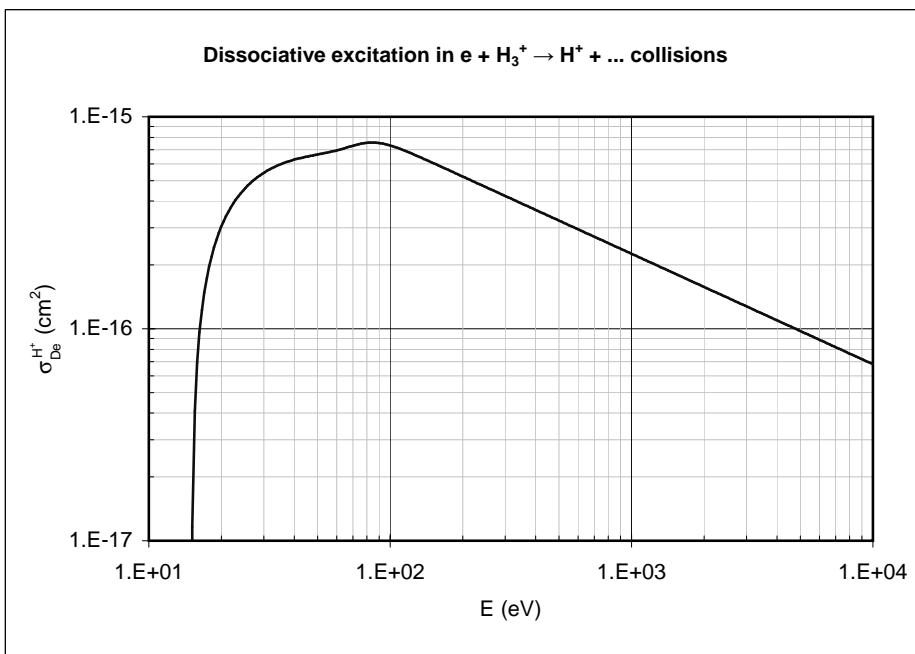


Figure 48: Dissociative excitation cross section in $e + H_3^+$ collisions, Eq. (228).

11 Figures

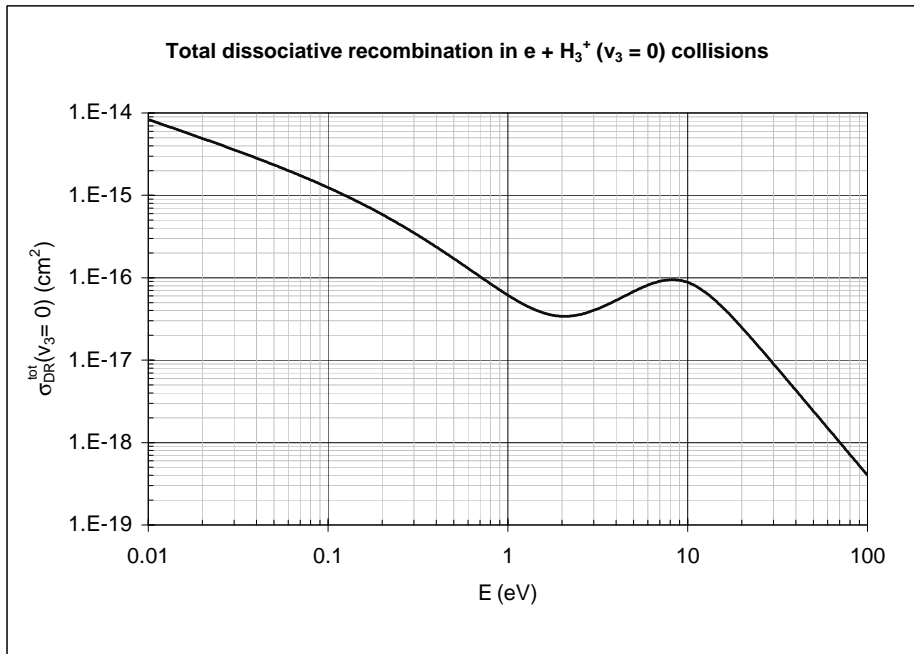


Figure 49: Total cross section for dissociative recombination in $e + H_3^+(v_3 = 0)$ collisions, Eqs. (230,231).

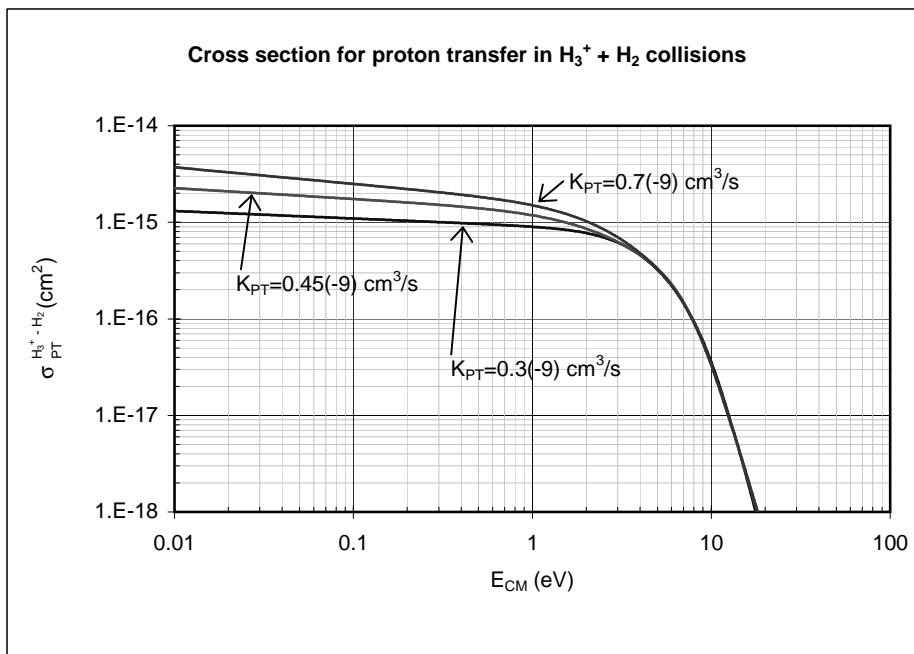


Figure 50: Cross section for proton transfer in $H_3^+ + H_2$ collisions for three values of thermal reaction rate coefficient K_{PT}^{th} , Eq. (239). [$a(-x)$ denotes $a \cdot 10^{-x}$.]

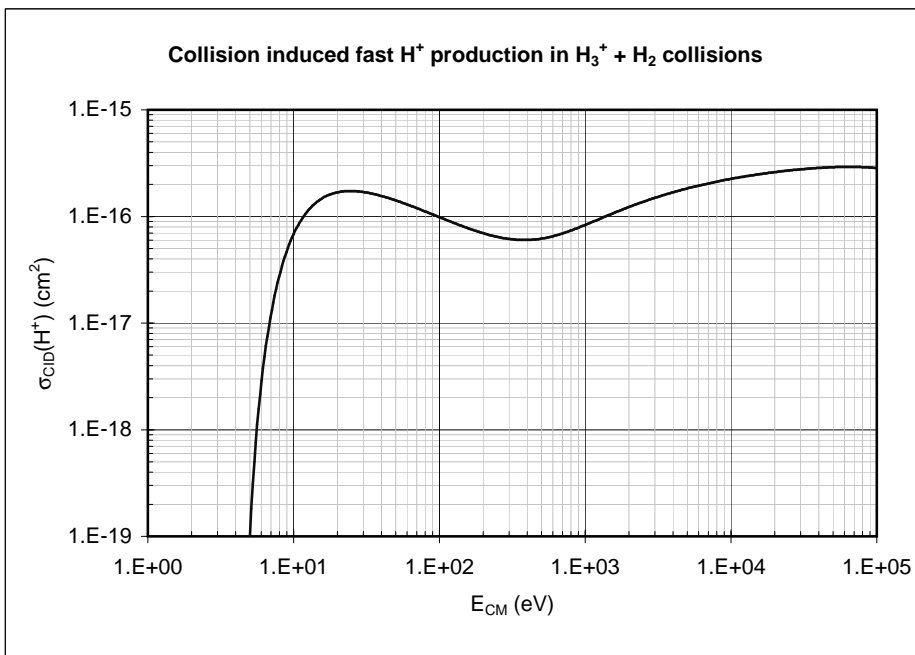


Figure 51: Cross section for fast H^+ production in $H_3^+ + H_2$ collisions, Eqs. (243).

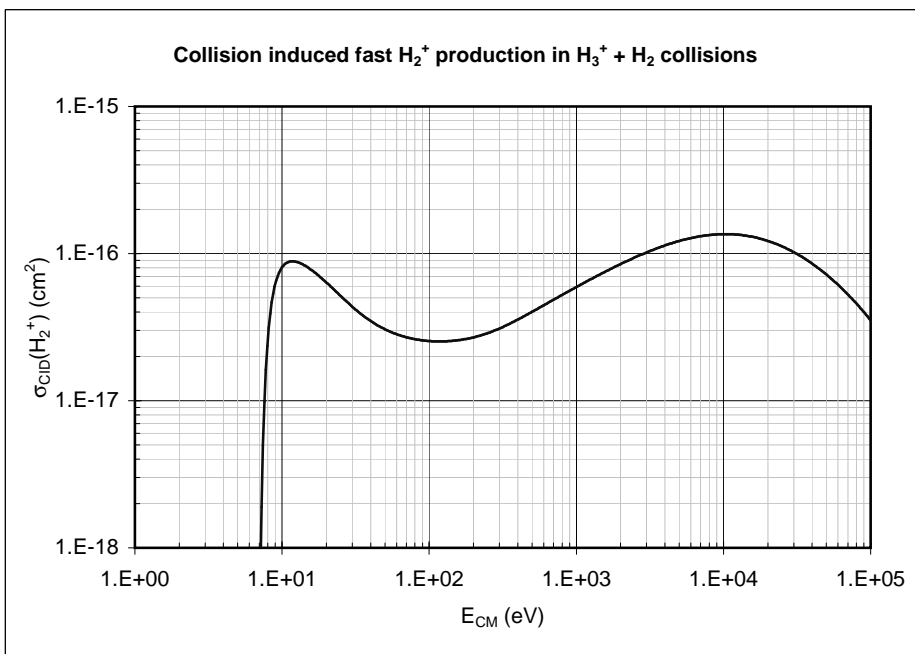


Figure 52: Cross section for fast H_2^+ production in $H_3^+ + H_2$ collisions, Eqs. (244).

11 Figures

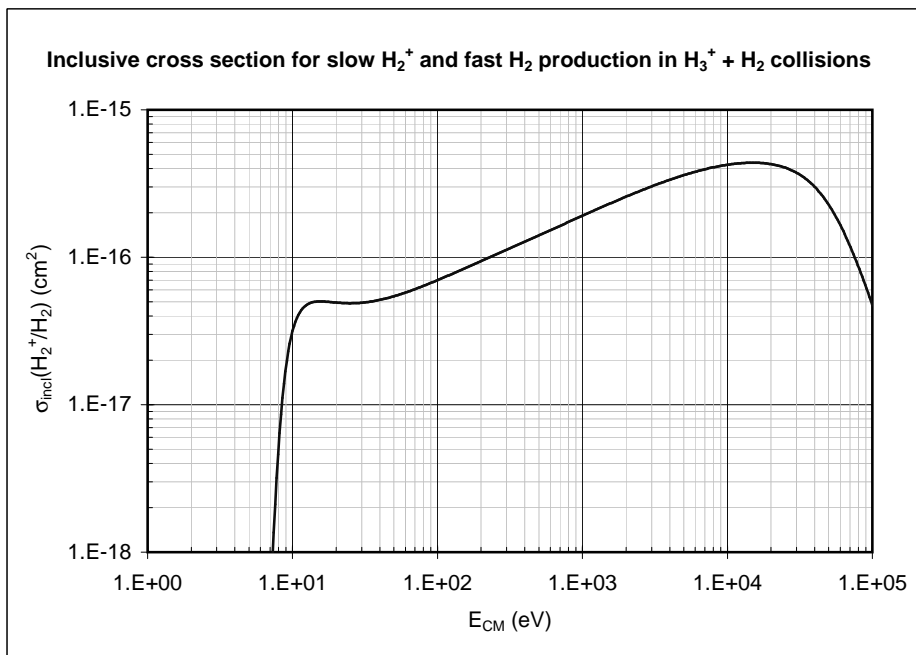


Figure 53: Inclusive cross section for slow H_2^+ and fast H_2 production in $H_3^+ + H_2$ collisions, Eqs. (248).

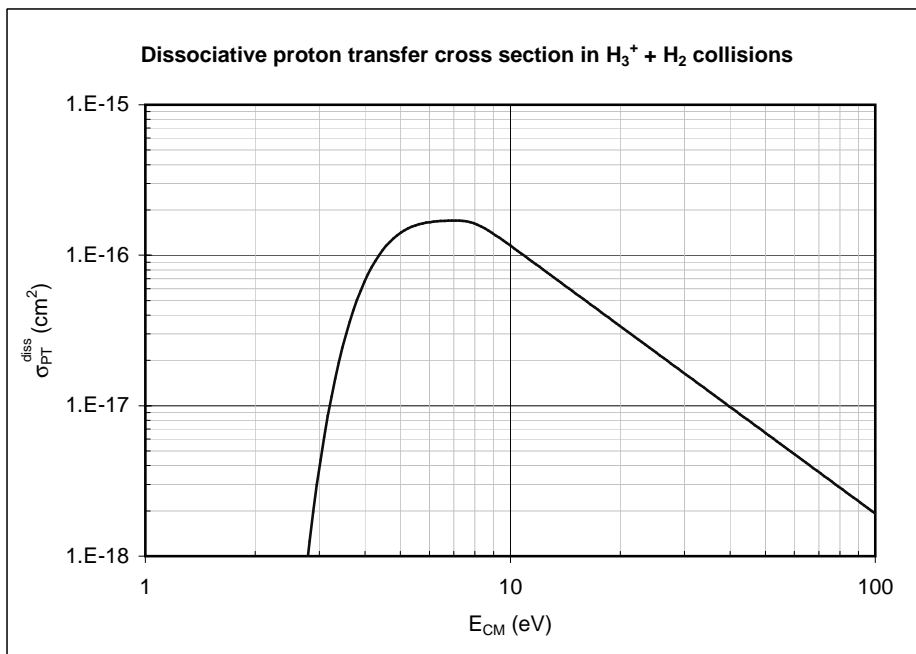


Figure 54: Dissociative proton transfer cross section in $H_3^+ + H_2$ collisions, Eq. (250).